ACOUSTIC EFFECTS ON PULSE FORMING IN ULTRASOUND TRANSIT TIME GAS FLOW METERS AT NO FLOW CONDITIONS

DISSERTATION FOR CAND. SCIENT. DEGREE

BY

MURUGENDRAN KANAGASUNDRAM

DEPT. OF PHYSICS

UNIVERSITY OF BERGEN

Bergen, June 1995

To my mother and father

Acknowledgements

First of all, I would like to thank my supervisor, Associate Professor Magne Westrheim, to suggest me such an interesting problem of diffraction of sound, among the other problems in acoustic instrumentation. His guidance through this work, suggestions to solve problems and discussions meant a lot to me. He was of great help in making this manuscript.

I wish to thank, a fellow student, Steinar Vervik. We did some programming and experimental works together in this research. His help in solving some practical problems and fruitful discussions on acoustics made a difference to this thesis.

I also want to thank Professor Halvor Hobæk and Dr. Kjell-Eivind Frøysa to patiently listen to me and help understand some problem in acoustics.

I take this opportunity to thank Ørjan Villanger and Kan Cao for their helps and discussions. The experiments and other researches related to my Cand. Scient. degree have been done in Chr. Michelson Research institute(CMR) and meetings with my supervisor were also took place at CMR. I like to thank the administration of CMR and the Ultrasound Group at CMR to give me a place to sit and do my works at CMR and to permit me to use the equipment and computer soft wares at CMR to my research work.

Finally, I would like to thank the Norwegian government to give me an opportunity to live and educate my self in Norway. My work, in return, I hope, can be useful to the people work in this field.

K.Murugendran.

CONTENTS

CHAPTER 1

INTRODUCTION

In ultrasonic transit time flow meters a sinusoidal tone burst is often used to measure the transit time and the transit time difference. A tone burst is sent into the medium and detected after travelled through it. The detected pulse which entirely different in shape from the input pulse, is used to make measurements. The correctness of the measurements, to the required accuracy, depend on the correct interpretation of the detected pulse. A good understanding of the pulse forming mechanism of the system help interpret the detected pulse correctly and make good measurements. This problem constitutes the theme of this thesis. There can be a number of factors involved in determining the form of the pulse. But, this thesis looks only into some of the acoustic aspects that contribute to the shape of the pulse.

The matters under discussion in this thesis are motivated towards the ultrasonic transit-time flow meter. However, the discussed effects are of fundamental importance in a variety of applications in the field of ultrasound technology.

This thesis consists of 8 chapters. In Chapter 2, the nature of the problem, studied in this work, is described. Zero crossing method, one of the flow measurement methods, is taken as an example to illustrate the problem and to indicate the importance of the knowledge of pulse forming in measurement systems. This knowledge can also be used in systems using other flow measurement principles.

Chapter 3 describes the measurement system both in frequency and time domains. The major parts of the system are represented as blocks. How the adjacent blocks are interfaced is mainly described in this chapter. With a simple proof, the open circuit output impedance of the receiving transducer is shown to be equal to the electrical input impedance. The same result can be found in an article written by Beissner[16], but the proof is omitted.

Chapter 4 is devoted to discuss the effect of diffraction on pulse forming. A system where two transducers of equal dimensions placed on their common axis is mainly considered. The transducer faces and the medium in between the transducers are considered as a linear, time invariant filter. The filter is described by a frequency domain transfer function which connects the particle velocity on the transmitter to the average pressure on the receiver. The impulse response of the filter is found using the transfer function. The impulse response is shown to be the same found by Rhyne[23], for a same type of configuration of the transducers, using pure time domain consideration. Using the impulse and frequency responses, the pressure pulses are calculated. The calculated pressure pulse forms are presented as a function of Seki parameters, S and ka values. The pressure pulses are compared with the well-known point receiver models; 1) Pressure due to a circular piston vibrator on the axis 2) Pressure due to a circular piston vibrator on its axis, with far-field approximation.

Khimunin[7] tabulated the diffraction correction for the transducer configuration described in the beginning of the above paragraph as a function of, S and ka values. Khimunin verified the diffraction correction for a few combinations of k and a values to show that the diffraction

correction is the same for any combination of k and a values. It is shown in this dissertation that this verification is not necessary (see Sec(4.4)).

In Chapter 5, the effects of the transducers on the shape of the transmitted pulse is studied. Mason's model for thickness extentional mode vibrations of a piezo electric plate is used as models for the transmitter and receiver. The basic mechanism of pulse forming is studied using a few terms of the impulse response of the transducer element. The pulse forms, calculated by the time domain method, are compared with that of the frequency domain method.

In Chapter 6, the total effect of the transmitter-medium-receiver system on the shape of the transmitted pulse is studied. A sinusoidal burst is used as the input voltage signal to the transmitting transducer. Using a frequency domain computer programme, the signals at every node is simulated and the pulse forms are discussed. That is, 1) Velocity signal at the face of the transmitter, 2) Free field pressure at the centre of the receiving transducer and 3) The open circuit voltage at the output terminal of the receiving transducer. The effects of matching layer is studied.

In Chapter 7, the experiment, performed in connection with the research, is described and the results are presented. The experimental results were analysed as follows. Measurements for two different separations of the transducers are involved in the analysis. Using the measured voltage signal for the first separation, the output voltage signal for the other separation is predicted. The predicted result is compared with the actual measurement. The deviations are discussed. The theoretical simulation of the measurements, using the parameters used in the experiment, and comparison with the measurements was intended. But, because of shortage of time, this was not done. However, this comparison is done and an excellent agreement in shape of the voltage signal is found by Vervik[15].

Conclusions of this work are presented in Chapter 8.

Mathematical derivations of some results are pretty long and involved. But they are an integral part of the thesis. The absence of the mathematical derivations, however, will not disturb the continuity of the thesis. Therefore they are placed in the appendices and classified as appendices(A-x). The computer programs used in calculations are listed out and placed in appendices(B-x) and constants and parameters used in the calculations are placed in appendices(C-x).

The problem for my Cand. Scient. degree was created in co-operation between the Dept. of physics, and the Chr. Michelsen Research institute(CMR), in connection with the project for developing an ultrasonic high-precision flow meter for natural gas at CMR. But this research has been done independently, not as a part of the project. At the same period another research on the transit time determination of the same flow meter was done by Mr. Steinar Vervik. Although these two researches have been started separately, in the course of the work we found the two problems are closely related to each other. As a result, most of the experimental and programming works have been done in co-operation between me and Mr.Vervik. Information on the variation of the transit-time due to properties of the various parts of the system can be found in the Cand. Scient thesis[15] of Mr. Vervik.

CHAPTER 2

MOTIVATION

2.1 INTRODUCTION

Ultrasound techniques have several advantages over the conventional methods, such as orifice plate, venturi and turbine meters, for the measurement of fluid flow. Munk[13] and Nolan and O'Hair[39] discussed some of the advantages. There are two principles widely used in commercially produced ultrasound flow meters; contra propagating and Doppler method. Of these two methods, Doppler method is not applicable for flow measurement of natural gas as it contains no particles which are necessary to scatter the sound waves. Tests[13] with 24-inch pipe lines show that the contra propagating ultrasound flow meter can be calibrated to accurately measure gas flow rates in large diameter pipe lines over a wide range of flow.

2.2 ULTRASOUND TRANSIT-TIME FLOW METER

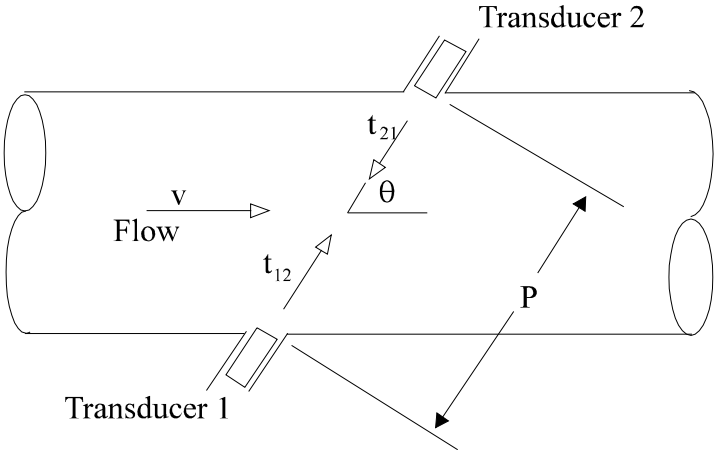

Figure(2.1) Transit-time flow meter with single path. P is the distance between transducers. The angle between the acoustical axis of the transducers and the direction of flow is θ. The mean flow velocity of the medium along the axis of the pipe is v.

The Fig.(2.1) illustrates a single beam transit-time flow meter. Transducers are oriented such that their common acoustical axis makes an angle θ with the direction of the flow. P is the distance between the transducers. t_{12} and t_{21} are the times taken for sound to travel(transit-times) from transducer 1 to transducer 2 and from transducer 2 to transducer 1 respectively. The expression for the velocity of flow can be found[13] as,

$$v = \frac{\Delta T}{t_{21} t_{12}} \frac{P}{2\cos\theta} \tag{2.1}$$

where

$$\Delta T = t_{21} - t_{12} \tag{2.2}$$

In the Eq.(2.1), v is the average velocity along the sound path. But in a real situation the flow velocity is not uniform over the cross-section of the pipe. As a result the flow rate calculated using the measured velocity would be different from the true. Therefore it is important to determine the flow profile correctly to find the correct flow rate. In high precision transit-time flow meters, several pairs of transducers are deployed and the velocity is measured at many places over the cross-section of the pipe.

Consider one sound transmission link in a multi-beam transit-time flow meter. The Fig.(2.2) illustrates such a single beam sound transmission. A voltage signal is applied to the transmitting transducer by the transmitting electronics. This signal, after travelled through the transmitting transducer, the medium and the receiving transducer, is received by the receiving electronics. The time interval between the transmitted and the received signals is registered. The registered times, obviously, contain the time delays in the non-liquid parts and has to be corrected for.

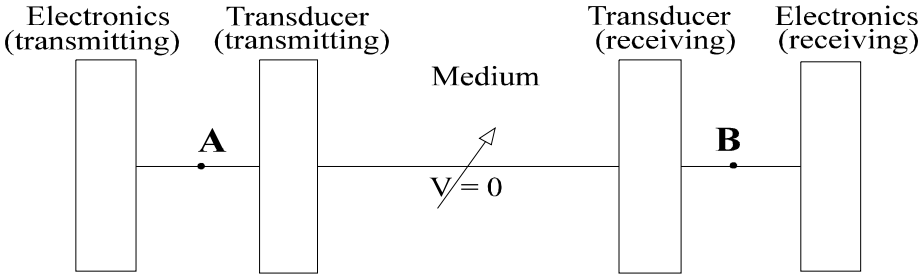

Figure(2.2) Simplified block diagram of a single beam sound transmission link in a transit-time ultrasonic flow meter.

2.3 NO-FLOW CONDITION

Transit-times at no-flow condition are utilised[20,43,44] to eliminate the time delays in the non-liquid parts of the meter from the measured transit-times. The transit times and the transit time difference at no-flow conditions are measured, for the required environmental conditions, and stored in the flow computer. This is known as zero calibration. Using these data, during the flow measurement, the transit-time measurements are corrected and the flow velocity is calculated according to the corrected transit-times.

The measurement errors occur in the measurement of the transit-time at no-flow conditions, thus, may reduce the accuracy of the meter. In this work an attempt has made to illustrate some possible source of errors due to the misinterpretation of the received signal. The signal transmission through transmitting and receiving electronics, shown in Fig.(2.2), can be modelled. Therefore the signal transmission between points A and B in the Fig.(2.2) is only investigated in this study.

In transit-time flow meters voltage signals of the form of sinusoidal bursts, chirps and spikes(an approximate delta function) are used to measure the transit-times. The choice of a particular form of the signal depends on the system. Sinusoidal tone bursts are usually used to measure low flow velocities(<30m/s)[33], like in gas transfer pipe lines, in narrow band systems.

A voltage signal of the form of a sinusoidal burst is applied to the electrical terminal of the transmitting transducer. This signal is detected by the receiving electronics after it has travelled through the transmitting transducer, the medium and the receiving transducer. Zero crossing method[43] is addressed here for the measurement of the transit-time. The detection unit of the receiving electronics is programmed to detect the zero crossings that come after a pre defined signal level. And these zero crossings are compared with the corresponding zero crossings of the transmitted signal to measure the transit-time. That is, the 1st zero crossing of the transmitted signal is compared with that of the received, 2nd zero crossing of the transmitted signal is compared with that of the received and so on and the time difference is taken to be the transit-time. If the pre defined signal level is misinterpreted as if it belongs to a particular cycle of the signal, for example as the first while it is being the second, then the measured time using the detected zero crossing will contain en error of one period.

Inter transducer distance divided by the propagation velocity of sound in the medium, ignoring the time delays in the transducer pockets, is taken to be the transit-time. This is the plane wave model for time calculations. Consider the time measured using the method described in the previous paragraph. To calculate the transit-time, the time delays in the non-liquid parts are subtracted from the measured time. Assume there is no absorption in the medium. The calculated transit-time will obey the time relationship of the plane wave model if the measurement were made using the first arrival of the received signal. For zero crossings in the signal to obey the time relationship of the plane wave model, the signal had to travel through the medium as a plane wave. But, this is not the case at all because of the finite size of the transmitter. The deviation of the measured signal from the plane wave depends on the geometrical configuration and the dimensions of the transducer-medium-transducer system. This deviation from the plane wave is found to be caused by the phenomena known as diffraction. If the zero crossings of the received burst are to be used for the measurements, which is often the case because the first few periods of the signal usually buried in the noise, the measured times of the zero crossings must be compensated for the above mentioned deviation from the plane wave. Otherwise, in high precision measurements, the accuracy will be reduced. The deviation of the measured signal from the plane wave due to diffraction is demonstrated and discussed in detail in Chapter 4.

With proper mathematical models for the transducers, diffraction and the electronics, the voltage level of each peak of the signal in the transient region and the entire form of the signal can be predicted. The predicted pulse may not match the real one. But, it will help the experimenter to interpret the measured signal correctly and to make the measurements more precisely. The knowledge of pulse forming effects will give a better understanding of the system which can be used to control and improve it.

2.4 DISCUSSION

The time of arrival of the received signal is strictly not equal to the time of arrival of the plane wave, d/c, if the medium is dispersive, where d is the distance between the transducers and c

is the phase velocity of the centre frequency of the signal. In a dispersive medium, high frequency components of the signal travel faster and arrive at the receiver earlier than the centre frequency. The zero crossings will also be altered by the absorption in a dispersive medium. If it can be assumed that variation of the velocity of sound is small for a large band width then this effect may be neglected. However, for the simulation of the received signal to be more close to the real one, absorption should be included in the model.

CHAPTER 3

SYSTEM MODEL

3.1 INTRODUCTION

In this chapter a simulation model[2,3,4] which is comparable to the experimental set-up that used to study the single beam ultrasound transmission through a medium is described. The model consists a number of blocks representing the major parts such as electronics(transmitting), transducer(transmitting), propagation medium, transducer(receiving), and electronics(receiving) of the experimental set-up. The input, output quantities involved in each block and how these quantities related to the adjacent blocks are discussed.

In coming chapters the influence of blocks, representing the medium and the transmitting and the receiving transducers, on the shape of the signal being transmitted are discussed. The analysis is done for isolated and integrated blocks. The suffixes of the parameters in the block diagram do not follow the numbers of the nodes.

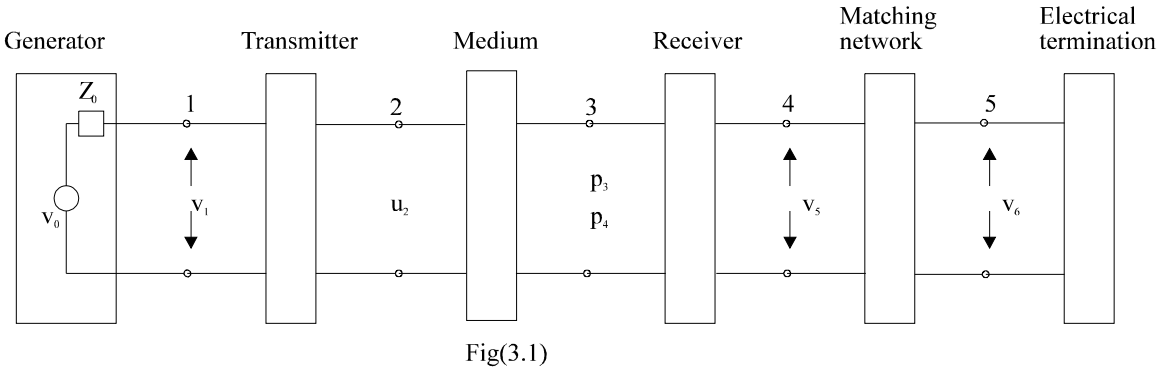

Figure(3.1) The block diagram of the system model.

$v_0(t)$ Voltage signal from the generator in volts.

$v_1(t)$ Input signal(volts) to the transducer(transmitting).

$u_2(t)$ Particle velocity of the radiating surface of the transmitting transducer.

$p_3(1m,t)$ Far-field pressure at a distance 1m on the axis of the transmitting transducer.

$p_4(t)$ Free field pressure at the centre of the receiving transducer.

$v_5(t)$ Output signal(volts) from the transducer(receiving).

$v_6(t)$ Output signal(volts) from the electrical matching network.

3.2 FREQUENCY DOMAIN DESCRIPTION OF THE SYSTEM MODEL

From basic signal analysis theory it is known that the output, y(t), of linear time invariant system for an input, x(t), is given by the inverse Fourier transform of the product of the spectrum of the input with the transfer function of the system, provided the Fourier transform of x(t) and y(t) are exist.

$$Y(\omega) = X(\omega)\, H(\omega) \tag{3.1}$$

where $Y(\omega)$, $X(\omega)$ are frequency spectrum of the output and the input signals respectively and $H(\omega)$ is the transfer function of the system.

The Fourier pair of a time function f(t) is defined as,

$$F(\omega) = \int_{-\infty}^{\infty} f(t) e^{-j\omega t} dt \tag{3.2a}$$

$$f(t) = \frac{1}{2\pi} \int_{-\infty}^{\infty} F(\omega) e^{j\omega t} d\omega \tag{3.2b}$$

Assuming the blocks in Fig(3.1) as linear time invariant filters, the inputs and outputs can be related through their respective frequency domain transfer functions. When the blocks are connected as shown in the Fig(3.1), the relationship between the input voltage, V_0, and output voltage, V_6 can be written[2] as follows.

$$\begin{aligned} \frac{V_6(\omega)}{V_0(\omega)} &= \frac{V_1(\omega)}{V_0(\omega)} \; \frac{U_2(\omega)}{V_1(\omega)} \quad \frac{P_4(\omega)}{U_2(\omega)} \; \frac{V_5(\omega)}{P_4(\omega)} \; \frac{V_6(\omega)}{V_5(\omega)} \\ &= H_{01}(\omega) \; H_{12}(\omega) \quad H_{24}(\omega) \; H_{45}(\omega) \; H_{56}(\omega) \end{aligned} \tag{3.3}$$

where,

$H_{01}(\omega)$ Transfer function relates the generator voltage to the transmitting transducer's input voltage.

$H_{12}(\omega)$ Transfer function relates the transmitting transducer's input voltage to the particle velocity of its radiating face.

$H_{24}(\omega)$ Transfer function relates the particle velocity of the surface of the transmitting transducer to the free field pressure at centre of the receiving transducer.

$H_{45}(\omega)$ Transfer function relates the free field pressure at the centre of the receiving transducer to the receiving transducer's output voltage.

$H_{56}(\omega)$ Transfer function relates the input voltage and output voltage of the electrical matching network.

The block representing the transmitting transducer is characterised by the voltage to velocity transfer function, $H_{12}(\omega)$. This transfer function is described by the Mason type of model for a thickness extensional piezoelectric vibrator. The transfer function, $H_{12}(\omega)$, using the above model, is found in Chapter 5.

The block representing the medium is characterised by the transfer function, $H_{24}(\omega)$. This transfer function is described by the following four different mathematical models.

1. Plane wave model

2. Near-field, point receiver model

3. Far-field model

4. Near-field, finite receiver model

These models are discussed in detail and the transfer function, $H_{24}(\omega)$, for each model are found in Chapter 4.

The transfer function $H_{45}(\omega)$ can be splited into two functions as,

$$H_{45}(\omega) = \frac{U(\omega)}{P_4(\omega)} \; \frac{V_5(\omega)}{U(\omega)} \tag{3.4}$$

where $U(\omega)$ is the spectrum of the particle velocity, u(t), of the active face of the receiving transducer.

The term, $\frac{U(\omega)}{P_4(\omega)}$, in Eq.(3.4) is the transfer function which relates the free-field pressure, P_4, to the particle velocity, U, of the receiving transducer. To calculate this transfer function, consider plane waves impinging on the receiver. This situation can be represented[16] by Thevenin equivalent circuit with the open circuit force, F_b, as the mechanical generator, the radiation impedance, Z_r, as its internal impedance and the acoustic input impedance of the transducer with a finite electrical termination, Z_{in}, as the load, as shown in Fig.(3.2). This representation is explained using the Thevenin theorem shortly. F_b, and P_4 are the Fourier transforms of their respective time functions.

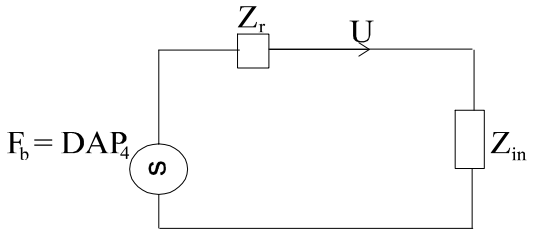

Figure(3.2) Thevenin equivalent circuit for plane waves incident on the transducer

Thevenin theorem can be found in any network analysis text book. However, in order to make the discussion easier, the theorem is stated here briefly in its technical form.

Thevenin theorem:

Suppose the current through an impedance in an electrical network is asked.

Step 1 Put the circuit in a black box, pull out the branch of the circuit with the impedance through which the current is under question and disconnect the impedance from the rest of the circuit as shown in Fig.(3.3).

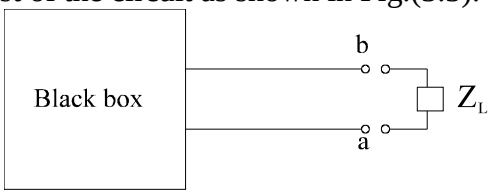

Figure 3.3 An electric network is put in a black box and the impedance through which the current under question is pulled out from the box and disconnected.

Step 2 Find the open circuit voltage between the terminals a and b. This is equivalent to find the voltage v_{AB} while the terminals a and b are connected to an infinite impedance. This is known as Thevenin equivalent voltage and denoted as E_{th}.

Step 3 Replace all the generators in the network with their internal impedance and find the impedance between the terminal a and b. This impedance can be found either by using simple resistor addition law or alternatively[32] by finding the voltage to current ratio at the test voltage source connected between the terminals a and b.

Thevenin equivalent circuit then would be,

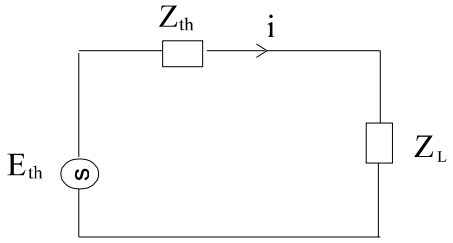

Figure 3.4 The Thevenin equivalent circuit for the electrical network considered in Fig.(3.3).

and the current, i, under question is given by,

$$i = \frac{E_{th}}{Z_L + Z_{th}}.$$

Now, consider the situation where a plane wave incident on the receiving transducer. Suppose the particle velocity of the transducer is to be found. The medium and the plane waves can be thought as an unknown electrical network of generators and resistance in the black box feeding a current(particle velocity U) in to a load(acoustic impedance of the transducer with the finite electrical termination, Z_{in}). To find the equivalent circuit, consider the following steps and compare with the corresponding steps under the Thevenin theorem.

Step 1 Disconnect the impedance, Z_{in}, from the rest of the circuit.

Step 2 Find the open circuit voltage(force). This is equal to the force on a blocked transducer while plane waves incident on it. That is $E_{th} \equiv F_b$, the force on the blocked transducer which can also be called, logically, as the open circuit force*.

The open circuit force, $F_b = DAP_4$, where D is the diffraction factor which, in the present case, is 2. A detailed proof of this relationship is given in Appendix(A-3).

Step 3 Remove all the generators. This means that there is no waves incident on the transducer now. There is only medium in the black box. Connect a test voltage(force) source to the terminal. This is equivalent to make any transducer to emit waves in to the same medium. Then the voltage to current ratio, voltage/current(force/velocity), at the test voltage(force) source gives the Thevenin equivalent impedance and which is, of course, the radiation impedance. That is Thevenin impedance $Z_{th} \equiv Z_r$.

The Thevenin equivalent circuit, then, would be as shown in Fig.(3.2), and from this circuit,

$$\frac{U(\omega)}{P_4(\omega)} = 2\frac{A}{Z_{in} + Z_r}. \tag{3.5}$$

The second term in Eq(3.4), $\frac{V_5}{U}$, the velocity to voltage transfer function of the receiving transducer while it is terminated with a finite impedance. This transfer function is considered here to formulate a general description of the system. But, in Chapter 5 and 6 only the transfer function with open circuit condition is considered.

3.3 SYSTEM TRANSFER FUNCTION IN TERMS OF SENSITIVITIES.

The overall transfer function of the system can also be expressed in terms of the sensitivities of the transmitting and receiving transducers. Before showing this, it is important to define the sensitivities.

Definition:

> *Free-field pressure[17] is the pressure due to a sound wave progressing freely.*

---

* Beissner[16] uses a same kind of representation for the plane waves incident on a transducer functioning as a receiver. In his discussion p_b is the open circuit pressure whereas in this thesis F_b is the open circuit force. $F_b = A\,p_b$ where A is the area of the transducer. He uses a two port Z parameter in his discussion, and Z_{22} is the open circuit acoustic impedance. In this thesis Z_{in} is the acoustic impedance of the transducer with a finite electrical termination.

Rhyne also uses a same kind of representation for this situation. The sentence "....This condition corresponds to an open-circuit loading of the wave and thus...." in page 319 of the article[23] is in support for this conclusion.

Definition:

> *Transmitting voltage sensitivity[18], S_v, of a transducer, for a given frequency, is defined as the ratio of the free-field pressure generated at a reference point to the voltage across the electrical terminal.*

A point at 1m on the axis from the transducer is used as the reference and the pressure is calculated according to the far-field model[1] in this discussion.

The transfer function $H_{24}(\omega)$ can be written as

$$H_{24}(\omega) = H_{23}(\omega)H_{34}(\omega), \tag{3.6}$$

where

$$H_{23}(\omega) = \frac{P_3(\omega)}{U_2(\omega)} \qquad \text{and} \qquad H_{34}(\omega) = \frac{P_4(\omega)}{P_3(\omega)}.$$

The overall transfer function can then be written as,

$$H_{06}(\omega) = H_{01}(\omega)\ H_{12}(\omega)\ H_{23}(\omega)\ H_{34}(\omega)\ H_{45}(\omega)\ H_{56}(\omega) \tag{3.7}$$

The transfer function, $H_{12}(\omega)H_{23}(\omega)$, transfers the input voltage, V_1, to the far-field pressure at 1m from the transducer. If $v_1(t)$ is chosen to be a sinusoidal voltage with frequency ω_0, $v_1(t)=V_0\exp(j\omega_0 t)$, then the far-field pressure is given by,

$$P_3(\omega) = H_{12}(\omega)H_{23}(\omega)V_0\delta(\omega-\omega_0) \tag{3.8}$$

where

$V_0\delta(\omega-\omega_0)$ is the frequency spectrum of $v_1(t)$.

Taking inverse Fourier transform to Eq.(3.8) and using sifting property of Dirac delta function gives,

$$p_3(t) = H_{12}(\omega_0)H_{23}(\omega_0)\ V_0\ \exp(j\omega_0 t) \tag{3.9}$$

The pressure at 1m, according to the above equation, is $V_0H_{12}(\omega_0)H_{23}(\omega_0)$. The source sensitivity is then found by dividing the pressure by voltage, V_0 , across the electrical terminals. That is,

$$S_v = H_{12}(\omega_0)H_{23}(\omega_0). \tag{3.10}$$

Since the choice of ω_0 is arbitrary Eq(3.10) can be written as,

$$S_v = H_{12}(\omega)H_{23}(\omega) \tag{3.11}$$

Definition:

> *Receiving sensitivity[19], M, of a transducer is defined as the ratio of the output open circuit voltage to the free-field pressure due to plane progressing wave, with the incident angle with the principal axis of the transducer being zero, at the centre of the transducer.*

The receiving transducer's output voltage, V_5. can be written using Thevenin theorem as,

$$V_5 = (V_5)_{open} \frac{Z_L}{Z_L + Z_{out}} \tag{3.12}$$

where

Z_{out} is the output impedance of the receiving transducer and

Z_L is the impedance due to the rest of the circuit that seen by the receiving transducer.

Z_{out} is same as the Thevenin equivalent impedance. This can be found as follows. The situation where plane waves incident on the transducer can be represented, as shown earlier in this section, by a generator and the radiation impedance, Z_r, as its internal impedance. The transducer can be represented as an electrical network of linear electric components. This representation is shown in Fig.(3.5). To find the Thevenin equivalent impedance, all the generators in the network, as described in step 3 of the Thevenin theorem stated earlier in this section, has to be removed and the impedance of circuit has to be found while the terminals are connected to a test voltage source. And this impedance is same as the electrical input impedance, Z_{in}^E, of the transducer while it is operating in the medium used in the application. That is,

$$Z_{out} \equiv Z_{in}^E.$$

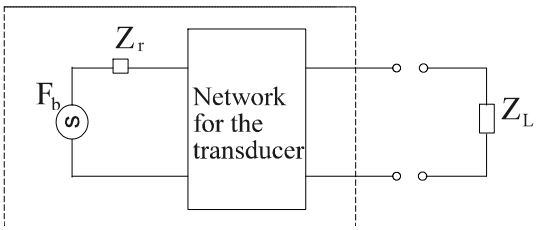

Figure 3.5 Representation of plane waves incident on a transducer as an electric circuit.

Dividing both sides of the Eq.(3.12) by the free-field plane wave pressure, P_4, gives,

$$\frac{V_5}{P_4} = \frac{(V_5)_{open}}{P_4} \frac{Z_L}{Z_L + Z_{out}} \tag{3.13}$$

$$H_{45}(\omega) = M \frac{Z_L}{Z_L + Z_{out}} \tag{3.14}$$

Now the Eq.(3.7) can be rewritten as

$$H_{06}(\omega) = S_{v1}\, M_2 \frac{Z_L}{Z_L + Z_{out}} H_{01}(\omega) H_{34}(\omega) H_{56}(\omega) \tag{3.15}$$

where,

S_{v1} transmitting sensitivity of the transmitting transducer and

M_2 receiving sensitivity of the receiving transducer.

The relationship in Eq(3.3) is mainly used to calculate the response of the total system. However, the time domain calculations also used in the analysis. Therefore, it is necessary to describe the system in the time domain. Next section is devoted to describe the system in the time domain.

3.4 TIME DOMAIN DESCRIPTION OF THE SYSTEM MODEL

The input, x(t), and the output, y(t), of a linear time invariant system are related through the time convolution as follows[9].

$$y(t) = h(t) \otimes x(t) \tag{3.16}$$

where

h(t) is the impulse response of the system and $\otimes$ is the convolution operation.

The time domain relationship in Eq(3.16) and the frequency domain relationship in Eq(3.1) are related through the Fourier transform as follows[9],

$$y(t) = h(t) \otimes x(t) \Leftrightarrow Y(\omega) = H(\omega)\, X(\omega). \tag{3.17}$$

The transfer function $H_{01}(\omega)$ in Eq.(3.3) is given by

$$V_1(\omega) = H_{01}(\omega) V_0(\omega).$$

Taking the inverse Fourier transform of the above equation gives,

$$v_1(t) = h_{01}(t) \otimes v_0(t) \tag{3.18a}$$

where, $h_{01}(t)$ is the impulse response between nodes 0 and 1 of the Fig.(3.1). Similarly, the time domain relationships of the input and output of each block in the Fig(3.1) can be written as follows.

$$u_2(t) = h_{12}(t) \otimes v_1(t) \tag{3.18b}$$

$$p_4(t) = h_{24}(t) \otimes u_2(t) \tag{3.18c}$$

$$v_5(t) = h_{45}(t) \otimes p_4(t) \tag{3.18d}$$

$$v_6(t) = h_{56}(t) \otimes v_5(t) \tag{3.18e}$$

where, $h_{nm}(t)$ are the impulse responses between the nodes n and m.

The overall response of the system in the time domain can then be written as,

$$v_6(t) = h_{01}(t) \otimes h_{12}(t) \otimes h_{24}(t) \otimes h_{45}(t) \otimes h_{56}(t) \otimes v_0(t) \tag{3.19}$$

As only the acoustic part of the system is studied in this work, only the impulse responses $h_{12}(t)$, $h_{24}(t)$ and $h_{45}(t)$ are presented in this thesis. $h_{12}(t)$ is found in Chapter 5, $h_{24}(t)$ is found in Chapter 4 and $h_{45}(t)$ is found, only for the open circuit case, in Chapter 5.

3.5 DISCUSSION

In calculating the transfer function $H_{45}(\omega)$, it was assumed that P_4, in Eq.(3.3),is the pressure due to a plane wave. But, this pressure, P_4, is calculated using four different mathematical models. Therefore it is important to justify that the pressure calculated by all these models are of plane wave pressure at the receiver.

In the plane wave model, a plane wave which propagates without changing its plane wave property is considered. Therefore, obviously, at the observation point the pressure wave is a plane. In the near-field, point receiver model, the receiver at the observation point has an infinitely small dimension. Therefore, even though the wave front is spherical, at the receiver, it can be considered as a plane. In the far-field model, the wave fronts are spheres with large radii. For receivers with small dimensions the wave fronts can be treated as planes. And for the near-field, finite receiver model, the pressure at the receiver is averaged over the surface of the receiver. Since the amplitude and the phase of the average pressure at every point over the receiver surface is equal, the average pressure can be considered[7] as the pressure due to a plane wave.

In the calculation of the open circuit force in Appendix(A-3), it is assumed that the receiving transducer is mounted on an infinite baffle. This is not true at all in practice. But, however, for frequencies where the dimension of the transducer is very much larger compare to the wave length of incident wave, the diffraction factor, for normal incidence, can be taken as 2. For smaller transducers the diffraction factor becomes smaller and reaches 1 for an ideal point receiver.

In the propagation models absorption has not been taken into consideration. Therefore, in a situation where the simulated sensitivity results are to be compared with the measurements, one has to correct the measurements for absorption.

One can measure the sensitivities of a transducer independently. The sensitivities characterises the behaviour of the transducer. As it has been recognised the sensitivities of the transmitting and receiving transducers as transfer functions in the system model, the output signal can be explained, qualitatively, in terms of the changes in transducers, for example with temperature. The description of the system model with the sensitivities contains both magnitude and the phase of the sensitivities. If the measurement lacks the phase information, a complete comparison of the simulated and experimental results would not be possible. However, with the magnitude of the sensitivities as a function of frequency, the magnitude of the output signal could be compared[15] with the simulated.

CHAPTER 4

EFFECT OF DIFFRACTION ON PULSE FORMING

4.1 INTRODUCTION

The diffracted field from a planar sound source is a century-old problem in acoustics. Lord Rayleigh[5] addressed the problem in his famous book "The Theory of Sound" in 1878. But, it gained more attention after 1940s. Numerous researches have been performed both theoretically and experimentally in this area in connection with ultrasound imaging and measurement of material properties, especially the measurement of attenuation of sound in materials. An overview on the works done in this field and a spectrum of references are given by Harris[38].

The pressure due to a circular radiator, averaged over a coaxial circular surface of equal radius in front of the source, is of interest. The transit time flow meters, calibration of transducers by self reciprocity method, absorption spectrometers etc. use a configuration where circular transducers of equal dimensions, placed coaxially, are used as transmitter and receiver or, equivalently, one transducer is used as transmitter and receiver with a reflector. These systems measure the average pressure. Williams[6] calculated the average velocity potential, for such a configuration as described above, for a sinusoidal excitation based on King's[22] expression, while Rhyne[23] calculated the average velocity potential for an impulse excitation based on Stepanishen's[24] impulse response results. In this dissertation, Rhyne's impulse response result(corresponding pressure) is found from the Williams' frequency response result(corresponding pressure). The results are essentially the same however, for the fact that both have the same origin; Stepanishen results and King's expression can be derived[45,10] from Rayleigh's integral.

Transit-time flow meter, which is under investigation in this work, uses two transducers of equal dimensions, placed on their common axis, as transmitter and receiver. As pointed out in Sec.(2.3), if the effect of diffraction is not considered, the accuracy of the transit-time meters may be reduced at high precision measurements. This chapter is devoted to study the effects of diffraction on the form of the pulse as it propagates between the transducers. The space between the planes passing through the transducer faces, also denoted as the "medium" block in Fig.(3.1), is considered as a linear, time invariant filter and the effects of diffraction is studied as the response of the filter both in frequency and time domains. Although the aim of the work is more concerned about the configuration of transducers described above, in order to explain and compare the pulse forms, some other special cases are also considered. The above mentioned filter is, therefore, described, by four different mathematical transfer functions based on piston type of model and the responses are compared and discussed.

4.2 THEORY

In this section, as proposed in Sec.(3.2), the transfer function that relates the particle velocity at transmitting transducer and free field pressure at the centre of the receiving transducer are found for all four models. The theory of the models to be discussed in this chapter is well established and can be found in the literature. However, for clarity, using the theories found in Ref.(45) and Ref.(1), the desired results are obtained. In the beginning of this section a general expression for the velocity to free field pressure transfer function is found. Using this general expression, the transfer functions for the three propagation models, namely the plane wave model, the near-field, point receiver model and the far-field model, and the corresponding impulse responses are found. Finally, the velocity to average pressure transfer function for the near-field, finite receiver model and the corresponding impulse response are found.

4.2.1 A GENERAL EXPRESSION FOR TRANSFER FUNCTION

The Fig.(4.1) shows the geometry of the configuration, which is to be described shortly, in the usual spherical polar co-ordinate system. Consider a circular sound source of radius, a, mounted on a rigid infinite baffle(not shown) that lies on the xy plane with its centre coincide with the co-ordinate origin. The co-ordinates with the suffix, 0, distinguish the points on the sound source from the points in the field and hence $\theta_0 = \pi/2$. The space defined by $z > 0$ is filled with an isotropic, homogeneous and non viscous medium. The source vibrates with a velocity, $u(r_0,\varphi_0,t)$ in the z direction.

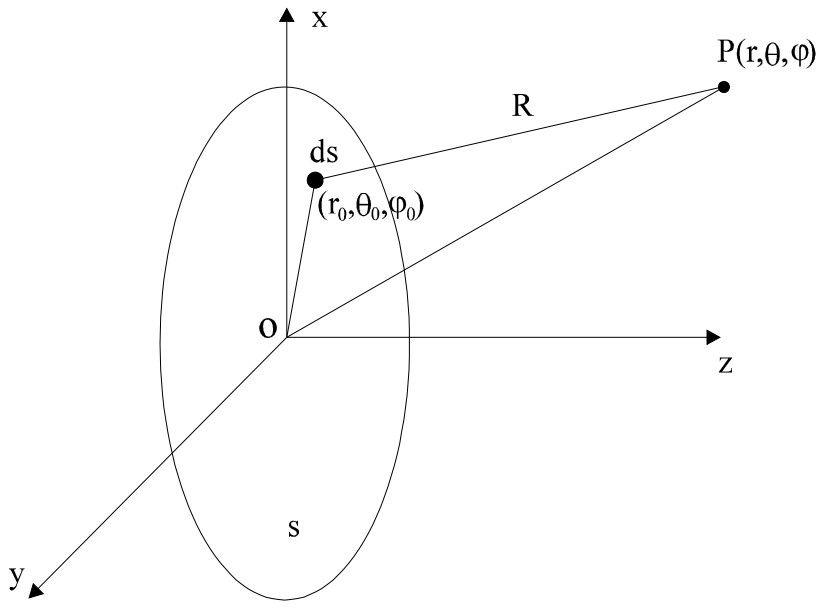

Figure(4.1) A circular piston source lies on the xy plane whose centre lies on the co-ordinate origin, O. The observation point, P, lies at (r,θ,φ) in the spherical co-ordinate system. ds is en elemental area on the source with co-ordinates (r_0,θ_0,φ_0) where $\theta_0 = \pi/2$.

The time dependent velocity potential, $\phi(\underline{r},t)$, at a point, P, and at time, t, is given by the well-known Rayleigh's integral[5],

$$\phi(\underline{r},t) = -\frac{1}{2\pi}\iint_s \left(\frac{\partial\phi}{\partial n}\right)_{z=0} \frac{e^{-jkR}}{R} ds \tag{4.1}$$

where ds is an infinitesimal elemental area on the source, R is the distance of the observation point from the infinitesimal elemental area, ds, r is the distance of the observation point from the origin, O, s is the surface of the source and n is the unit normal to s. $\left(\frac{\partial\phi}{\partial n}\right)_{z=0}$ is the normal particle velocity at the source.

The following expressions[1] for particle velocity, u, and pressure, p, are used in this dissertation.

$$u(\underline{r},t) = -\nabla\phi(\underline{r},t) \tag{4.2}$$

and

$$p(\underline{r},t) = \rho_0 \frac{\partial}{\partial t}\left(\phi(\underline{r},t)\right) \tag{4.3}$$

where ρ_0 is the density of the medium.

At the source region,

$$-\left(\frac{\partial\phi}{\partial n}\right)_{z=0} = u(r_0,\varphi_0,t)\,. \tag{4.4}$$

If $u(r_0,\varphi_0,t) = e^{j\omega t}$, the Eq.(4.1) can be written as,

$$\phi(\underline{r},t) = \frac{1}{2\pi}\iint_s \frac{e^{-jkR}}{R} ds \cdot e^{j\omega t}\,. \tag{4.5}$$

Then the frequency domain expressions for the velocity potential, $\phi(\underline{r},t)$, for an arbitrary velocity function, $u(r_0,\varphi_0,t)$, assuming the system to be linear, can be written[9] as,

$$\Phi(\underline{r},\omega) = \frac{1}{2\pi}\iint_s U(r_0,\varphi_0,\omega)\frac{e^{-jkR}}{R} ds \tag{4.6}$$

where, $U(r_0,\varphi_0,\omega)$ is the Fourier transform of $u(r_0,\varphi_0,t)$, $k = \omega/c$ and c is the thermodynamic speed of sound in the medium,

The frequency domain expression of the pressure, using Eq.(4.3), can be written as,

$$P(\underline{r},\omega) = j\omega\rho_0\Phi(\underline{r},\omega) \tag{4.7}$$

The formula given in Eq.(3.2) is used for Fourier transformation.

Now, assume the velocity is uniform over the surface of the source. Then, $U(r_0,\varphi_0,\omega)$ can be written as $U(\omega)$ and the Eq.(4.6) becomes,

$$\Phi(\underline{r},\omega) = U(\omega)\left(\frac{1}{2\pi}\iint_s e^{-jkR}\,\frac{ds}{R}\right) \tag{4.8}$$

or

$$\Phi(\omega) = U(\omega)G(\underline{r},\omega) \tag{4.9}$$

where

$$G(\underline{r},\omega) = \left(\frac{1}{2\pi}\iint_s e^{-jkR}\,\frac{ds}{R}\right). \tag{4.10}$$

The expression for pressure will then be,

$$P(\underline{r},\omega) = j\omega\rho_0 U(\omega)G(\underline{r},\omega) \tag{4.11}$$

or

$$P(\underline{r},\omega) = U(\omega)H(\underline{r},\omega) \tag{4.12}$$

where

$$H(\underline{r},\omega) = j\omega\rho_0 G(\underline{r},\omega) \tag{4.13}$$

For linear time invariant systems the ratio of the output to input spectrum gives[9] the transfer function. Therefore, $H(\underline{r},\omega)$ is the general expression for the velocity to pressure transfer function. By taking the inverse Fourier transform of the Eq.(4.12), in principle, one can find the pressure, $p(\underline{r},t)$, at the observation point, P, for a given velocity, u(t). Some special cases of interest which constitute the three propagation models mentioned earlier in this chapter are described and their transfer functions and their impulse responses are presented in the coming sections. The function $G(\underline{r},\omega)$, as it is being a part of the transfer function and depends only on the spatial co-ordinates, is called the spatial transfer function of the system.

4.2.1.1 PLANE WAVE MODEL

This section describes a very simple and often used model. In Sec.(2.3), it is said that the transmitted signal does not propagate like a plane wave in the medium due to diffraction. In order to demonstrate the deviation and to calculate the corrections, this model is used as a reference model in this work. A transfer function is developed for this model in this section which can be used to simulate plane pressure waves at the observation point for a given velocity function.

TRANSFER FUNCTION

Consider an infinite rigid plane(not shown) lies on the xy plane of a spherical polar co-

ordinate system as shown in Fig.(4.2). The plane vibrates back and forth with a uniform velocity, u(t), in the z direction. Denote the velocity to pressure transfer function for this model, as $H_p(\underline{r},\omega)$. The corresponding spatial transfer function, denoted as $G_p(\underline{r},\omega)$, has to be calculated first to calculate $H_p(\underline{r},\omega)$.

If the elemental area ds in the expression for $G_p(\underline{r},\omega)$ is chosen as follows, the integration can be calculated easily. Now, consider the Fig.(4.2). O' is the projection of the observation point, P, on the xy plane. A reference axis, x', is drawn, parallel to x-axis, from O'. The radial distance of an arbitrary point on the xy-plane from O' is r' and the angle, measured anti clock wise, between the line connecting the arbitrary point and O' and x'-axis is φ'. The shaded portion in the Fig.(4.2) is the chosen elemental area, denoted as ds', and can be written as,

$$ds' = r'dr'd\varphi'. \tag{4.14}$$

Then Eq.(4.10) takes the form for this case as

$$G_p(\underline{r},\omega) = \left(\frac{1}{2\pi} \iint_s e^{-jkR} \frac{ds'}{R} \right). \tag{4.15}$$

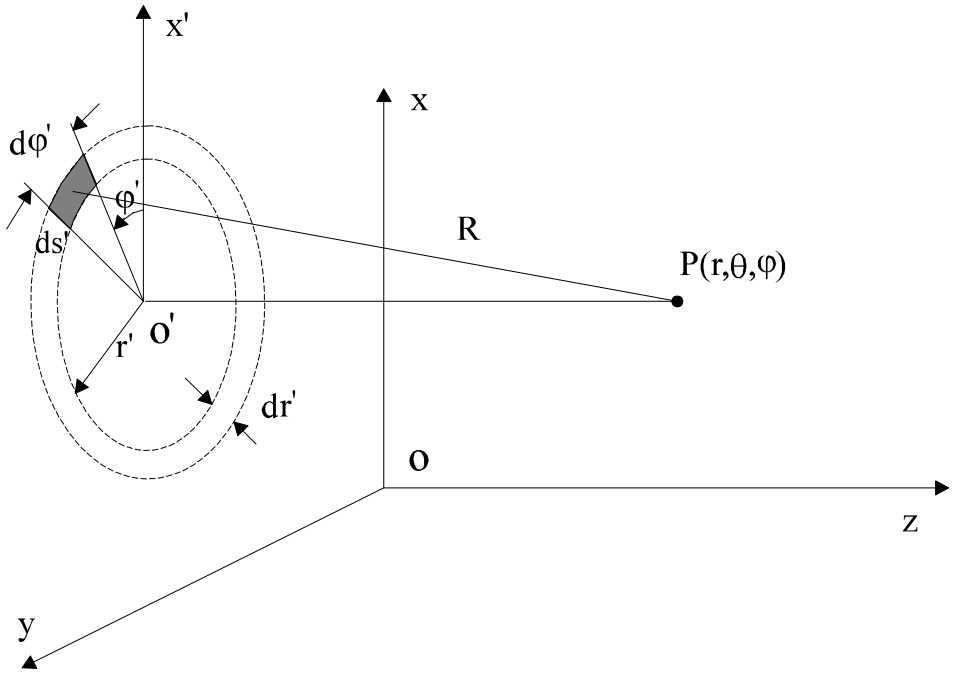

Figure(4.2) An infinite plane lies on the xy plane. Observation point, P, lies at (r,θ,φ) in spherical co-ordinate system. Projection from the point P to the xy plane is O'. R is the distance between the observation point and the elemental area, ds'.

Let the distance of the observation point, P, from the xy plane be z(= rcosθ)

Since

$$R = \sqrt{z^2 + r'^2} \tag{4.16}$$

$$G_p(\underline{r},\omega) = \frac{1}{2\pi}\int_0^{2\pi}\int_0^{a'} \frac{e^{-jk\sqrt{z^2+r'^2}}}{\sqrt{z^2+r'^2}} r'dr'd\varphi' \tag{4.17}$$

where a', a very large number, is the upper limit for the integration variable r'. The integrand in the above integration[21] can be written as an exact differential,

$$G_p(\underline{r},\omega) = -\frac{1}{jk}\int_0^{a'} d\left[e^{-jk\sqrt{z^2+r'^2}}\right] \tag{4.18}$$

and then further can be written as,

$$G_p(\underline{r},\omega) = \frac{1}{jk}\left[e^{-jkz} - e^{-jk\sqrt{z^2+a'^2}}\right]. \tag{4.19}$$

Then, $H_p(\underline{r},\omega)$, using Eq.(4.13), can be written as,

$$H_p(\underline{r},\omega) = \rho_0 c\left[e^{-jkz} - e^{-jk\sqrt{z^2+a'^2}}\right] \tag{4.20}$$

The pressure at point, P, $p(\underline{r},t)$, for a velocity function, u(t), can be found by multiplying $H_p(\underline{r}, \omega)$ with the spectrum of u(t), $U(\omega)$, and taking inverse Fourier transform.

$$p(\underline{r},t) = \rho_0 c\left[u\left(t-\frac{z}{c}\right) - u\left(t-\frac{\sqrt{z^2+a'^2}}{c}\right)\right] \tag{4.21}$$

This equation consists two wave components; one placed at z/c on the time axis and the other at $(z^2+a'^2)^{1/2}/c$. By letting a' tend to infinity, the contribution of the second term, for applications with time limited signals, can be made negligible. The resulting wave would be a plane wave. This corresponds to dropping the second term in Eq.(4.20). Hence, the plane wave transfer function can be written as,

$$H_p(\underline{r},\omega) = \rho_0 c\, e^{-jkz} \tag{4.22}$$

Since this transfer function depend only on the distance of the observation point from the xy plane and not on the distance from the origin of the co-ordinate system the transfer function can simply be written as,

$$H_p(z,\omega) = \rho_0 c\, e^{-jkz}, \tag{4.23}$$

and called as plane wave transfer function. This is the first of the four transfer functions represent $H_{24}(\omega)$ mentioned in Chapter 3.

IMPULSE RESPONSE

The velocity to pressure impulse response is the inverse Fourier transform of the velocity to pressure transfer function in Eq.(4.23) and is given by,

$$h_p(z,t) = \rho_0 c\, \delta(t-z/c) \tag{4.24}$$

where δ is the Dirac delta function. The formula given in Eq.(3.2) is used to calculate the inverse Fourier transform.

4.2.1.2 NEAR-FIELD, POINT RECEIVER MODEL

The Fig(4.3) shows the sketch of a circular sound source of radius, a, placed in the xy plane, whose centre coincides with the origin of the co-ordinate system. An infinitesimal point receiver is placed on the axis of the source. The expression for pressure for this model, as will be shown, turns out to be very simple and compact. The forming of pulses can be explained easily and may be considered as base to understand the pulse forming in the models explained in later sections.

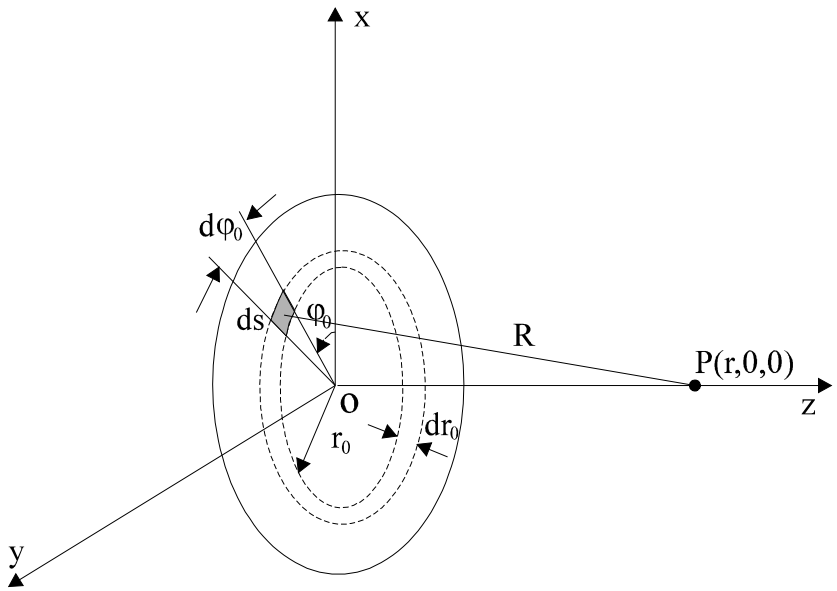

Figure(4.3) A circular plane sound source lies on the xy plane being its centre coincide with the origin of the co-ordinate system. An infinitesimal point receiver is placed on the axis of sound source. R is the distance between the observation point and the elemental area, ds.

TRANSFER FUNCTION

The spatial transfer function for this arrangement, $G_n(r,\omega)$, is readily found using Eq.(4.10). The points on the piston are denoted with a subscript, 0. From the geometry,

$$ds = r_0 dr_0 d\varphi_0 \tag{4.25}$$

Since the observation point always lies on the axis, r is simply replaced by the axial distance z, $r \equiv z$.

Since

$$R = \sqrt{z^2 + r_0^2} \tag{4.26}$$

$$G_n(z,\omega) = \frac{1}{2\pi}\int_0^{2\pi}\int_0^{a} \frac{e^{-jk\sqrt{z^2+r_0^2}}}{\sqrt{z^2+r_0^2}} r_0 dr_0 d\varphi_0 \tag{4.27}$$

The above integration is similar to that in the Eq.(4.17), and can be written as,

$$G_n(z,\omega) = \frac{1}{jk}\left[e^{-jkz} - e^{-jk\sqrt{z^2+a^2}}\right]. \tag{4.28}$$

Then the velocity to pressure transfer function, $H_n(z,\omega)$, using Eq.(4.13), can be written as,

$$H_n(z,\omega) = \rho_0 c\left[e^{-jkz} - e^{-jk\sqrt{z^2+a^2}}\right], \tag{4.29}$$

and called as near-field point receiver transfer function. This is the second of the four transfer functions represent $H_{24}(\omega)$ mentioned in Chapter 3.

IMPULSE RESPONSE

Taking inverse Fourier transform for the Eq.(4.25), gives the impulse response of this model as,

$$h_n(z,t) = \rho_0 c\left[\delta\left(t - \frac{z}{c}\right) - \delta\left(t - \frac{\sqrt{z^2+a^2}}{c}\right)\right] \tag{4.30a}$$

or

$$h_n(z,t) = \rho_0 c[\delta(t - t_z) - \delta(t - t_{za})] \tag{4.30b}$$

where $\delta(.)$ is the Dirac delta function, $t_z = \frac{z}{c}$, $t_{za} = \frac{\sqrt{z^2+a^2}}{c}$ and $h_n(z,t)$ is the velocity to pressure impulse response for this model. The meanings of the above times will be explained under the discussion of impulse responses in Sec.(4.2.3).

4.2.1.3 FAR-FIELD MODEL

This is an often used model for the situations where the measurements are made at distances very much larger compared to the dimension of the source. The Fig(4.4) shows the geometry of a circular sound source of radius, a, being placed on the xy plane, with its centre coincide with the origin of the co-ordinate system. An observation point, P, is at (r,θ,φ), in the spherical polar co-ordinate system.

TRANSFER FUNCTION

The spatial transfer function, $G_f(\omega)$, for this model is found, as for the previous models, using Eq.(4.10), as,

$$G_f(\underline{r},\omega) = \frac{1}{2\pi}\int_0^{2\pi}\int_0^{a} \frac{e^{-jkR}}{R} r_0 dr_0 d\varphi_0 . \tag{4.31}$$

For observation points lies at large distance compare to the dimension of the source, the following approximations[25] can be made.

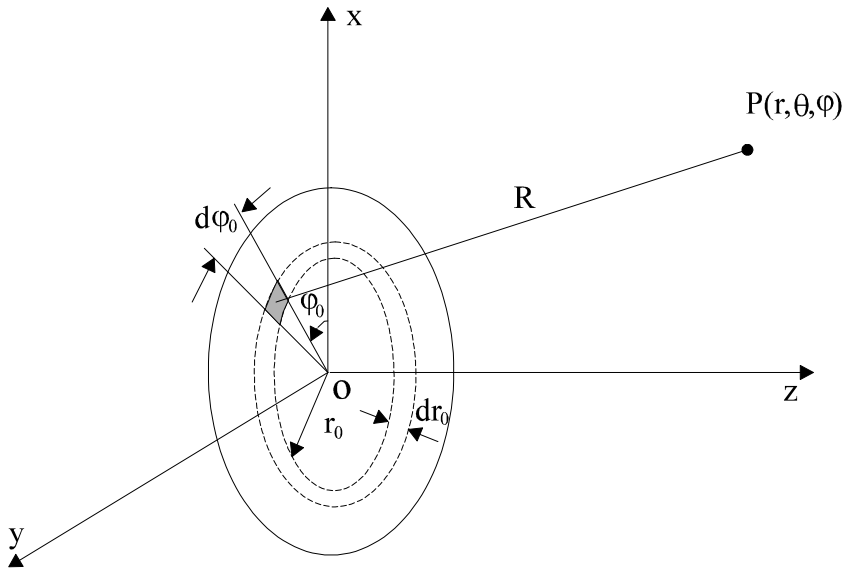

Figure(4.4) A circular sound source is placed in the xy plane being its centre coincide with the origin of the co-ordinate system. Observation point, P, is at (r,θ,φ), in the spherical polar co-ordinate system. R is the distance between the observation point and the shaded elemental area on the sound source.

$$\frac{1}{R} \approx \frac{1}{r} \tag{4.32}$$

and

$$R \approx r - r_0 \cos\varphi_0 \sin\theta \tag{4.33}$$

This approximation implies that the equidistant points on the source from the observation point are on straight lines instead of an arc length. Stepanishen has mentioned about this approximation in (page 1632 of Ref.(24)).

then

$$G_f(\underline{r},\omega) = \frac{1}{2\pi r}\int_0^{2\pi}\int_0^{a} e^{-jk(r - r_0\cos\varphi_0\sin\theta)} r_0 dr_0 d\varphi_0 \tag{4.34a}$$

or

$$G_f(\underline{r},\omega) = \frac{1}{2\pi r} e^{-jkr}\pi a^2 \frac{2J_1(ka\sin\theta)}{(ka\sin\theta)} \tag{4.34b}$$

The Eq.(4.34b) can be found elsewhere[47]. The velocity to pressure transfer function, $H_f(\underline{r},\omega)$, will then be,

$$H_f(\underline{r},\omega) = j\rho_0\omega\ e^{-jkr}\frac{a^2}{2r}\ \frac{2J_1(ka\sin\theta)}{(ka\sin\theta)}. \tag{4.35}$$

For an observation point on the axis, $\theta = 0$,

$$H_{fa}(\underline{r},\omega) = j\rho_0\omega\ e^{-jkr}\frac{a^2}{2r}. \tag{4.36}$$

The above expression for $H_{fa}(\underline{r},\omega)$ is the velocity to pressure transfer function for observation points on the axis in the far-field. As only the on axis response is considered in this discussion, the above transfer function will be denoted hereafter in this text simply as,

$$H_f(z,\omega) = j\rho_0\omega\ e^{-jkz}\frac{a^2}{2z} \tag{4.37}$$

and called as far-field transfer function, where z is the axial distance from the centre of the source. This is the third of the four transfer functions represent $H_{24}(\omega)$ mentioned in Chapter 3.

IMPULSE RESPONSE

The impulse response, as in the previous cases, is found by taking the inverse Fourier transform of the far-field transfer function, $H_f(z,\omega)$ in (4.37),as,

$$h_f(z,t) = \rho_0\frac{a^2}{2z}\delta'\left(t-\frac{z}{c}\right), \tag{4.38}$$

where

δ' is the time derivative of the Dirac delta function

4.2.2 NEAR-FIELD, FINITE RECEIVER MODEL

In the previous models the receiving probes were treated as of point dimension. In this model the receiving probe is an imaginary coaxial circular surface of same dimension as the source in front it.

TRANSFER FUNCTION

The average velocity potential on such a circular surface as mentioned above, for a continuous sinusoidal velocity of the source, was found by Williams[6] as,

$$\langle \phi(z,t) \rangle = \frac{U_0 e^{j\omega t}}{jk} \left[e^{-jkz} - \frac{4}{\pi} \int_0^{\pi/2} e^{-jk(z^2+4a^2\cos^2\theta)^{\frac{1}{2}}} \sin^2\theta d\theta \right] \tag{4.39}$$

where $k = \frac{\omega}{c}$. Later this expression was used by Khimunin[7] to find the diffraction correction for the same system.

The average pressure corresponds to the average velocity potential in Eq.(4.39), using the Eq.(4.3) is given by,

$$\langle p(z,t) \rangle = U_0 e^{j\omega t} \rho_0 c \left[e^{-j\frac{\omega}{c}z} - \frac{4}{\pi} \int_0^{\pi/2} e^{-j\frac{\omega}{c}(z^2+4a^2\cos^2\theta)^{\frac{1}{2}}} \sin^2\theta d\theta \right] \tag{4.40a}$$

or

$$\langle p(z,t) \rangle = U_0 e^{j\omega t} H(z,\omega) \tag{4.40b}$$

where

$$H(z,\omega) = \rho_0 c \left[e^{-j\frac{\omega}{c}z} - \frac{4}{\pi} \int_0^{\pi/2} e^{-j\frac{\omega}{c}(z^2+4a^2\cos^2\theta)^{\frac{1}{2}}} \sin^2\theta d\theta \right]. \tag{4.40c}$$

Assuming the system to be linear, as done in Sec.(4.2.1), the expression for pressure, $\langle p(z,t) \rangle$, in Eq.(4.40b) can be extended to a more general velocity function, u(t). Calling $H(z,\omega)$ the near-field finite receiver transfer function and denoting as $H_{nf}(z,\omega)$, the expression for the average pressure will be,

$$\langle P(z,\omega) \rangle = U(\omega)\, H_{nf}(z,\omega), \tag{4.41a}$$

where $\langle P(z,\omega) \rangle$ and $U(\omega)$ are the Fourier transforms of $\langle p(z,t) \rangle$ and u(t) respectively and

$$H_{nf}(z,\omega) = \rho_0 c \left[e^{-j\frac{\omega}{c}z} - \frac{4}{\pi} \int_0^{\pi/2} e^{-j\frac{\omega}{c}(z^2+4a^2\cos^2\theta)^{\frac{1}{2}}} \sin^2\theta d\theta \right]. \tag{4.41b}$$

This is the forth of the four transfer functions represent $H_{24}(\omega)$ mentioned in Chapter 3.

IMPULSE RESPONSE

The velocity to average pressure impulse response for this model is given by Eq.(4.42a) or Eq(4.42b). The impulse response of the same type of model was first found by Rhyne[23], by pure time domain consideration, from Stepanishen's[24] impulse response results for point receiver model. In this work the impulse response is found by taking the inverse Fourier transform of the velocity to average pressure transfer function, $H_{nf}(z,\omega)$, in Eq.(4.41b). A detailed derivation of the impulse response from the transfer function is given in Appendix(A-1).

$$h_{nf}(z,t)=\begin{cases}0 & t<t_z\\ \rho_0 c\left[\delta(t-t_z)-\dfrac{c^2 t}{\pi a^2}\sqrt{\dfrac{4a^2-c^2t^2+z^2}{c^2t^2-z^2}}\right] & t_z\le t\le t_{4az}\\ 0 & t>t_{4az}\end{cases} \tag{4.42a}$$

where

$$t_z=\frac{z}{c} \qquad \text{and} \qquad t_{4az}=\frac{\sqrt{4a^2+z^2}}{c}$$

or

$$h_{nf}(z,t)=\begin{cases}0 & t<t_z\\ \rho_0 c\left[\delta(t-t_z)-\dfrac{c^2 t}{\pi a^2}\sqrt{\dfrac{t_{4az}^2-t^2}{t^2-t_z^2}}\right] & t_z\le t\le t_{4az}\\ 0 & t>t_{4az}\end{cases}. \tag{4.42b}$$

The times t_z and t_{4az} can be considered just as abbreviations for the moment and the meanings of these times will be cleared under the discussion of impulse responses in the next section. The results given in Eq.(4.42b), differs from that of Rhyne's by the factor of $\rho_0 c$ as he calculated the force to force impulse response. This can be explained as follows. Since $h_{nf}(z,t)$ in Eq.(4.42b) is the velocity to average pressure impulse response, $\pi a^2 h_{nf}(z,t)$ is the velocity to force impulse response, where, πa^2 is the area of the receiver. Since[46] the force to velocity ratio at the transmitter is the impedance $Z = \pi a^2 \rho_0 c$, dividing the velocity to force impulse response by Z gives the force to force impulse response as $h_{nf}(z,t)/\rho_0 c$.

4.2.3 DISCUSSION

In the previous section, the transfer function and the impulse responses of the different models were calculated. In this section, transfer functions and the impulse responses are represented graphically and the behaviours of the functions are discussed.

TRANSFER FUNCTIONS

Figure(4.5) (a), (b) and (c) show the graphical representation of $H_n(z,\omega)$, $H_f(z,\omega)$ and $H_{nf}(z,\omega)$ respectively. The magnitude and the phase, for example, of the near-field transfer function are presented as $20\log|H_n(z,\omega)/H_p(z,\omega)|$ and $\angle(H_n(z,\omega)/H_p(z,\omega))$ respectively. Similar quantities are presented for other two transfer function too. All three plots are calculated for the same parameters; a = 4.5mm, z = 0.1m and c = 344.35m/s. A similar plot for the plane wave transfer function would be just straight lines though 0dB for magnitude and 0^o for phase.

The near-field, point receiver transfer function has strong oscillation with increasing frequency. This can easily be explained by simplifying the expression of its transfer function further as follows. Consider the near-field, point receiver transfer function in Eq.(4.29)

Using Euler's relation

$$e^{jkx} = \cos kx + j\sin kx \tag{4.43}$$

the Eq.(4.29) can be written as,

$$H_n(z,\omega) = 2\rho_0 c \sin\omega\left(\frac{t_{za}-t_z}{2}\right)e^{j\left(\frac{\pi}{2}-\omega\frac{t_{za}+t_z}{2}\right)} \tag{4.44}$$

The sine term in the above expression explains the oscillating behaviour of the magnitude of the transfer function shown in Fig.(4.5)(a). The amplitude response takes minimum and maximum values for frequencies equal to the even and odd harmonics of $1/(2[t_{za}-t_z])$ respectively. For the particular choice of parameters of the plot in Fig.(4.5)(a) maxima and minima occur at odd and even multiples of 1701.35kHz. respectively. The minima are exactly zero.

The phase of the transfer function can be written as,

$$\frac{\pi}{2} - \omega\left(\frac{t_{za}-t_z}{2}\right) - \omega t_z \tag{4.45}$$

and the phase relative to the plane wave, also shown in Fig.(4.5)(a) ,then will be,

$$\frac{\pi}{2} - \omega\left(\frac{t_{za}-t_z}{2}\right) \tag{4.46}$$

The above expression shows that the phase relative to plane wave decreases with increasing frequency. But, it changes from -90^0 to $+90^0$ at frequencies equal to the even multiples of $1/(2[t_{za}-t_z])$, as shown in Fig.(4.5)(a), because of the sine term in the expression for $H_n(z,\omega)$.

The magnitude of the far-field transfer function, shown in Fig(4.5)(b), is zero at zero frequency, which can be seen from its expression in Eq.(4.37), and increases monotonically with frequency. The phase is $(\pi/2 - \omega t_z)$. This shows that the phase of all frequency components of the input signal is advanced by $\pi/2$ relative to plane wave.

The magnitude of the near-field finite receiver transfer function, shown in Fig(4.5)(c), increases with frequency and reaches a limit at high frequencies. And it is zero at zero

frequency which can easily be shown by putting $\omega = 0$ in its expression in Eq.(4.41b). The phase of the transfer function relative to that of the plane wave decreases with frequency from 90 degrees and approaches zero at high frequencies.

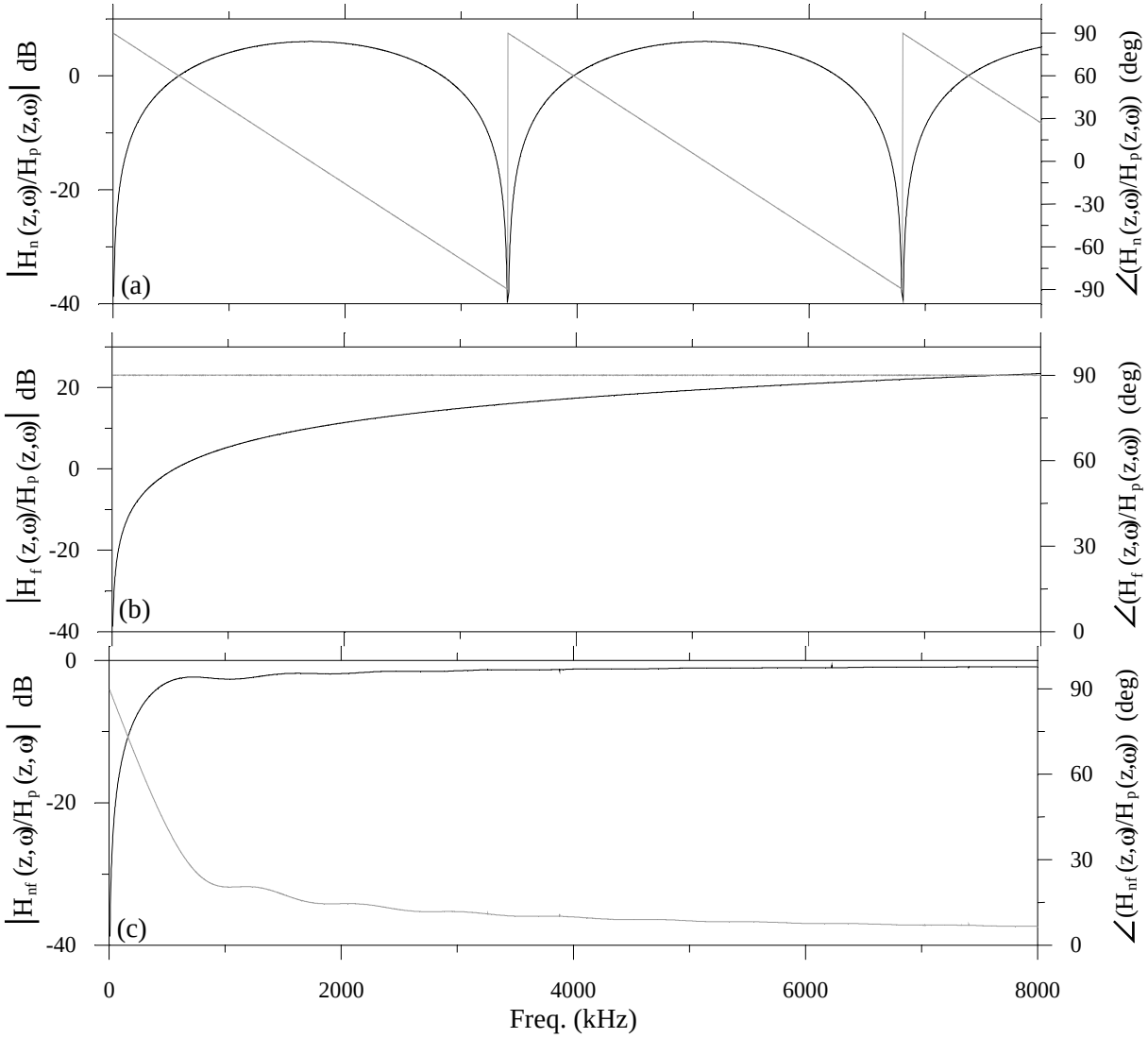

Figure(4.5) Transfer function. (a) near-field, point receiver, (b) far-field, (c) near-field finite receiver. Magnitude is normalised to the plane wave magnitude and phase is calculated relative to the plane wave phase. Calculations are made for z = 0.1m, a = 4.5mm, and c = 344.35m/s.

Change in the axial distance will not change the basic shape, except the amplitude, of the pressure wave according to the far-field model.

This can be easily shown considering two different axial distances as follows. If z_1 and z_2 are two axial distances, then,

$$H_f(z_1,\omega) = j\rho_0\omega\, e^{-jkz_1}\,\frac{a^2}{2z_1} \tag{4.47}$$

$$H_f(z_2,\omega) = j\rho_0\omega\, e^{-jkz_2}\,\frac{a^2}{2z_2} \tag{4.48}$$

or

$$H_f(z_2,\omega) = H_f(z_1,\omega)H_f(z_1,z_2,\omega), \tag{4.49}$$

where

$$H_f(z_1,z_2,\omega) = \frac{z_1}{z_2}e^{-j\frac{\omega}{c}(z_2-z_1)}. \tag{4.50}$$

Since the term responsible for the time delay, $(z_1 - z_2)$, of the signal in the above transfer function is independent of frequency, there is no phase distortion in the signal. And since the magnitude of the transfer function is also independent of frequency, the change in axial distance will not give any change to the basic shape of the signal. The term z_1/z_2 gives only an amplitude reduction, if $z_2>z_1$, to the signal.

IMPULSE RESPONSES

Fig.(4.6) (a), (b), (c) and (d) show the graphical representation of the impulse responses $h_p(z,t)$ in Eq.(4.24), $h_n(z,t)$ in Eq.(4.30b), $h_f(z,t)$ in Eq.(4.38) and $h_{nf}(z,t)$ in Eq.(4.42) respectively. The magnitude axis of the plots are normalised with $\rho_0 c$. Therefore the weights of the Dirac delta functions are 1. With the same normalisation, the weight of the time derivative of the Dirac delta function, $\delta'(\cdot)$, of the far-field model is $\frac{a^2}{2cz}$. Time axis of the plots are presented as $(t - t_z)$ where $t_z = z/c$. That is, the arrival time of the plane wave is made the time origin of the plots.

There are two delta functions in Fig.(4.6)(b). It is evident from the time of arrival, in Eq.(4.30b), that the first delta function is due to the direct plane wave and the second is due to the wave from the edge of the piston. This facts has been discussed also by some other authors[24,26]. According to Huygens principle, every point on the piston vibrator acts like an independent sound source. When the piston face is vibrating with an impulse velocity, disturbance from different point on the piston reach the receiver at different times. Obviously, the first arrival, $t_z(= z/c)$, corresponds to the centre of the piston, the nearest point to the receiver, and the last arrival, $t_{za}\left(=\sqrt{z^2+a^2}/c\right)$ corresponds to the points on the circumference of the piston, the farthest points to the receiver. After the time t_{za} and before t_z, there is no response. The duration of the impulse response is, therefore, $(t_{za}-t_z)$.

$$(t_{za} - t_z) = \frac{z}{c}\left[\sqrt{1+\frac{a^2}{z^2}} - 1\right] \tag{4.51}$$

It can be seen from the expressions for t_{za} and t_z that $t_{za} > t_z$. And, as z increases the difference between t_{za} and t_z becomes small and the delta functions in Fig.(4.6)(b) become close to each other. At large distances compared to the radius of the source, the impulse response approaches the far-field impulse response in Fig.(4.6)(c).

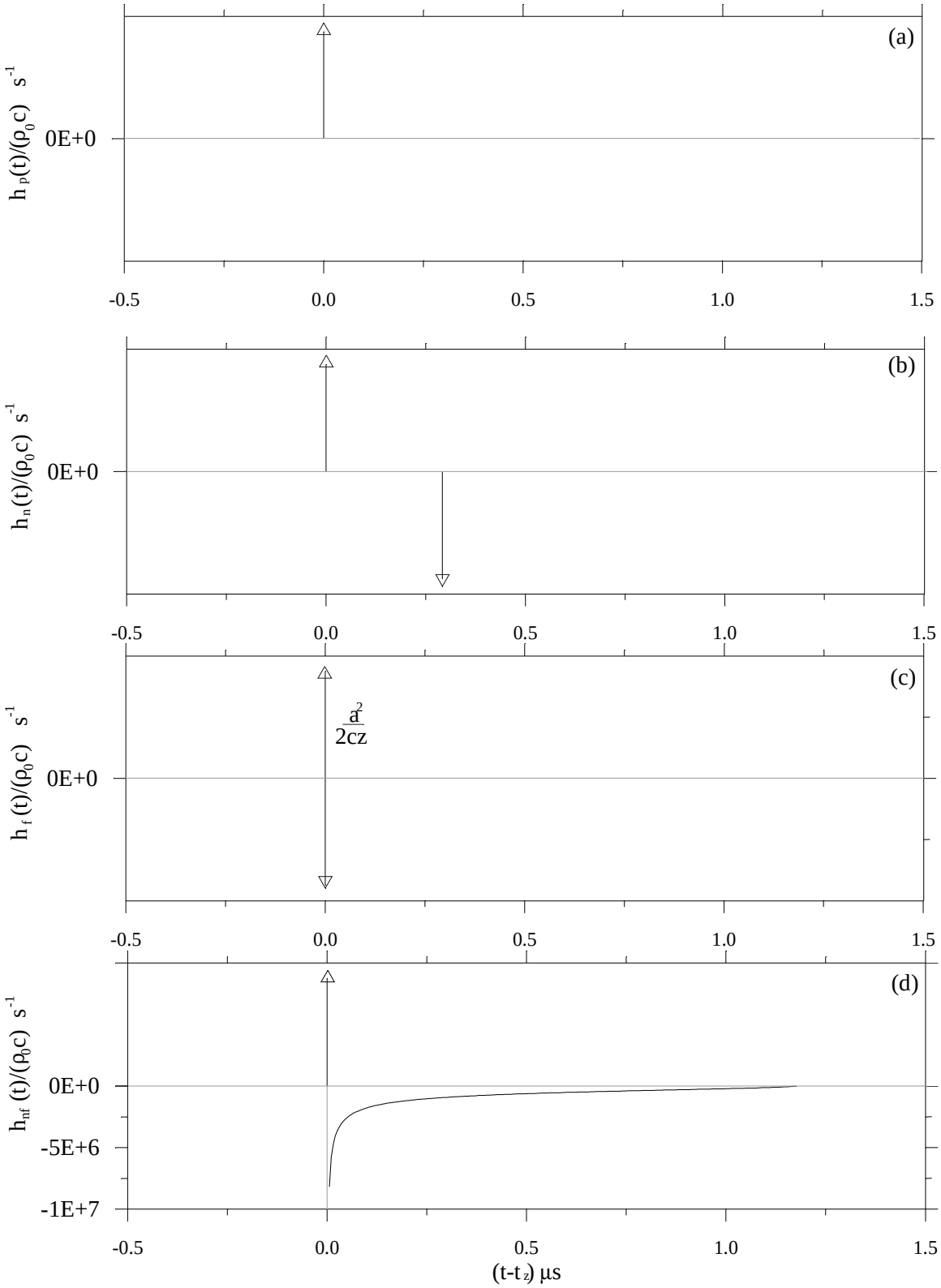

Figure(4.6) Impulse response. (a) Plane wave model, (b) Near-field point receiver model, (c) Far-field model and (d) Near-field finite receiver model. Magnitudes are normalised to the magnitude of the plane wave impulse response. The Dirac delta functions are indicated by arrows and the time derivative of the Dirac delta function is indicated by two opposite arrows. All the simulations are made for the following parameters; a = 4.5mm, z = .1m and c = 344.35m/s

The impulse response of the far-field model is the derivative of delta function. Therefore, the far-field model is a differentiating filter. The derivative of delta function is represented[40] by a pair of delta functions as in Fig.(4.6)(c). The impulse response of an ideal high pass filter can be represented[9] with a positive delta function and a negative sinc function. The width of the sinc function is $1/f_0$, where f_0 is the lower cut-off frequency of the ideal high pass filter. When the lower cut-off frequency of the filter increases, the width of the sinc function becomes narrower and approaches to a delta function, at high frequencies. This situation is comparable to the far-field model. But, the frequency response of the far-field model is zero at zero frequency. However, the impulse response reveals that the far-field model is a high pass filter. Rhyne[23] puts forward a similar argument to say that the near-field finite receiver model is also a high pass filter, as it contain a delta function and a negative singularity function which goes to zero with time, in its impulse response.

Fig.(4.6)(d) shows the impulse response of the near-field finite receiver model. With reasons similar to those given under the near-field point receiver case, the first arrival, t_z, corresponds to the communication between the points on the receiver and the points immediately in front of them on the piston source. The last arrival, $t_{4az}\left(=\sqrt{4a^2+z^2}/c\right)$, corresponds to the communication between the points on the circumference of the receiver and the points on the farthest edge on the piston source. There is no response before t_z and after t_{4az}. The duration of the impulse response is, then, $(t_{4az} - t_z)$.

$$(t_{4az} - t_z) = \frac{z}{c}\left[\sqrt{\frac{4a^2}{z^2}+1}-1\right] \tag{4.52}$$

Fig(4.7) shows the impulse response of the near-field finite receiver model for three different values of z.By taking t_z as time origin of the plot, all the impulse responses are made to start at the same place. All the impulse responses have delta functions at $t = t_z$. But, these delta functions are omitted here in the plot for simplicity. It is evident from the figure and from the expression for $(t_{4az} - t_z)$ that, as z increases the duration of the impulse response become shorter and approaches the far-field impulse response.

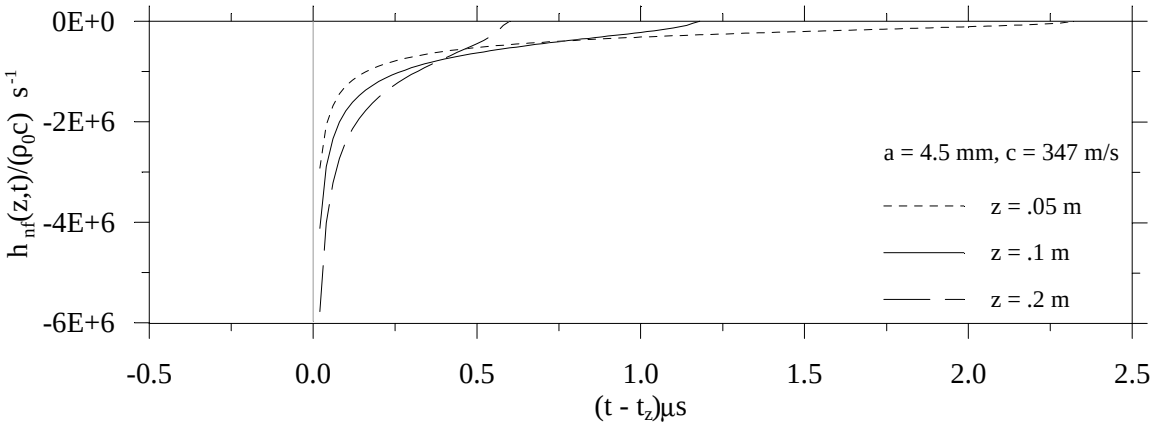

Figure(4.7) Impulse response, $h_{nf}(z,t)$, for three different distances, 0.05 m, 0.1 m and 0.2 m. In all cases a = 4.5 mm, c = 347m/s. The delta functions of all plots are omitted for simplicity.

4.3 CALCULATIONS

In the previous sections velocity to pressure transfer functions of the four models and their corresponding impulse responses were found and their behaviours were discussed. In this section using the impulse responses and the transfer functions the pressure will be calculated. This pressure is same as the free field pressure, denoted as p_4, in the system model in Chapter3. A sinusoidal burst with three cycles and a sinusoidal continuous wave are used as the velocity signals for illustration. And the pressure wave form for the sinusoidal bursts are discussed. But, the velocity signal will not be a sinusoidal burst in a system like that addressed in Chapter 3. However, similar pressure signals, as mentioned above, for a more realistic velocity input are presented in Chapter 6.

The pressure wave forms, for each model, are calculated by convolving the velocity wave form with the respective impulse responses of the propagation models. Calculation of the pressure signal for the first three models, for this particular velocity wave, is quiet easy. But for the near-field, finite receiver model the problem has not been solved so far analytically. Therefore the calculation of the convolution integral is done numerically. The procedure for the calculation is given in Appendix(A-2). The program code is given in Appendix(B-1).

The following signals are used as input signals in the calculations.

1. Continuous wave : $u_C(t) = U_0 \sin\omega_0 t$,

2. Pulsed sine wave : $u(t) = U_0\left[\mathbf{U}(t) - \mathbf{U}(t-T')\right]\sin\omega_0 t$, where $\mathbf{U}$ is the unit step function, $T' = 3T$ and T is the period of the input signal. The following abbreviations,

$$t_z = \frac{z}{c}, \qquad t_{za} = \frac{(z^2 + a^2)^{\frac{1}{2}}}{c} \qquad \text{and} \qquad t_{4az} = \frac{(4a^2 + z^2)^{\frac{1}{2}}}{c}, \tag{4.53}$$

the meanings of which has already been discussed in the previous section, will be used.

4.3.1 PLANE WAVE MODEL

The pressure pulse due to this model is well-known and can be found in any text book on waves. However, in order to make the discussion easier, the pressure pulses are presented here and their characteristics are discussed. The results will be used in the coming sections. The pressure, $p_p(t)$, at a distance, z, from the source can be calculated as follows,

$$p_p(z,t) = u(t) \otimes h_p(z,t) \tag{4.54}$$

where u(t) is the velocity function given in the beginning of this section and $h_p(z,t)$ is the plane wave impulse response found in Eq.(4.24).

$$p_p(z,t) = \int_{-\infty}^{\infty} U_0\left[\mathbf{U}(t-\tau) - \mathbf{U}(t-\tau-T')\right]\sin\omega_0(t-\tau)\rho_0 c\,\delta(\tau - t_z)\,d\tau \tag{4.55}$$

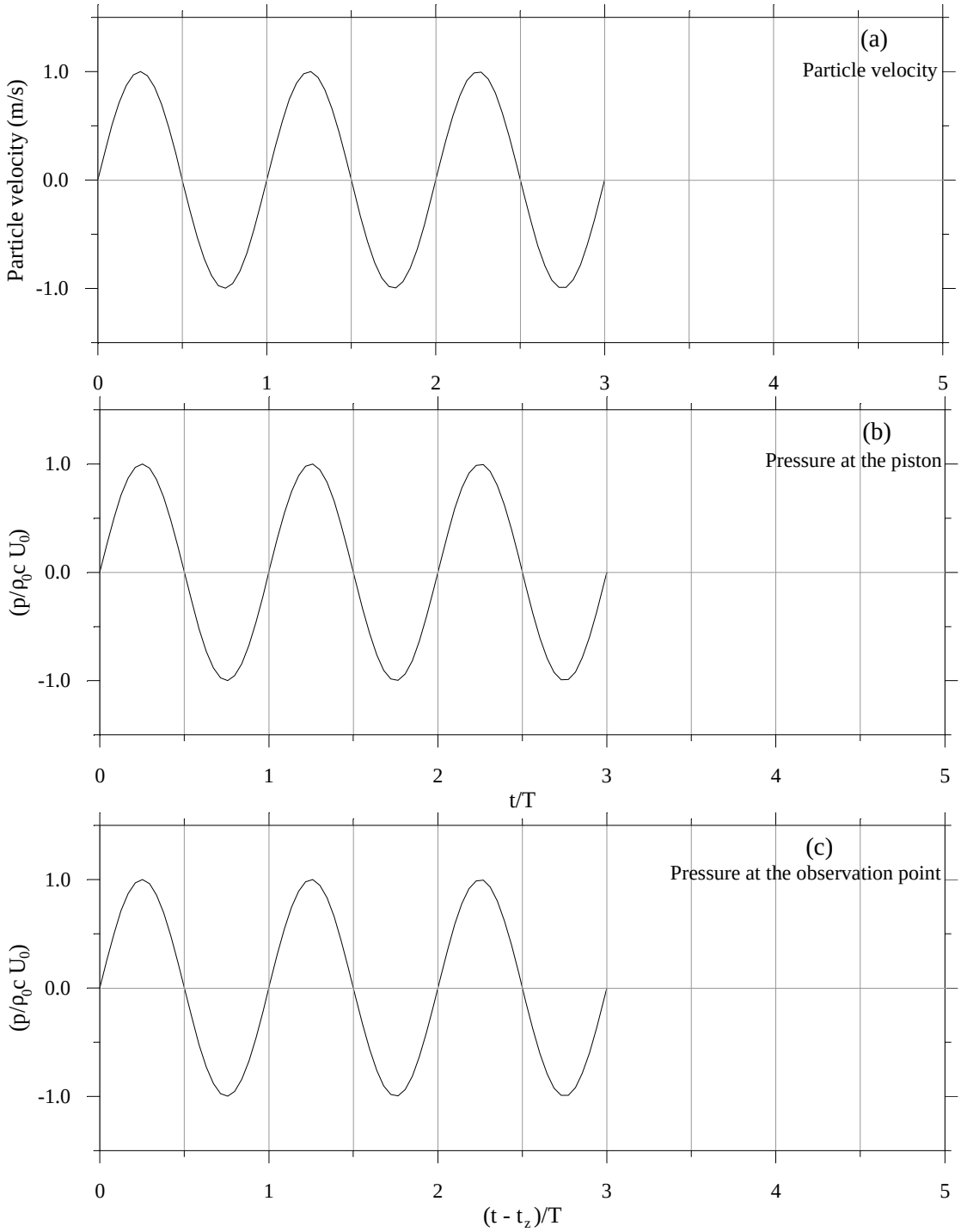

Figure(4.8) The wave forms of particle velocity and normalised pressure for the plane wave model. The time axis of all figures are normalised to the period of the input signal. The arrival time of the pulse is made the time origin. (a) Particle velocity of the face of the transducer (b) Pressure wave at the piston face (c) pressure wave at an observation point.

using sifting property[41] of the Dirac delta function, the above expression can be written as,

$$p_p(z,t) = \rho_0 c U_0 \left[\mathbf{U}(t-t_z) - \mathbf{U}(t-T'-t_z) \right] \sin \omega_0 (t-t_z) \tag{4.56}$$

The particle velocity at the piston face, the pressure at the piston face and the pressure at an arbitrary observation point are shown in Fig.(4.8). The time axis of the plots are normalised to the period of the velocity signal. By subtracting the arrival time of the pulse from the absolute time, the arrival time is made as the time origin of the plot in Fig.(4.8)(c). It is clear from the expression for pressure, $p_p(z,t)$ and from Fig.(4.8)(b)&(c), that the pressure wave is only shifted in time and has not changed its form due to propagation. This simple wave is used as a reference to compare the wave forms predicted by the other models in the coming sections. It can be seen from Fig.(4.8)(c) that the zeros of the signal coincides with the period and half period #s of the time axis. This fact is used in the coming sections. For example, it may not be possible to accommodate the plane wave and the pressure wave due to the other models in one plot, because of the large difference in the relative size of the two waves, but, still the period and half period #s of the time axis denote the plane wave zero crossings. This is not true for an input signal other than a sinusoidal burst, but, still one can have a plane wave.

4.3.2 NEAR-FIELD, POINT RECEIVER MODEL

CONTINUOUS WAVE

Pressure at a distance, z, for a continuous excitation, $u_C(t)$ is found as,

$$p_{nC}(z,t) = u_C(t) \otimes h_n(z,t) \tag{4.57}$$

where $h_n(z,t)$ is the impulse response of this model found in Eq.(430b).

$$p_{nC}(z,t) = \int_{-\infty}^{\infty} U_0 \sin \omega_0 (t-\tau) \rho_0 c \left[\delta(\tau - t_z) - \delta(\tau - t_{za}) \right] d\tau \tag{4.58}$$

Using sifting property of the Dirac delta function, the above expression can be written as,

$$p_{nC}(z,t) = \rho_0 c U_0 \left(\sin \omega_0 (t-t_z) - \sin \omega_0 (t-t_{za}) \right) \tag{4.59}$$

$$p_{nC}(z,t) = 2\rho_0 c U_0 \sin \omega_0 \left(\frac{t_{za} - t_z}{2} \right) \cos \omega_0 \left(t - \frac{t_z + t_{za}}{2} \right) \tag{4.60}$$

PULSED SINE WAVE

For the sinusoidal burst, u(t), the pressure at a distance, z, from the source is given by,

$$p_n(z,t) = u(t) \otimes h_n(z,t) \tag{4.61}$$

$$\begin{aligned} p_n(z,t) = \int_{-\infty}^{\infty} U_0 \left[\mathbf{U}(t-\tau) - \mathbf{U}(t-\tau-T') \right] \sin \omega_0 (t-\tau) \\ \bullet \rho_0 c \left[\delta(\tau - t_z) - \delta(\tau - t_{za}) \right] d\tau \end{aligned} \tag{4.62}$$

Using sifting property of the Dirac delta function, the integration is simplified as follows.

$$p_n(z,t) = \rho_0 c U_0 \left[\mathbf{U}(t-t_z) - \mathbf{U}(t-t_z-T') \right] \sin \omega_0 (t-t_z) \tag{4.63}$$

$$-\left[\mathbf{U}(t-t_{za}) - \mathbf{U}(t-t_{za}-T') \right] \sin \omega_0 (t-t_{za})$$

The pressure, $p_n(z,t)$, is the resultant of two sinusoidal bursts. The first one is the direct plane wave, and the other is the negative of its replica arrived with the delay, t_{za}. The resultant can be written, if $T' > (t_{za} - t_z)$, as,

$$p_n(z,t) = \begin{cases} 0 & 0 \le t \le t_z \\ \rho_0 c U_0 \sin \omega_0 (t - t_z) & t_z \le t \le t_{za} \\ 2\rho_0 c U_0 \sin \omega_0 \left(\frac{t_{za} - t_z}{2} \right) \cos \omega_0 \left(t - \frac{t_z + t_{za}}{2} \right) & t_{za} \le t \le t_z + T' \\ -\rho_0 c U_0 \sin \omega_0 (t - t_{za}) & t_z + T' \le t \le t_{za} + T' \\ 0 & t_{za} + T' \le t \le \infty \end{cases} \tag{4.64}$$

In the above expression, one can notice that the second and the fourth terms last for the same time duration, $(t_{za}-t_z)$, and this time is equal to the time duration of the impulse response, discussed under the subheading, "impulse responses", in Sec.(4.2.3). And the middle term can be recognised as a continuous wave expression. That is, the expression is the same as that of the pressure for continuous velocity signal, $u_C(t)$, found in Eq.(4.60). As shown in Fig.(4.9), the signal passes a transient region and reaches steady state and then again through a transient region decays to zero.

If $T' < (t_{za} - t_z)$ then,

$$p_n(z,t) = \begin{cases} 0 & 0 \le t \le t_z \\ \rho_0 c U_0 \sin \omega_0 (t - t_z) & t_z \le t \le t_z + T' \\ 0 & t_z + T' \le t \le t_{za} \\ -\rho_0 c U_0 \sin \omega_0 (t - t_{za}) & t_{za} \le t \le t_{za} + T' \\ 0 & t_{za} + T' \le t \le \infty \end{cases} \tag{4.65}$$

Since the time interval between the start of the two signals are longer than the duration of the

signals or in other words the duration of the impulse response is longer than the duration of the input signal, they do not interfere with each other and remain separated.

Since the impulse response, $h_n(z,t) = 0$, for $t < t_z$, by inspecting the convolution integral[9], one can say that the signal starts at $t = t_z$.

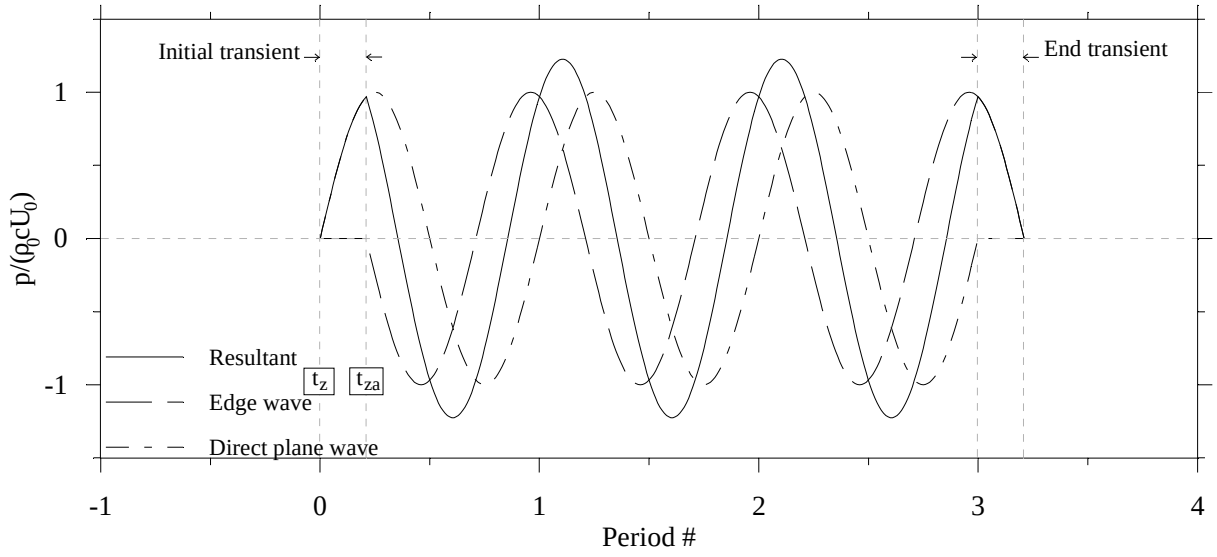

Figure(4.9) Axial response of near-field point receiver model for the case $T' > t_{za} - t_z$. Transient regions of the pulse are indicated by dotted lines parallel to the amplitude axis. The amplitudes are normalised to the plane wave amplitude. The time axis is normalised to the period of the velocity signal. The simulation was made for the following parameters; z = 55mm, a = 6.5mm, f = 200kHz and c = 344.35m/s.

The pressure $p_n(z,t)$ found in Eq.(4.64) can be written in a different form as,

$$p_n(z,t) = \begin{cases} 0 & 0 \le t \le t_z \\ \rho_0 c U_0 \sin\omega_0(t-t_z) & t_z \le t \le t_{za} \\ 2\rho_0 c U_0 \sin\omega_0\left(\frac{t_{za}-t_z}{2}\right)\sin\left(\omega_0(t-t_z)+\frac{\pi}{2}-\omega_0\frac{t_{za}-t_z}{2}\right) & t_{za} \le t \le t_z + T' \\ -\rho_0 c U_0 \sin\omega_0(t-t_{za}) & t_z + T' \le t \le t_{za} + T' \\ 0 & t_{za} + T' \le t \le \infty \end{cases} \tag{4.66}$$

Consider the third term of the expression, in Eq.(4.66). As pointed out earlier, this is the continuous part of the signal. With this expression, some important and, of course, known results, for continuous excitation, can be deduced. Let,

$$\Theta = \left(\omega_0 \frac{t_{za}-t_z}{2}\right). \tag{4.67}$$

In the following discussion the observation point moves towards the source from infinity. At infinity, with Eq.(4.51), $\Theta \approx 0$. Then from the expression in Eq.(4.66), since $\omega_0(t - t_z)$ is the phase of the plane wave, the continuous part of the signal leads the plane wave by $\pi/2$. As the observation point moves towards the source Θ increases. If Θ can be written as $N\pi/2$, where N = 1,2...,then for odd values of N the continuous part of the signal is in phase with the plane wave and the amplitude is double that of the plane wave and for even values of N the continuous part of the signal becomes zero. For example, for N = 1, substituting $\Theta = \pi/2$ in Eq.(4.66) gives the continuous part of $p_n(z,t) = 2\rho_0 c U_0 \sin(\omega_0(t-t_z))$, and for N = 2, substituting $\Theta = \pi$ in the Eq.(4.66) makes the continuous part of $p_n(z,t)$ zero and so on. This is a well-

known result[1]. That is, as the observation point moves towards the source on the axis from an infinite distance the pressure, for a continuous excitation of the piston, reaches its maximum at $\Theta = \pi/2$ and then alternates its value between $2\rho_0 cU_0$ and zero. And also the pressure waves lags the plane wave when the observation point moves from a pressure maximum to a pressure minimum and leads when the observation point moves from a pressure minimum to a pressure maximum. Consider, for example, the observation point, as it moves towards the source, at which the pressure lies between the first maximum and first minimum. Substituting for Θ, which is $\pi/2 < \Theta < \pi$, in the continuous part of $p_n(z,t)$ gives,

$$2\rho_0 cU_0 \sin\omega_0\left(\frac{t_{za}-t_z}{2}\right)\sin\left(\omega_0(t-t_z)-\varphi\right), \tag{4.68}$$

where

$$\varphi = \Theta - \frac{\pi}{2} \tag{4.70}$$

This shows that the continuous part of the wave lags the plane wave. Similarly, for the placement of the observation point between the first minimum and the second maximum, it can be shown that the pressure wave leads the plane wave as follows. Since $\pi < \Theta < 3\pi/2$ for this case, substituting $\Theta = (\pi+\alpha)$, where $\alpha < \pi/2$, in the expression for the continuous part of $p_n(z,t)$ gives,

$$2\rho_0 cU_0 \sin(\pi+\alpha)\sin[\omega_0(t-t_z) + \pi/2-(\pi+\alpha)] \tag{4.71}$$

and this can be written as,

$$2\rho_0 cU_0 \sin\alpha \sin[\omega_0(t-t_z) + (\pi/2-\alpha)] \tag{4.72}$$

This shows that the continuous part of the signal leads the plane wave.

The phase of the continuous part of the pressure wave relative to the plane wave,$(\pi/2-\Theta)$, is also found earlier from the transfer function in Eq.(4.44). This can be expressed in terms of the parameters, known as seki parameters, S and ka, where $S = z/(a^2/\lambda)$, $k = 2\pi/\lambda$ and λ is the wave length of the input signal. Substituting for t_{za} and t_z in Eq(4.67) from Eq.(4.53) and with some manipulations one can easily show the above mentioned phase relationship is given by the following formula,

$$\frac{\pi}{2} - \Theta = \frac{\pi}{2} - \frac{(ka)}{2}\left[\sqrt{S^2\frac{(ka)^2}{4\pi^2}+1} - S\frac{(ka)}{2\pi}\right] \tag{4.73}$$

The amplitude of the signal relative to the plane wave can easily be found simply by dividing the amplitude by the plane wave amplitude, $\rho_0 cU_0$. And this relative amplitude, $2\sin\Theta$, can be written in terms of S and (ka) as,

$$2\sin\left(\frac{(ka)}{2}\left[\sqrt{S^2\frac{(ka)^2}{4\pi^2}+1} - S\frac{(ka)}{2\pi}\right]\right). \tag{4.74}$$

These are the plane wave diffraction correction factors for phase and amplitude, when a measurement is made on the axis of a piston type sound source, with a receiver which can be considered as a point.

4.3.3 FAR-FIELD MODEL

CONTINUOUS WAVE

The pressure at a distance, z, from the source for the continuous excitation, $u_C(t)$ is ,as in the previous cases, given by,

$$p_{fC}(z,t) = u_C(t) \otimes h_f(z,t) \tag{4.75}$$

$$p_{fC}(z,t) = \int_{-\infty}^{\infty} U_0 \sin\omega_0(t-\tau)\rho_0 \frac{a^2}{2z}\delta'(\tau - t_z)d\tau \tag{4.76}$$

where

δ' is the time derivative of the Dirac delta function.

using sifting property of the Dirac delta function,

$$p_{fC}(z,t) = \rho_0\omega_0 \frac{a^2}{2z} U_0 \cos\omega_0(t-t_z) \tag{4.77}$$

PULSED SINE WAVE

The pressure at a distance, z, from the source for u(t) as the input is given by,

$$p_f(z,t) = u(t) \otimes h_f(z,t) \tag{4.78}$$

$$p_f(z,t) = \int_{-\infty}^{\infty} U_0\left[\mathbf{U}(t-\tau) - \mathbf{U}(t-\tau-T')\right]\sin\omega_0(t-\tau)\rho_0 \frac{a^2}{2z}\delta'(\tau - t_z)d\tau \tag{4.79}$$

using sifting property of the Dirac delta function, gives,

$$p_f(z,t) = \rho_0\omega_0 \frac{a^2}{2z} U_0 \left[\mathbf{U}(t-t_z) - \mathbf{U}(t-t_z-T')\right]\cos\omega_0(t-t_z) \tag{4.80}$$

This equation can also be written as,

$$p_f(z,t) = \rho_0\omega_0 \frac{a^2}{2z} U_0\left[\mathbf{U}(t-t_z) - \mathbf{U}(t-t_z-T')\right]\sin\left(\omega_0(t-t_z) + \frac{\pi}{2}\right) \tag{4.81}$$

The above expression shows that the pressure, $p_f(z,t)$, has $\pi/2$ phase lead over the plane wave. Fig(4.10) shows the plot of the amplitude normalised version of the Eq.(4.80) and the plane wave. Since $h_f(z,t) = 0$ for $t < t_z$, the signal starts at $t = t_z$. And, since the impulse response is momentary, there is no transient region in the signal. The signal reaches its steady state immediately after it started and after 3 periods suddenly decays to zero. As a consequence, the length of the output pressure wave is equal to the input velocity wave.

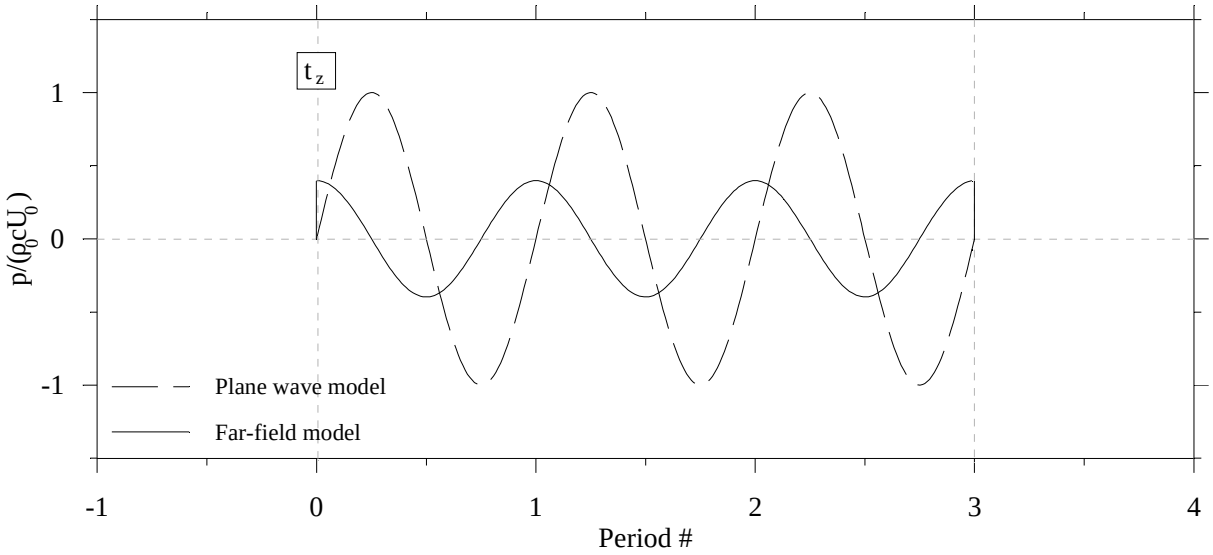

Figure(4.10) Axial response of the far-field model. The amplitude is normalised to the amplitude of the plane wave. The time axis is normalised to the period of the velocity signal. The simulation is made for the following parameters. z = .1m, a = 4.5mm, f = 215kHz c = 344.35m/s.

The amplitude of the pressure relative to the plane can easily be found by dividing the magnitude of $p_f(z,t)$ by the plane wave amplitude, $\rho_0 c U_0$. And this relative amplitude can be written simply as π/S, where $S = a^2/\lambda$.

4.3.4 NEAR-FIELD, FINITE RECEIVER MODEL

CONTINUOUS WAVE

In this model, as described in sec.(4.2.2), the pressure is averaged over an imaginary circular area, coaxially placed on the axis of the source. But, though it is an average pressure, in the following discussion, it is simply called as pressure and denoted for a continuous excitation as $p_{nfC}(z,t)$ and for a burst as $p_{nf}(z,t)$.

The pressure, p_{nfC} ,at a distance, z, from the source for a continuous excitation, $u_C(t)$, is given by,

$$p_{nfC}(z,t) = u_C(t) \otimes h_{nf}(z,t) \tag{4.82}$$

$$= u_C(t) \otimes (h_{1nf}(z,t) + h_{2nf}(z,t)) \tag{4.83}$$

where

$$h_{1nf}(z,t) = \rho_0 c\delta(t-t_z), \tag{4.84}$$

$$h_{2nf}(z,t) = -\frac{\rho_0 c^3 t}{\pi a^2}\left[\sqrt{\frac{t_{4az}^2 - t^2}{t^2 - t_z^2}}\right] \quad t_z < t \le t_{4az} \tag{4.85}$$

$$p_{nfC}(z,t) = \int_{-\infty}^{\infty} U_0 \sin\omega_0(t-\tau)(h_{1nf}(z,\tau) + h_{2nf}(z,\tau))d\tau \tag{4.86}$$

using the sifting property of Dirac delta function and since $h_{2nf}(z,t)$ has values only between t_z and t_{4za}, the above integration can be written as,

$$p_{nfC}(z,t) = \rho_0 c U_0 \sin\omega_0(t-t_z) + \int_{t_z}^{t_{4az}} U_0 \sin\omega_0(t-\tau)h_{2nf}(z,\tau)d\tau \tag{4.87}$$

PULSED SINE WAVE

The pressure at a distance, z, from the source for u(t) as an input is,

$$p_{nf}(z,t) = u(t) \otimes h_{nf}(z,t) \tag{4.88}$$

$$p_{nf}(z,t) = \int_{-\infty}^{\infty} U_0[\mathbf{U}(t-\tau) - \mathbf{U}(t-\tau-T')]\sin\omega_0(t-\tau)h_{nf}(z,t)d\tau \tag{4.89}$$

Using sifting property of the Dirac delta function, Eq.(4.89) can be written as,

$$\begin{aligned} p_{nf}(z,t) = {} & U_0\rho_0 c[\mathbf{U}(t-t_z) - \mathbf{U}(t-t_z-T')]\sin\omega_0(t-t_z) \\ & + U_0\int_{-\infty}^{\infty}[\mathbf{U}(t-\tau) - \mathbf{U}(t-\tau-T')]\sin\omega_0(t-\tau)h_{2nf}(z,\tau)d\tau \end{aligned} \tag{4.90}$$

For an input signal with length, $T' > (t_{4za}-t_z)$, the above expression can be written, remembering $h_{2nf}(z,t)$ has values only between t_z and t_{4za}, as,

$$p_{nf}(z,t) = \begin{cases} 0 & 0 \le t \le t_z \\ \rho_0 c U_0 \sin\omega_0(t-t_z) + \int_{t_z}^{t} \sin\omega_0(t-\tau) h_{2nf}(z,\tau) & t_z \le t \le t_{4za} \\ \rho_0 c U_0 \sin\omega_0(t-t_z) + \int_{t_z}^{t_{4az}} \sin\omega_0(t-\tau) h_{2nf}(z,\tau) & t_{4az} \le t \le t_z + T' \\ \int_{t-T'}^{t_{4az}} \sin\omega_0(t-\tau) h_{2nf}(z,\tau) dt & t_z + T' \le t \le t_{4az} + T' \\ 0 & t_{4az} + T' \le t \le \infty \end{cases} \quad (4.91)$$

The third term in the above expression is same as that of the pressure output for a continuous input velocity, $u_C(t)$. Second and fourth terms are transient parts at the beginning and at the end of the signal respectively. As in the near-field, point receiver case, the pressure, $p_{nf}(z,t)$, has an initial transient region, continuous region and an end transient region. The time duration of the transients at the both ends of the signal are equal to $(t_{4az} - t_z)$. Since $h_{nf}(z,t) = 0$ for $t < t_z$ the output signal starts at $t = t_z$. These facts are sketched in a plot in the Fig.(4.11). The case with the velocity signal whose length $T' < (t_{4az} - t_z)$ is illustrated in Appendix(A-2).

The pressure pulse shown in Fig.(4.11) was calculated using two different methods. The transient parts at the ends of pulse were calculated using numerical calculation of the convolution integral explained in Appendix(A-2). This method was preferred over the usual Fourier transform(FFT) method in order to avoid any aliasing problem. Though the same method can be used to calculate the whole pulse, as it consumes a lot of time for calculation, a different method was used to calculate the continuous part of the pulse.

The velocity to pressure transfer function of this model, $H_{nf}(\omega)$, is given in Eq.(4.41b). The pressure, for a velocity, $u_C(t)$,can be found as follows. Consider a sinusoidal velocity wave $U_0 e^{j\omega_0 t}$. Its Fourier transform is $U_0\delta(\omega-\omega_0)$. The pressure corresponding to this velocity is given by,

$$p_{nfC}(z,t) = \mathrm{IFT}(H_{nf}(z,\omega)\, U_0\delta(\omega-\omega_0)) \quad (4.92)$$

or

$$p'_{nfC} = H_{nf}(z,\omega_0) U_0 e^{j\omega_0 t}. \quad (4.93)$$

The desired pressure, that corresponds to the velocity $u_C(t)$, is,

$$p_{nfC}(z,t) = \mathrm{Im}\left(H_{nf}(z,\omega_0) U_0 e^{j\omega_0 t}\right). \quad (4.94)$$

Since this method does not involve any numerical calculation with frequency spectrum, the result is free from time aliasing due to truncation of the frequency spectrum. The Eq.(4.94) was used to calculate the continuous part of the pulse shown in Fig.(4.11). The time axis and the amplitude axis of the plot are normalised to the period and the magnitude of the ideal plane wave respectively. And the signals are given an arbitrary start.

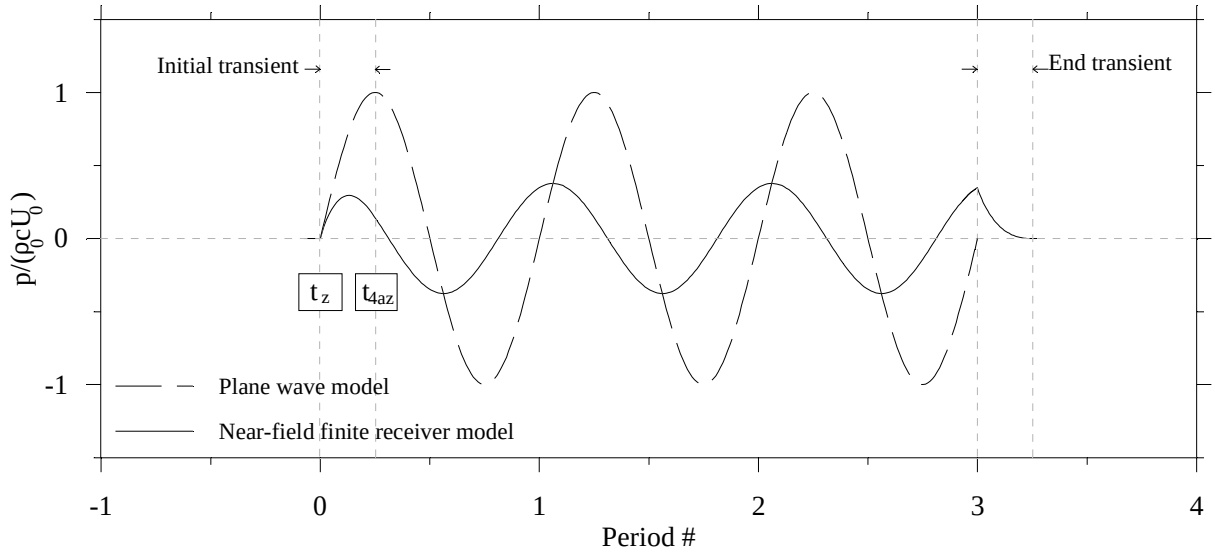

Figure(4.11) Average pressure of the near-field finite receiver model, normalised to the ideal plane wave pressure. Time axis is normalised to the period of the ideal plane wave. z = 0.1m, a = 4.5mm, f = 215kHz and c = 344.35m/s.

The Fig.(4.11) shows that the continuous region of the signal has advanced in phase compare to the ideal plane wave.

The duration of the transient regions, t_{tr}, at both ends of the signal normalised with period of the input signal is a function of S and (ka) only. That is,

$$\frac{t_{4za} - t_z}{T} = \frac{t_{tr}}{T} = \frac{(ka)^2}{4\pi^2}\left[\sqrt{S^2 + \frac{16\pi^2}{(ka)^2}} - S\right] \tag{4.95}$$

The Fig(4.12) shows $\frac{t_{tr}}{T}$ as a function of S for three different values of (ka).

As S increases the transient duration becomes smaller and smaller, for all ka values, and goes towards zero. This means that this model tends to the far-field model at larger S values for all ka values. At small S values, transient duration becomes larger for larger ka values. At S = 1 the expression for the normalised transient duration in Eq(4.95) can be further simplified as follows. Substituting S = 1 in Eq(4.95) gives,

$$\frac{t_{tr}}{T} = \frac{(ka)^2}{4\pi^2}\left[\sqrt{1 + \frac{16\pi^2}{(ka)^2}} - 1\right] \tag{4.96}$$

for large ka values

$$\frac{t_{tr}}{T} \approx \frac{(ka)^2}{4\pi^2}\left[1 + \frac{1}{2}\frac{16\pi^2}{(ka)^2} - 1\right] \tag{4.97}$$

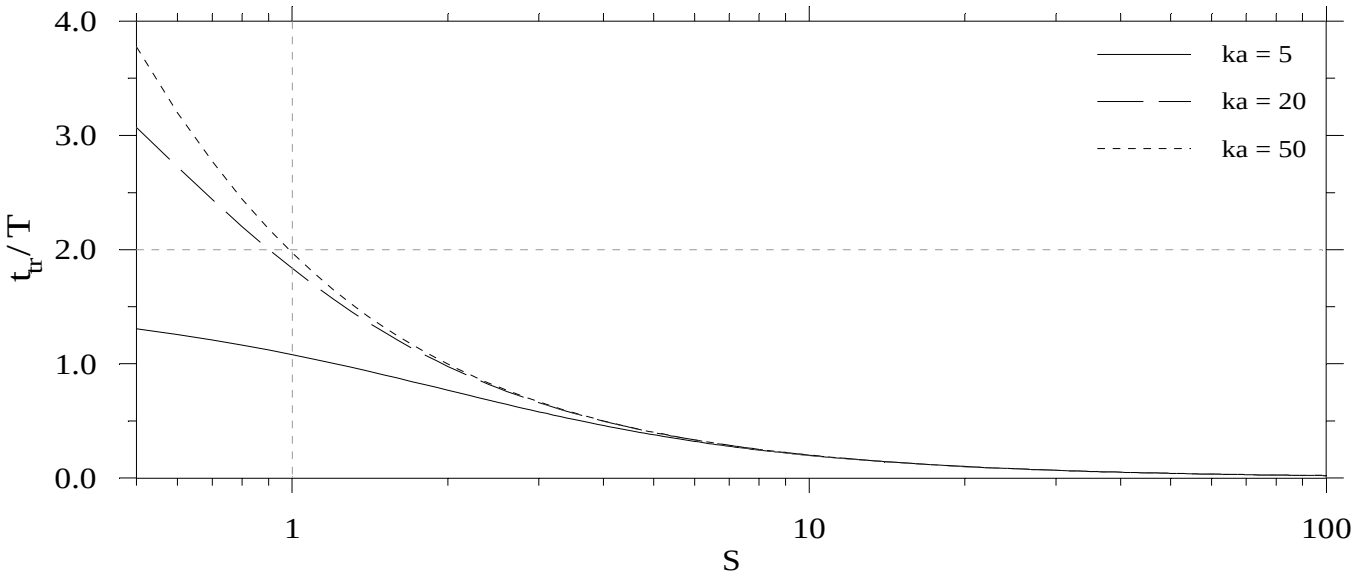

Figure(4.12) Transient duration for the near-field finite receiver model as a function of S. The S axis is in log scale. The transient time, t_{tr}, is normalised to the period of the ideal plane wave.

$$\frac{t_{tr}}{T} \approx 2 \tag{4.98}$$

The transient duration is less than two periods for all ka values in the range S > 1.

PULSE FORMS

In the previous sections methods to calculate the pressure waves for a sinusoidal velocity burst and the explanations for the shapes of the calculated pressure waves were presented. The basic shape of the pressure wave is determined by the parameters; radius of the source, a, distance between the source and the observation point, z and the velocity of the medium, c, and the frequency of the velocity wave, f. This can be seen from the expression for the convolution integral, Eq.(4.90), and the expression for the impulse response, $h_{nf}(z,t)$. The density of the medium, ρ_0, and the amplitude of the velocity wave, U_0, are just multiplication factors and hence do not contribute to the basic shape of the wave.

In this section the changes in shape of the pressure wave due to above mentioned parameters, a, z, c and f, are discussed. It is cumbersome to take all four variables in to the analysis. But, fortunately, it is possible to express the pressure pulse in terms of Seki parameters, S and ka, provided the time axis of the pulse is normalised to the period of the ideal plane wave. A proof that the pressure pulse can be written in terms of S and ka is given in Appendix(A-4). But, as the plot in Fig.(4.11), the continuous part of the pulse was calculated according to the Eq.(4.94) for the same reasons stated in the related text. Consider the transfer function

$$H_{nf}(z,\omega) = \rho_0 c\left[e^{-jkz} - \frac{4}{\pi}\int_0^{\pi/2} e^{-jk(z^2+4a^2\cos^2\theta)^{\frac{1}{2}}} \sin^2\theta d\theta \right]. \tag{4.41b}$$

This equation can be written as follows,

$$H_{nf}(z,\omega) = \rho_0 c\left[e^{-j(kz)} - \frac{4}{\pi}\int_0^{\pi/2} e^{-j((kz)^2+4(ka)^2\cos^2\theta)^{\frac{1}{2}}} \sin^2\theta d\theta \right] \quad (4.99)$$

Since (kz) can be written as $\frac{S}{2\pi}(ka)^2$, $H_{nf}(z,\omega)$ is a function of S and ka only. θ does not consist any physical quantity, ρ_0 and c are constants. Therefore Eq.(4.94) can be written, defining $\hat{t} = \frac{t}{T}$ to be the normalised time, as

$$p_{nfC}(z,\hat{t}) = U_0 |H_{nf}(S,ka)| \sin\left(2\pi\hat{t} + \angle H_{nf}(S,ka)\right). \quad (4.100)$$

This proves that this method of calculation of the continuous part of the pulse is also consistent with the normalisation and hence the representation of the pulse in terms of S and ka values.

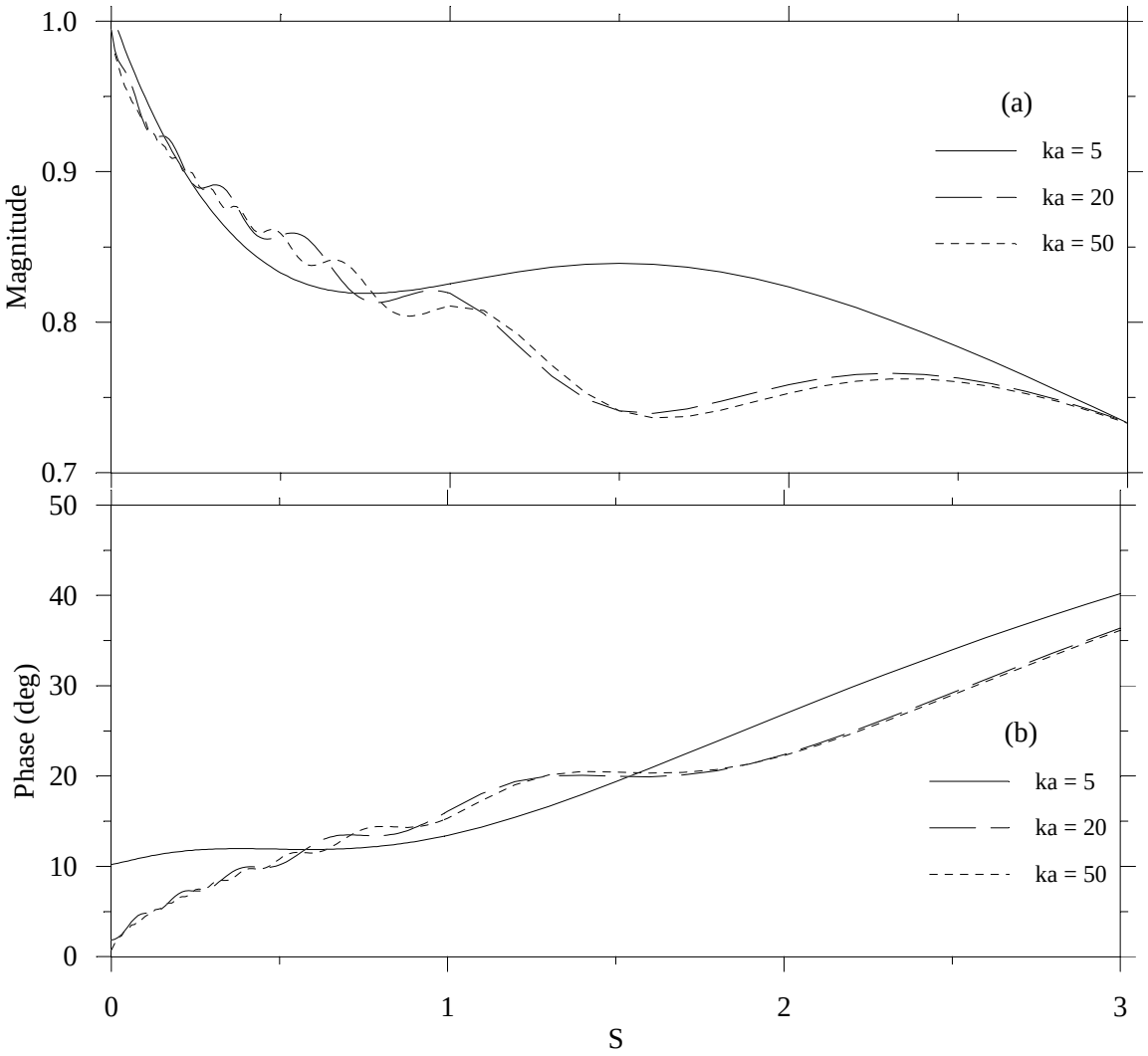

Figure(4.13) The (a) magnitude and (b) phase of the transfer function $H_{nf}(S,ka)/H_p(S,ka)$ as a function of S, up to S = 3, for ka values 5, 20 and 50.

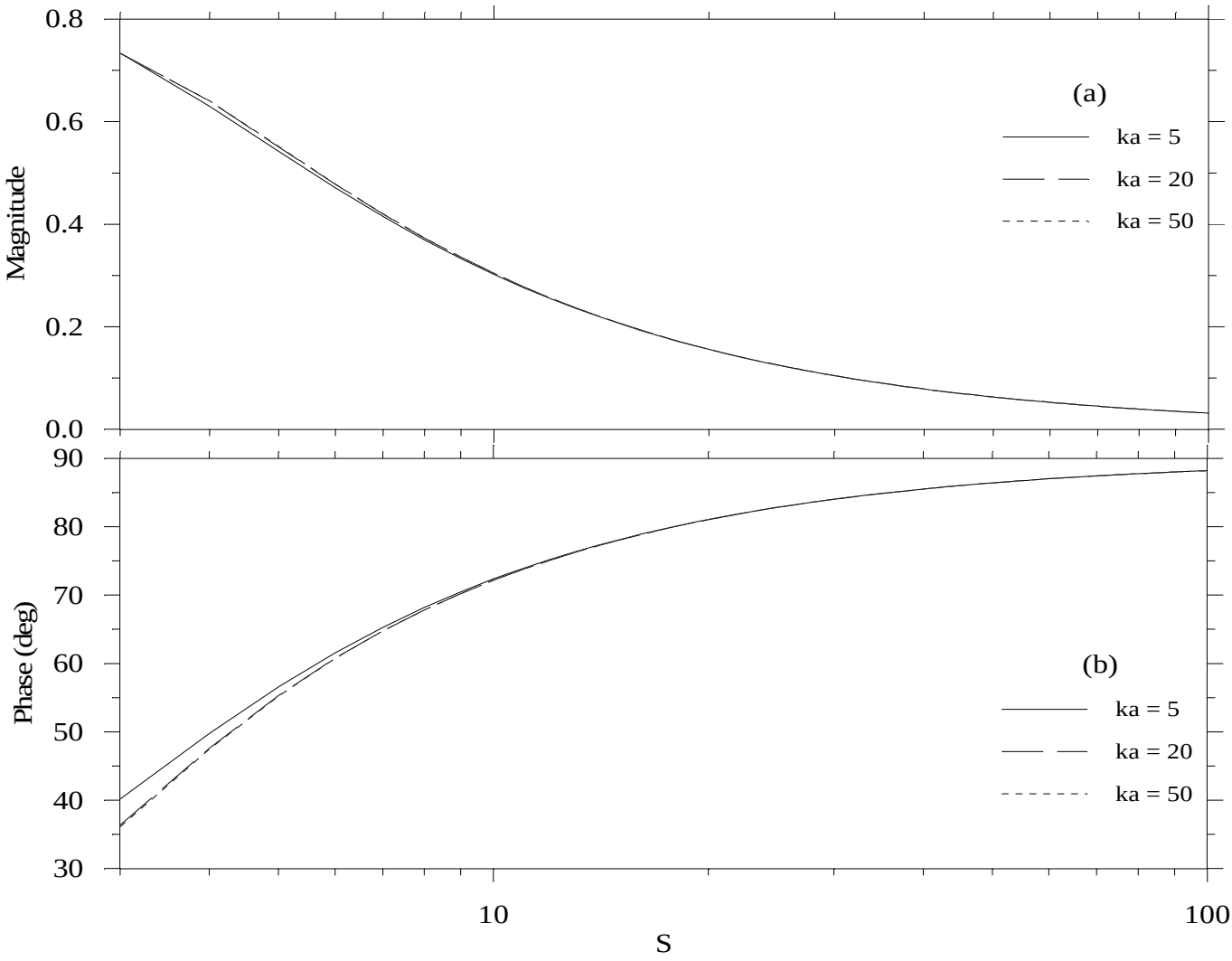

Figure(4.14) The (a) magnitude and (b) phase of the transfer function $H_{nf}(S,ka)/H_p(S,ka)$ as a function of S for ka values 5, 20 and 50. S axis is in log scale from 3 to 100.

Now, it is natural to study the variation in the shape of the pulse due to one variable keeping the other constant. Before this analysis, it may be useful to plot the transfer function, $H_{nf}(z,\omega)$, as a function of S and ka values. The Figs.(4.13) & (4.14) show the magnitude and phase of transfer function, relative to the plane wave, $H_{nf}(S,ka)/H_p(S,ka)$, for three different ka values; 5, 20 and 50. The Fig.(4.13) show the magnitude and phase of the transfer functions from S = 0 to 3 in linear scale and the Fig.(4.14) show from S = 3 to 100 in log scale.

In the analysis of the pulse forms with S and ka values, first, the pressure pulses for two different ka values for three different S values were simulated. These simulations are plotted in Fig.(4.15). In all simulations a 4-period pulse was used. The time axes are normalised to the period of the ideal plane wave. The extension of the transients, at both ends of the pulses, are denoted by round marks. The initial transients start at the beginning of the pulses and end at the first round marks. The end transients start after 4 periods and end at the round marks. The duration of the transients are calculated, using Eq.(4.95), and tabulated in Table(4.1).

From the table, it can be seen that as S increases, the change in ka value becomes immaterial, concerning the transient duration.

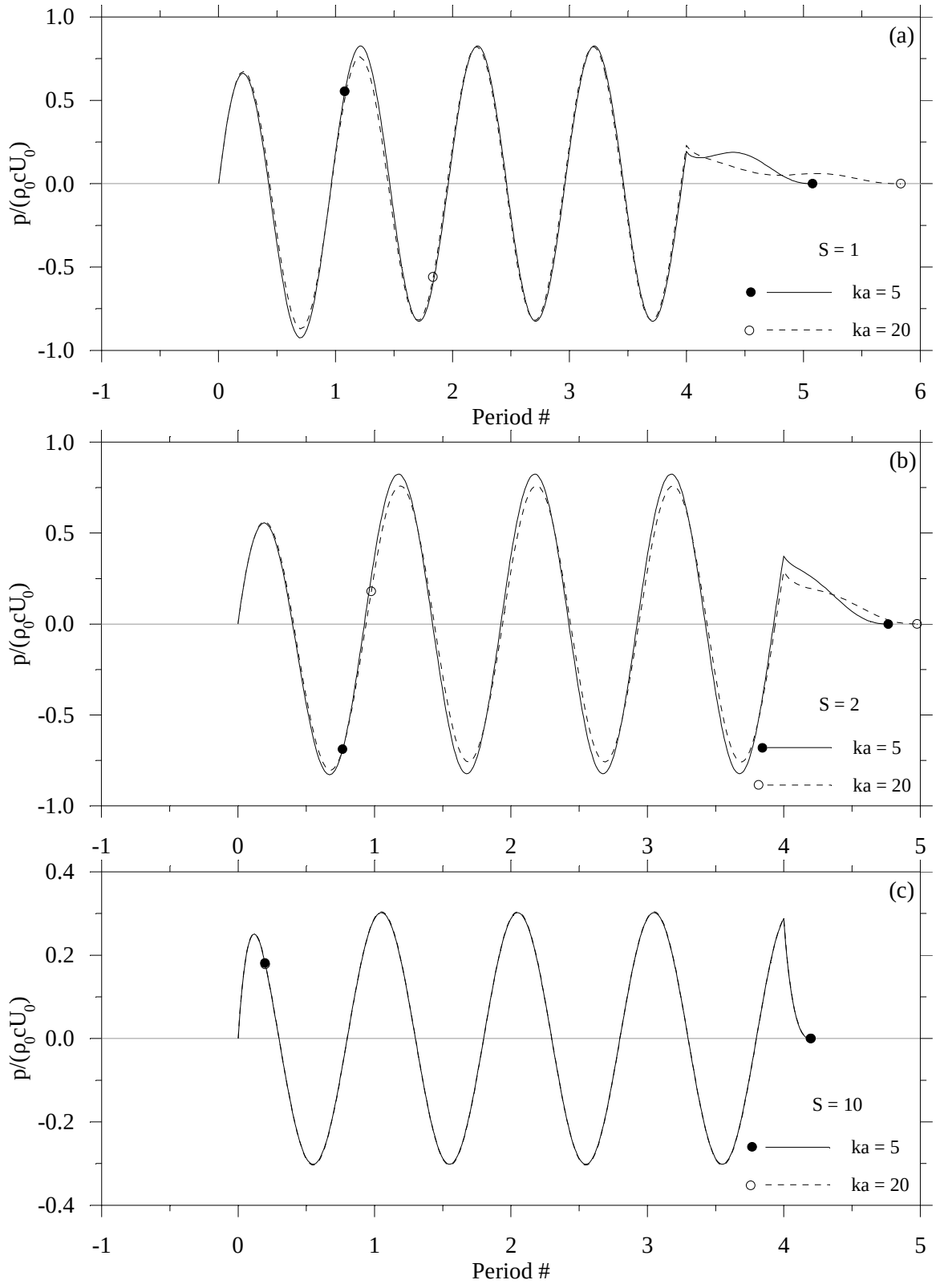

Figure(4.15) Change in pulse form due to ka value, for a constant S value. Pressure amplitude is normalised to the plane wave amplitude. Time axis is normalised to the period of the ideal plane wave. Pulse forms are presented for ka values 5 and 20 at (a) S = 1, (b) S = 2 and (c) S = 10. The round marks denote the end of the transient regions.

	S = 1	S = 2	S = 10
ka = 5	1.079	0.767	0.196
ka = 20	1.834	0.976	0.199

Table (4.1) Calculated transient duration of the pulses shown in Fig.(4.15), using Eq.(4.95).

At S = 1, the difference between the magnitudes and the phases in the continuous part of the two signals are very small. At S = 2 these differences become, comparatively, large and at S = 10 become small again. These variations in the continuous part of the pulse due to the variation in ka value can be related to the transfer function, $H_{nf}(S,ka)$, in Figs.(4.13) and (4.14). The transfer functions are normalised to the plane wave and the pulses under consideration are also normalised to the plane wave. Therefore, the differences in the pulses, both in magnitude and phase, can be compared directly to corresponding differences in the transfer functions. From the plots of the transfer functions, it can be seen that the difference between the magnitudes and phases for ka values 5 and 20 at S = 1 is small, at S = 2 is large and at S = 10 is very small.

Fig.(4.16)(a), (b) and (c) show the variation in the pulse form with increasing S value while ka being constant at 20. The time axis of the plots are normalised to the plane wave periods. The amplitude of the signals in Fig.(4.16)(a) decreases with increasing S. This effect is in agreement with the behaviour of the transfer function shown in Fig.(4.14)(a). The length, in time, of the pulse is decreasing with increasing S value and approaches to the length of the input signal, four periods in this simulations. This is due to the reduction in the transient region of the pulse with increasing S value which is also shown in Figs.(4.16)(b) and (c). The relation between the transient duration and the S value is shown in Fig.(4.12). Fig.(4.16)(a) shows that, as S increases, the peaks of the continuous part approach the zeros of the plane wave. This indicates that the phase difference between the continuous part of the pulse and the plane wave increases with increasing S and approaches 90 degrees, which is also evident from the phase of the transfer function, $H_{nf}(S,ka)/H_p(S,ka)$, shown in Fig.(4.14)(b).

Fig.(4.16)(b) shows the initial transient portion of the signals shown in Fig.(4.16)(a). Fig.(4.16)(c) shows the end transient and a small portion of the continuous part of the signals shown in Fig.(4.16)(a). The amplitudes of the pulses in figs.(4.16)(b) and (c) are normalised to their respective steady state values. Therefore, Fig(4.16)(b) shows the change in the relative size of the first peak of the pulse to the continuous part with increasing S value. At very large values of S, the first peak of the signal becomes equal to the continuous part.

So far, the pulse forms of the near-field point receiver model ,far-field model and the near-field finite receiver model are discussed individually comparing to the plane wave model. The Fig.(4.17) compares the pulse forms of last three of the four models calculated for three different transmitter-receiver separations. The amplitude of the waves are normalised to the plane wave amplitude. The time axes of the plots are normalised to the period of the ideal plane wave. The parameters radius, frequency and velocity of sound in the medium are same for all three plots; a = 5.52mm, f = 200kHz and c = 347m/s. The transmitter-receiver separation, z, are 35.2, 175.7 and 352mm for plots (a), (b) and (c) respectively. These parameters correspond to ka = 20 and S value 2, 10, and 20 for plots (a), (b) and (c) respectively.

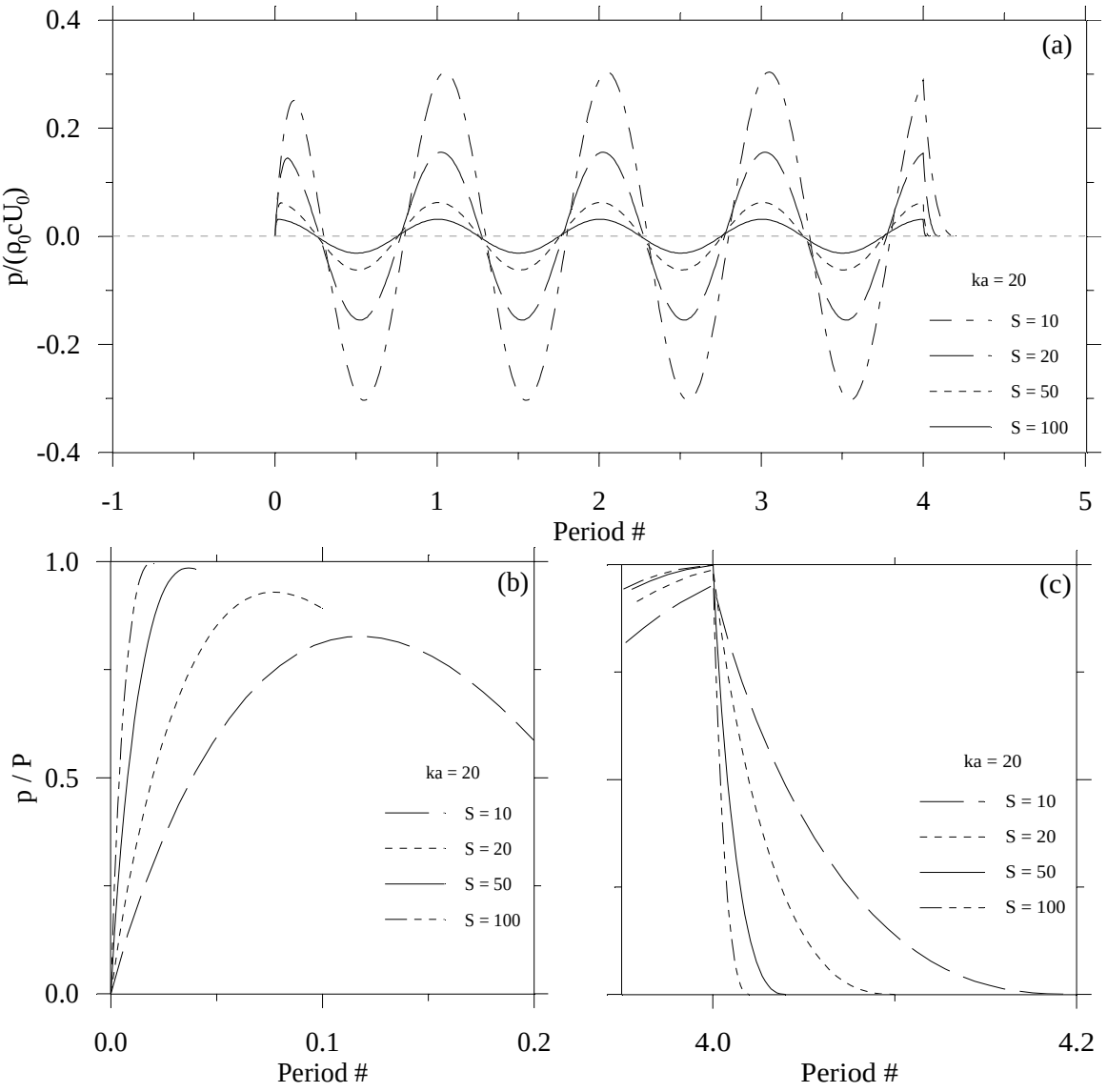

Figure(4.16)

Variation in pulse form due to the change in S for a constant ka value. Form of (a) the whole pulse, (b) beginning of the pulses up to the continuous region and (c) end transient of the pulses ,with a small portion of the continuous part, for S values 10, 20, 50 and 100 at ka = 20. The amplitudes of the pulses in (a) are normalised to the amplitude of the ideal plane wave. The amplitudes of the pulses in (b) and (c) are normalised to their respective steady state values. Time axes of all the plots is normalised to the period of the ideal plane wave.

As z increases the pulses predicted by the near-field point receiver and near-field finite receiver models approach to that predicted by the far-field model. This is an anticipated result, as similar behaviour was observed in the impulse responses of the three models. That is, the impulse response of the near-field models approach that of the far-field model for large transmitter-receiver separations. But, one might wonder about the physics behind this. It may be explained as follows. High frequency signals are more directive than the low frequency signals. That is, high frequency components of a signal lie in narrow cones around the axis while the low frequency components lie in wide cones. When the transmitter-receiver separation increases, most of the low frequency components do not reach the receiver, only higher frequency components do. Then the received signal contains more high frequency components.

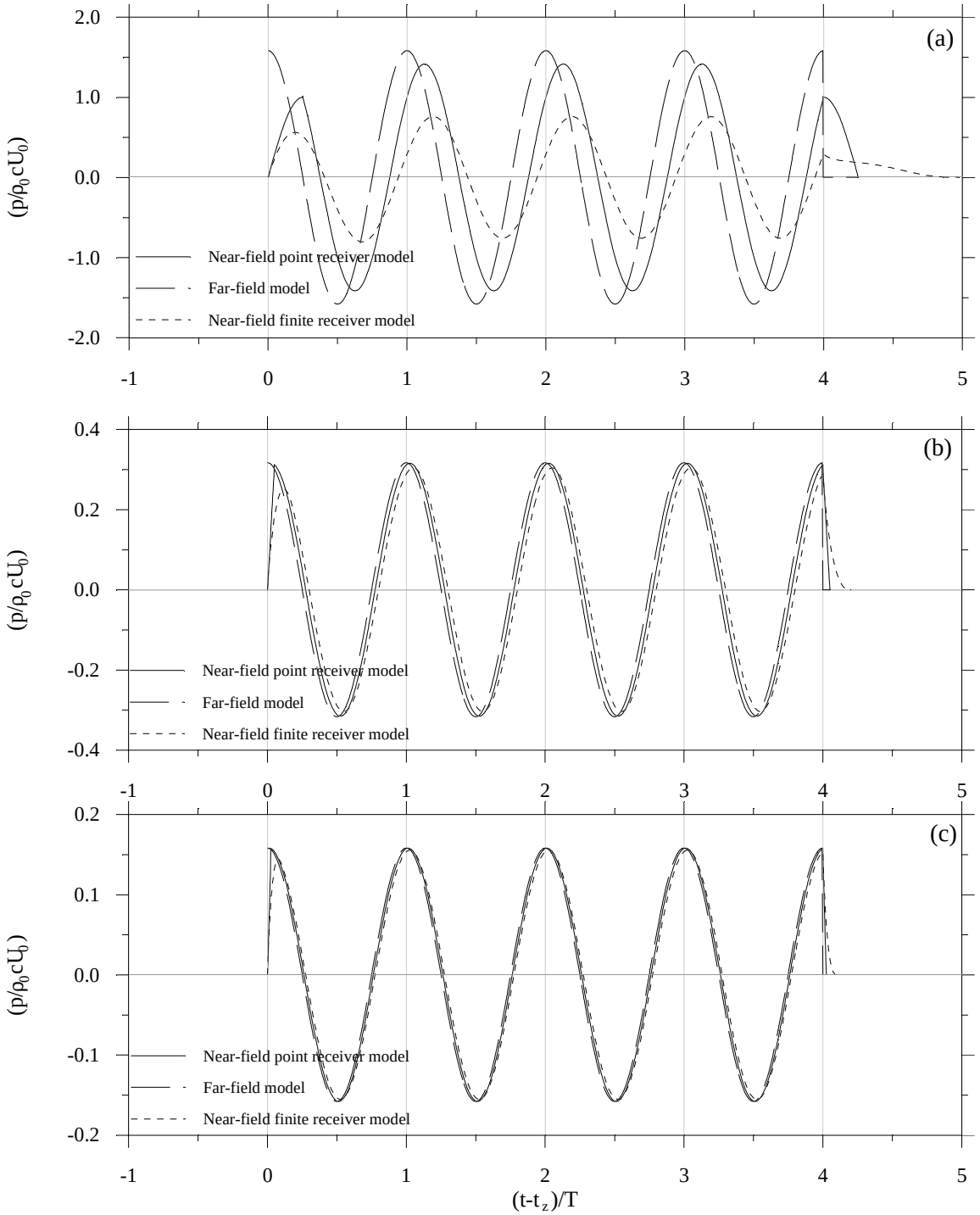

Figure 4.17 Pulse forms of near field point receiver, far-field and near-field finite receiver models for different transmitter-receiver separations. The parameters used in the calculations are: a = 5.52mm, f = 200kHz, c = 347m/s and (a) z = 35.2mm, (b) z = 175.7mm and (c) z = 352mm.

The reduction in amplitude can be accounted by the energy lost with the low frequency components. The far-field model is a high pass filter(see under the subheading "impulse responses"). The signal calculated by the near-field models, for large transducer separations, and the far-field model contain the high frequency portion of the initial spectrum. Therefore, the near-field models approach the far-field model at large transmitter-receiver separations. The enhancement of high frequency components in the transmitted signal with increasing transmitter-receiver separation is shown experimentally by Cassereau *et al*[42].

4.4 DISCUSSION

Pressure pulse forms due to a uniform sinusoidal velocity pulse transmitted by a piston type transducer through a non viscous medium are studied. Pulse forms due to the near-field finite receiver model are presented as a function of S and ka values. With this presentation one can compare and study the pulse forms in different medium at different environmental conditions. These differences can be accounted as a change in the parameter for velocity of sound in the medium.

It has been showed that the pulse predicted by far-field model has continuous region for input pulses of any length in time. But the pulse predicted by the other two models has continuous region for sufficiently long input pulses. The continuous region of the pulse predicted by the near-field finite receiver model and the far-field model has advanced in phase compared to the plane wave because of diffraction effects. In the near-field point receiver model the pulse lags and leads the plane wave alternatively in the region close to the receiver. The advancement in phase for the far-field case is $\pi/2$ for all frequencies. For the other two cases the advancement in phase is a function of S and ka values. In calculations using plane wave model, the advancement in phase has to be corrected. Otherwise, for example, in the calculation of the velocity of sound one will end up with a velocity which is larger than the actual one.

The Eq.(4.41) shows the function, $H_{nf}(z,\omega)$ and Eq.(4.23) shows $H_p(z,\omega)$. $H_{nf}(z,\omega)/H_p(z,\omega)$ is the diffraction correction. The magnitude and phase of this function, are tabulated by Khimunin[7,36] as a function of S and ka values. Khimunin verified the diffraction correction for a few combinations of k and a values, which give the same ka value, and concluded that the diffraction correction depends on the ka value, no matter what the combinations of k and a values are. This verification may not be necessary because of the following reason. It is shown in Eq.(4.99) and in the related text that $H_{nf}(z,\omega)$ is a function of S and ka only. Since kz can be written in terms of S and ka values $H_p(z,\omega)$ is also a function of S and ka values only. Therefore, $H_{nf}(z,\omega)/H_p(z,\omega)$, the diffraction correction, is a function of S and ka only. The magnitude and the phase of this function are plotted in Figs.(4.13) and (4.14) respectively.

CHAPTER 5

EFFECTS OF TRANSDUCER DYNAMICS ON PULSE FORMING

5.1 INTRODUCTION

The transducers, in an acoustical system such as one described in Chapter 3, play an important roll in determining the shape of the transmitted pulse. Therefore it is of perticular important to study the effect of transducers on pulse forming to understand the system. In this chapter the dynamic characteristics of the transmitting and receiving transducers and the pulse forming machanism are discussed.

A frequency domain equivalant circuit representation of the one dimensional, thickness extentional vibrations of a piezo-eletric transducer element was devoloped by Mason[28]. To study the transient response of the piezo-electric transducer element, Redwood[30] devoloped its time domain response for the special case where the negative capacitance, $-C_o$, in the equivalant circuit is ignored. Later Vervik[15], Guo[43] and others devoloped the time domain response including $-C_o$.

In this work, the equivalent circuit of the one dimensional Mason model is taken as the starting point for the discussion. The voltage to velocity transfer function of the equivalant circuit is found. Then the transfer function is converted to Laplace domain to get the time domain responses of Redwood and Vervik for the cases where $-C_o$ is excluded and included respectively. Using these results the transducer dynamics and the pulse forming effects are studied. The time domain responses are too large and too complex to use to simulate the total response of the transducer. Therefore, two frequency domain models, TRANSCAD and FLOSIM, developed at CMR for transducer modelling and for flow simulation purposes, have been used for simulations of the total response of the transducer. These are also one-dimensional Mason type models except for the elastic, dielectric and piezoelectric losses are included. In addition, TRANSCAD and FLOSIM models are designed so that the transducer element can have many matching and backing layers. But, in this chapter the option for no matching and no backing layer was chosen.

5.2 TRANSMITTER

In this section theoretical models for a transmitting transducer are developed and the transfer functions and impulse responses of the models are presented and explained. Then a method to calculate the particle velocity of the transducer for a sinusoidal voltage excitation and some examples of calculated velocity, with and without $-C_0$, are presented and discussed.

5.2.1 THEORY

In the beginning of this section, the voltage to velocity transfer function and the impulse responses for the Mason's model are derived. Then, the simplified model is deduced and similar transfer function and impulse response are derived. Finally, the TRANSCAD model, actually the implementation of loss factors in the model, is briefed.

5.2.1.1 THE MASON MODEL

The cross-sectional view of the thickness expander piezoelectric plate is shown in the Fig.(5.1). The cross-section lies in a plane parallel to the electric field and perpendicular to the radiating face. The electric field is parallel to the vibration. F_1^p and F_2^p are the forces acting on the plate from the medium at acoustic port 1 and 2 respectively. v_1^p and v_2^p are the particle velocity of the transducer faces at ports 1 and 2 respectively. These quantities are taken to be positive in their respective directions shown in Fig.(5.1). Z_{r1} and Z_{r2} are impedance of the backing and radiation medium respectively.

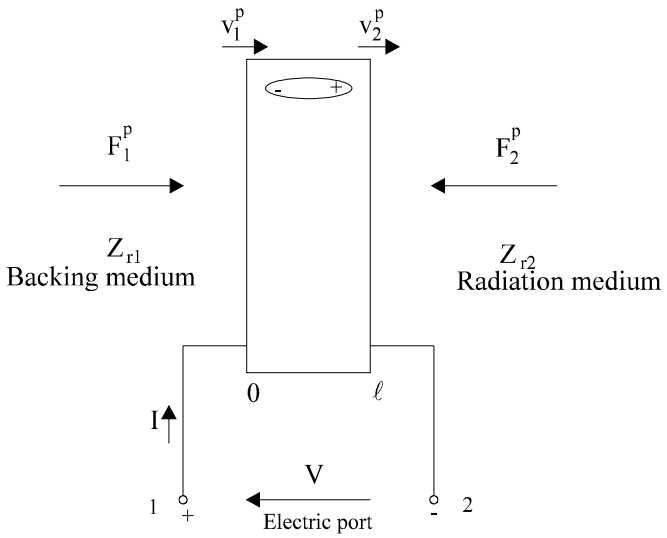

Fig.5.1 Thickness expander piezoelectric plate. Electric field parallel to the thickness of the plate.

The equivalent circuit for the thickness mode vibrations of a piezoelectric transducer element is well established and the derivation of it could be found in the literature[27,28]. The Fig.(5.2) shows the equivalent circuit of a thickness expander transducer.

In the equivalent circuit ,

$$Z_a = jZ_0 \tan\left(\frac{k\ell}{2}\right) \tag{5.1a}$$

and

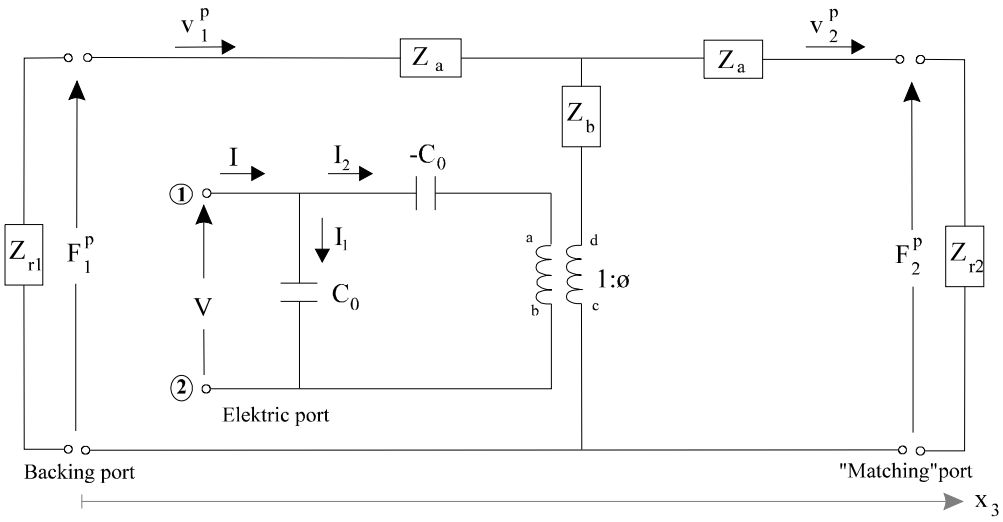

Fig. 5.2 The equivalent circuit for one-dimensional thickness extensional vibrations in a thin piezoelectric plate.

$$Z_b = \frac{Z_0}{j\sin(k\ell)} \tag{5.1b}$$

are the transmission line impedance represent the acoustic reverberations in the transducer,

$$Z_0 = \rho c A \tag{5.1c}$$

is the mechanical impedance of the transducer, where, ρ is the density of the piezoelectric material, c is the speed of sound in the piezoelectric material and A is the area of the transducer plate,

$$C_0 = \frac{A}{\ell}\varepsilon_{33}^S \tag{5.1d}$$

is the clamped capacitance of the plate, where ℓ is the thickness of the plate and ε_{33}^S is the permittivity of the piezo electric material at constant strain and

$$\phi = \frac{A}{\ell}e_{33} \tag{5.1e}$$

is a factor represents the electromechanical conversion where e_{33} is the stress coefficient of the piezo electric material.

VOLTAGE TO VELOCITY TRANSFER FUNCTION

The relationships between voltage, forces, electric current and the particle velocities are found by applying the basic network analysis laws to the equivalent circuit shown in Fig(5.2).

For the transformer,

$$V_{ba} = \frac{F_{cd}}{\phi} \tag{5.2a}$$

and

$$(v_1^p - v_2^p)\phi = -I_2, \tag{5.2b}$$

where F_{cd} is the mechanical force produced at the transformer.

For the rest of the circuit,

$$V = \frac{I_1}{j\omega C_0}, \tag{5.2c}$$

$$I = I_1 + I_2, \tag{5.2d}$$

$$V = V_{ba} + \frac{I_2}{j\omega(-C_0)}, \tag{5.2e}$$

$$F_1^p = (Z_a + Z_b)v_1^p - Z_b v_2^p + V_{ba}\phi \tag{5.2f}$$

and

$$F_2^p = Z_b v_1^p - (Z_a + Z_b)v_2^p + V_{ba}\phi. \tag{5.2g}$$

The boundary conditions give,

$$F_1^p = - Z_{r1}\, v_1^p, \tag{5.2h}$$

$$F_2^p = Z_{r2}\, v_2^p. \tag{5.2i}$$

The negative sign in Eq.(5.2h) is because, the force on the medium and the particle velocity are in opposite directions.

The relationship between the voltage and velocity is found, using the above relationships, as

$$\frac{v_2^p}{V} = \frac{\phi}{\left(Z_a + Z_b^* + Z_{r2}\right) + Z_b^* \dfrac{\left(Z_a + Z_{r2}\right)}{\left(Z_a + Z_{r1}\right)}} \tag{5.3a}$$

where

$$Z_b^* = Z_b - \frac{\phi^2}{j\omega C_0} \tag{5.3b}$$

If the voltage, $V = e^{j\omega t}$ then,

$$v_2^p = \frac{\phi}{\left(Z_a + Z_b^* + Z_{r2}\right) + Z_b^* \dfrac{\left(Z_a + Z_{r2}\right)}{\left(Z_a + Z_{r1}\right)}} \cdot e^{j\omega t}. \tag{5.3c}$$

Assuming the system to be linear, the velocity for an arbitrary input voltage, V(t), can be written[9] as,

$$V_2^p(\omega) = \frac{\phi}{\left(Z_a + Z_b^* + Z_{r2}\right) + Z_b^* \dfrac{\left(Z_a + Z_{r2}\right)}{\left(Z_a + Z_{r1}\right)}} \cdot V(\omega) \tag{5.3d}$$

where $V_2^p(\omega)$ and $V(\omega)$ are the Fourier transforms of $v_2^p(t)$ and V(t) respectively.

$$V_2^p(\omega) = H_{tr1}(\omega) \cdot V(\omega) \tag{5.3e}$$

where,

$$H_{tr1}(\omega) = \frac{\phi}{\left(Z_a + Z_b^* + Z_{r2}\right) + Z_b^* \dfrac{\left(Z_a + Z_{r2}\right)}{\left(Z_a + Z_{r1}\right)}}, \tag{5.3f}$$

the ratio of the output spectrum to the input spectrum, is the voltage to velocity transfer function[9].

The transfer function of a linear time invarient system is the Fourier transform of its impulse response[9].Therefore, the inverse Fourier transform of $H_{tr1}(\omega)$ gives the corresponding impulse response. But the inverse Fourier transform of Eq.(5.3f) is not straight forward. In order to make the inverse transform easy the equivalent circuit is represented[14] in its Laplace transforms. In the Laplace domain, jω is represented by s. Substituting for jω in Eqs.(5.1a) and (5.1b) gives,

$$Z_a = jZ_0 \tan\left(\frac{k\ell}{2}\right) = Z_0 \left(\frac{e^{\frac{s\tau_0}{2}} - e^{-\frac{s\tau_0}{2}}}{e^{\frac{s\tau_0}{2}} + e^{-\frac{s\tau_0}{2}}} \right) \tag{5.4a}$$

and

$$Z_b = \frac{Z_0}{j\sin(k\ell)} = \frac{2Z_0}{e^{s\tau_0} - e^{-s\tau_0}} \tag{5.4b}$$

where, $k = \frac{\omega}{c}$, $\tau_0 = \frac{\ell}{c}$ and s is the Laplace variable. Substituting for Z_b and jω in Eq.(5.3b) gives,

$$Z_b^* = \frac{2Z_0}{e^{s\tau_0} - e^{-s\tau_0}} - \frac{\phi^2}{sc_0} \tag{5.4c}$$

Substituting for Z_a and Z_b in the Eq(5.3a) and with some manipulations, it can be shown that the transfer function in the Laplace domain takes the following form.

$$H_{tr1}(s) = \phi \frac{(Z_0 + Z_{r1}) - 2Z_0 e^{-s\tau_0} + (Z_0 - Z_{r1}) e^{-2s\tau_0}}{k_1 + k_2 e^{-s\tau_0} - k_3 e^{-2s\tau_0}} \tag{5.5}$$

where

$$k_1 = (Z_0+Z_{r1})(Z_0+Z_{r2}) - \frac{\phi^2}{sC_0}(2Z_0+Z_{r1}+Z_{r2}), \tag{5.6a}$$

$$k_2 = 4\frac{\phi^2}{sC_0}Z_0 \tag{5.6b}$$

and

$$k_3 = (Z_0 - Z_{r1})(Z_0 - Z_{r2}) - \frac{\phi^2}{sC_0}(2Z_0 - Z_{r1} - Z_{r2}). \tag{5.6c}$$

Some intermediate steps in the manipulation to arrive the final form of the transfer function in Eq.(5.5) are given in Appendix(A-5).

IMPULSE RESPONSE

The voltage to velocity impulse response of the transducer element is given by the inverse Laplace transform of $H_{tr1}(\omega)$. Having expanded the denominator of the Eq(5.5) by the binomial theorem using partial fraction method the voltage to velocity impulse response is found[15] as,

$$h_{tr1}(t) = \frac{\phi(1-r_2)}{2Z_{r2}}\big(f(t) + g(t)\big), t \geq 0 \tag{5.7a}$$

where

$$f(t) = \left\{ \begin{array}{lll} \delta(t) - (1+r_1)\delta(t-\tau_0) & + & r_1(1+r_2)\delta(t-2\tau_0) \\ -r_1 r_2(1+r_1)\delta(t-3\tau_0) & + & r_2 r_1^2(1+r_2)\delta(t-4\tau_0) \\ -r_1^2 r_2^2(1+r_1)\delta(t-5\tau_0) & + & r_2^2 r_1^3(1+r_2)\delta(t-6\tau_0) \\ \cdots & & \cdots \\ \cdots & & \cdots \end{array} \right\}, \tag{5.7b}$$

$$
\begin{aligned}
g(t) &= (k_{00}) \cdot e^{\beta t} u(t) \\
&- \left(k_{10} + k_{11} \frac{(t-\tau_0)}{1!} \right) \cdot e^{\beta (t-\tau_0)} u(t-\tau_0) \\
&+ \left(k_{20} + k_{21} \frac{(t-2\tau_0)}{1!} + k_{22} \frac{(t-2\tau_0)^2}{2!} \right) \cdot e^{\beta (t-2\tau_0)} u(t-2\tau_0) \\
&- \left(k_{30} + k_{31} \frac{(t-3\tau_0)}{1!} + k_{32} \frac{(t-3\tau_0)^2}{2!} + k_{33} \frac{(t-3\tau_0)^3}{3!} \right) \cdot e^{\beta (t-3\tau_0)} u(t-3\tau_0)
\end{aligned}
\tag{5.7c}
$$

$\cdots \qquad \cdots \qquad \cdots$

$\cdots \qquad \cdots \qquad \cdots,$

$$\beta = \frac{\phi^2}{2C_0} \left(\frac{2 + r_1 + r_0}{Z_0} \right), \tag{5.7d}$$

$$r_1 = \frac{Z_0 - Z_{r1}}{Z_0 + Z_{r1}} \qquad r_2 = \frac{Z_0 - Z_{r2}}{Z_0 + Z_{r2}}, \tag{5.7e}$$

and τ_0 is the reverbaration period of the transducer element.

The above expression for the impulse response contains the effect of the negative capacitance, $-C_0$. The effect of $-C_0$ could be isolated and studied by comparing the above impulse response with the impulse response in which the terms due to $-C_0$ are ignored. A model, called "simplified model" in which the $-C_0$ is ignored, and the impulse response of it are presented in the next section.

5.2.1.2 SIMPLIFIED MODEL

In this model the $-C_0$ is ignored in the Mason equivalent circuit. This does not mean any removal of the negative capacitance from the Mason equivalent circuit. Such a circuit represents[29] a length expander bar with electric field perpendicular to length. Therefore no special equivalent circuit is needed. But, the equations for this model are found by ignoring the terms involving $-C_0$ in the Eqs.(5.2a)...(5.2g). This modification of the equations of the Mason equivalent circuit is exactly the same as that found in Redwood's[30] article, except for the modifications are made by Redwood to the basic wave equations.

TRANSFER FUNCTION

There is only one equation, Eq.(5.2e) involve $-C_0$. Ignoring the term involving $-C_0$ from the Eq.(5.2e) leaves,

$$V = V_{ba}, \tag{5.8}$$

This equation together with other circuit equations, Eqs.(5.2a)...(5.2g), and with the equations of the boundary conditions, Eqs.(5.3a),(5.3b), give the relationship between the voltage and the velocity as,

$$\frac{v_2^p}{V} = \frac{\phi}{(Z_a + Z_b + Z_{r2}) + Z_b \dfrac{(Z_a + Z_{r2})}{(Z_a + Z_{r1})}}. \tag{5.9}$$

Using the same arguments given for the Mason model earlier in this section, the voltage to velocity transfer function can be written as,

$$H_{tr2}(\omega) = \frac{\phi}{(Z_a + Z_b + Z_{r2}) + Z_b \dfrac{(Z_a + Z_{r2})}{(Z_a + Z_{r1})}}. \tag{5.9a}$$

IMPULSE RESPONSE

The voltage to velocity impulse response of this model can be found by taking the inverse Fourier transform of the Eq.(5.9a). But, for the reason stated in the previous section, the transfer function in Eq.(5.9a) is transformed in to Laplace domain. As in the previous section, substituting for Z_a and Z_b in the above transfer function and with some manipulations, it can be shown that the transfer function in the Laplace domain takes the form as,

$$H_{tr2}(s) = \phi \frac{(Z_0 + Z_{r1}) - 2Z_0 e^{-s\tau_0} + (Z_0 - Z_{r1}) e^{-2s\tau_0}}{(Z_0 + Z_{r1})(Z_0 + Z_{r2}) - (Z_0 - Z_{r1})(Z_0 - Z_{r2}) e^{-2s\tau_0}} \tag{5.10}$$

or

$$H_{tr2}(s) = \frac{\phi(1 - r_2)}{2Z_{r2}} \frac{1 - (1 + r_1) e^{-s\tau_0} + r_1 e^{-2s\tau_0}}{1 - r_1 r_2 e^{-2s\tau_0}} \tag{5.11}$$

where r_1 and r_2 are same as that defined in Eq.(5.7e).

Some intermediate steps in the manipulation to arrive the final form of the transfer function in Eq.(5.10) are given in Appendix(A-5).

Then, the voltage to velocity impulse response can be found[15] by expanding the denominator of Eq.(5.11) by binomial theorem and taking its inverse Laplace transform. And it is given by,

$$h_{tr2}(t) = \frac{\phi}{(Z_0 + Z_{r2})} \left\{ \begin{array}{ccc} \delta(t) - (1 + r_1)\delta(t - \tau_0) & + & r_1(1 + r_2)\delta(t - 2\tau_0) \\ -r_1 r_2 (1 + r_1)\delta(t - 3\tau_0) & + & r_2 r_1^2 (1 + r_2)\delta(t - 4\tau_0) \\ -r_1^2 r_2^2 (1 + r_1)\delta(t - 5\tau_0) & + & r_2^2 r_1^3 (1 + r_2)\delta(t - 6\tau_0) \\ \cdots & & \cdots \\ \cdots & & \cdots \end{array} \right\} \tag{5.12}$$

5.2.1.3 TRANSCAD MODEL

The cross-sectional view of the transducer element with the electrical terminals is the same as that shown in Fig.(5.1). Fig.(5.3) shows the equivalent circuit of a thickness mode transducer with losses. F_1^p and F_2^p are forces acting on the transducer from the backing and radiation medium respectively. v_1^p and v_2^p are particle velocity of transducer faces at the backing and radiation ports respectively.

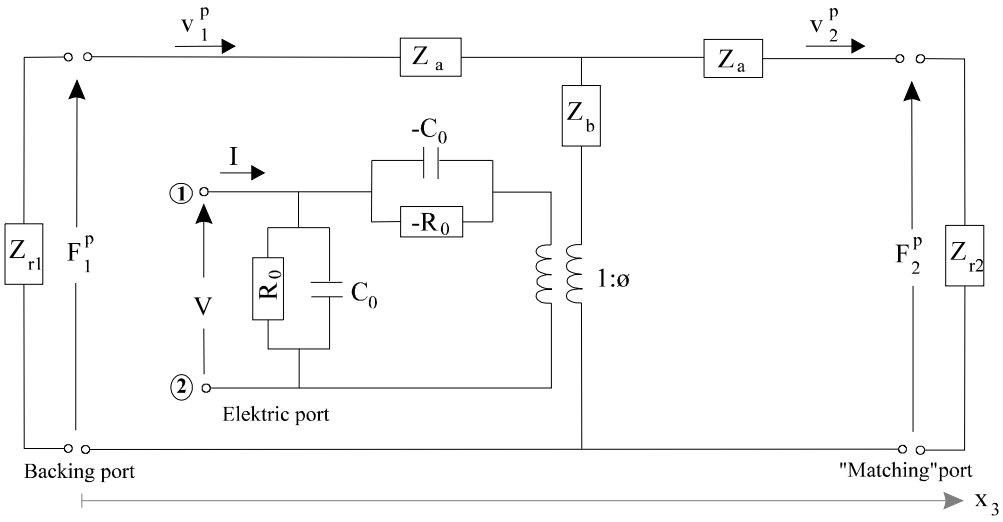

Figure(5.3) Distributed, lossey equivalent circuit for a thickness extensional mode transducer.(From Ref.(3))

The losses in the transducer are accounted for by using complex quantities for elastic, dielectric and piezoelectric constants in the derivation of the equivalent circuit of the lossles transducer model. The complex elastic, dielectric and piezoelectric constants used are as follows:

The complex elastic constant,

$$c_{eff}^{E} = c^{E} + j\omega\eta^{E}, \tag{5.13a}$$

where c^E is the stiffness and η^E is the viscoelastic loss coefficient of the piezoelectric material at constant electric field. The complex dielectric constant,

$$\varepsilon_{eff}^{S} = \varepsilon^{S} - j\nu^{S}, \tag{5.13b}$$

where ε^S is the permittivity and ν^S is the dielectric loss coefficient of the piezoelectric material at constant strain. The complex piezoelectric constant,

$$e_{eff} = e + j\gamma, \tag{5.13c}$$

where e is the piezoelectric stress constant and γ is the piezoelectric loss coefficient.

Making the elastic, dielectric and piezoelectric constants complex result a complex wave number and hence a complex speed of sound in the piezoelectric material. The complex wave number, k, is given by $\mathbf{k} = \frac{\omega}{\mathbf{c}}$, where **c** is the complex speed of sound in the piezoelectric material, given by,

$$\mathbf{c} = \sqrt{\frac{c_{33}^{E} + \frac{(e_{33} + j\gamma_{33})^2}{\varepsilon_{33}^{s} - j\nu_{33}^{s}} + \mathrm{j}\omega\eta_{33}^{E}}{\rho}}\,. \tag{5.14}$$

Since the coefficients η, ν, and γ are not available in data sheets, the expression for the complex speed of sound cannot be used as it is given in Eq.(5.14). There fore, an approximated expression for the complex speed of sound, **c**, in terms of the mechanical quality factor, Q_m , which represents the elastic, dielectric and piezoelectric losses in the transducer material, is used. The approximated complex speed of sound is given by,

$$\mathbf{c} = c\left(1 + j\frac{1}{2Q_m}\right) \tag{5.15}$$

and hence

$$k = \frac{\omega}{c}\left(1 - j\frac{1}{2Q_m}\right) \tag{5.16}$$

And since the piezoelectric absorption coefficient, γ, is not available, the imaginary part of the mechanical coupling factor, ϕ, is set to zero.

$$R_0 = \frac{\left(1 - k_p^2\right)\left(1 - (k_{33}^t)^2\right)}{\omega C_0 (\tan\delta)^T} \tag{5.17}$$

is the shunt resistance which represents the dielectric loss in the piezoelectric material

Transfer function

The voltage to velocity transfer function can easily be found as follows. First write down the equations governing the equivalant circuit shown in Fig.(5.3) along with the boundary conditions, as done for the Mason model, and calculate the expression for v_2^p /V. Then find the frequency domain expression, using the arguments given under the Mason model earlier in this section. And this transfer function is given by,

$$H_{tr3}(\omega) = \frac{\phi}{\left(Z_a + Z_b^* + Z_{r2}\right) + Z_b^* \dfrac{\left(Z_a + Z_{r2}\right)}{\left(Z_a + Z_{r1}\right)}} \tag{5.18a}$$

where

$$Z_b^* = Z_b - \frac{\phi^2}{j\omega C_0 + \dfrac{1}{R_0}}, \tag{5.18b}$$

Z_a and Z_b are similar to that given in Eqs.(5.1)(a) and (b) with the complex velocity of sound given in Eq.(5.15).

5.2.2 CALCULATIONS

In this section the impulse response and the transfer function of the transmitting transducer devoloped in the previous section are presented in plots and their behaviours are discussed. The simplified model and the Mason model are compared to demonstrated the effects of $-C_0$.

CALCULATION OF VELOCITY

The velocity output of the transducer, for an arbitrary input voltage can be calculated by convolving the input voltage with the appropriate impulse response found in the previous sections.

$$u(t) = h(t) \otimes v(t) \tag{5.19}$$

or

$$u(t) = \int_0^\infty h(\tau)v(t-\tau)d\tau \tag{5.20}$$

where u(t) is the velocity output of the transducer, h(t) is the impulse response of the transducer and v(t) is the input voltage.

This integral cannot be calculated, by analytical means, for an arbitrary input voltage function. And, even for an input voltage function which gives a closed form for the particle velocity, u(t), the integration is evidently tedious because of the complexity of the expression of the impulse response, h(t). However, in the above integral, the terms involve Dirac delta function, for any input voltage function, can be calculated easily using the symmetry and sifting property of the Dirac delta function.

$$\int_{-\infty}^{\infty} \delta(\tau)v(t-\tau)d\tau = v(t) \tag{5.21}$$

For the above reasons, the terms involve Dirac delta function, in the integral in Eq.(5.20), are calculated analytically and the rest are calculated numerically. A computer program in FORTRAN to calculate the particle velocity, as described above, is given in Appendix(B-3).

IMPULSE RESPONSE

The impulse response of the Mason and the simplified models are given in Eq.(5.7a) and in Eq.(5.12) respectively. These expressions contain Dirac delta functions of various weights. It is not possible to show these delta functions on a plot by direct simulation of the expressions mentioned above. Therefore an approximate impulse response is presented using the following method.

Response, h'(t), to an impulse function, δ(t), is given by

$$h'(t) = h(t) \otimes \delta(t) \tag{5.22}$$

or

$$h'(t) = \int_{-\infty}^{\infty} h(\tau)\delta(t-\tau)d\tau\,. \tag{5.23a}$$

Using the symmetry property of the delta function, Eq.(5.23a) can be written as

$$h'(t) = \int_{-\infty}^{\infty} h(\tau)\delta(\tau-t)d\tau\,. \tag{5.23b}$$

Using the sifting property of the delta function to the above equation gives

$$h'(t) = h(t). \tag{5.23c}$$

The Dirac delta function can be represented as,

$$\delta(t) = g(t) = \lim_{\varepsilon\to 0}\frac{\pi}{2\varepsilon}\sin\left(\frac{\pi t}{\varepsilon}\right) 0 \le t \le \varepsilon\,, \tag{5.24}$$

since g(t) satisfy,

$$\int_{-\infty}^{\infty} g(t)\phi(t) = \phi(0) \tag{5.24a}$$

for an arbitrary function, φ(t), which is continuous at t = 0.

Proof

$$\lim_{\varepsilon\to 0}\frac{\pi}{2\varepsilon}\int_{-\infty}^{\infty}\sin\left(\frac{\pi t}{\varepsilon}\right)\phi(t)dt \cong \phi(0)\frac{\pi}{2\varepsilon}\int_{0}^{\varepsilon}\sin\left(\frac{\pi t}{\varepsilon}\right)dt = \phi(0)\,. \tag{5.24b}$$

A proof comparable to the above is found in Ref.31.

The Fig(5.5)(a) and (b) show the voltage to velocity impulse response of the simplified and the Mason model respectively. The function defined in Eq.(5.24) with $\varepsilon = \tau_0/50$ is used as the voltage impulse for the simulations where τ_0 is the reverberation period of the transducer element. The specifications of PZT-5A with no absorption was used as the parameters of the transducer for simulations. Specifications of PZT-5A are given in Appendix(C-1). The thickness and the radius of the transducer element used for simulations are 10.128mm and 4.51mm respectively. The specific impedance of the backing material and the radiation medium used are 1Mrayl and 419.35rayl respectively.

The Fig.(5.5)(a) can be explained[10] as follows. Suppose a unit voltage impulse is applied to the electrical terminals of the transducer. The mechanical force produced by the piezoelectric(inverse) effect is given by the equations for the transformer in the equivalant circuit of the simplified model. The equations of the simplified model are same as that of the Mason model except for Eq.(5.8). Combining the Eqs.(5.2a) and (5.8) gives the mechanical force, F_{cd}, which is equal to ϕ, for unit impulsive voltage. This force acts on both surfaces of the transducer and produce force waves into the medium and the transducer as shown in Fig.(5.4). Force transmitted into the medium1 is F_1 and into the transducer from face1 is F_0^1. The forces F_2 and F_0^2 are defined in a similar way. The velocity of face1 is v_1 and of face2 is v_2. The characteristic impedance of medium1 is Z_1, of medium2 is Z_2 and of transducer material is Z_0. Consider the front face, face 2, of the transducer. Since the total force on the mass less plane is zero,

$$(F_2 - F_0^2) = \phi \tag{5.25}$$

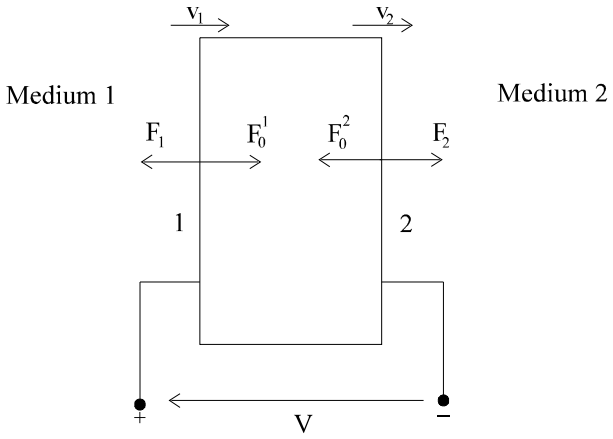

Figure(5.4) Forces and velocities on the transducer faces immediately after the voltage impulses is applied to the electrical terminals.

The characteristic impedance of the medium and the transducer material, the forces and the velocities, according to the directions shown in the Fig.(5.4), have the following relationships.

$$Z_0 = -F_0^2/v_2 \qquad \text{and} \qquad Z_2 = F_2/v_2 \tag{5.26}$$

From the above two equations,

$$F_2 = \frac{\phi}{Z_0 + Z_2} Z_2 \tag{5.27a}$$

and

$$F_0^2 = -\frac{\phi}{Z_0 + Z_2} Z_0. \tag{5.27b}$$

With similar arguments it can be shown that,

$$F_1 = \frac{\phi}{Z_0 + Z_1} Z_1 \tag{5.27c}$$

and

$$F_0^1 = -\frac{\phi}{Z_0 + Z_1} Z_0 \qquad (5.27d)$$

The transmitted force waves in to medium1 and medium2 will never come back because of the asssumption of the model that the medium1 and 2 are of infinite extend. The waves transmitted into the transducer element propagate as plane waves and at discontinuties a portion reflected back and the rest transmitted into the medium. The reflected and transmitted portions can be calculated using reflection and transmission coefficients. These coefficients can be found in any text book on waves, see, for instance, page 126 of Ref.(1). The reflection coefficients of face1 and 2, r_1 and r_2 respectively, are defined in Eq.(5.7e). The transmission coefficients of face 1 and 2 are, then, given by $(1 + r_1)$ and $(1 + r_2)$ respectively. It should be noted here that the coefficients are defined for waves incident on the transducer-medium interface from the medium. For waves travelling in the opposite directions, the reflection coefficients, r_1 and r_2, should have a minus sign infront of them and hence the corresponding transmission coefficients are given by $(1 - r_1)$ and $(1 - r_2)$.

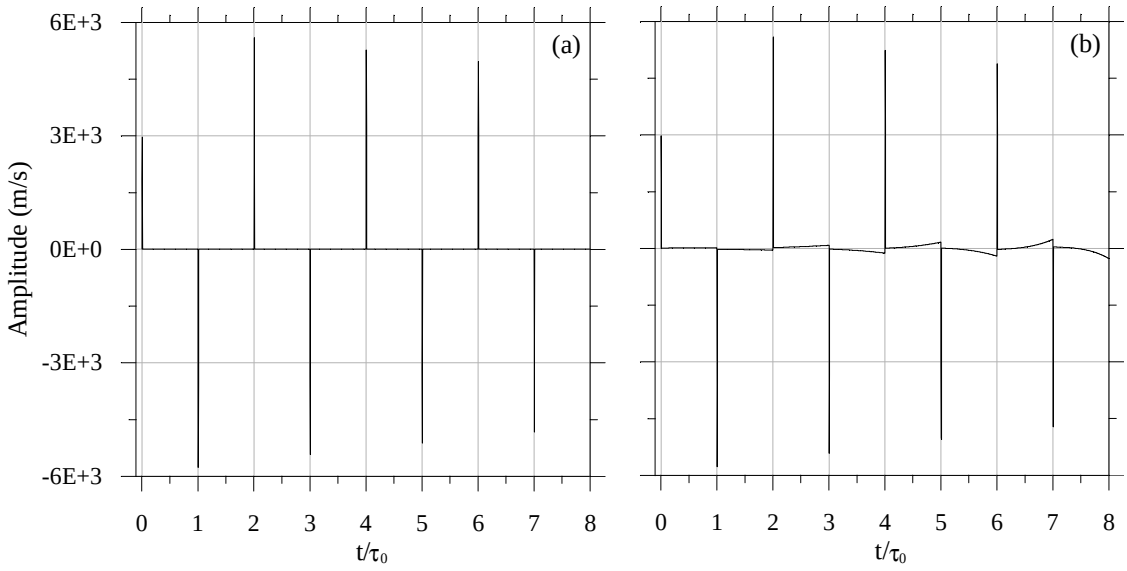

Figure(5.5) Impulse response of transmitting transducer. (a) Simplified model (b) Mason model. The time axis is normalised to $\tau_0 (= \ell/c)$, the reverberation period.

The quantity considered and calculated in this discussion is force. To calculate the velocity one has to use the Eq.(5.26).

Now, F_2 is the magnitude of the first wave that comes out from the transducer front face at time t = 0. And this can easily be identified, with Eq.(5.26), as the first term in the voltage to velocity impulse response in Eq.(5.12). The second term in the voltage to velocity impulse response corresponds to the transmitted part of the wave that comes from the back face, face1, at time $t = \ell/c$ and is given by $(1-r_2)F_0^1$. Substituting for r_2 from Eq.(5.7e) and F_0^1 from Eq.(5.27d) and substituting for r_1 in the second term of Eq.(5.12), with Eq.(5.26), give the same result, $-\frac{2\phi Z_0}{(Z_0 + Z_{r1})(Z_0 + Z_{r2})}$. The third term corresponds to the wave sent into the element from the front face at time t = 0 and transmitted into the medium2 through the front face at time $t = 2\ell/c$ after one reflection at the back face, face1 at $t = \ell/c$. And this is given by -

$r_1(1-r_2)F_0^2$. Similarly, the magnitude and the placement in time of the rest of the terms in the voltage to velocity impulse response can easily be verified.

As described above, there is no response from the transducer between the reverberation periods. But this is not true for a real transducer. The response of the transducer in between the reverberation periods are shown in Fig.(5.5)(b). Obviously, the $-C_0$ in the equivalent circuit is responsible for the additional response. The mathematical result does not tell anything about the physical insight of this behaviour. Discussions on this problem can be found in the litrarure. The effect of $-C_0$, also known as regeneration effect, on pulse forming will be discussed in this section.

The effect of the $-C_0$ on a uniform sinusoidal pulse is shown in Fig(5.6). The response of the transducer for a 4-period uniform sinusoidal pulse is calculated using the two models. The frequency of the pulse was equal to the half wave resonance frequency of the transducer and the amplitude was 1 volt. The specification of the transducer was the same as that used for the simulation of impulse responses above.

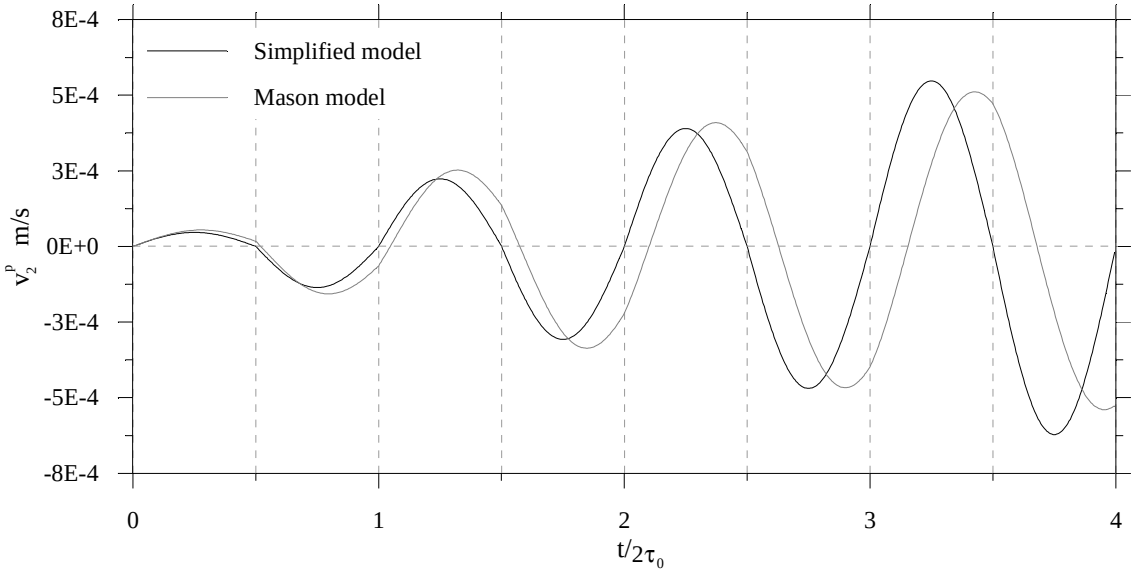

Figure(5.6) Response of the transducer models to a 4 - period uniform sinusoidal pulse. The time axis is normalised to $2\tau_0 = 2\ell/c$, which is also equal to the period of the input signal.

Consider the response of the simplified model in Fig.(5.6). This response was calculated using the Eq.(5.19) with

$$h(t) = h_{tr2}(t)$$

where $h_{tr2}(t)$ is given by Eq(5.13) and,

$$v(t) = \sin\omega t \qquad 0 \leq t \leq 8\tau_0,$$

where $\omega = \pi/\tau_0$ and τ_0 is the reverberation time of the transducer element. The convolution of the uniform sinusoidal function with the delta functions result again uniform sinusoidal functions of the same frequency as the original sinusoidal function and with pure time delays. This time delays, given by the corresponding delta functions, are integer multiples of τ_0. The amplitudes are equal to the amplitude of the input function multiplied with the weight of the

corresponding delta function which are just real numbers. Therefore the total response, the summation of the functions resulted from the convolutions, becomes as a sinusoidal function of the same frequency as the original function and the zero crossings coincide with the integer multiples of τ_0.

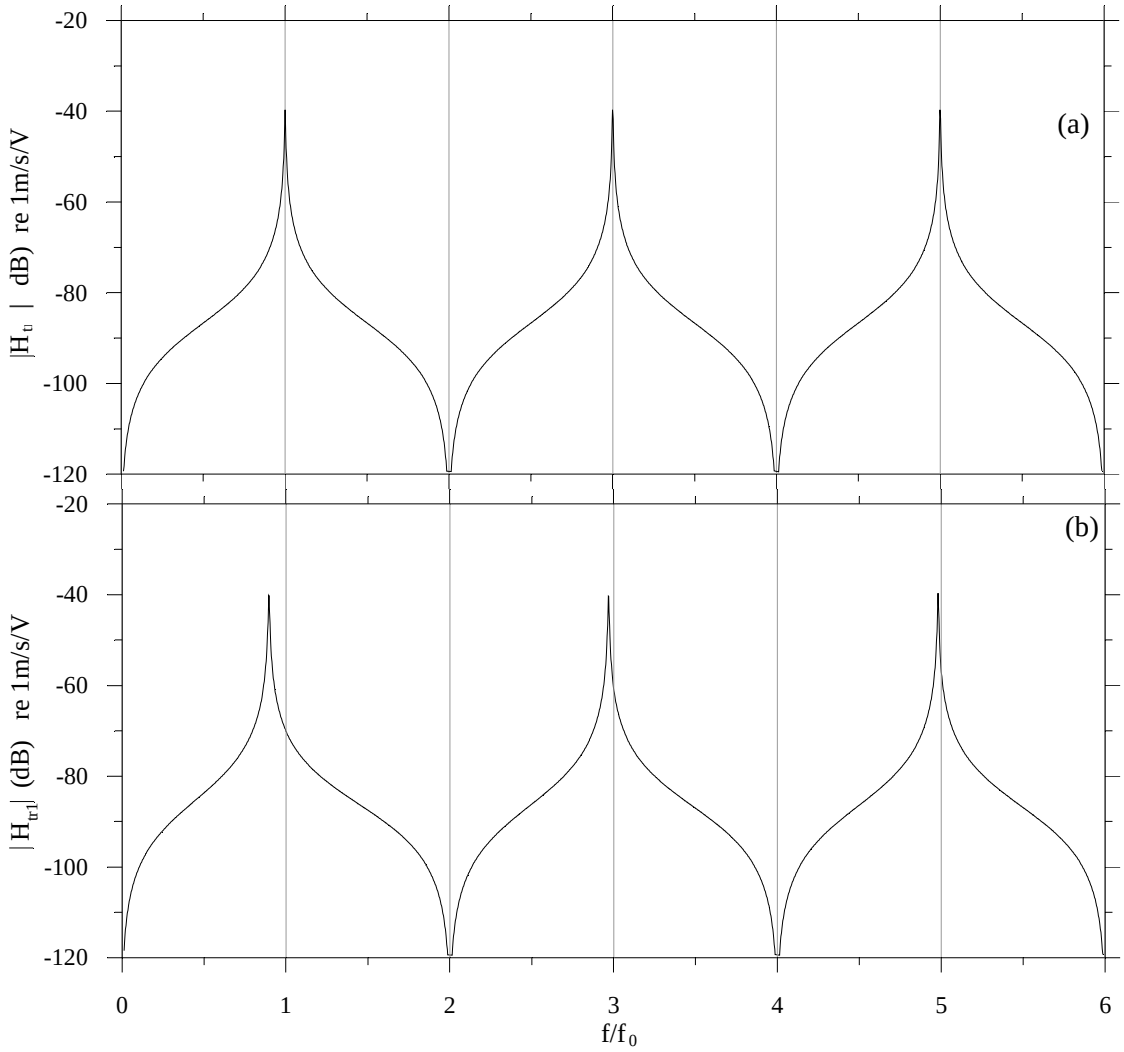

Figure(5.7) The magnitude of the voltage to velocity transfer function. (a) Simplified model, (b) Mason model. Frequency axes are normalised to the half-wave resonance frequency, f_0.

In addition to the delta functions, the impulse response of the Mason model contains response due to the regeneration effect. Since this response acts in the same direction with the delta functions the signal, in the first couple of periods, is larger than that of the simplified model. But, later the regenerative response becomes larger and the delta functions become small. Therefore, the signall becomes smaller than that of the simplified model. The later behaviour of the transducer is not shown as only 8 terms in the impulse response is avaialble(rest are not calculated because of the large size of the expressions). In Fig.(5.13), the impulse response upto 40 reverberation periods, calculated using the frequency domain calculations, is shown.

The Fig.(5.7)(a) and (b) show the magnitude of the voltage to velocity transfer function of the simplified and the Mason model respectively. The frequency axes are normalised to the half-wave resonance frequency, $f_0 = 2\ell/c$. The transfer function of the simplified model, as anticipated, has a resonance at frequency $f = f_0$. But the Mason model reveals the resonance of

the transfer function at a frequency which smaller than f_0. This is, evidently, a consequence of the negative capacitance, $-C_0$, in the equivalent circuit of the Mason model.

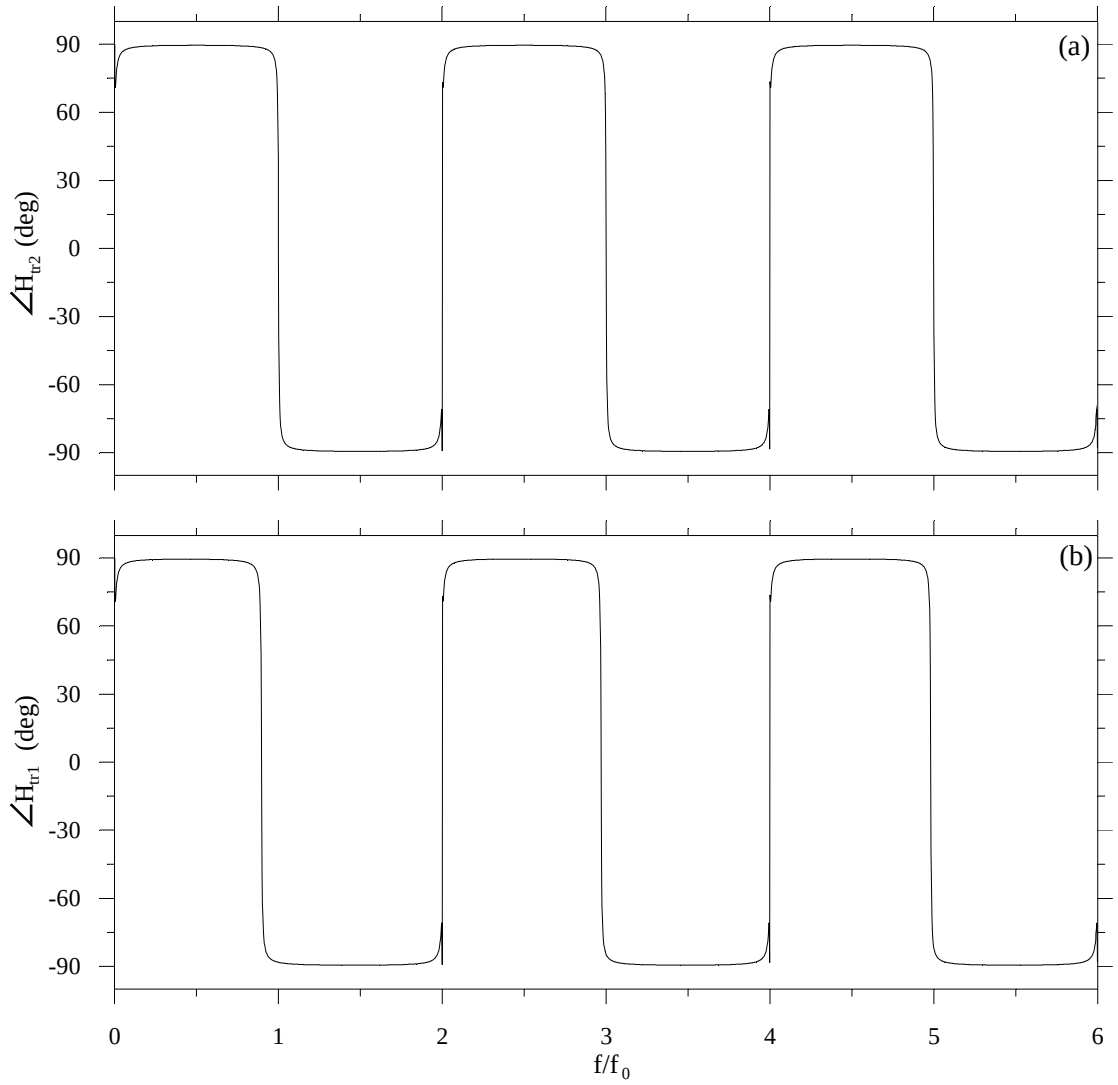

Figure(5.8) The phase response of the voltage to velocity transfer function. (a) Simplified model, (b) Mason model. Frequency axes are normalised to the half-wave resonance frequency, f_0.

Fig.(5.8)(a) and (b) show the phase response of the voltage to velocity transfer function of the simplified and the Mason model respectively. The plots start at 90deg. and go down and increase again. This behaviour repeats at every zeros of the transfer function. From the Fig.(5.9) it can be seen that this effect increases with the backing impedance for a constant radiation medium(air). But this effects of the backing impedance are not analysed in detail in this thesis. However, for the backing impedance, 0.3Mrayl, used in all the simulations presented in this work, the frequency components at the neighbourhood of the zeros of the transfer function have magnitudes, roughly, more than 60dB down to the maximum and hence will not alter the shape of the signal very much.

Even though the behaviour of the transfer function with backing impedance is not analysed thoroughly, the general tendancy of the transfer function of the simplified model can be easily checked for some special cases. Consider the case where the backing impedance is same as that of the radiation medium. That is $Z_{r1} = Z_{r2}$. Then the Eq.(5.9) becomes as,

$$H_{tr2}(\omega) = \frac{\phi}{(Z_a + 2Z_b + Z_{r2})}. \tag{5.28a}$$

Using the expressions for Z_a and Z_b in Eqs.(5.1a) and (5.1b), the above equation can be written as,

$$H_{tr2}(\omega) = \phi \frac{j \tan\left(\frac{\pi}{2}\frac{\omega}{\omega_0}\right)}{Z_0 + jZ_{r2}\tan\left(\frac{\pi}{2}\frac{\omega}{\omega_0}\right)} = \phi \frac{j}{Z_0 \cot\left(\frac{\pi}{2}\frac{\omega}{\omega_0}\right) + jZ_{r2}}, \tag{5.28b}$$

where $\omega_0 = \pi c/\ell$.

The argument of the numerator of the Eq.(5.28b) is $\pi/2$. At very low frequencies, $\omega \ll \omega_0$, the argument of the denominator is almost zero. Therefore the argument of H_{tr2} is $\pi/2$. As ω increases the argument of the denominator increases steadily and hence the argument of H_{tr2} decreases steadily. This is true for any value of $Z_{r2} < Z_0$. But, the size of Z_{r2} will decide how fast the argument of H_{tr2} would decrease. This is shown in Fig.(5.9) using the impedance of air and 10Mrayl. At $\omega = \omega_0$, the argument of the denominator is $\pi/2$ and hence the argument of H_{tr2} is zero. When $\omega > \omega_0$, the argument of H_{tr2} is approximately $-\pi/2$ and as ω increases it reaches $-\pi/2$. At $\omega = 2\omega_0$, the argument of H_{tr2} again becomes $\pi/2$. The magnitude of the transfer function is zero at very low frequencies, increases with ω and reaches the maximum, ϕ/Z_{r2}, at $\omega = \omega_0$ and then decreases with ω to zero at $\omega = 2\omega_0$.

The other special case is "matched backing". That is, the impedance of the backing material is same as that of the transducer material, $Z_{r1} = Z_0$(= 33.75Mrayl). A direct simplification of Eq.(5.9) may not be easy for this case. But, imposing this condition in Eqs.(5.10) and (5.11), remembering $s = j\omega$ and some simple manipulations will give the following expression for the transfer function. That is,

$$H_{tr2}(\omega) = \frac{\phi(1-r_2)}{2Z_{r2}} 2\sin\left(\frac{\pi}{2}\frac{\omega}{\omega_0}\right) e^{-j\frac{\pi}{2}\left(1-\frac{\omega}{\omega_0}\right)}. \tag{5.29}$$

The phase of the above function decreases linearly from $\pi/2$ to $-\pi/2$, while the frequency increases from zero to $2\omega_0$ and at $\omega = 2\omega_0$, the phase changes sudenly back to $\pi/2$. At $\omega = \omega_0$, the phase is zero. The magnitude varies sinusoidaly because of the sine term in the expression. This transfer function is compareable to that of the point receiver on axis propagation model in Chapter 4. As this model, the above perticular case of the transducer model has two delta function in its impulse response; one from the front face of the transducer and the other from the back face, all the others are totally lost in the backing medium.

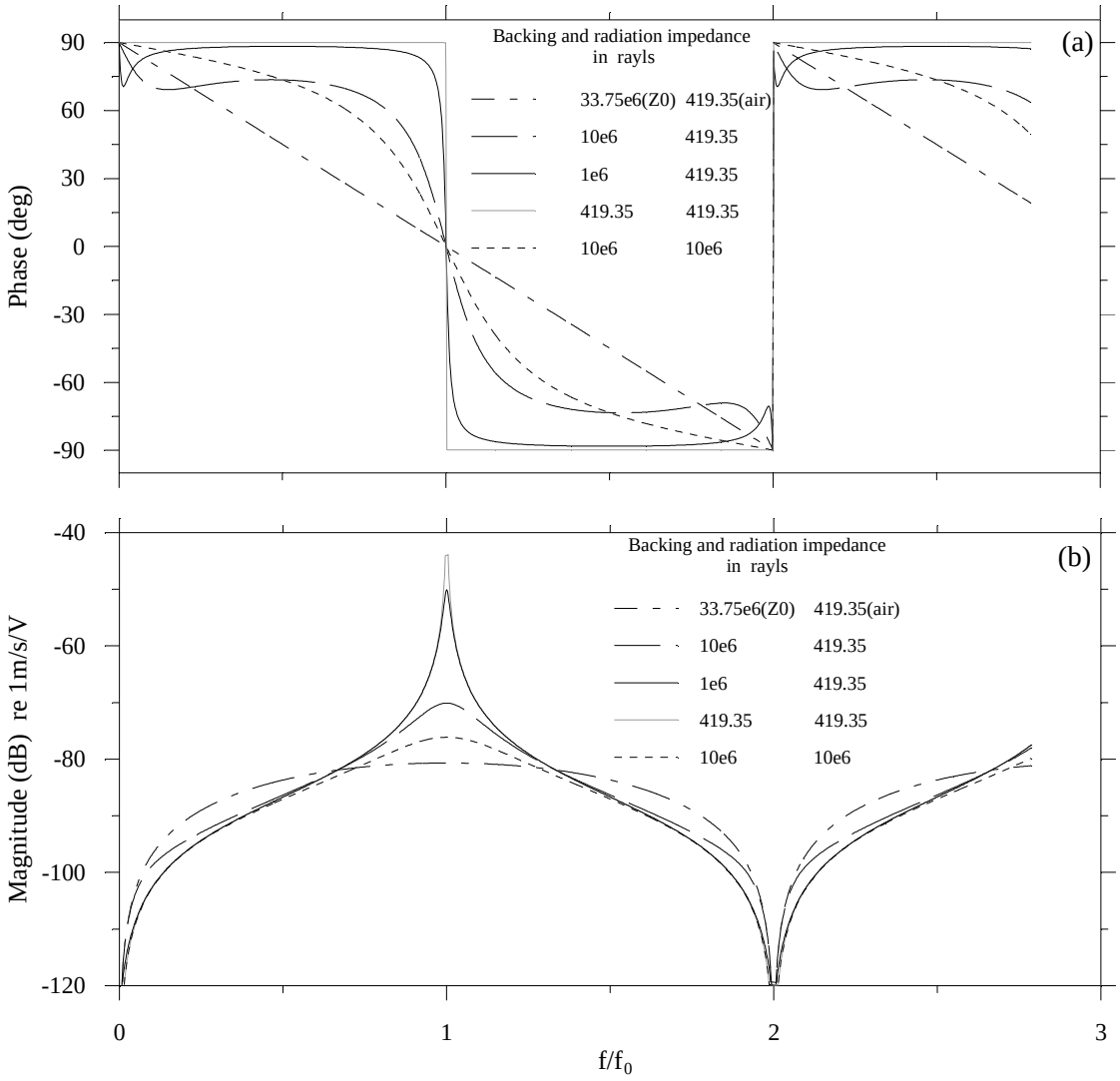

Figure (5.9) The voltage to velocity transfer function of the simplified model for some special set of backing and radiation impedance. (a) Phase and (b) Magnitude. The frequency axes are normalised to the half wave frequency of the transducer element.

MODEL COMPARISON

The basic transducer action is explained using a simple plane wave model. And, how the regeneration is superimposed with the principal response is also demonstrated. Forming of the velocity pulse for a 4-period sinusoidal voltage pulse is explained. The effect of regeneration also demonstrated. All these calculations were done using the time domain methods. But, however, the time domain method, as pointed out at the beginning of this section, is tedious and thus limited. There fore, for calculations of signals required in the rest of this chapter and in Chapter 6, TRANSCAD and FLOSIM models are used. But, before making results using this models, it is reasonable to compare these models with the Mason model. The impulse response is being taken to begin with.

The impulse response contains Dirac delta functions. These delta functions were modelled and presented, using a high frequency(10.75MHz) half sine wave as the voltage input, in Fig.(5.5). Simulating the velocity function for such a high frequency voltage pulse in FLOSIM requires a large memory. Thus a same kind of treatment for the delta functions as

shown in Fig.(5.5) is not possible. Therefore, the regenerative response, in the impulse response, only matched with the similar response of the Mason model.

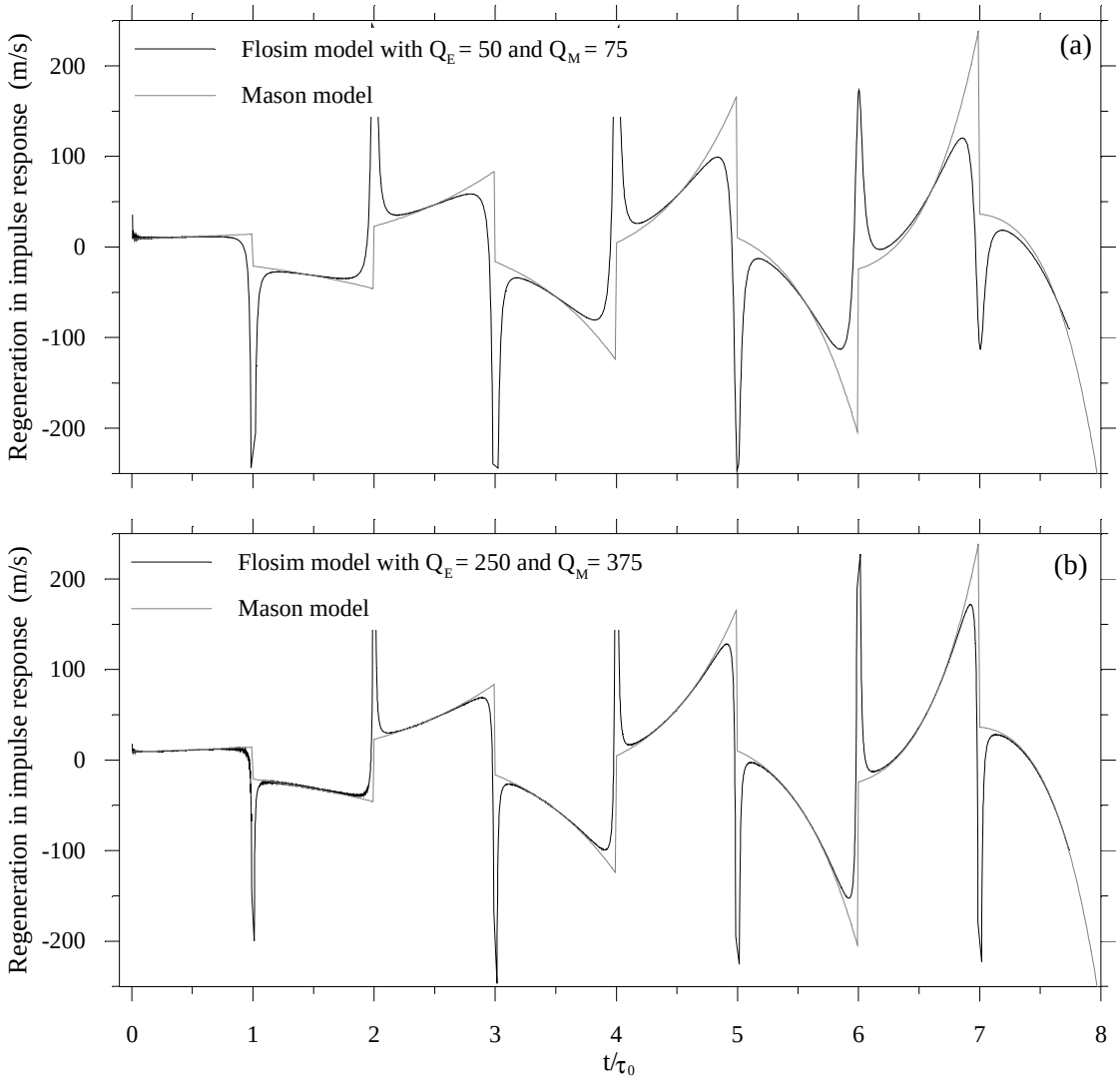

Figure(5.10) Regeneration in the impulse response of Transcad and Mason models for two different sets of absorption parameters, (a) Q_E = 50,Q_M = 75 and (b) Q_E = 250,Q_M = 375.

In the Fig(5.10) the regenerative response in the impulse response of the Mason model is compared with that of the FLOSIM model for two different sets of absorption parameters. The radius and the thickness of the element used in the simulation are 4.51mm and 10.128mm respectively. The specifications of PZT-5A was used for the material constants of the transducer element in both cases except for the absorption parameters for the plot in Fig.(5.10)(b).

The Flosim model calculates the impulse response by inverting the frequency domain transfer function using IFFT. Thus the delta functions cannot be left out. Therefore the response of the Flosim model in Fig.(5.10) contains some portion of the delta functions. The plots Fig.(5.10)(b) are in more agreement than the plots in Fig.(5.10)(a). This is because, the absorption in the FLOSIM model in Fig.(5.10)(b) is smaller, which corresponds to larger Q values, than that of in Fig.(5.10)(a). Because of the large absorption, the delta functions in Fig.(5.10)(a) are broadened by smearing effect and this can make the system non causal.

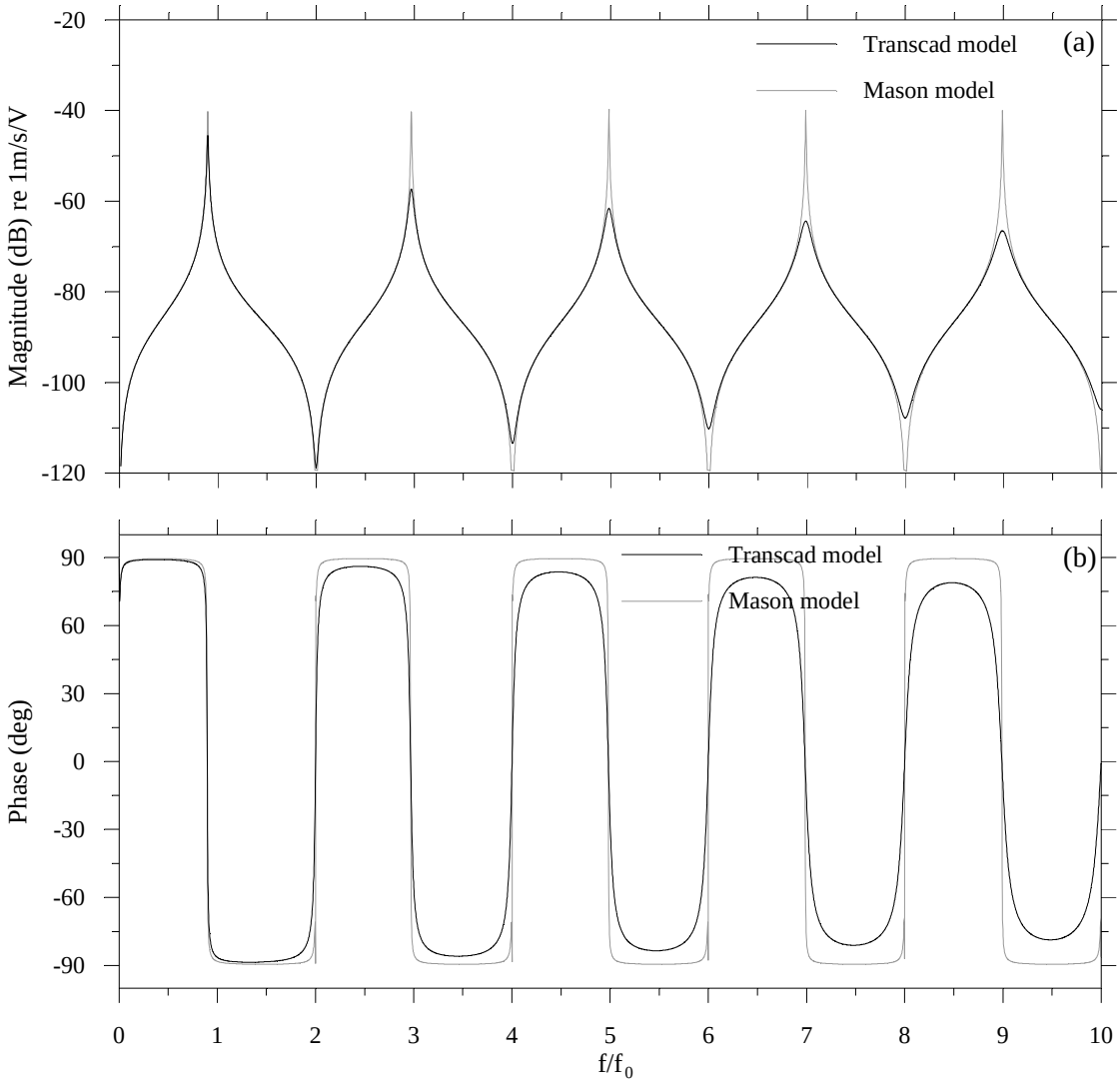

Figure(5.11) Voltage to velocity transfer functions of the transmitter due the Transcad model and the Mason model, (a)magnitude and (b)Phase. The frequency axis is normalised to the half wave frequency, $f_0 = c/2\ell$, of the transducer element.

The voltage to velocity transfer functions of the transmitting transducer due to Transcad and the Mason models are compared in Fig.(5.11). The plots are in good agreement. The plots due to Transcad is diminishing with frequency because of the absorption. Absorption increases with frequency. Since always there is a response from the front face of the transducer, the transfer function approaches a finite value. At this high frequencies the wave produced by the back face does not reach the front face, completely absorbed by the transducer material. The phase of the emerging wave is zero, ie., it follows the exciting voltage wave.

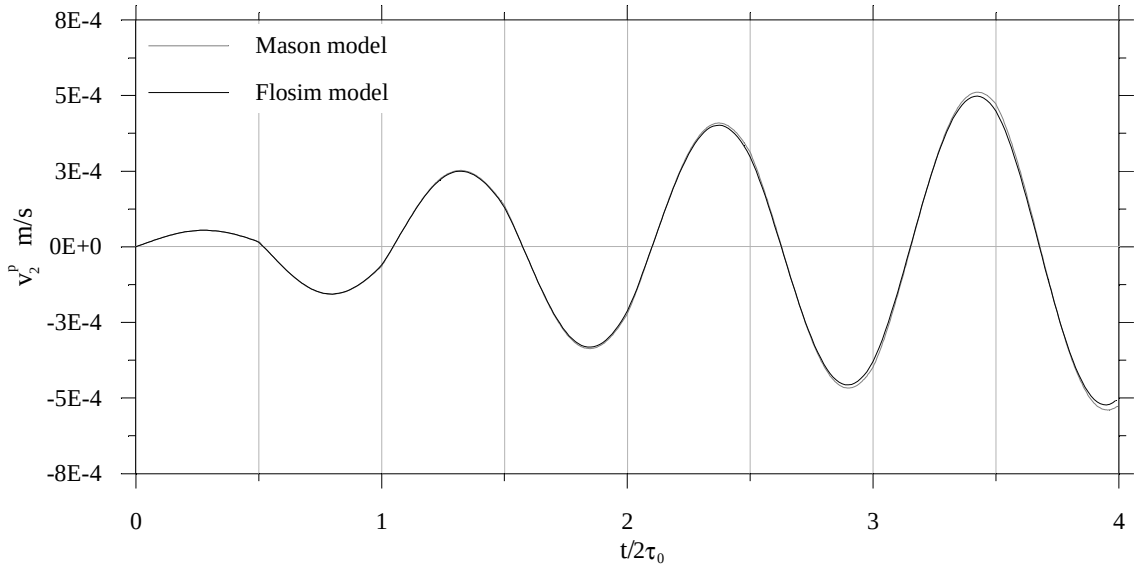

Figure(5.12) Velocity output for a 4-period uniform sinusoidal voltage input due to Transcad and Mason models.

The response of the transducer element for a 4-period sinusoidal voltage input calculated by Transcad and Mason models are compared in Fig.(5.12). At the beginning, both signals are prety much the same. But as the time increases the signal, while it travels back and forth in the transducer, looses energy to absorption. This is the reason the signal calculated by the Flosim model is smaller than that of the Mason model.

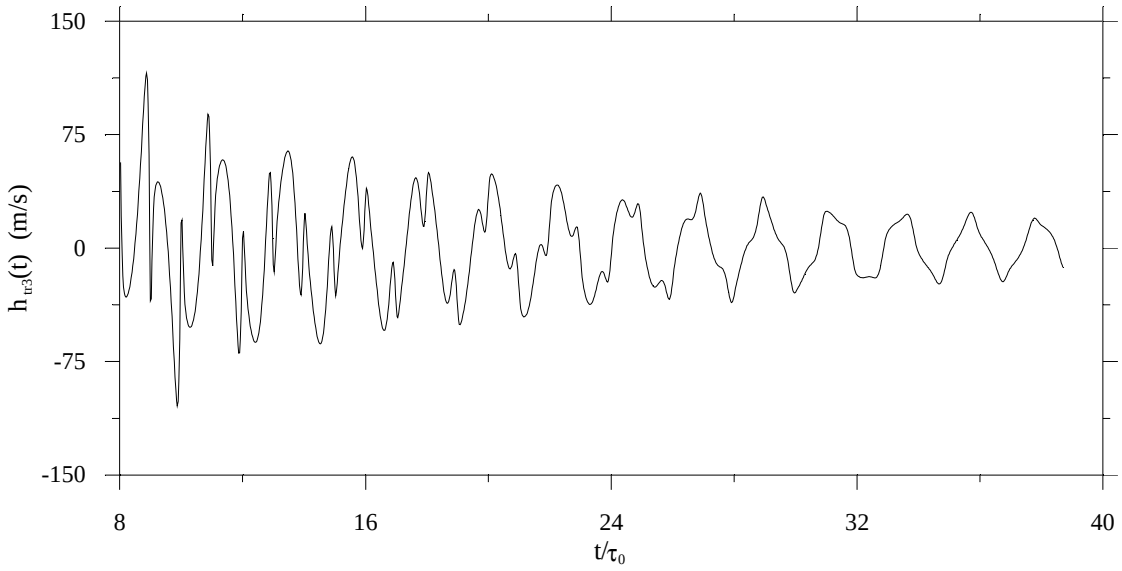

Figure(5.13) Impulse response of the transducer element up to 40-reverberation periods due Flosim model. Absorption parameters $Q_E = 50$ and $Q_M = 75$.

The Fig.(5.13) shows the impulse response from the 8th reverberation period up to the 40th reverberation period. The simulation was made for a PZT-5A transducer element with the same dimensions as before. As time goes on the deltafunctions become smaller and the response being smoothed out.

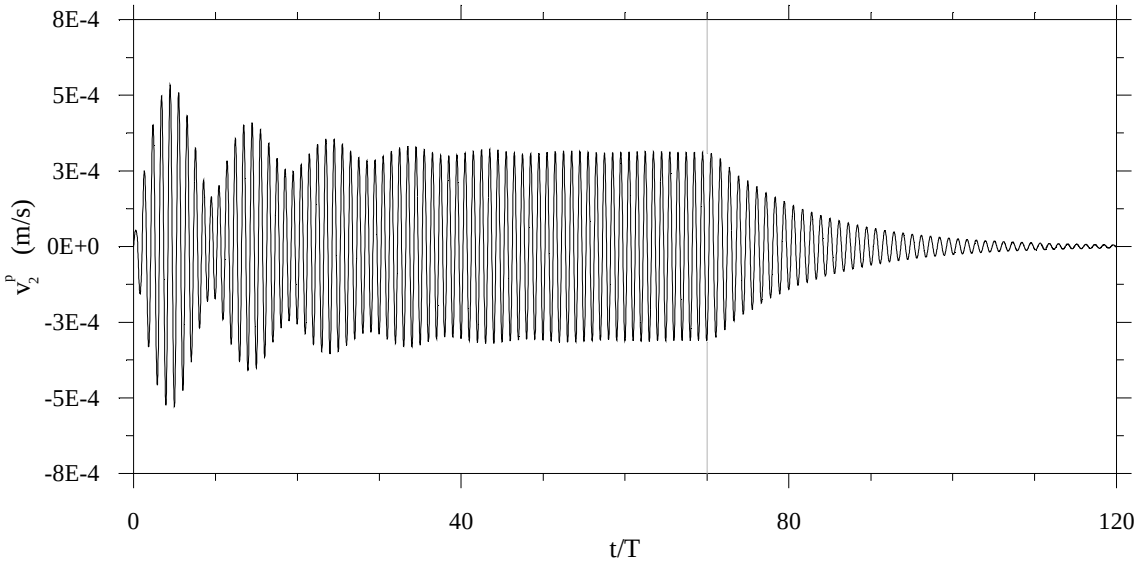

Figure(5.14) Velocity output for a 70-period uniform sinusoidal voltage input due to Flosim model. The time axis is normalised to the period of the input signal.

The Fig.(5.14) shows the velocity output of the transducer element for a 70-period uniform sinusoidal voltage input calculated by the Flosim model. The time axis is normalised to the period of the input signal. Since there is no driving force the signal dies off after 70 periods. The oscillating behaviour of the onvelope of the signal is also a consequence of the $-C_0$ in the equivalant circuit of the transducer model. The transducer element has the resonance frequency at little less than 215kHz and the exciting frequency is 215kHz. This two frequencies interact and give a beating type effect, seen in the transient part of the signal. This fact is discussed in little more detail in Chapter 6.

5.3 RECEIVER

In this section, free field pressure to open circuit voltage transfer function and the corresponding impulse response of a piezo electric receiving transducer are developed and their behaviours are presented in plots.

5.3.1 THEORY

A piezo electric element, which is similar to that used as the transmitter, in all respects, is used as a receiver. In the derivation of the equivalent circuit of the transmitter, a one-dimensional wave equitation is solved for the appropriate boundary conditions. There is no presumption to distiguish the derivation is for the transmitter. Therefore, the same equivalent circuit used for the transmitter, with the appropriate boundary conditions, can be used for receiver.

5.3.1.1 MASON MODEL

The Fig.(5.15) shows the cross-sectional view of the receiving transducer element. The cross-section lies on a plane parallel to the electrical field and perpendicular to the active surface. The area of the active face is A. Plane waves incident, normally, on the element. v_1^p and v_2^p are the particle velocities of the transducer faces and F_1^p and F_2^p are forces on the transducer element from the medium. The velocities and forces are taken to be positive in their respective directions shown in the figure.

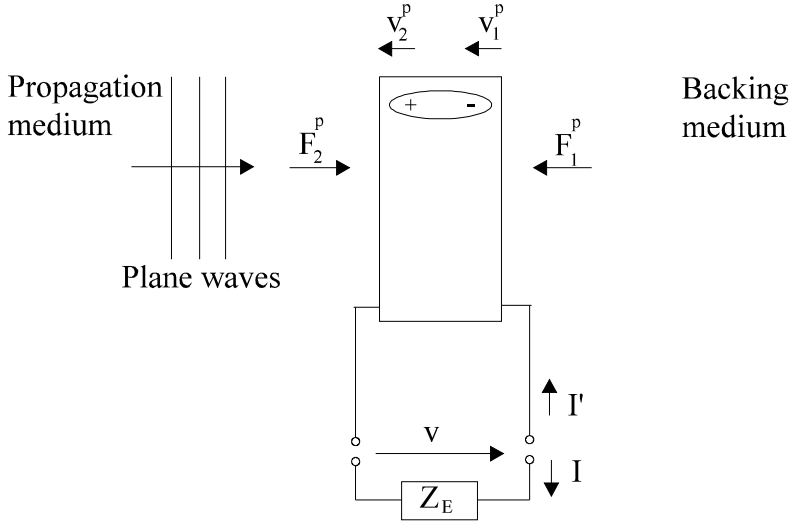

Figure 5.15 Cross-sectional view of plane waves incident on the receiving transducer. Cross-section is parallel to the electrical field and perpendicular to the active face of the element

The Fig.(5.16) shows the equivalent circuit of the receiving transducer. In the receiving mode, Z_{r2} is the input mechanical impedance of the transducer element. That is, $Z_{r2} \equiv Z_{in}$.

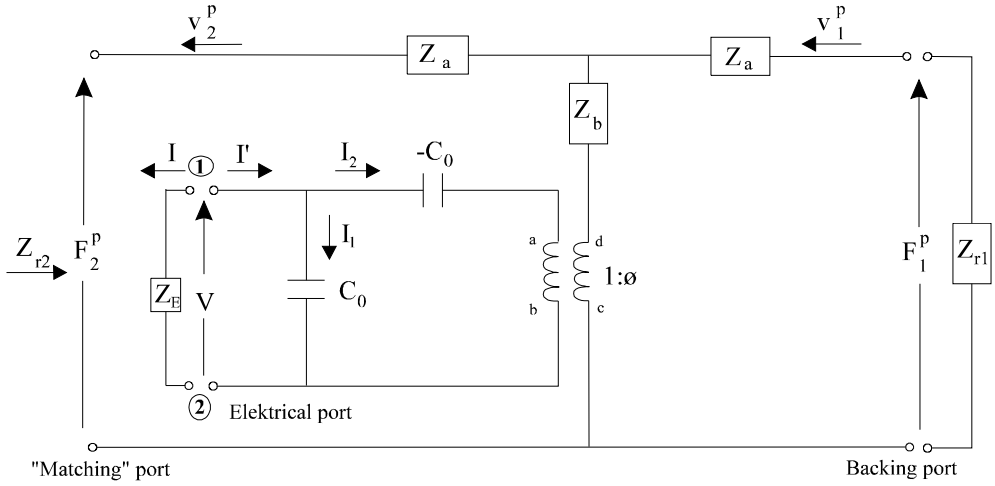

Figure(5.16) Equivalant circuit of the Mason model for the receiving transducer element.

The equations governing the above equivalent circuit, using basic network analysis laws, are found as follows.

For the transformer,

$$V_{ba} = \frac{F_{cd}}{\phi} \tag{5.30a}$$

and

$$(v_1^p - v_2^p)\phi = -I_2 \tag{5.30b}$$

and for the rest of the circuit,

$$V = \frac{I_2}{j\omega(-C_0)} + V_{ba}, \tag{5.30c}$$

$$V = IZ_E \tag{5.30d}$$

$$I' = I_1 + I_2, \tag{5.30e}$$

$$I = -I', \tag{5.30f}$$

$$F_1^p = (Z_a + Z_b)v_1^p - Z_b v_2^p + F_{cd} \tag{5.30g}$$

and

$$F_2^p = Z_b v_1^p - (Z_a + Z_b)v_2^p + F_{cd}. \tag{5.30h}$$

The boundary conditions give,

$$F_1^p = - Z_{r1}\, v_1^p, \tag{5.30i}$$

$$F_2^p = - Z_{r2}\, v_2^p. \tag{5.30j}$$

At open circuit condition $Z_E = \propto$ and $I = 0$.

TRANSFER FUNCTION

Using the Eqs.(5.30), the relationship between the velocity and the open circuit voltage is found as,

$$\frac{V}{v_2^p} = \frac{-\phi(Z_a + Z_{r1})}{j\omega C_0 (Z_a + Z_b + Z_{r1})}. \tag{5.31}$$

If the velocity input, $v_2^p(t)$ is assumed to be an exponential function, $e^{j\omega t}$, then the open circuit voltage output will be,

$$V(t) = \frac{-\phi(Z_a + Z_{r1})}{j\omega C_0 (Z_a + Z_b + Z_{r1})} \cdot e^{j\omega t}. \tag{5.31a}$$

Assuming the system to be linear, the open circuit voltage output for an arbitrary velocity function can be written[9] as,

$$V(\omega) = \frac{-\phi(Z_a + Z_{r1})}{j\omega C_0 (Z_a + Z_b + Z_{r1})} \cdot V_2^p(\omega), \tag{5.31b}$$

where $V_2^p(\omega)$ and $V(\omega)$ are Fourier transforms of $v_2^p(t)$ and $V(t)$ respectively.

$$V(\omega) = H'_{re1}(\omega) \cdot V_2^p(\omega), \tag{5.31c}$$

where,

$$H'_{re1}(\omega) = \frac{-\phi(Z_a + Z_{r1})}{j\omega C_0 (Z_a + Z_b + Z_{r1})}, \tag{5.31d}$$

the velocity to open circuit transfer function of the receiving transducer.

But, the desired one is the transfer function is the one from the free field pressure, P, to open circuit voltage, V. This transfer function, $H_{re1}(\omega)$, can be written as,

$$\frac{V(\omega)}{P(\omega)} = \frac{V(\omega)}{V_2^p(\omega)} \cdot \frac{V_2^p(\omega)}{P(\omega)}. \tag{5.32}$$

The first term in Eq.(5.32) is found in Eq.(5.31d) and the second term is found in Eq.(3.5) in Chapter 3. The Fig.(3.2) in Chapter 3 shows the equivalant circuit representing plane waves incident on the receiving transducer, where P_4 is the free field pressure, Z_{in} is the input mechanical impedance of the receiving transducer, U is the particle velocity of the transducer face, Z_r is the radiation impedance and A is area of receiver. The notations in Fig.(3.2) have the following relationship with the notations used in this chapter; $P_4 \equiv P$, as pointed in the beginning of this section $Z_{in} \equiv Z_{r2}$, $U = -V_2^p$. Then the Eq.(3.5) in the present notation would be,

$$\frac{V_2^p}{P} = -2\frac{A}{Z_{r2} + Z_r}. \tag{5.33}$$

Combining Eqs.(5.31d) and (5.33) gives,

$$H_{re1}(\omega) = \frac{2A\phi}{j\omega C_0} \frac{(Z_a + Z_{r1})}{(Z_a + Z_b + Z_{r1})(Z_r + Z_{r2})}. \tag{5.34}$$

Using the Eqs.(5.30), Z_{r2} is found as,

$$Z_{r2} = Z_r + Z_a + Z_b - \frac{Z_b^2}{Z_a + Z_b + Z_{r1}} \tag{5.35}$$

Substituting for Z_{r2} in (5.34) gives,

$$H_{re1}(\omega) = \frac{2A\phi}{j\omega C_0} \frac{(Z_a + Z_{r1})}{(Z_a + Z_b + Z_{r1})\left(Z_r + Z_a + Z_b - \dfrac{Z_b^2}{Z_a + Z_b + Z_{r1}}\right)} \tag{5.36a}$$

or

$$H_{re1}(\omega) = \frac{2A\phi}{j\omega C_0} \frac{(Z_a + Z_{r1})}{(Z_a + Z_r)(Z_a + Z_b + Z_{r1}) + Z_b(Z_a + Z_{r1})} \tag{5.36b}$$

or

$$H_{re1}(\omega) = \frac{2A}{j\omega C_0} \frac{\phi}{(Z_a + Z_b + Z_r) + Z_b \dfrac{(Z_a + Z_r)}{(Z_a + Z_{r1})}} \tag{5.36c}$$

IMPULSE RESPONSE

The inverse Fourier transform of the Eq.(5.36c), in principle, will give the impulse response. But, for the same reasons stated under the sec(5.2.1.1), Eq.(5.36c) is transformed to Laplace domain. The Eq.(5.36c) looks the same as Eq.(5.9) except the factor $2A/j\omega C_0$. Therefore, the free field pressure to open circuit voltage transfer function, $H_{re1}(s)$, can be written in the Laplace domain as,

$$H_{re1}(\omega) = \frac{A\phi(1 - r_0)}{sC_0 Z_r} \frac{1 - (1 + r_l)e^{-s\tau_0} + r_l e^{-2s\tau_0}}{1 - r_l r_0 e^{-2s\tau_0}} \tag{5.37a}$$

where

$$r_0 = \frac{Z_0 - Z_r}{Z_0 + Z_r} \qquad \text{and} \qquad r_l = \frac{Z_0 - Z_{r1}}{Z_0 + Z_{r1}} \tag{5.37b}$$

Taking inverse Laplace transform of Eq.(5.37a) gives,

$$h_{re1}(t) = \frac{A\phi(1 - r_0)}{C_0 Z_r} \begin{Bmatrix} u(t) - (1 + r_l)u(t - \tau_0) & + r_l(1 + r_0)u(t - 2\tau_0) \\ -r_l r_0(1 + r_l)u(t - 3\tau_0) & + r_0 r_l^2(1 + r_0)u(t - 4\tau_0) \\ -r_l^2 r_0^2(1 + r_l)u(t - 5\tau_0) & + r_0^2 r_l^3(1 + r_0)u(t - 6\tau_0) \\ \cdots & \cdots \\ \cdots & \cdots \end{Bmatrix} \tag{5.38}$$

5.3.1.2 TRANSCAD MODEL

The Fig.(5.17) shows the equivalent circuit of the receiver due to the Transcad model.

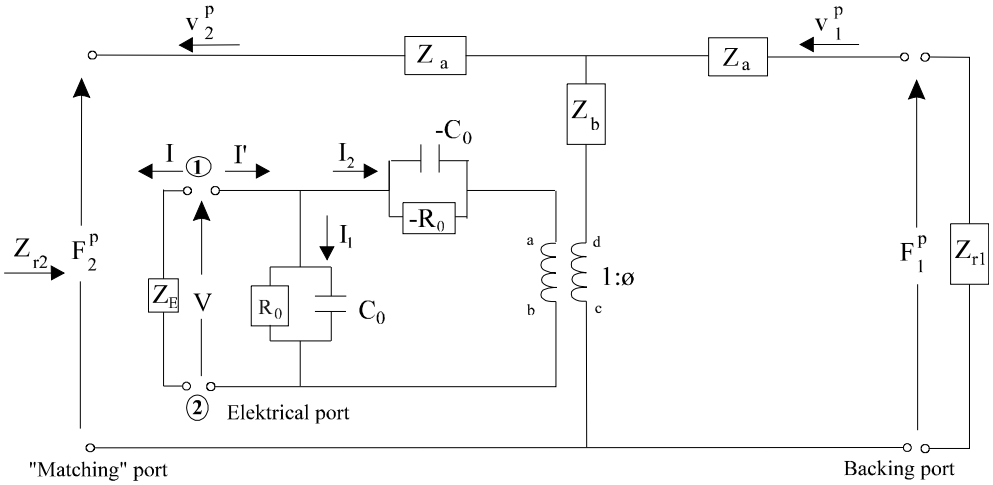

Figure 5.17 Equivalant circuit of the distributed, lossey model for the receiving transducer element.(From Ref.3)

TRANSFER FUNCTION

The free field pressure to open circuit voltage transfer function of the receiver, $H_{re3}(\omega)$, due to the Tranacad model is given by,

$$H_{re3}(\omega) = \frac{V(\omega)}{P(\omega)} = \frac{2A}{\left(\frac{1}{R_0} + j\omega C_0\right)} \frac{\phi}{(Z_a + Z_b + Z_r) + Z_b \dfrac{(Z_a + Z_r)}{(Z_a + Z_{r1})}}. \qquad (5.39)$$

This transfer function is not explicitly given in the Transcad report[3]. But it can easily be found using the following equations in the TRANSCAD report. Substituting the Eq.(2.1.1) with $\theta = 0$, Eq.(2.2.3) with $Z_N^m = Z_{r2}$, Eq.(2.2.5) for the no matching condition, and Eq.(2.2.14) with $Z_E = \infty$ in the Eq.(2.1.3) gives the transfer function, $H_{re3}(\omega)$. Z_{r2} can be found from the Eq.(2.2.13) imposing the condition $Z_E = \infty$.

5.3.2 CALCULATIONS

In this section the impulse response and the transfer function of the receiving transducer, developed in the previous section, are presented in plots and the behaviour of the plots are discussed.

IMPULSE RESPONSE

The Fig.(5.18) shows the free field pressure to open circuit impulse response of the receiving transducer.

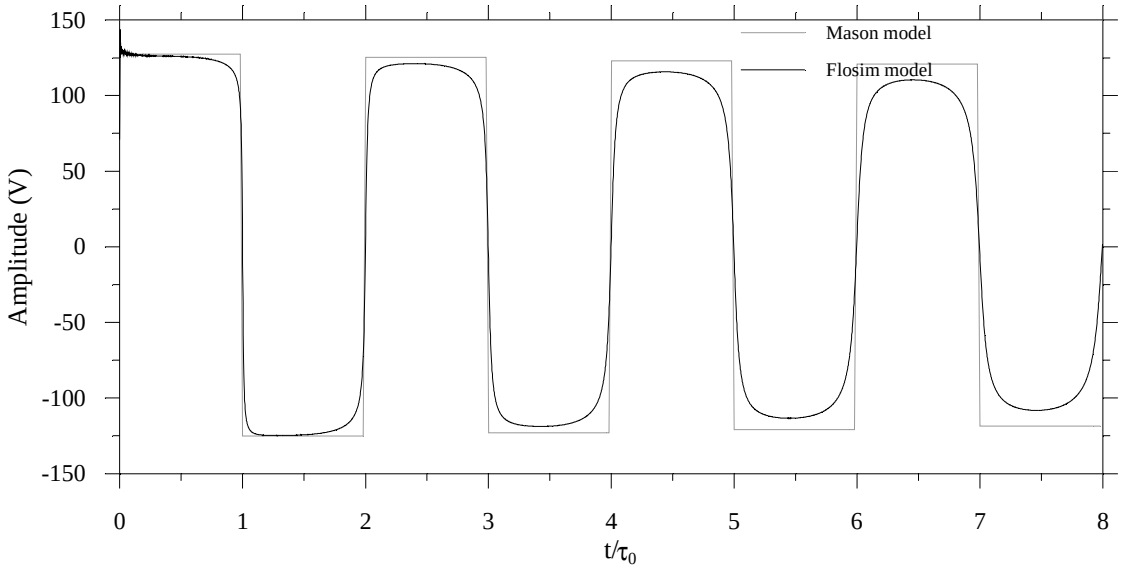

Figure 5.18 Free field pressure to open circuit voltage impulse response of the receiving transducer. The time axis is normalised to the reverberation period, τ_0, of the transducer element.

The Eq.(5.38) is simulated, for the Mason model, with a = 4.51mm, ℓ = 10.128mm and the specifications of the PZT-5A for the material constants. The backing and radiation impedance are 3.0e5 and 419.35rayls respectively. With the same parameters as above, for the Flosim model, absorption, Q_E = 50 and Q_M = 75, is included. And for the Flosim model, the inverse Fourier transform of the open circuit transfer function was calculated using IFFT.

The impulse response of the Flosim model starts with that of the Mason model and because of the absorption in the element, deviates as time increases. In the beginning of the response, the Flosim model shows some oscillation. This is because of the trunction of the frequency spectrum.

TRANSFER FUNCTION

The Fig.(5.19) shows the free field pressure to open circuit voltage transfer function of the receiving transducer. The parameter used for the simulations are the same as those used for the impulse response.

The transfer function of the receiving transducer at open circuit conditions, found in Eq.(5.36c), is comparable to the transfer function of the simplified model of the transmitter, found in Eq.(5.9), except the factor, $2A/j\omega C_0$. Z_{r2} in Eq.(5.9) denotes the radiation impedance, Z_r. Because of the ω in the denominator, the magnitude of the transfer function of the receiver decreases with frequency. The absorption has reduced the resonant tops compared to that of the Mason model.

The phase of the transfer function of the transmitter changes between $\pi/2$ and $-\pi/2$, whereas, because of the j in the denominator in the Eq.(5.36c), the phase of the receiver changes between 0 and $-\pi$. The phase response of the transfer function due to the Flosim model starts out with that of the Mason model and later, at high frequencies, deviates because of the absorption. It should be noted that the phase response due to the Flosim model is shifted in the

positive direction than that of the Mason model. It is very much visible in low frequencies of the response. This may be a consequence of the way of implementation of absorption in this model. This may be explained as follows. The plane wave pressure to open circuit voltage transfer function of the receiver due to Flosim model is given in Eq.(5.39). This equation may be further simplified using the expression for R_0 given in Eq.(5.17) as follows.

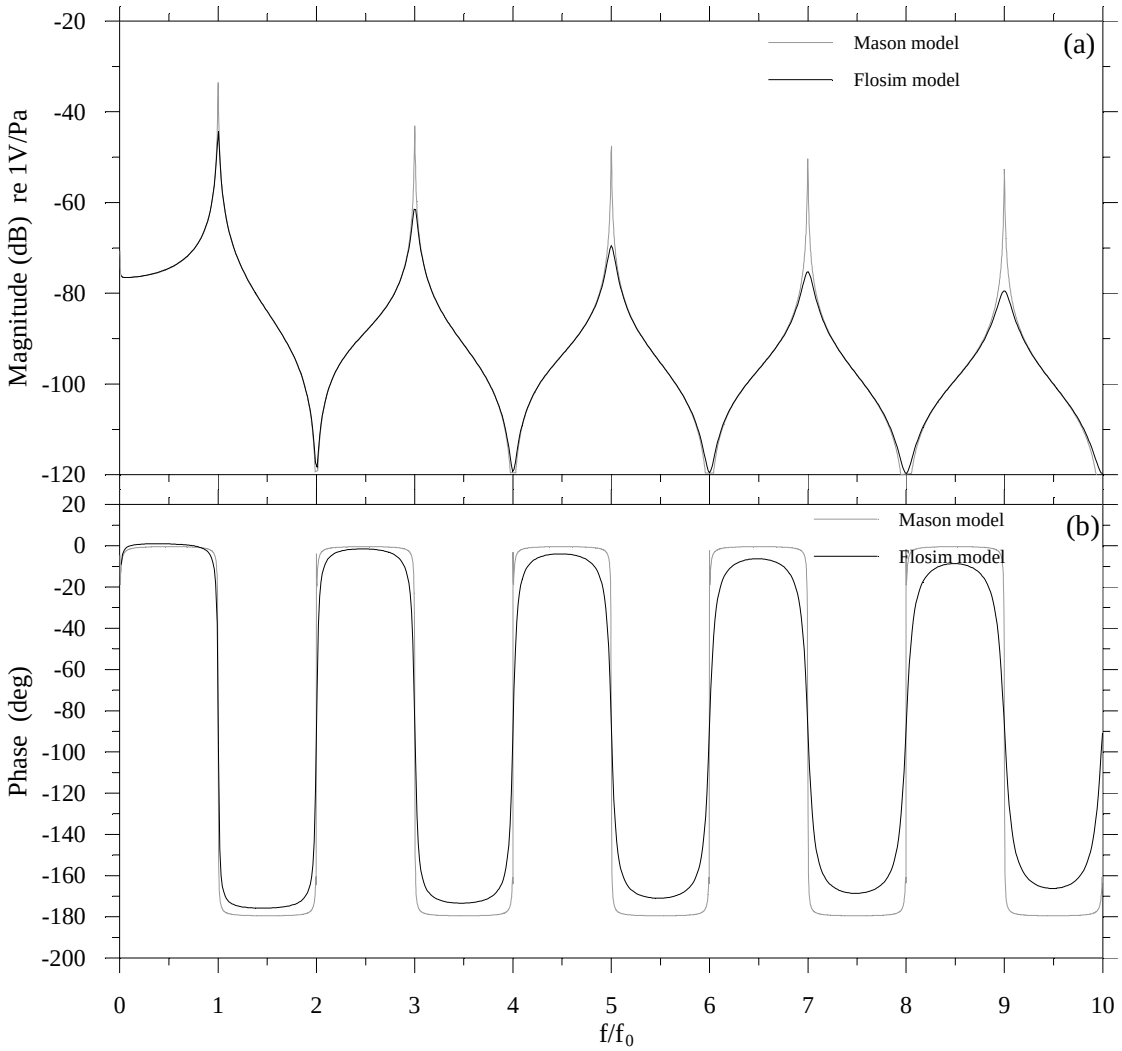

Figure 5.19 Free field pressure to open circuit voltage transfer function of the receiving transducer. (a)Magnitude and (b)Phase. The frequency axis is normalised to the half wave frequency of the transducer element.

$$H_{re3}(\omega) = \frac{2A}{\frac{\omega C_0}{C_{R0}}\left(1 + jC_{R0}\right)(Z_a + Z_b + Z_r) + Z_b \frac{(Z_a + Z_r)}{(Z_a + Z_{r1})}} \frac{\phi}{}, \tag{5.40a}$$

where,

$$C_{R0} = \frac{(1 - k_p^2)(1 - (k_{33}^t)^2}{(\tan\delta)^T}. \tag{5.40b}$$

Consider the transfer function due to the Mason model in Eq.(5.36c). As explained in the previous pargraph, the phase of the first term, $-\pi/2$, reduce the phase of the second term from ($\pi/2$ — $-\pi/2$) to (0 — $-\pi$). But, in the transfer function due to the Flosim model, Eq.(5.40a), the phase of the first term is greater than $-\pi/2$ and faild to reduce the phase of the second term to (0 — $-\pi$). This may be the reason for the phase of the transfer function is more positive than that of the Mason model in the low frequencies.

Since the phase of the first term of Eq.(5.40a) is indipendant of frequency, the whole spectrum is given a positive phase shift. The Mason model is causal, known from its impulse response. Since, as seen before, the phase response of the Flosim model is shifted in the positive side compared to that of the Mason model, the Flosim model will give a non causal response.

CHAPTER 6

TOTAL ACOUSTIC RESPONSE

6.1 INTRODUCTION

In Chapter 4 and in Chapter 5 the effects on the form of the transmitted pulse due to diffraction and transducer dynamics were discussed separately. In all circumstances a uniform sinusoidal burst was used to illustrate the effects. In this chapter a sinusoidal voltage signal is used as an input signal to the transmitting transducer and the changes on its form are observed at nodes 2, 3 and 5, shown in Fig.(3.1) in Chapter 3, and explained.

In Chapter 5 the effects of the dynamics of a transducer element with backing was discussed. In this chapter a backed transducer with a matching layer is considered and the major effects of the matching layer on pulse forming are discussed. In order to distinguish the difference the signal produced by the matched transducer is compared with that of an unmatched transducer.

A time domain convolution was mainly used to calculate the pulse forms in Chapters 4 and 5. It was realised that the time domain techniques are tedious and time consuming. Therefore the frequency domain techniques were preferred to calculate the total pulse. At the end of each of the chapters 4 and 5 the pulse forms calculated by the time domain techniques have been compared with the corresponding results calculated by their frequency domain counterparts. In this chapter the pulse forms are calculated using only frequency domain techniques namely the Fourier methods.

6.2 TRANSDUCER MODEL

In chapter 5 a single transducer element was used to explain the basic transducer action and its influence on pulse forming. In this chapter a more realistic transducer models are used for the transmitting and receiving transducers. Actually the models represent the transducers used in the experiment; mas01 as transmitter and mas02 as receiver. The details of the modelling of the transducers is found in Ref.15. The models are achieved by empirically fitting the magnitude of transmitting sensitivity of the model to the magnitude of the measured transmitting sensitivity of the transducer. The models have two main discrepancies; 1) some parameters found for the transducer model is different from that of the real transducer, 2) the electrical properties of the model is not in agreement with that of the measured. The later gives an incorrect simulation result for output voltage of the receiving transducer. However in Ref.15, the author cleverly over come the problem by replacing the electrical input impedance by its measured data, i.e. by multiplying the spectrum of the voltage signal with the transfer function, $Z^{E}_{in,M}/Z^{E}_{in,S}$, where $Z^{E}_{in,M}$ is the measured electrical input impedance of the transducer and $Z^{E}_{in,S}$ is simulated electrical input impedance of the transducer model. This is possible because, the electrical input impedance of the transducer is explicitly show up in the expression for the output voltage while it is written in terms transmitting sensitivity of the receiving transducer instead of its receiving sensitivity, assuming the transducer is reciprocal. The electrical input impedance of the receiving transducer(mas02) and of its model are shown in Fig.(6.1).

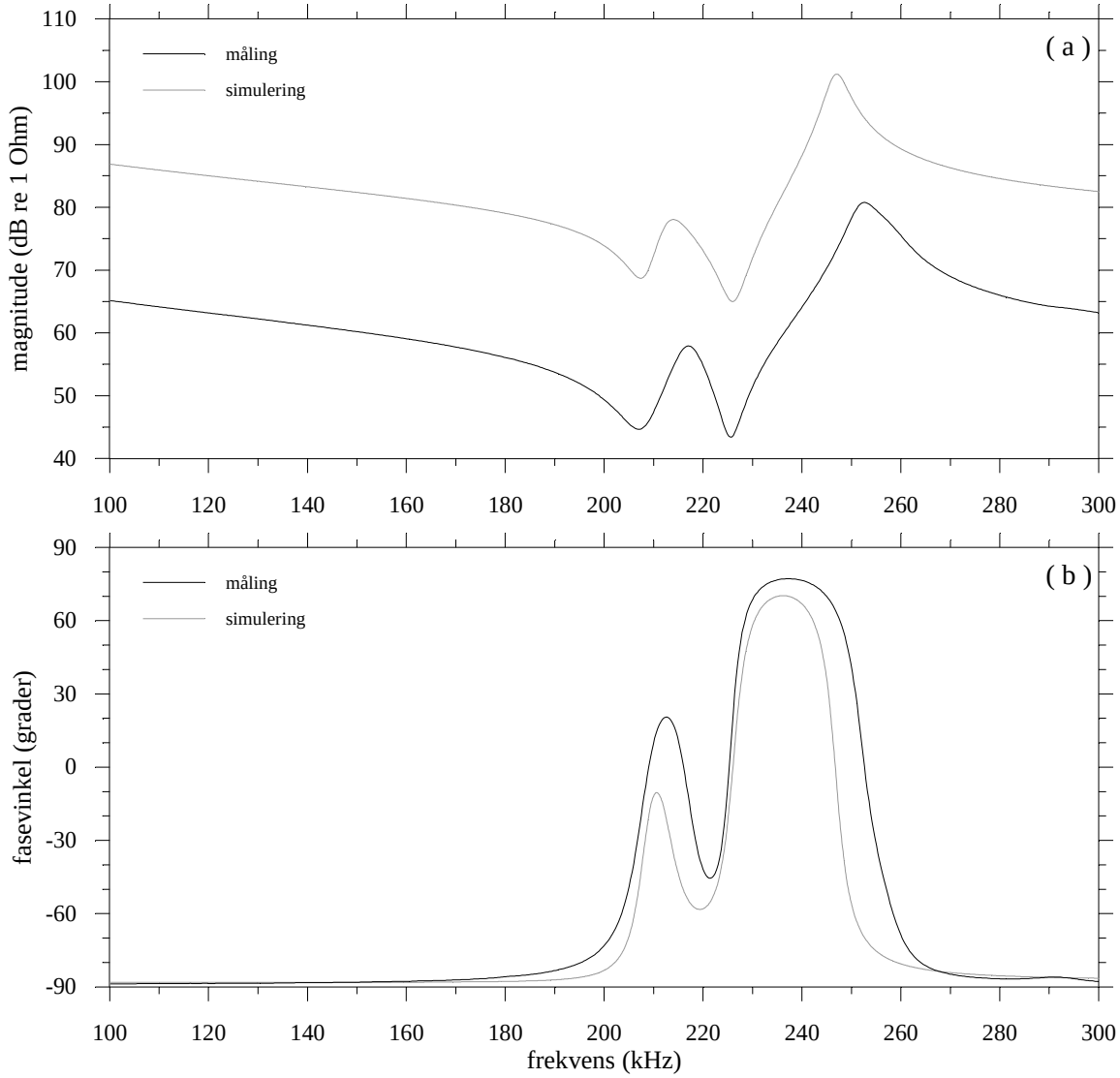

Figure 6.1 The measured(måling) electrical input impedance of mas02 and the simulated(simulering) electrical input impedance of the fitted transducer model as functions of frequency(frekvens). (a) Magnitude and (b) Phase angle(fasevinkel) in degrees(grader). These plots are copied from Ref.15 with the permission of the author.

6.3 CALCULATION

The velocity signal, $u_2(t)$, and its frequency spectrum, $U_2(\omega)$, of the transmitting transducer for a uniform sinusoidal voltage burst are calculated using the FLOSIM program. Then, using the FIELDSIM program the free field pressure, $p_4(t)$, and its frequency spectrum, $P_4(\omega)$, are calculated. Finally, the output voltage, for the calculated free field pressure, is calculated using the FIELDSIM program. This program uses the free field pressure to voltage transfer function

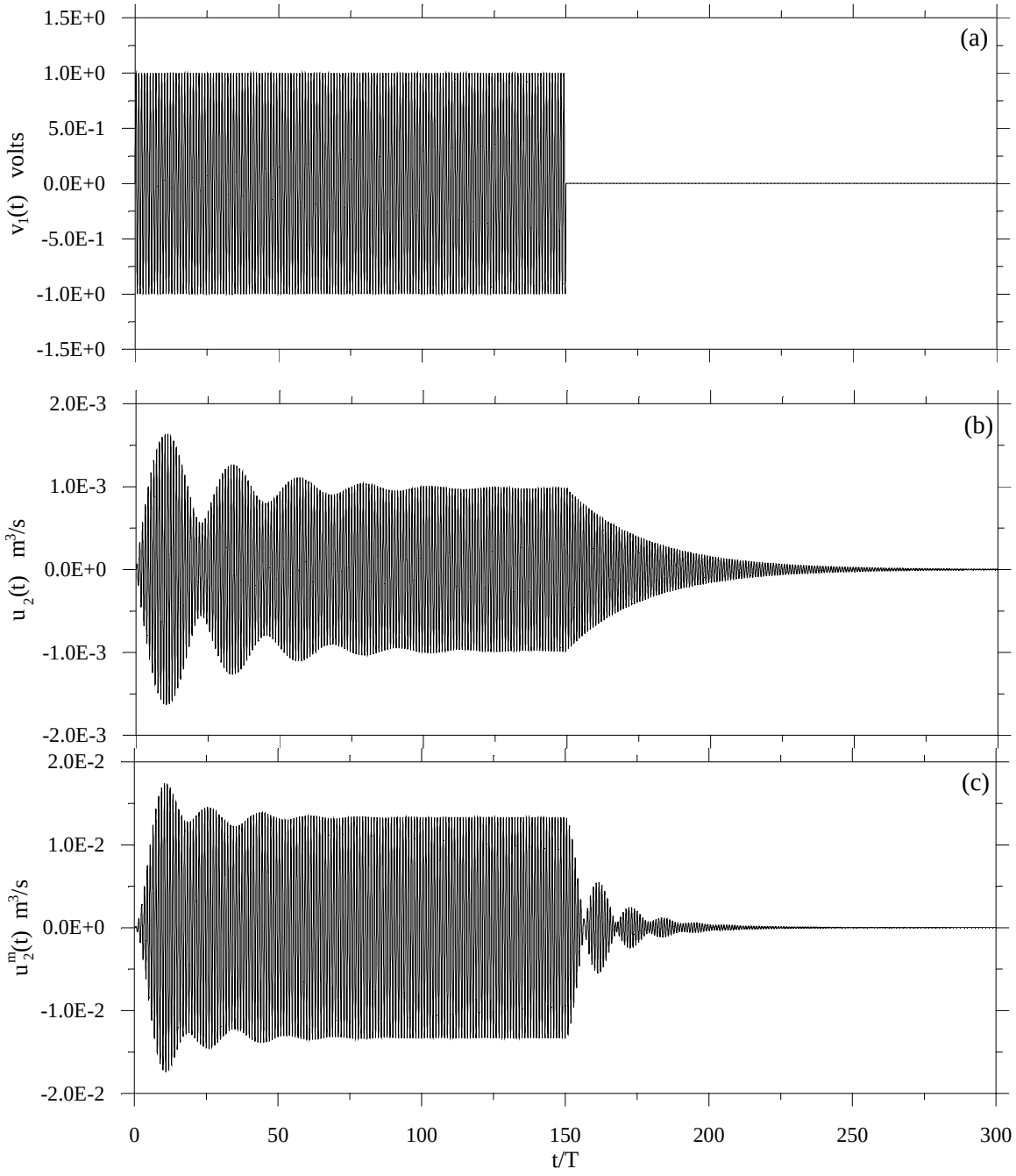

Figure 6.2 Form of the (a) Input signal, the velocity signal at node 2 while the transducer is (b) not matched and (c) matched to the medium. The particle velocity is multiplied by the area of the transducer.

calculated by the FLOSIM program to calculate the voltage output. The volume velocity is presented instead of the particle velocity as FLOSIM calculates. The volume velocity is the particle velocity multiplied by the area of the transducer. The transfer functions are used accordingly. That is, for transmitter, voltage to volume velocity transfer function; for propagation, volume velocity to pressure transfer function. But for simplicity, volume velocity is called velocity in the following discussion.

The input signal used for the simulation in this chapter is a CW type sinusoidal burst of frequency 215kHz and amplitude 1 volt with 150 cycles, as shown in Fig.(6.2)(a). Its frequency spectrum is shown in Fig.(6.3)(a). The velocity output of the unmatched transducer

for the above input signal is shown in Fig.(6.2)(b). The nature of this signal may be explained, qualitatively, as follows. The frequency spectrum of this signal, shown in Fig.(6.3)(c), is

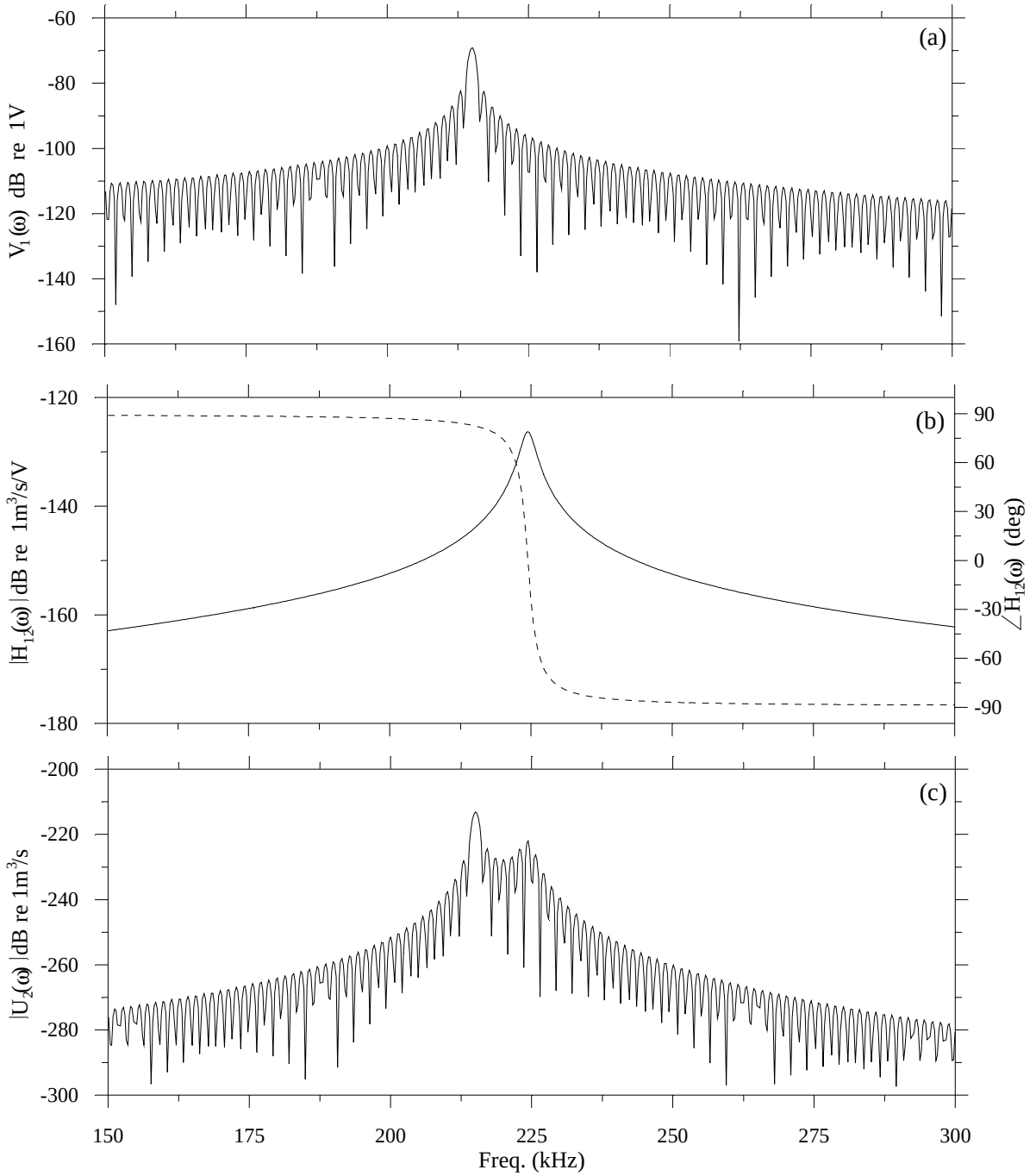

Figure 6.3 Magnitude of the frequency spectrum of (a) Input signal shown in Fig.(6.1)(a) and (c) signal at node 2 shown in Fig.(6.1)(b). (b)The magnitude and phase of the voltage to velocity transfer function of the unmatched transducer.

found by multiplying the frequency spectrum of the input signal with the voltage to velocity transfer function, shown in fig.(6.3)(b). Since the transfer function has one resonance peak at 225kHz, the velocity spectrum has two prominent peaks at 215kHz and 225kHz. The interaction of these two frequencies is seen mainly in the beginning of the signal, i.e., the beating type of behaviour. However, as time goes on the strongest of the frequency components takes over. That is, the signal stabilises at 215kHz. After 150 cycles there is no

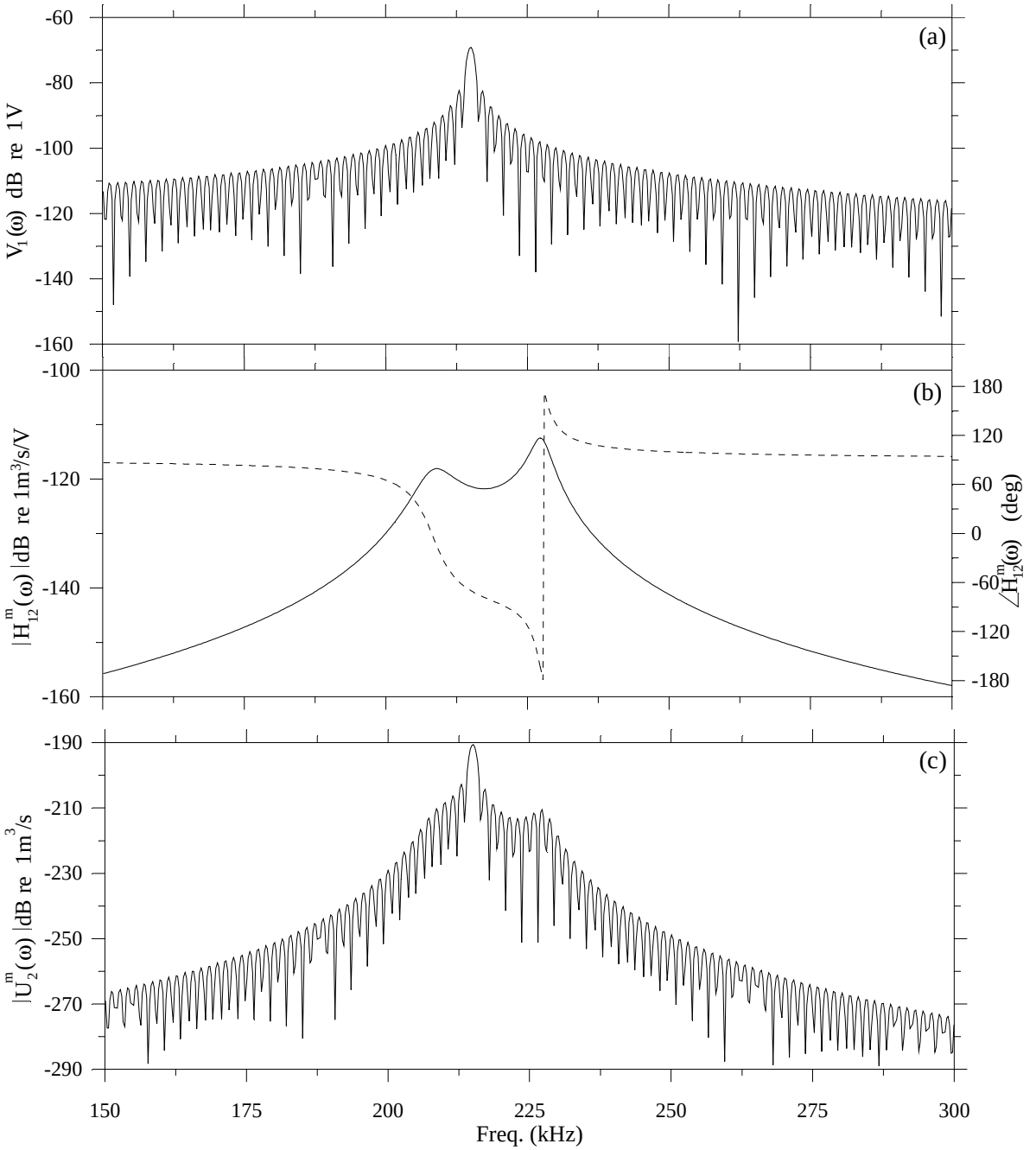

Figure 6.4 Magnitude of the frequency spectrum of (a) Input signal shown in Fig.(6.2)(a) and (c) signal at node 2 shown in Fig.(6.2)(c) and the magnitude and phase of the (b) voltage to velocity transfer function of the matched transducer.

driving signal, the transducer vibrates at its natural resonance frequency, 225kHz and the signal dies off gradually. The frequency variation through the signal is estimated using the consecutive zero crossings and plotted in Fig.(6.5). The zero crossings are calculated by linear interpolation method using every pair of consecutive positive and negative values of the signal and their corresponding times. The velocity output of the matched transducer is shown in Fig.(6.2)(c) and its frequency spectrum in Fig.(6.4)(c). This spectrum is found, as in the previous case, by multiplying the frequency spectrum of the input signal with the voltage to velocity transfer function of the matched transducer shown in Fig.(6.4)(b). The transfer function has two resonance peaks around 210kHz and 228kHz. Since the input spectrum has its peak at 215kHz, beating type of behaviour of the transient region of the velocity signal

must be the result of the interaction of these three frequencies. After a while the signal stabilises to the strongest of these three frequencies, 215kHz. As in the previous case, after 150 cycles the signal dies off gradually. But, since the transducers has two resonance frequencies, as shown in Fig.(6.4)(b), the decaying part of the signal, unlike the unmatched case, shows a beating effect of the two frequencies. And as the time goes on the transducer vibrates at its stronger resonance frequency, 228kHz. The frequency variation through this signal also estimated and plotted in Fig.(6.5) with the unmatched case.

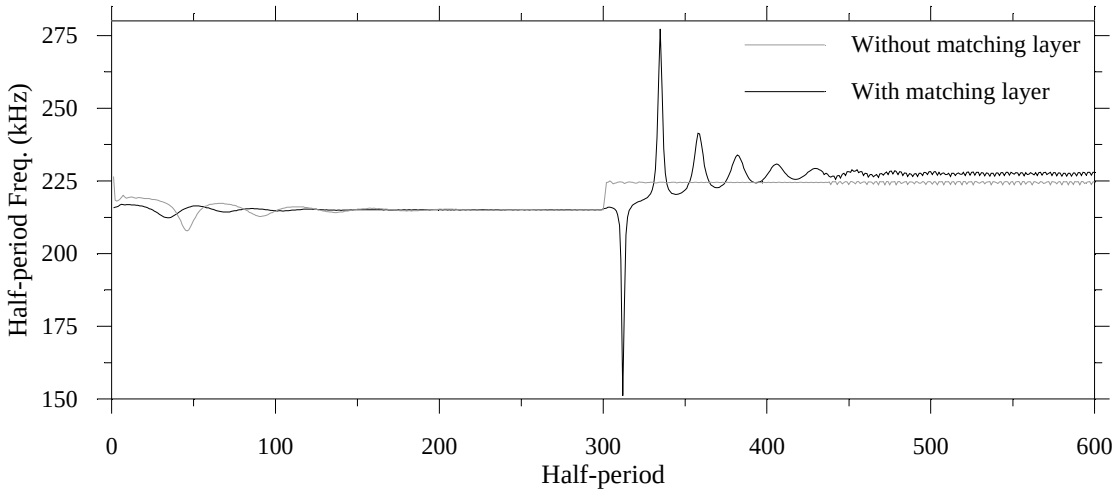

Figure 6.5 The frequency variation through the pulse calculated using consecutive zero crossings.

The Fig.(6.6)(a) and (b) show the first 1.5 periods and the first 12 periods of the velocity signals shown in Fig.(6.2) respectively. The velocity signal for the unmatched case starts at time t = 0, i.e. immediately after the voltage is applied to the transducer. And, for the matched case the signal starts with a time delay. This time delay is the time taken by the wave to travel through the matching layer. In this particular simulation where the velocity of sound in the matching material, c_M = 1027m/s, thickness of the matching layer, t_M = 1.215mm and the frequency of the input signal f = 215kHz, the delay, $t_M f/c_M$, is approximately 0.25 period of the input signal.

In addition to the difference in time delays, there are some other important differences between the velocity bursts produced by the unmatched and the matched transducers. The velocity burst produced by the unmatched transducer is small in amplitude and long in duration compared to that of the matched transducer. This differences may be explained qualitatively, in terms of flow of energy, as follows. The reflection coefficient, r, is defined in Eq.(5.7e) and can be found[1] in any text book on waves. The power reflection and transmission coefficients are given[1] by $R_\pi = |\mathbf{r}|^2$ and $T_\pi = 1 - R_\pi$ respectively and, for normal incidence, the power transmission is equal to the energy flow per unit time.

In the case of the unmatched transducer, because of the large difference in the impedance of the transducer material and the load(air) a large amount of the energy of the wave hitting the transducer-air interface is reflected back into the transducer. This makes the transducer to vibrate for a long time until it looses all the energy. As a result the output signal is long in time and small in amplitude. In contrast, comparatively more energy of the wave hitting the transducer-matching layer interface is transmitted into the matching layer and of which a large amount of energy is transmitted at the matching-load interface in to the load(air). This makes the output velocity signal large in amplitude and short in duration compared to that of the unmatched case. An approximate calculation would show the difference clearly. The

impedance of the transducer, matching layer and the load used in the simulation are Z_0(33.75Mrayl), Z_M(0.144Mrayl) and Z_L (415rayl) respectively. The power transmission coefficient in the unmatched transducer is

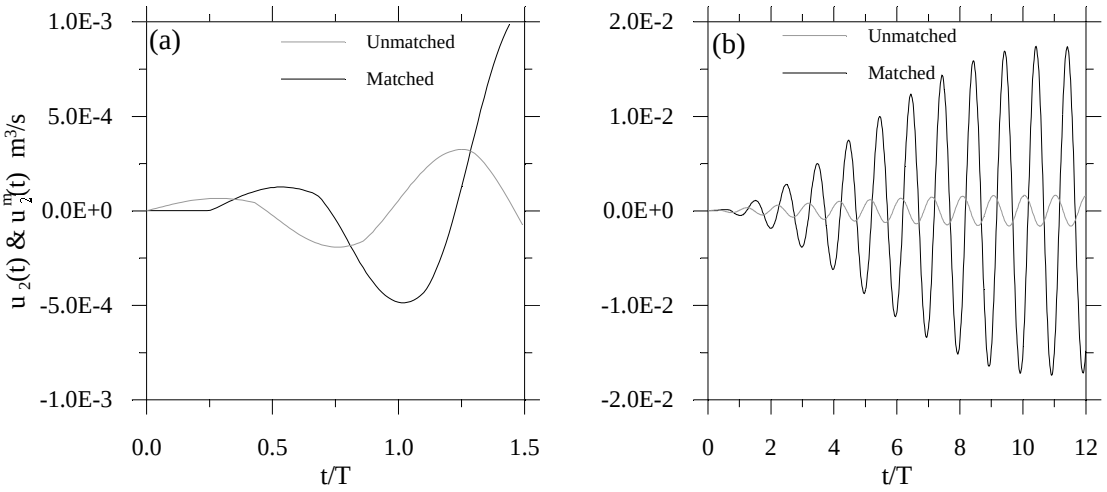

Figure 6.6 The start of the velocity signals shown in Fig.(6.2)(b) and (c). (a) First 1.5 periods and (b) First 12 periods.

$$\left(\frac{2Z_L}{Z_L+Z_0}\right)^2 \frac{Z_0}{Z_L}. \tag{6.1}$$

Similarly, for the matched transducer, if the absorption is omitted, the power transmission coefficient is

$$\left(\frac{2Z_M}{Z_M+Z_0}\right)^2 \frac{Z_0}{Z_M}\cdot\left(\frac{2Z_L}{Z_L+Z_M}\right)^2 \frac{Z_M}{Z_L}. \tag{6.2}$$

Since Z_L « Z_M « Z_0, the transmitted power in the matched transducer is approximately four times larger than that in the unmatched transducer. This shows that the power transmission is increased by using a matching layer. The transmitted force can also be found in a similar fashion using the corresponding force transmission coefficient. But this estimated force is just for one wave. The output signal is the addition of several such waves reflected between the transducer faces and the matching layer faces and thus of different magnitudes and phase. In addition, the output signal contains the regeneration contribution and the absorption reductions due to both transducer and matching layer materials.

The calculation of the output signal using the above method is very difficult. However, the first cycle of the output signal can be calculated easily using this method. The following is the calculation of the signal up to the first reverberation time, i.e. until the time of arrival of the wave originated at the back face of the transducer element.

The voltage input used in the simulation can be represented as,

$$v(t) = \sin\omega t \qquad 0 \le t \le 150T, \tag{6.3}$$

where T is the period.

The velocity output, $y_1(t)$, of the transducer up to the first reverberation time is given by the convolution of v(t) with the first term of the voltage to velocity impulse response of the transducer given in Eq.(5.7a).

$$y_1(t) = \frac{\phi}{Z_0 + Z_2} \cdot \left[\delta(t) + \beta e^{\beta t}\right] \otimes v(t) \qquad 0 \le t \le \tau_0, \tag{6.4a}$$

where τ_0 is the reverberation time of the transducer element.

$$y_1(t) = \frac{\phi}{Z_0 + Z_2}\left[\int_0^t \left(\delta(\tau) + \beta e^{\beta\tau}\right)\sin(t-\tau)\,d\tau\right] \qquad 0 \le t \le \tau_0. \tag{6.4b}$$

A simple manipulation will result,

$$y_1(t) = \frac{\phi}{Z_0 + Z_2}\left[\left(1 - \frac{\beta^2}{\omega^2 + \beta^2}\right)\sin\omega t + \frac{\omega\beta}{\omega^2 + \beta^2}\cos\omega t - \frac{\omega\beta}{\omega^2 + \beta^2}e^{\beta t}\right] \qquad 0 \le t \le \tau_0 \tag{6.4c}$$

Assume Z_2 is real. If $Z_2 = Z_L$ then $y_1(t) = y_1^{ta}(t)$, the velocity of the transducer-air interface of the unmatched transducer.

Similarly, if $Z_2 = Z_M$ then $y_1(t) = y_1^{tm}(t)$, the velocity of the transducer-matching interface. The force transmitted into the matching layer is then $y_1^{tm}(t)\cdot Z_M$ and the velocity at the matching layer-air interface, $y_1^{ma}(t)$, is,

$$y_1^{ma}(t) = y_1^{tm}(t) \cdot Z_M \cdot \left(\frac{2Z_L}{Z_M + Z_L}\right)\cdot\left(\frac{1}{Z_L}\right) \qquad \tau_M \le t \le \tau_M + \tau_0, \tag{6.5a}$$

where τ_M is the transit time in the matching layer. Since $Z_L \ll Z_M$,

$$y_1^{ma}(t) \approx 2y_1^{tm}(t). \qquad \tau_M \le t \le \tau_M + \tau_0 \tag{6.5b}$$

Since $Z_L \ll Z_M \ll Z_0$,

$$\beta \approx \left(\frac{3 + r_0}{\tau_0}\right)\left(k_{33}^t\right)^2 \qquad \text{and} \qquad y_1^{ta}(t) \approx y_1^{tm}(t) \tag{6.6}$$

Comparing the Eqs.(6.6) and (6.5b) gives the velocity output of the matched transducer up to the first reverberation time is approximately two times larger than that of the unmatched transducer. It should be noted that the velocity signal of the matched transducer is suffered an absorption loss. However, this loss may be neglected since the matching layer is very thin and the absorption coefficient is very small. In the simulation where the thickness of the matching layer, ℓ_M = 1.215mm and the absorption coefficient, α/ω = 1.623e-5 Nepers*sec/rad*m, the reduction in amplitude for 250kHz wave is approximately 0.004dB. The parameter used here are found for the model fitted for the real transducer element.

The matching has shorten the length of the output signal. In other words the matching has increased the bandwidth of the transducer. The increase in bandwidth can also be achieved by increasing the backing impedance but at a cost of the efficiency of the transducer.

The effect of matching on the shape of velocity signal has been discussed. In the rest of the analysis and discussion velocity output of the matched transducer will be used. The Fig.(6.7)(a), (b) and (c) show the free-field pressure wave form at the centre of the receiving transducer calculated by the plane wave model, far-field model and the near-field finite receiver model respectively for the velocity signal, shown in Fig.(6.2)(c), produced by the matched transducer.

The Fig.(6.8) show (a)the spectrum of the input velocity signal, (b)velocity to free field pressure transfer function and (c)the spectrum of the output free field pressure signal due to the far-field model. Since the overall shape of the far-field and near-field pressure signals are very much the same, spectrum of one of the signals, due to the far-field model, is shown. For comparison, the transfer functions of both models are shown in Fig.(6.8)(b). The parameters used in the simulations are; $c = 344.35$m/s, $a = 4.51$mm, $\rho_0 = 1.20$kg/m^3

The pressure wave due to the plane wave model is just a multiplication of the velocity by the characteristic impedance of air($\rho_0 c = 414.6$rayl) and with a pure time delay. This can be seen from the plane wave transfer function, Eq.(4.19) in Chapter 4. Therefore, it looks like the velocity signal except the amplitude.

The Fig.(6.9)(a) shows the beginning of the pressure signals shown in Fig.(6.7) up to one period. Fig.(6.9)(b) compares the first 12 periods of the plane wave and near-field pressures and Fig.(6.9)(c) compares the same number of periods of the far-field and near-field pressures. Fig.(6.9)(b) shows the reduction in amplitude and the advancement in phase due to diffraction. The reduction in amplitude in the initial periods as shown in Fig.(6.9)(a) will give difficulties in signal detection. The Fig.(6.9)(c) shows the difference between the signals due to the near-field finite receiver model and that of the far-field model.

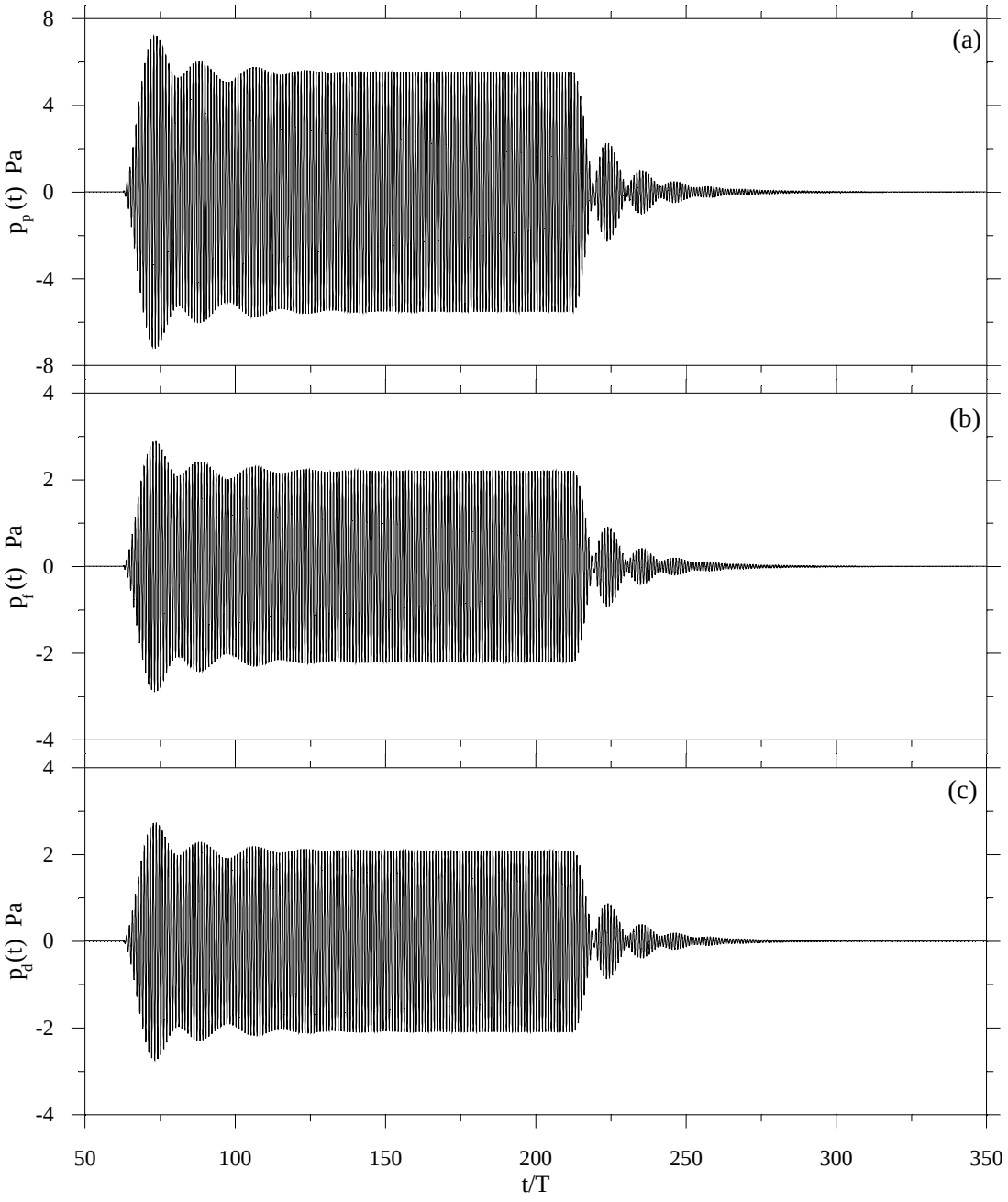

Figure 6.7 Free-field pressure at the centre of the receiving transducer by (a) Plane wave model, (b) Far-field model and (c) Near-field finite receiver model.

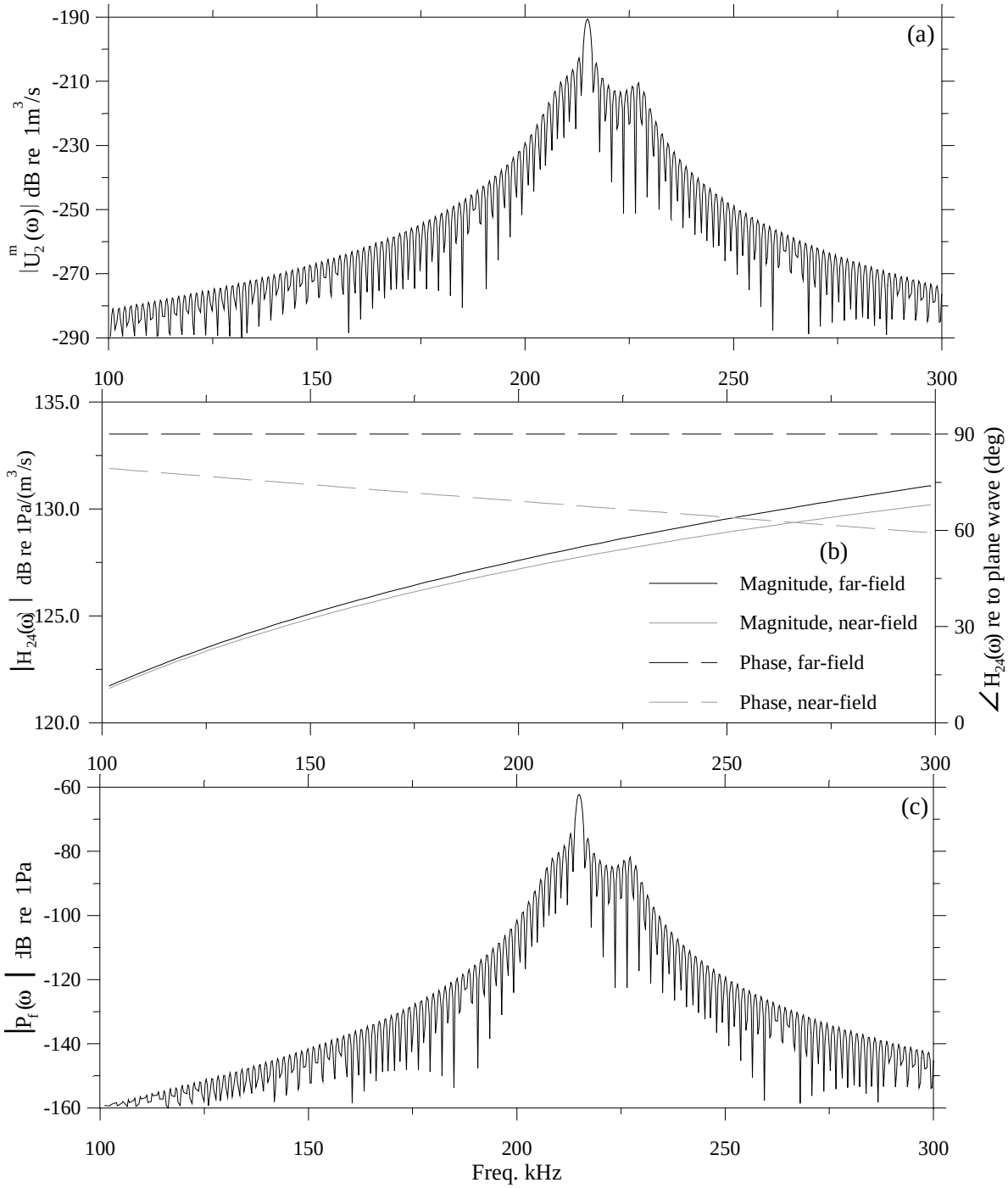

Figure 6.8 (a)The frequency spectrum of velocity signal at the transmitter face. (b)The velocity to free field pressure transfer function. (c)The spectrum of the free field pressure wave at the centre of the receiver due to the far-field model.

The pressure signal due to the far-field model shows some undulating variations. This can be explained as follows. Consider the velocity signal produced by an unmatched transducer. The major contributors in building up the first few cycles of this signal are the waves resulted from direct reflections and transmissions at the transducer faces. This construction process is explained in Chapter 5. Since these waves are of different amplitudes and come at time $t = N\tau_0$,

where N is an integer and τ_0 is the reverberation time of the transducer element, the velocity signal has breaking points at times $t = N\tau_0$. The first breaking point is visible, for example see Fig.(5.6), and the rest are smoothed out, by the addition of several such waves and the

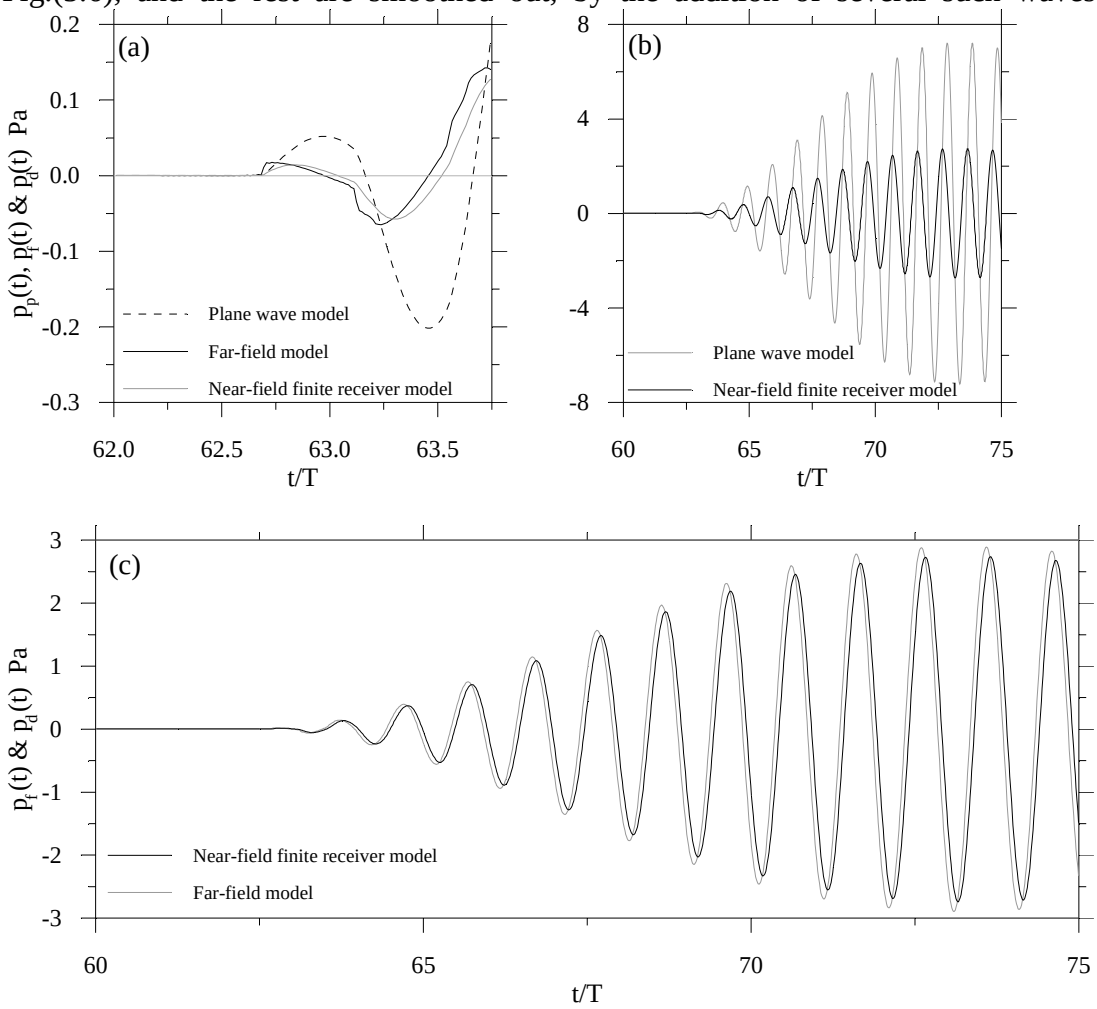

Figure 6.9 The start of the pressure signals at the centre of the receiving transducer shown in Fig.(6.8). (a)First period, (b) First 12 periods of the signals due to Near-field finite receiver model and plane wave model and (c)First 12 periods of the signals due to Far-field model and Near-field finite receiver model.

regeneration contributions, and thus not visible. In a matched transducer the number of breaking points are increased because of the waves result from reflections at the matching layer faces. The breaking points are associated with high frequency components. When this signal is send through the filter of the far-field model the high frequency components are amplified. And the invisible breaking points in the velocity signal are represented by jumps and visible in the far-field pressure signal. In the voltage to velocity impulse response of the transducer, the waves mentioned earlier in this paragraph are represented by impulse spikes. Therefore the spikes in the impulse response can be used to locate the breaking points in the signals. The Fig.(6.10) shows the voltage to velocity impulse response of the matched transducer and the far-field pressure signal. The impulse response is shifted by propagation time in the medium in order to match its time scale with that of the pressure signal. It can be seen from the Fig.(6.10) that every jump in the pressure signal is associated with an impulse spike in the impulse response. Let the transducer-matching layer interface, transducer-backing interface and matching layer-medium interface are denoted by face numbers 1,2 and 3 respectively. When a

voltage signal is applied to the transducer acoustic waves are produced at both faces 1 and 2 and after reflections and transmissions at the transducer and matching layer faces these waves finally transmitted to the medium through face 3. The path followed by each of these spikes in the transducer element and in the matching layer are shown in Fig.(6.10).

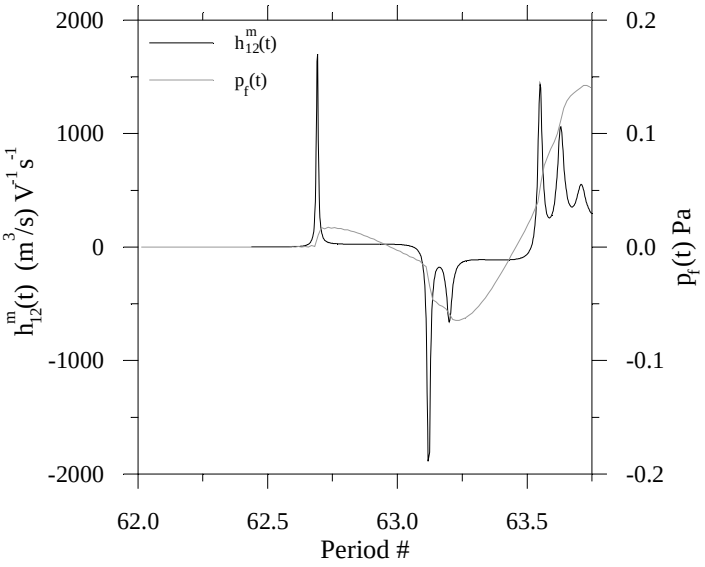

Spike #	Path
1	1→3
2	2→1→3
3	1→3→1→3
4	1→2→1→3
5	2→1→3→1→3
6	1→3→1→3→1→3

Figure 6.10 The voltage to velocity impulse response of the transducer with the corresponding far-field pressure and the paths followed by impulse spikes in the transducer element and in the matching layer.

The impulse spikes are smeared around their centre because of the absorption. This may cause some error in the size of the jump shown in the plot.

In the propagation model no absorption is implemented. But, in a practical situation, where the absorption is in action, the effects shown in the signal will be smoothed out and the undulating variations may not be visible. Further more, the far-field model is very idealistic whose transfer function is increasing monotonically with frequency and the phase is $\pi/2$, independent of the frequency. The near-field finite receiver model is more realistic and approaches the far-field model at larger distances. At larger distances the absorption loss also will be large. Therefore the chance of detecting the above described effects is reduced.

The Fig.(6.11)(a),(b) and (c) show the open circuit voltage output signal of the receiving transducer for the free-field pressure calculated by the plane wave model, far-field model and the near-field finite receiver model respectively. The time axes are normalised to the period of the input voltage burst.

The Fig(6.12)(a),(b) and (c) show the frequency spectrum of the free field pressure wave form due to the far-field model, free field pressure to open circuit transfer function of the receiving transducer and the frequency spectrum of the open circuit voltage output of the receiver respectively. Since the overall shapes of the pulses are very much the same, the spectrums of the pulse due to the far field model is only shown in Fig.(6.12).

The overall shape of the signals are very much the same because the input pressure signals are very much the same. The transient parts of the signals are greatly reduced compared to the corresponding pressure signals in Fig.(6.7). In other words, the band width of the signals are increased. This may be explained by the change in the spectrums shown in Fig.(6.12). The spectrum around 245kHz is improved by the peak of the receiver transfer function at 245kHz.

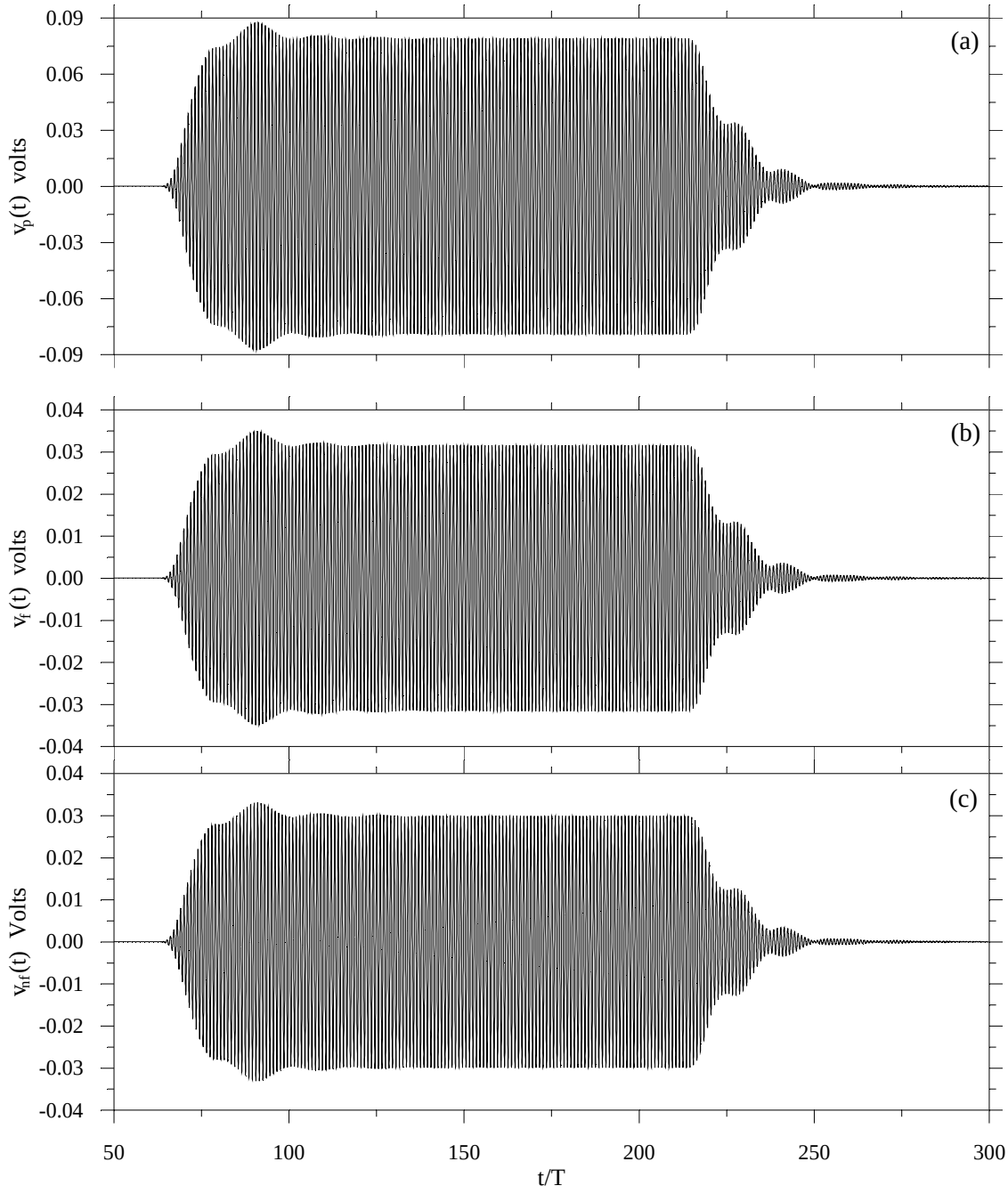

Figure 6.11 Open circuit voltage output of the receiving transducer for the input free field pressure calculated by (a) Plane wave model, (b) Far-field model and (c) Near-field finite receiver model.

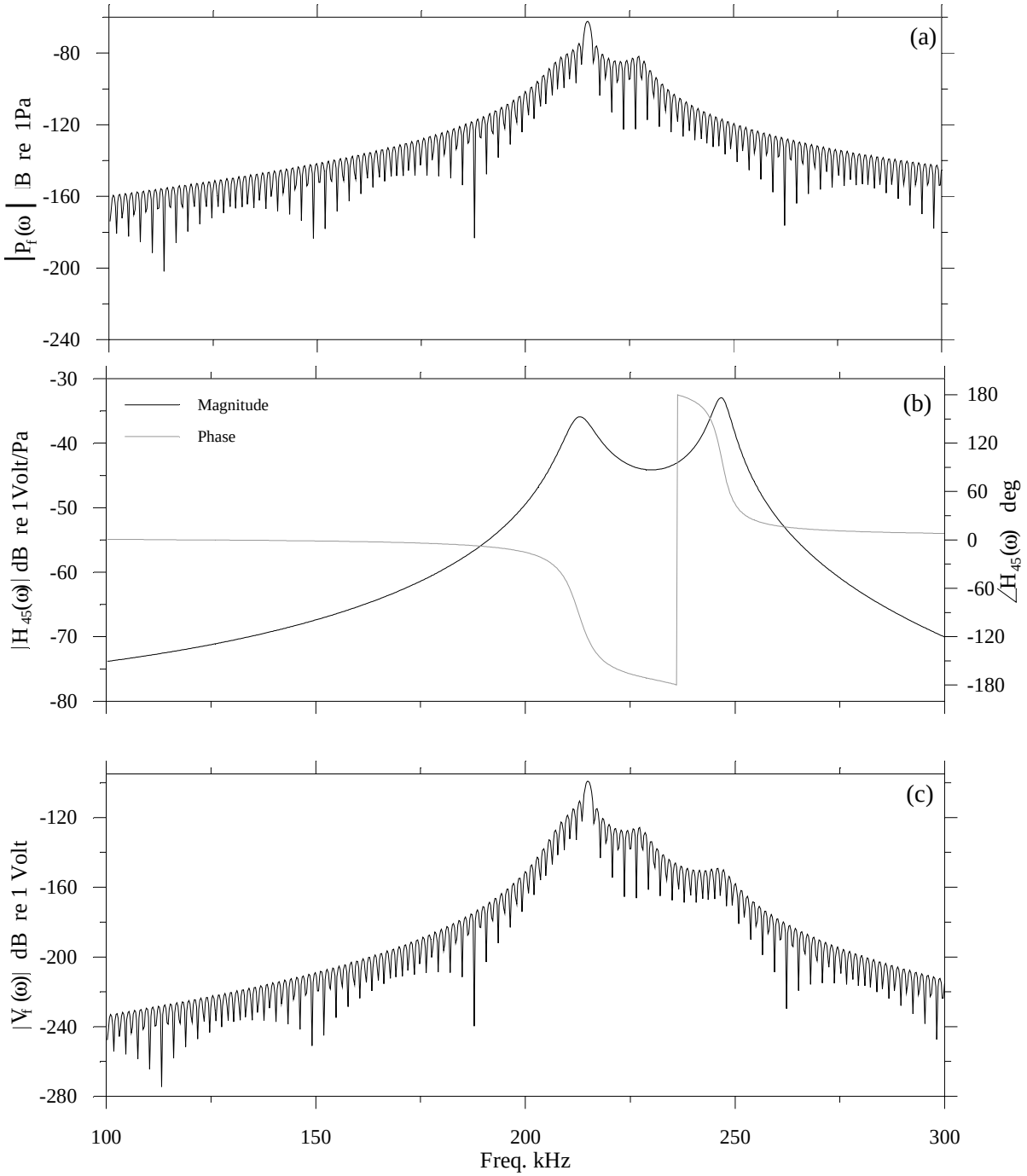

Figure 6.12 (a) The frequency spectrum of the free-field pressure at the centre of the receiving transducer due to the far-field model, (b) The free-field pressure to open circuit transfer function of the receiving transducer and (c) The frequency spectrum of the open circuit voltage output signal of the receiving transducer.

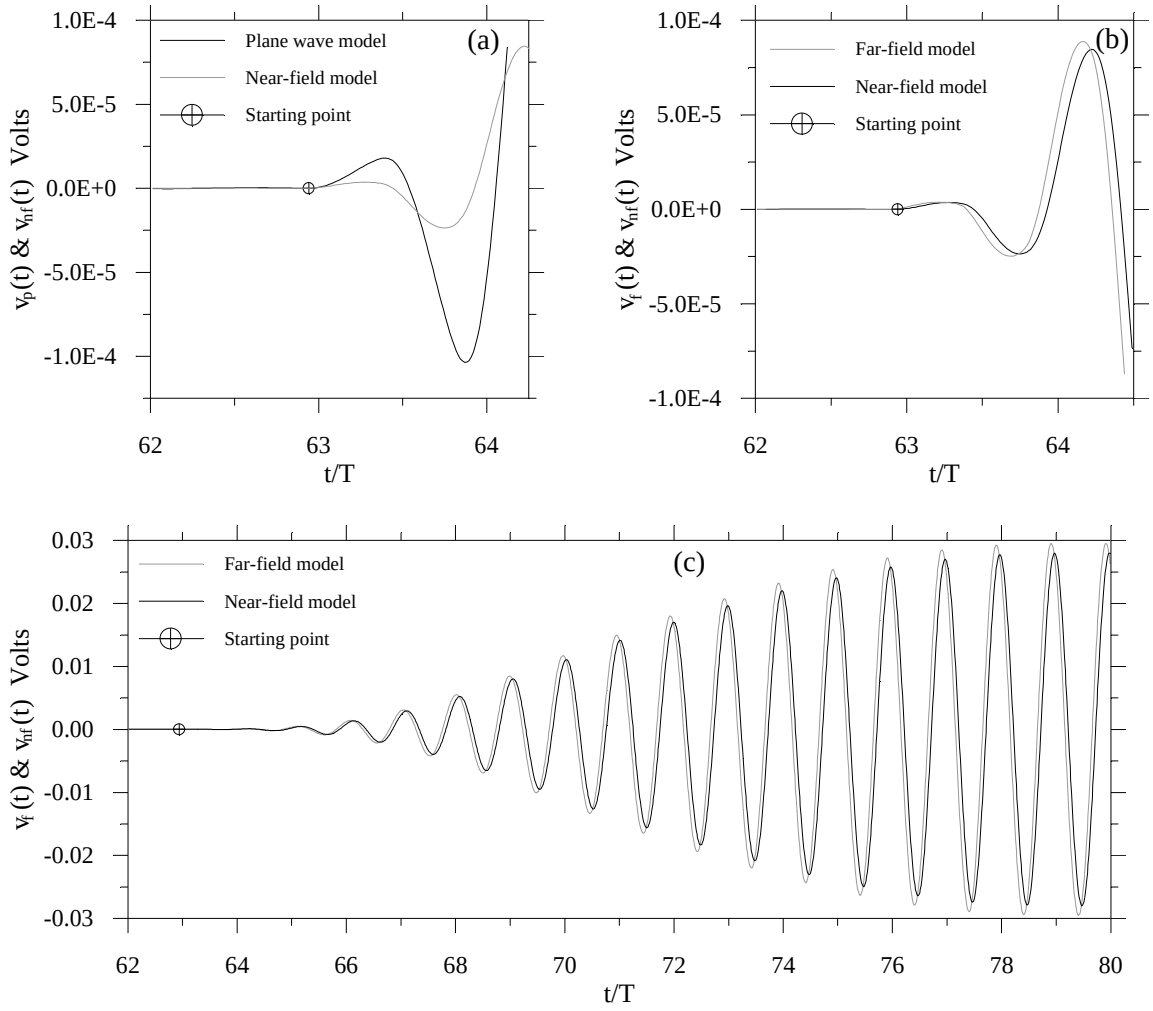

Figure 6.13 The start of the open circuit voltage output signals of the receiving transducer shown in Fig.(6.11). (a) First period of the signals due to Plane wave and Near-field models. (b) First period of the Near-field and far-field models. (c) First 17 periods of the signals due to Near-field and far-field models.

The Fig.(6.12)(a) compares the first period in beginning of the open circuit voltage output signal calculated from the free field pressure due to plane wave and near-field finite receiver models and (b) compares the similar quantities due to far-field and near-field finite receiver models. The expected start of the signals are indicated by small circles. This time is the time taken by the sound wave to travel from the matching layer-transducer interface of the sending transducer to the matching layer-transducer interface of the receiving transducer. That is $(t_{T,M}/c_{T,M} + t_{R,M}/c_{R,M} + d/c)$, where $t_{T,M}$ and $t_{R,M}$ are the thickness of the matching layers of the transmitting and receiving transducers respectively, $c_{T,M}$ and $c_{R,M}$ are the velocity of sound in the matching layers of the transmitter and the receiver respectively, d is the inter transducer distance and c is the velocity of sound in the medium.

The voltage signals shown in Fig.(6.12), as pointed out in Sec.(6.2), is not final. To find the exact value, the signals have to be modified with the frequency domain transfer function $Z^E_{in,M}/Z^E_{in,S}$. This modification is not done here. But the general behaviour of the transfer function is used in the qualitative discussion of certain aspects. From the Fig.(6.1) it is seen that the magnitude of the transfer function is almost -20dB with some fluctuation approximately between 170 and 270 kHz. And, except in this frequency range, the phase is almost zero. The fluctuation in the transfer function would cause distortions in the shape of the signal. The

magnitude of the steady state part of the signal will be reduced. It cannot be predicted whether the individual peaks in the transient part of the signal become larger or smaller.

The first, second and third positive half cycles(peaks) of the voltage signal due to the near field finite receiver model in Fig.(6.12) are 98dB, 71dB and 56dB down to the steady state value respectively. These numbers will be altered after the modification mentioned in the previous paragraph. However, since the fluctuation in the transfer function is not very large, it can be expected that the relative sizes of the peaks to the steady state value will not altered very much. If it can be assumed that the signal conditioning units in the rest of the system are ideal, i.e. the amplifier, filter and termination have very large input and very low output impedance and have wide band widths, then the above mentioned relative sizes of peaks to the steady state value will be unchanged. For a system which capable to give, for example, 50dB S/N ratio, the first two peaks are undetectable. And the third can be detected and identified correctly.

6.4 DISCUSSION

In this chapter the transmission of a sound signal through the acoustic part of an experimental system is studied. The effects of the matching layer is discussed. The changes on the shape of the signal in terms of the transfer function are discussed. The size of initial half periods indicate that they may not be detectable. These are just an indication of the use of a simulation model. Using such a model like this one can study the system for transducers with different matching and backings, for different excitation frequencies, different termination of the receiving transducer and so on. The knowledge from the study will help one to plan the experiment efficiently and make the measurements correctly.

In the simulations in this chapter, a sinusoidal burst of amplitude 1 volt is used. And the rest of the discussions are based on the assumption that the system is linear and the transmitting sensitivity of the transducer which used to model the transducer was measured in the same environmental conditions as used in the simulation. But the real system was found to have non-linear behaviour. That is the response of the system to varying input voltage is not linear. In such a situation the transmitting sensitivity of the transducers must be measured not only with the same environmental parameters but also with the same input voltage as used in the simulation and the model for the transducers have to be found accordingly. This is not a complete remedy for the problem. However, if the non linearity is not large then the simulated result can be used for qualitative identification of the experimental result.

CHAPTER 7

EXPERIMENT

7.1 INTRODUCTION

An experiment was performed to verify some of the effects shown in chapter 4 and chapter 5. In the beginning of this chapter the experimental arrangement is presented and the necessary features of the instruments involved in the experiment are described. Then the experimental procedure is described in detail. Finally the results of the experiment are analysed and discussed. The experiment was done by me and Vervik in co-operation.

7.2 EXPERIMENTAL ARRANGEMENT

An experimental set-up which designed and already in use at CMR was used in our experiment. The Fig.(7.1) shows the block diagram of the experimental arrangement. The instruments represented by the different blocks are described bellow.

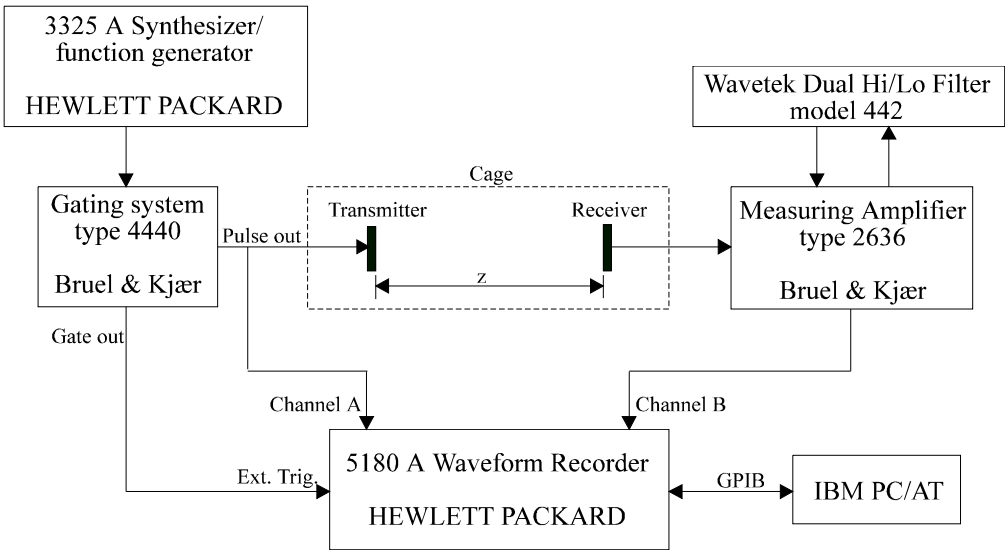

Fig.(7.1) Block diagram of the experimental arrangement

SYNTHESIZER / FUNCTION GENERATOR (3325A, Hewlett-Packard)

This generator outputs a sinusoidal signal with accuracy of ±1Hz at the frequency range used in the experiment.

GATEING SYSTEM (4440, Brüel & Kjær)

The transmitting section of the instrument, used in the experiment, is capable of giving out maximum 15V peak tone bursts of frequency up to 200kHz ±0.5dB through output terminal, PULSE OUT, while the input terminal, GEN. INPUT, is connected to a signal generator. The pulse rate and duration are adjustable within 0.5 to 15Hz and 100μs to 1s respectively. The GEN. INPUT can accept maximum of 1Vrms. The output impedance of PULSE OUT is less than 1Ω. Another terminal, PULSE GATE OUT, delivers a digital signal which, contains the time information of the starting of the tone burst send by the PULSE OUT, can be used to trigger off the measuring device. The PULSE GATE OUT is TTL compatible and has an output impedance of 50Ω.

MEASURING AMPLIFIER(2636, Brüel & Kjær)

This instrument amplifies the signal fed into its DIRECT INPUT terminal then sends the amplified signal through a filter, finally amplifies the filtered signal once again and delivers at the output terminal, AC OUTPUT. The overall gain(the total amplification at input and at output) is from -30 to 100dB and can be selected in (10 ± 0.5)dB steps. The DIRECT INPUT terminal accepts maximum of 42Vrms and has an input impedance of 1MΩ. The output impedance at the terminal delivers the signal to the external filter, TO(Ext.filter)INPUT, is 5k ΩThe input impedance of the terminal accepts the signal from the filter, FROM(Ext.filter)OUTPUT is 1MΩ. The output impedance of the AC OUTPUT terminal is 10kΩ.

FILTER(Wavetek Dual Hi/Lo Filter, model 442)

This instrument consists two separate sections; one functions as high pass filter and the other as low pass filter. Each section has a frequency band width of 10Hz - 1.1MHz and roll off of 24dB/octave. By connecting the output terminal of the high pass filter, OUT1, to the input terminal of the low pass filter, IN2, the instrument can be made to operate in a band pass mode. The input signal should be fed through the input terminal of the high pass filter, IN1, and the output can taken out from the output terminal of the low pass filter, OUT2. The input impedance and the output impedance of the instrument are 100kΩ and 50Ω respectively. The maximum input to the instrument is ±100Volts.

WAVEFORM RECORDER(5180 A, HEWLETT PACKARD)

This device(WR) can sample the analogue signal fed into one of its input channels with a sampling frequency up to 20MHz and store as 10 bit digital codes in a 16K memory. The stored wave form can be transferred to a computer diskette through a GPIB for further analysis. In the chop mode the signals connected to the channels A and B are sampled at the same time and stored. The sampling takes place alternatively between the two channels and the maximum sampling frequency is 5MHz per channel. The input channels accept from ± 100mV to ±10V. The input impedance of the channels are 10MΩ.

PulseLog

This is a manu driven computer programme[35] can be run on a IBM-AT compatible computer. The different options in the manu enable the user to document the important information of the experiment, initialise the WR and the signal generator and transfer the logged data to the computer.

PC

This is an IBM-AT personal computer. This control the WR and the signal generator using the **PulseLog** program and transfers the measurements made by the WR to a computer diskette.

TRANSDUCERS(MAS 01 & MAS 02)

MAS01 & MAS02 are high frequency narrow beam ultrasonic transducers, Model E-188/215 of the Massa Products Corporation. MAS01 was used as the sender and MAS02 as the receiver. The maximum driving voltage of the transducers is 50Vp-p. Thickness and diameter of the transducer elements are 1.57mm and 9.02mm respectively.

7.3 PROCEDURE & RESULTS

The transmitting and receiving transducers were clamped, facing each other, to the stands of an optical bench. The transducers were positioned so that their acoustical axes coincide. The distance between the transducers was set to ~100mm and measured with an internal micrometer. Then the optical bench was placed in the cage together with the sensors of the thermometer and the hygrometer. The cage was used here to reduce any air currents which cause jittering of the signal and to reduce fast changes in the environment. The inside wall of the cage was made of cotton in order to reduce any possible reflections from the wall. The cage was kept in a chamber for several hours until the environmental conditions to be stabilised.

When the environmental parameters changes very slowly the transducer terminals were connected to the rest of the experimental set-up as shown in the Fig.(7.1). The input voltage and frequency of the signal generator were set as such the gating system give out the intended voltage at the desired frequency. Then, the amplification of the measuring amplifier and the cut off frequencies of the filter were adjusted so that a good wave form is seen on the WR. With this measurement set-up a ten quick measurements were taken. That is; when the option "logdata" in the PulseLog program is chosen, the WR is set to the "output" mode. The WR immediately digitise the one shot input and the corresponding output signals and transfer the digitised data to the computer. And the computer save it in a diskett. The logging process being done in a matter of seconds. When the logging of the data is finished the WR is switched manually to the normal position and computer is returned to log the data again. This procedure was repeted ten times. Then another frequency for the input burst was chosen and the above procedure was repeated. Similarly, several measurement sets with different combinations of input voltages and input frequencies were taken. These measurements are denoted as X_1-X_{10}, X_{11}-X_{20},...X_{91}-X_{100} and called "X" measurements. Then the cage was taken out of the chamber and the separation of the transducers was changed to ~200mm and measured with the internal micrometer. The set-up was put again in to the chamber and left

for hours to the environment to stabilise. Then measurements were taken as in the X measurements. The measurements were recorded as Y_1-Y_{10}, Y_{11}-Y_{20},...Y_{51}-Y_{60} and called "Y" measurements. Similarly, measurements for the transducer separation ~400mm were taken and called "Z" measurements. A sample measurement set is shown bellow.

	Temper-ature[°C]	Humid-ity[%]	Pressu-re[mbar]
X_{11}	20.139	50.1	1010
X_{12}	20.140	50.1	1010
X_{13}	20.141	50.1	1010
X_{14}	20.142	50.1	1010
X_{15}	20.143	50.1	1010
X_{16}	20.144	50.1	1010
X_{17}	20.144	50.1	1010
X_{18}	20.145	50.1	1010
X_{19}	20.145	50.1	1010
X_{20}	20.146	50.1	1010

Input voltage	15Vp-p
Frequency of the input signal	210kHz
Band-pass filter	(40-400)kHz
Amplfication	40Db
WR channel A, rang	10
WR channel B, rang	2

7.4 ANALYSIS

In this section the effect of diffraction on pulse forming will be discussed using the experimental results. The theory under the near-field finite receiver model in Chapter 4 is used for the analysis. Therefore, the analysis also can be considered as a varyfication of the diffraction model. The analysis is done in the following way. Consider the signal measured for two different separations of the transducers, z_1 and z_2. Using the signal measured for z_1, the voltage signal for z_2 is calculated. The calculated signal is then compared with the actual measured signal for z_2. By doing this, the diffraction effect can be isolated. The theory for the calculation is derived shortly.

THEORY

Assuming the two measurements were taken at exactly the same environmental conditions and with the same input voltage and using Eq.(3.3) of Chapter 3, the spectrum of the voltage signal measured at distance z_1, $V_6(z_1,\omega)$, can be written as,

$$V_6(z_1,\omega) = H_{01}(\omega)H_{12}(\omega)H_{24}(z_1,\omega)H_{45}(\omega)H_{56}(\omega)V_0(\omega) \tag{7.1}$$

and the spectrum of the voltage signal measured at distance z_2 can be written as,

$$V_6(z_2,\omega) = H_{01}(\omega)H_{12}(\omega)H_{24}(z_2,\omega)H_{45}(\omega)H_{56}(\omega)V_0(\omega). \tag{7.2}$$

Comparing the above two equations gives,

$$V_6(z_2,\omega) = \frac{H_{24}(z_2,\omega)}{H_{24}(z_1,\omega)} V_6(z_1,\omega) \tag{7.3}$$

In the experiment described above the measurement were not made at same environmental condition. Therefore, it is further assumed that the transducers and the electronics are stable for small change in the environmental parameters. The change in the environmental condition was considered only for the propagation medium. That is, the transfer function for the medium was calculated for the appropriate density(medium) and velocity of sound in the medium,

$$V_6(z_2,\omega) = \frac{H_{24}(z_2,\rho_2,c_2,\omega)}{H_{24}(z_1,\rho_1,c_1,\omega)} V_6(z_1,\omega). \tag{7.4}$$

This idea was implemented in a computer programme, DIF2FILD, in FORTRAN. The programme code is given in appendix(B-4). This program prompts the user for the voltage signal(time function) measured for distance between the transducers z_1. It also ask the user for the following information of the two different measurement situations;(1) the density of the medium, (2) the velocity of sound in the medium, and (3) the distance between the transducers. Then outputs the predicted voltage signal that would be measured for the distance between the transducers, z_2. The predicted wave form is compared with the wave form of the corresponding measured signal. The predicted output signal, however, cannot be expected to match with the actual measurement both in amplitude and in phase, specially, because of the absorption.

Before using this programme to analyse the measured data, it was tested with purely simulated data. As all the simulated signal do not contain absorption, one can expect an exact match between the compared signals. The test was done as follows.

Test 1

First the voltage output signal for the separation of the transducers, z_1, was simulated as described in sec.(6.3). This calculation is denoted as occasion1 for future reference. Similarly the output voltage signal for the separation of the transducers, z_2, was simulated. And this calculation is denoted as occasion2. Then, using the voltage signal of occasion1, the voltage output for the separation of the transducers, z_2, was calculated with the programme DIF2FILD and denoted as occasion12. Finally, with the plane wave option of the programme DIF2FILD, using the voltage wave form of occasion1, a plane wave form for the distance z_2 was calculated. In the plane wave option of the programme DIF2FILD Eq.(7.4) was implemented with the corresponding plane wave transfer functions for $H_{24}(z_2,\rho_2,c_2,\omega)$ and $H_{24}(z_1,\rho_1,c_1,\omega)$.

The parameters chosen for the calculations are,

	Occasion1	Occasion2
z(mm)	100.50	401.86
c(m/s)	344.073	344.229
$\rho(kg/m^3)$	1.19476	1.17585

The frequncy and the radius of the transducer used in this calculation are 210kHz and 4.51mm respectively. The difference between the calculated plane wave form and the wave form of occasion12 is due to geometrical diffraction and diffraction alone as absorption is not implemented. The Fig.(7.2) shows the difference between the zero crossings of the two wave forms. The difference in amplitude and in the zero crossings in the continuous part of the wave forms can be calculated directly from the diffraction correction formulas for continuous excitations, for example, the one in Ref.7. The diffraction correction formula in Ref.7 is implemented in the programme DIFFKORR in FORTRAN by Vervik[15]. Using this programme the diffraction correction between occasion1 and occasion2 is calculated and compared with that of calculated using the wave forms of occasion12 and the corresponding plane wave. This diffraction correction is same as that seen in the steady state part of Fig.(7.2). The diffraction correction in the Fig.(7.2) reaches 216.1ns, except a few points. The deviation of these few points is not explained. The mathematical calculation of the comparison is shown shortly.

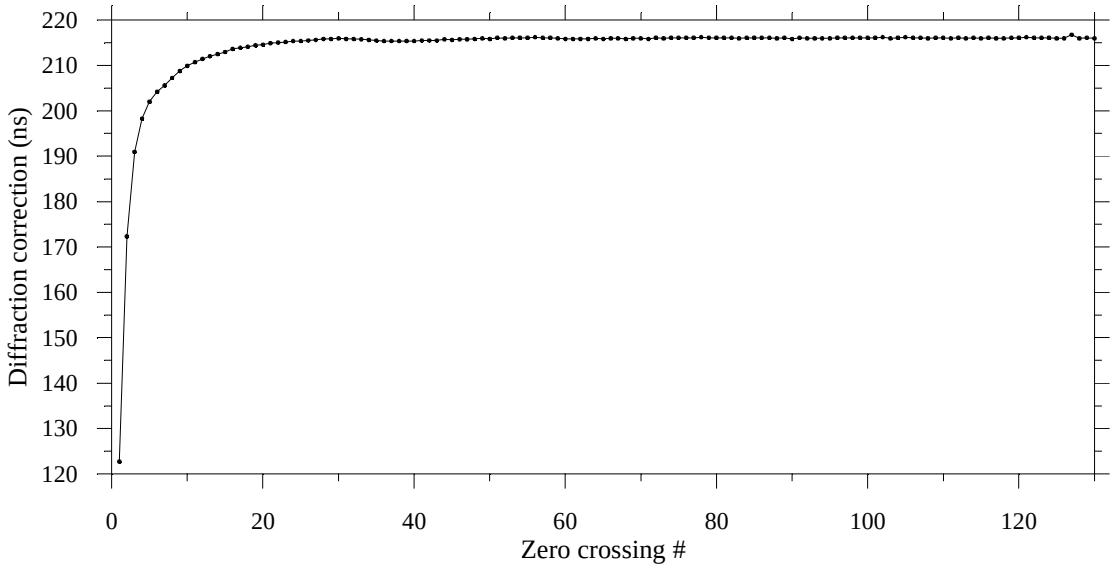

Figure 7.2 Diffraction correction of the zero crossings, from the first to 125th, of the voltage signal for separation between the transducers, z_2(occasion2) and z_1(occasion1) calculated using the wave forms of occasion12 and the corresponding plane wave.

	Occasion1	Occasion2
$S(= \frac{z}{a^2/\lambda})$	8.09	32.38
ka	17.29	17.28
diffraction correction(phase) using DIFFKORR	68.06^0	84.44^0

Therefore the diffraction correction between occasion1 and occasion2 is $(84.44-68.06)^0$

$= \underline{16.38}^0$

The diffraction correction(phase) between occasion1 and occasion2 using the wave forms (continuous part) as described in the above paragraph is = 216.1ns * 210kHz * 360

$= \underline{16.34}^0$

The difference in the above two calculations is 0.04^0. This difference in phase corresponds to 0.5ns in time.

The diffraction correction in the transient part could not be checked with any other alternative method.

Test 2

The wave forms of occasion2 and occasion12 are compared. The Fig.(7.3) shows this comparison.

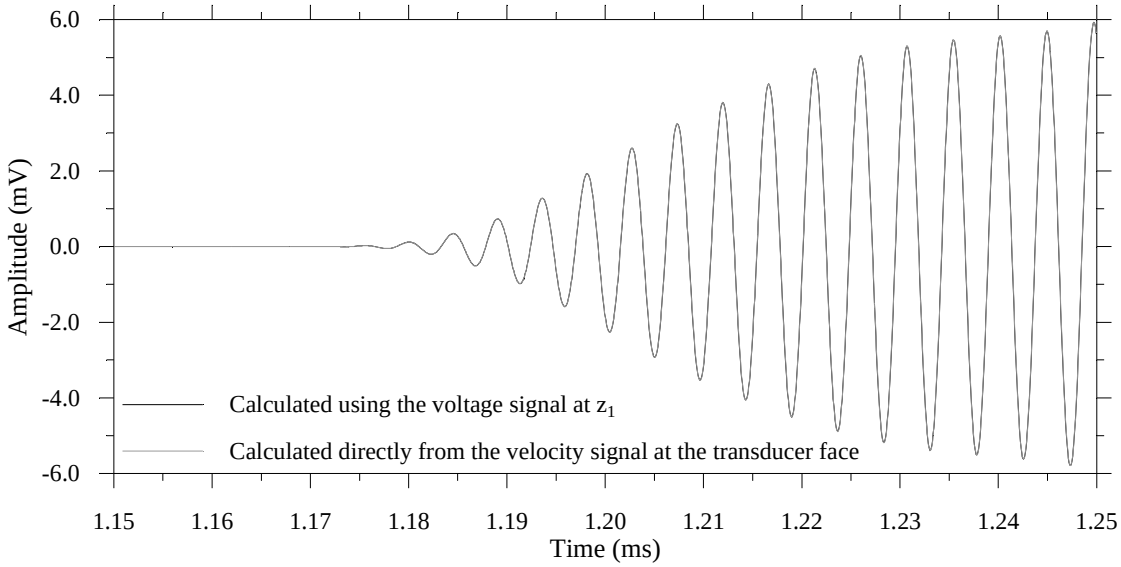

Figure 7.3 The wave forms calculated using the voltage signal at z_1(occasion12) and calculated directly from the velocity signal at the transducer face(occasion2).

The two wave forms overlaps each other so that they cannot be distinguished.

The above two tests show that DIF2FILD predicts the voltage signal correctly for a given separation of the transducers using the output voltage signal for another given separation(smaller) of the transducers with the assumption that the transducers and the rest of the experimental system are remain unchanged for small environmental changes. Now, the programme DIF2FILD is ready to use.

There are measurements, X, Y and Z, for three different transducer separations as presented in Sec(7.3). In the following analysis measured signals of Y and Z are predicted theoretically(with programme DIF2FILD) using the measured signal of X and compared with the corresponding measurements. In order to comply with the assumption, pairs of sets of measurements with minimum temperature difference were chosen. Each set of ten measurements were averaged to reduce the noise. For each set, for their respective averaged

temperature and humidity, velocity of sound and density of the medium(air) were calculated. Programmes LYDHAST and TETTHET in FORTRAN written by Vervik[15] were used to calculated the velocity of sound in the medium and the density of the medium respectively. Absorption coefficients are calculated using the programme ABSORB in FORTRAN written by Cao[35]. The parameters of the chosen first pair of measurements are shown Table(7.1). The frequency of the bursts used in both cases was 210kHz.

	Temperature .(°c)	Pressure (mbar)	Humidity (%)	Velocity (m/s)	Density (kg/m^3)	Amplifica-tion.(dB)	Absorp. coef. (dB/m)
X_{11}-X_{20}	20.142	1010	50.1	344.073	1.19476	40	8.9471
Z_1-Z_{10}	20.395	995	49.9	344.229	1.17585	40	9.0970

Table 7.1 Measured and calculated parameters of pair 1.

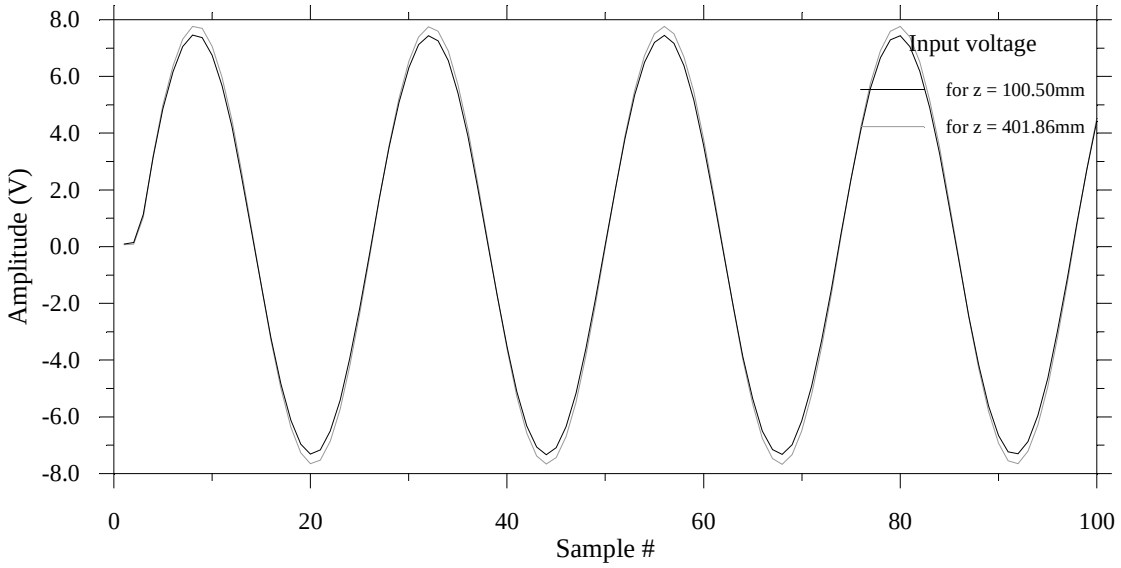

Figure 7.4 A portion of the measured input voltage signals used in a set of X_{11}-X_{20}(z = 100.50mm) measurements and Z_1-Z_{10}(z = 401.86mm) measurements.

One of the assumptions of the analysis is that the input voltage signals used in the two measurement situations are same. The Fig.(7.4) shows the input voltage signals applied in the X_{11}-X_{20} and Z_1-Z_{10} measurements. The input signals have a small difference in amplitude. But this difference in amplitude can easily be accounted for, as long as the signals have same frequency. And these signals have very much the same frequency.

Using the averaged signal of the measurements X_{11}-X_{20}, first, signal with plane wave propagation for the transducer separation z = 401.86mm is found. This signal is shown in Fig.(7.5)(a). As it propagated as plane wave, this signal is a time shifted version of the original signal, that is, the signal measured for the transducer separation 100.50mm.

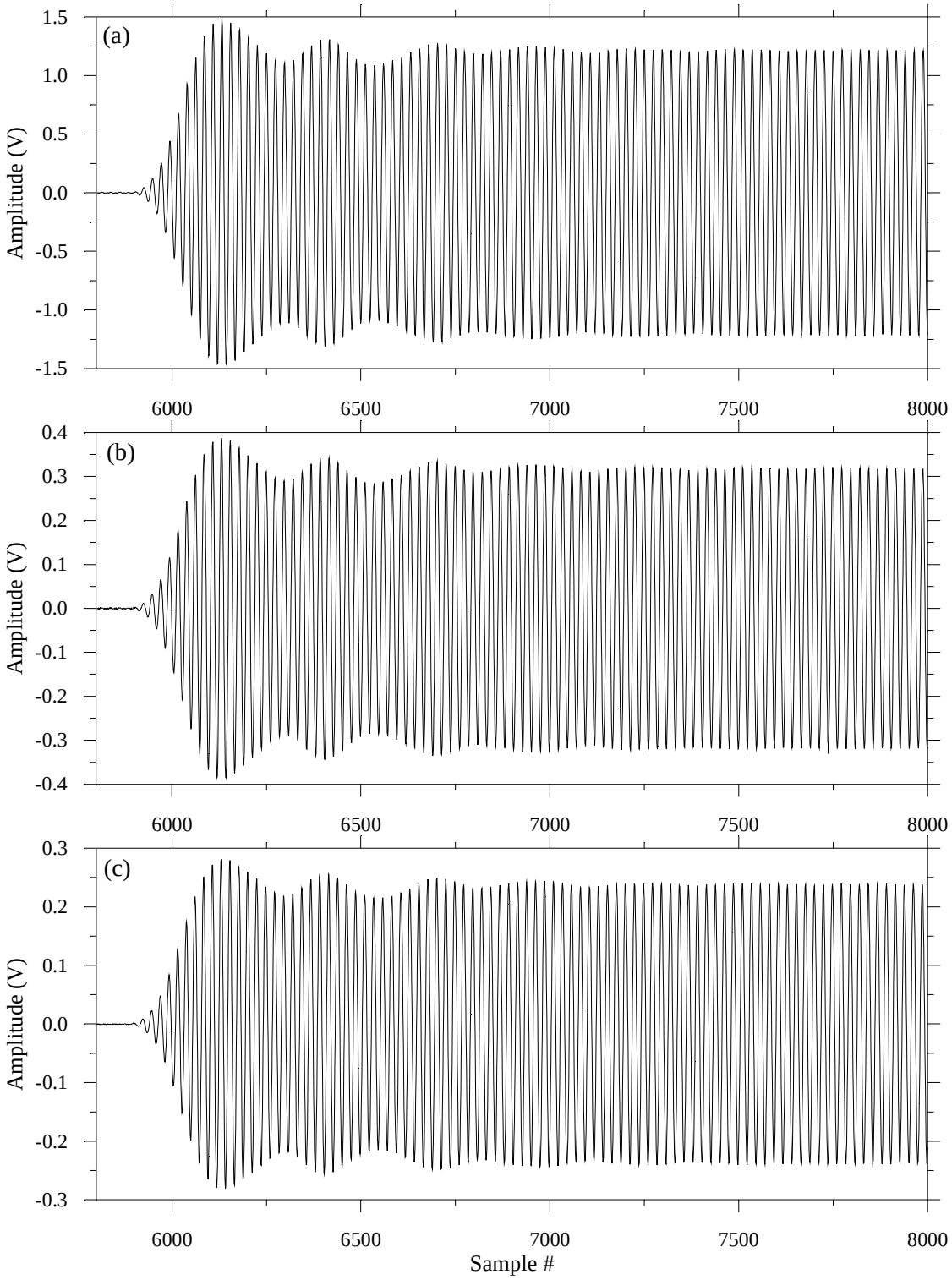

Figure 7.5 Simulated output voltage signals for the transducer separation z = 401.86mm using the measured output voltage signals, measured for transducer separation z = 100.50mm with (a) Plane wave model, (b) Near-field finite receiver model. (c) is the measured output voltage signal for transducer separation z = 401.86mm. Measured signal belongs to the set Z_1-Z_{10} and the signal used for the simulation belongs to the set X_{11}-X_{20}.

Therefore this signal can be used as a reference to see the change in the signal due to diffraction between the measurements for z = 100.50mm and z = 401.86mm. Fig.(7.5)(b) shows the simulated output voltage signal for the transducer separation z = 401.86mm with the programme, DIF2FILD, using the signal of X_{11}-X_{20}. Fig.(7.5)(c) shows the actual measured signal for the transducer separation z = 401.86mm. As the same amplification factor was used during the two measurements, as shown in Table(7.1), the relative values are presented to compare the signals in Fig.(7.5).

The overall shape of the three signals are very much the same. Diffraction has not alter the overall shape of the signal. There are difference in the magnitude among the signals. The difference in level of the signals in Fig.(7.5)(a) and (b) is due to diffraction. The simulated signal in Fig.(7.5)(b) is larger than the measured signal, shown in Fig.(7.5)(c). This is generally anticipated as absorption is not implemented in the simulation programme and the actual signal suffered absorption. However, the predicted signal is smaller than it should be, because of the difference in the input signals shown in Fig.(7.4).

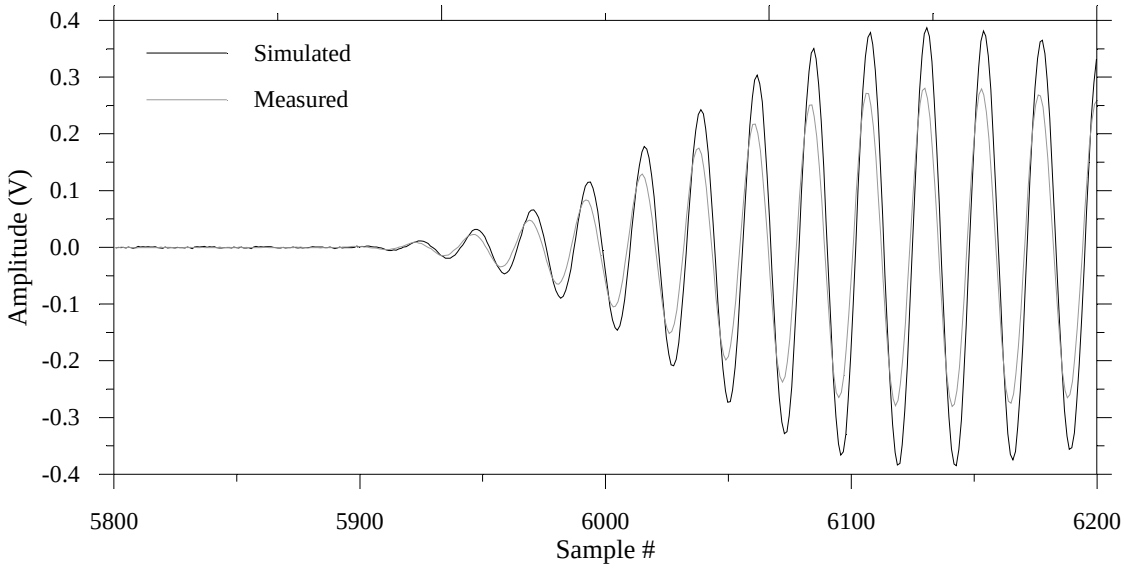

Figure 7.6 A portion in the start of the measured and simulated output voltage signals for the transducer separation 401.86mm are shown. The simulated signal was calculated using the measured output voltage signal, measured for transducer separation z = 100.50mm. The measured signal belongs to the set Z_1-Z_{10} and signal used to the simulation belongs to the set X_{11}-X_{20}.

To see the predicted and the measured signals more closely, a portion in the beginning of these signal are plotted and shown in Fig.(7.6). There is a considerable difference between the two signals. There can be number of factors caused this deviation; (1)the assumption that the characteristics of the transducers remain unchanged for the temperature difference(0.25^{0}c) might be wrong. (2)absorption has not been implemented in the model, (3)errors in the measurements of temperature, humidity and transducer separation and (4)physical radius of the transducers has been used in the calculation instead of the effective radius, To check the first of the four factors listed above, another pair of measurements with even smaller temperature was chosen and analysed.

Measurement sets of X_{91}-X_{100} and Z_{31}-Z_{40} were chosen as the second pair for the analysis. The necessary parameters of this pair are shown in Table(7.2). The frequency of the signal burst used in both measurements was 216kHz.

	Temperature. (°c)	Pressure (mbar)	Humidity (%)	Velocity (m/s)	Density (kg/m^3)	Amplificat -ion.(dB)	Absor. coeff. (dB/m)
X_{91}-X_{100}	20.480	1010	50.4	344.289	1.19324	30	9.4353
Z_{31}-Z_{40}	20.472	995	50.0	344.279	1.17551	40	9.5350

Table 7.2 Measured and calculated parameters of pair 2.

First, as in the previous case, the input signals used in the two measurements are checked. The input signals are shown in Fig.(7.7). The signals are very much the same both in amplitude and in frequency.

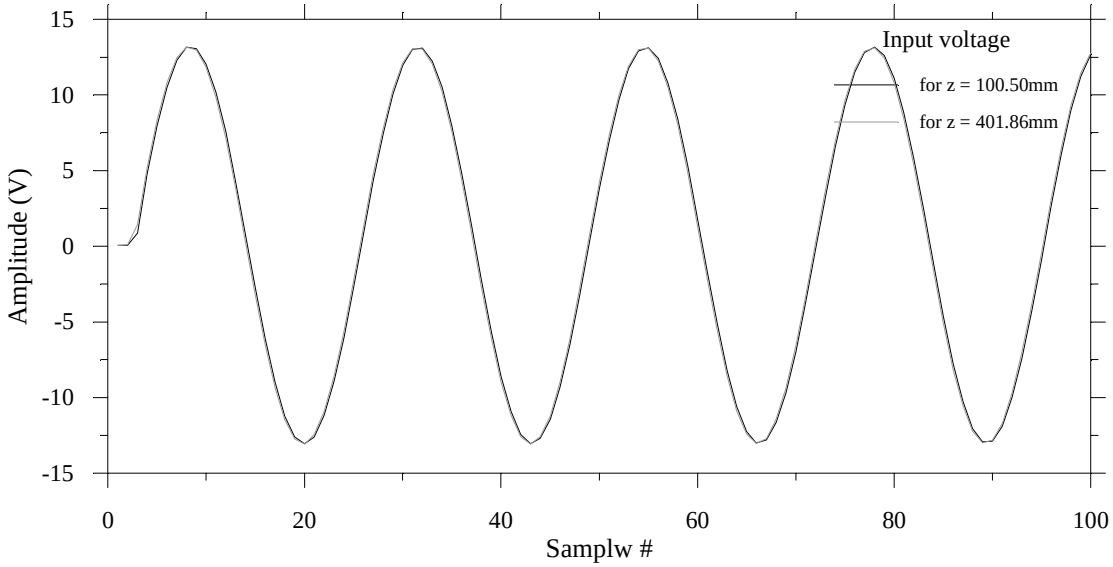

Figure 7.7 A portion of the measured input voltage signals used in a set of X(z = 100.50mm) measurements and Z(z = 401.86mm) measurements.

The Fig.(7.8)(a) and (b) show the predicted output voltage signal for the transducer separation z = 401.86mm, using the measured output voltage signal, measured for the transducer separation z = 100.50mm, with the plane wave model and the near-field finite receiver model respectively. Fig.(7.8)(c) shows the measured output voltage signal for the transducer separation z = 401.86mm. Different amplification factors has been used during the two measurements, X_{91}-X_{100} and Z_{31}-Z_{40}, as shown in the Table(7.2). Therefore, to compare the signals, unlike the signals in Fig.(7.5), the absolute values of the signals are presented in Fig.(7.8).

The plots in Fig.(7.8) also show that diffraction has not alter the main shape of the signal. The shape of the signals in Fig.(7.8) differ from that of in Fig.(7.5), the signals of the pair used in the previous analysis. This difference is due to the transducer dynamics. In the pair of measurements, used in the previous analysis, the transducer was excited with 210kHz frequency and in the pair, used in the later, with 216kHz. The Fig.(7.9) show a portion in the beginning of the predicted and the measured signals, shown in Fig.(7.8)(b) and (c). There is a considerable difference between the signals. The difference between this two signals looks very much the same as the difference between the signals in Fig.(7.6), the simulated and the measured signals of the previous case. The difference between the zero crossings of the two

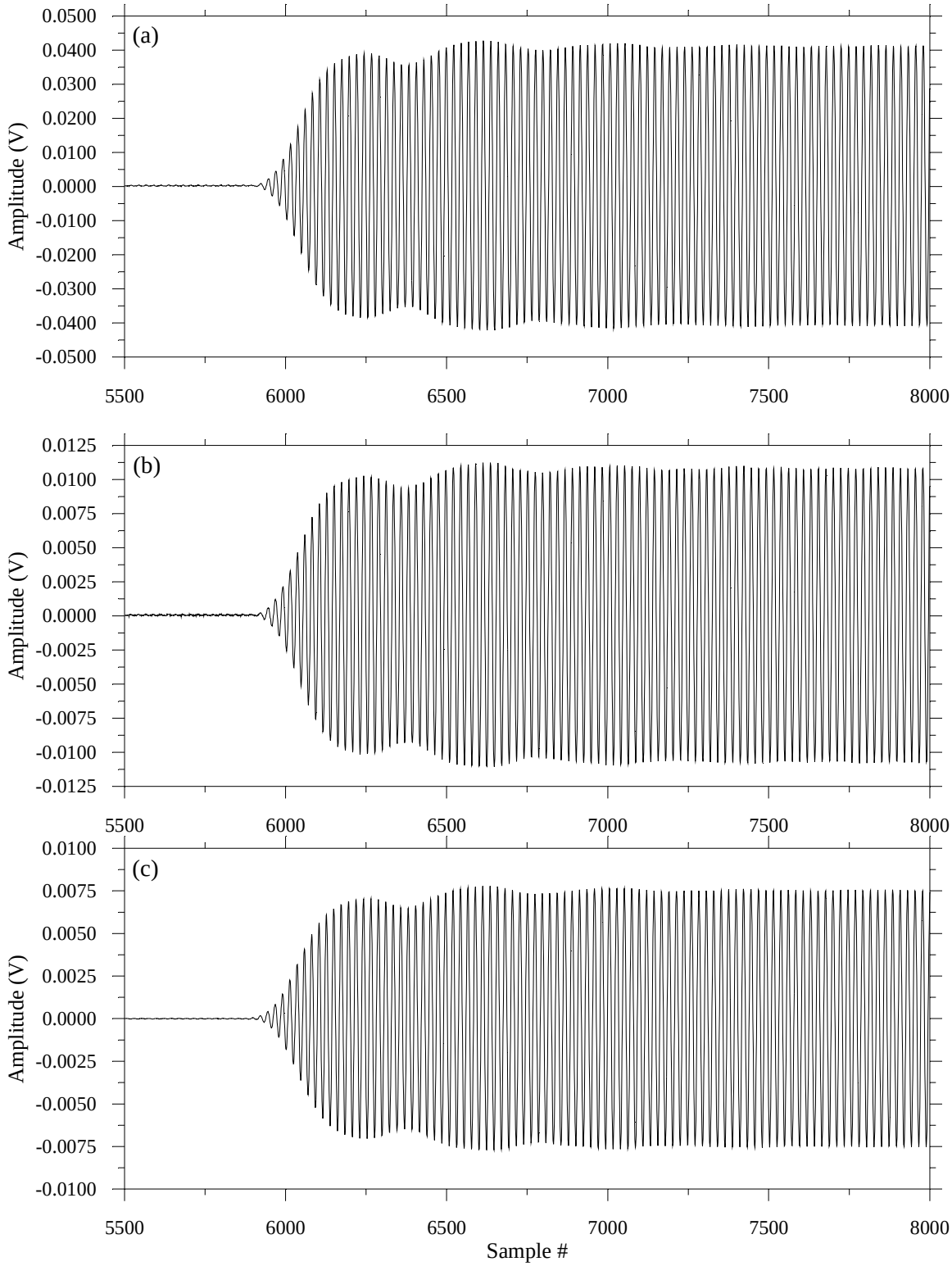

Figure 7.8 Simulated output voltage signals for the transducer separation z = 401.86mm using the measured voltage signals, measured for transducer separation z = 100.50mm, with (a) Plane wave model, (b) Near-field finite receiver model. (c) is the measured output voltage signal for transducer separation z = 401.86mm. Measured signal belongs to the set Z_{31}-Z_{40} and the signal used for the simulation belongs to the set X_{91}-X_{100}.

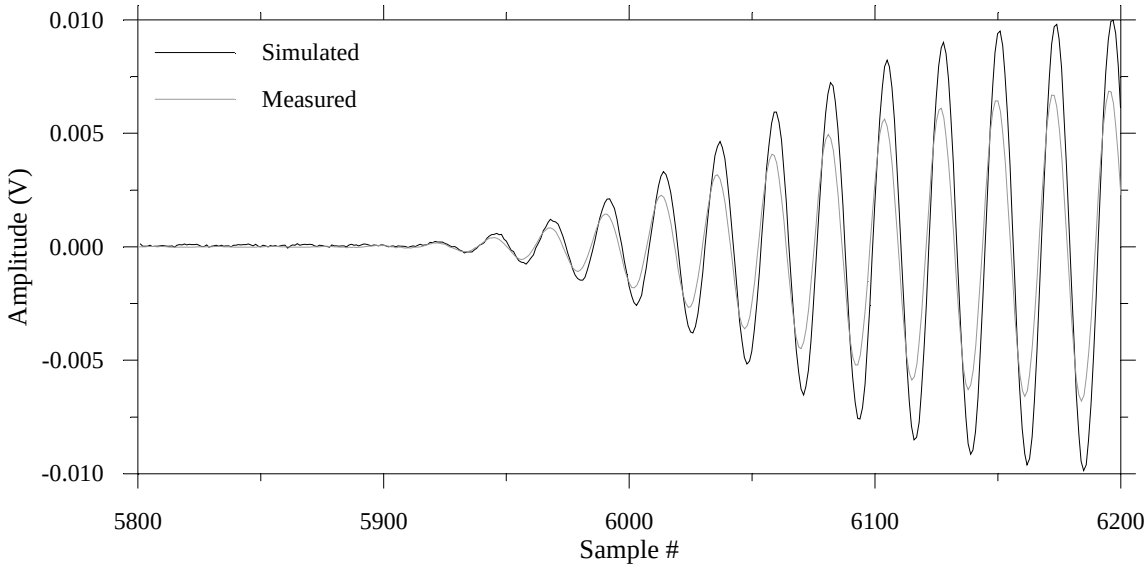

Figure 7.9 A portion in the start of the measured and simulated output voltage signals for the transducer separation 401.86mm are shown. The simulated signal was calculated using the measured output voltage signal for transducer separation z = 100.50mm. The measured signal belongs to the set Z_{31}-Z_{40} and signal used to the simulation belongs to the set X_{91}-X_{100}.

signals in both cases are found to be about 200ns.

In the analysis of the second pair a more agreement in phase(zero-crossings) between the simulated and measured signals than in the previous pair, was expected. The reason is the temperature difference between the mesurements of the pair2 is smaller(0.008^0c) than that of the pair1(0.253^0c). Had the temperature difference between the measurements of pair1 been the reason for the difference in the zero-crossings of the simulated and measured signals of pair1 then the difference between the zero-crossings of simulated and measured signals of pair2 should be smaller than that of pair1.

But, the results indicate that the variation in the transducer dynamics due to temperature difference in both cases cannot be a reason for the disagreement. And it also indicate that there must be some other systematic error to give a same amount of disagreement(~200ns). There are three posibilities for the source of error which is common for both pairs; 1)The speed of sound in the medium used in the simulations are calculated using the programme, LYDHAST, based on theoritical and experimental data. The error in the data could have caused the systematic error. 2)Some inherent error in the measurement of the separation of the transducers, 3)Using the physical radius of the transducer instead of the effective radius. The disagreement can be a combination of the three possible errors mentioned above.

Let the speed of sound, for example, be 344.289m/s. An error of 0.08m/s in the speed of sound could easily have caused approximately 200ns difference for the separation of 301.86mm.

To demonstrate, how an inherent error in the measurement of separation of transducers can cause a disagreement mentioned above, the following simulations were made for both pairs with z = 401.80mm instead of z = 401.86mm. The results for pair1 and pair2 are shown in Fig.(7.10) and Fig.(7.11) respectively.

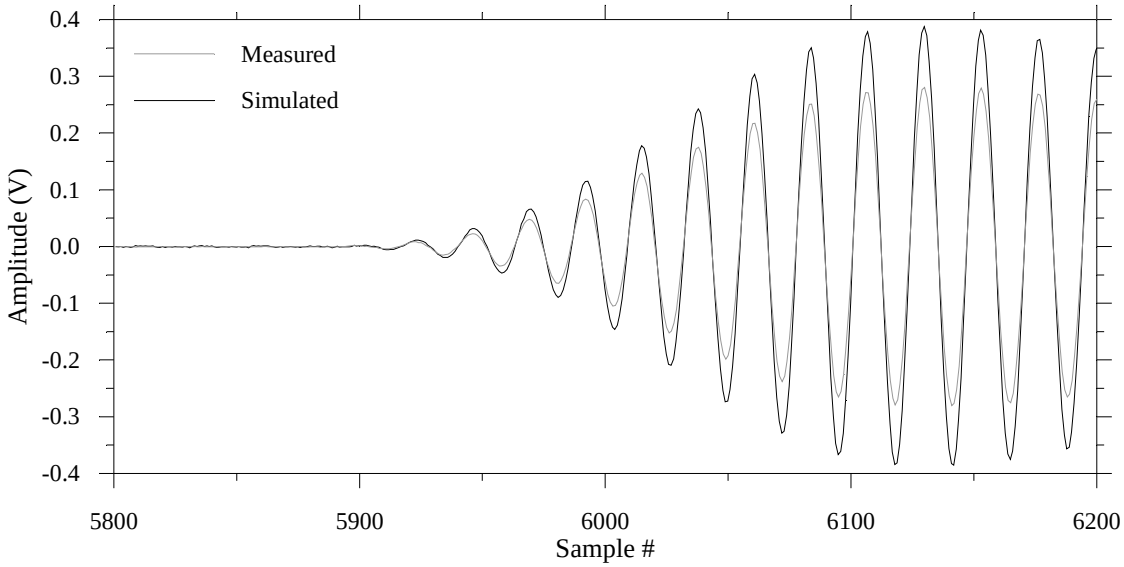

Figure 7.10 A portion in the start of the measured voltage output signal for the transducer separation z = 401.86mm and simulated output voltage signals for the transducer separation 401.80mm are shown. The simulated signal was calculated using the measured output voltage signal of the set X_{11}-X_{20} for transducer separation z = 100.50mm. The measured signal belongs to the set Z_1-Z_{10}.

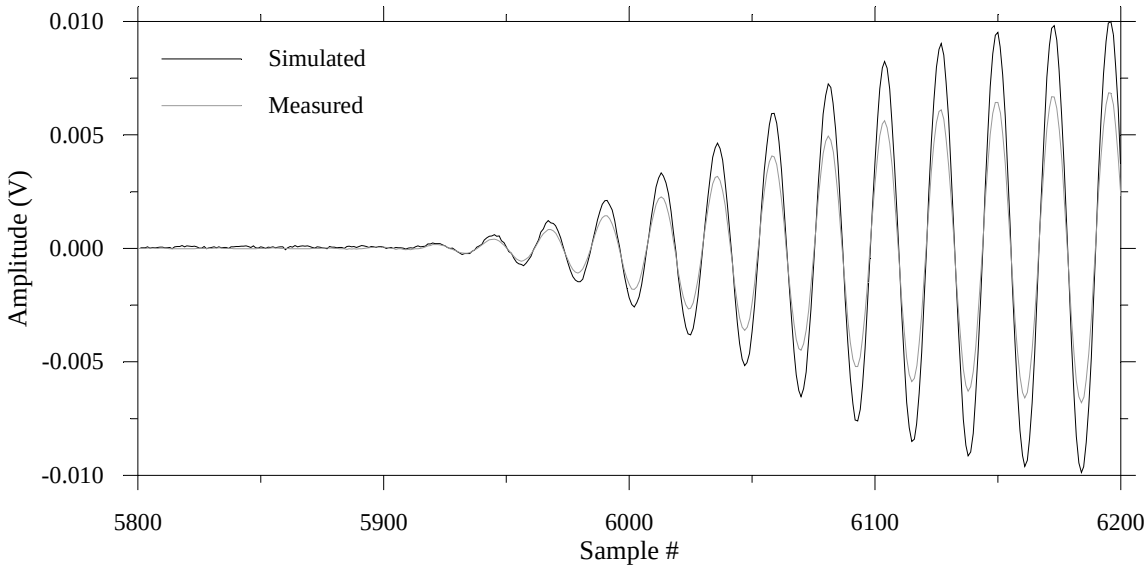

Figure 7.11 A portion in the start of the measured output voltage signal for the transducer separation z = 401.86mm and simulated output voltage signals for the transducer separation 401.80mm are shown. The simulated signal was calculated using the measured output voltage signal of the set X_{91}-X_{100} for transducer separation z = 100.50mm. The measured signal belongs to the set Z_{31}-Z_{40}.

CALCULATION OF ABSORPTION

A decaying plane wave can be written as,

$$p = P_0 \, e^{-\alpha z} \, e^{j(\omega t - kz)} \tag{7.5}$$

where α is the attenuation coefficient whose unit is m^{-1}.

The amplitude attenuation in dB is given by,

$$20\log\left(\frac{p_{rms}}{(P_0)_{rms}}\right)=20\log\left(\frac{(P_0)_{rms}e^{-\alpha z}}{(P_0)_{rms}}\right)=20\log\left(e^{-\alpha z}\right). \tag{7.6}$$

Consider the near-field finite receiver model described in Sec.(4.2.2). The average pressure on the circular plane placed on the common axis with the sender, for continuous excitation, $U_0e^{j\omega t}$, is given by Eq.(4.35). Absorption can be included to this case by putting $\omega/c = \mathbf{k}$, a complex wave number, and $\mathbf{k} = (k_0\text{-}j\alpha)$. Then the average pressure, $\langle p_{ab}(z,\omega)\rangle$, can be written as,

$$\left\langle p_{ab}(z,\omega)\right\rangle=\rho_0cU_0e^{j(\omega t-k_0z)}e^{-\alpha z}\left[1-e^{j(k_0-j\alpha)z}\frac{4}{\pi}\int_0^{\pi/2}e^{-j(k_0-j\alpha)(z^2+4a^2\cos^2\theta)^{1/2}}\sin^2\theta d\theta\right], \tag{7.7}$$

or

$$\left\langle p_{ab}(z,\omega)\right\rangle=p_0e^{-\alpha z}\left[1-e^{j(k_0-j\alpha)z}\frac{4}{\pi}\int_0^{\pi/2}e^{-j(k_0-j\alpha)(z^2+4a^2\cos^2\theta)^{1/2}}\sin^2\theta d\theta\right], \tag{7.8}$$

where

$$p_0=\rho_0c_0U_0e^{j(\omega t-k_0z)} \tag{7.9}$$

is the plane wave. The diffraction correction both in magnitude and in phase, as in Ref.(7) and in Ref.(36), is given by the ratio of the average pressure to the exponentially decaying plane wave. That is,

$$\frac{\left\langle p_{ab}(z,\omega)\right\rangle}{p_0e^{-\alpha z}}=\left[1-e^{j(k_0-j\alpha)z}\frac{4}{\pi}\int_0^{\pi/2}e^{-j(k_0-j\alpha)(z^2+4a^2\cos^2\theta)^{1/2}}\sin^2\theta d\theta\right]. \tag{7.10}$$

It has been shown in Ref.(7) that, for $\alpha \ll k_0$, the effect of intrinsic absorption in the magnitude of the diffraction correction can be neglected. It is shown in Ref.(36) that the effect of intrinsic absorption in the phase of the diffraction correction can also be neglected when $\alpha \ll k_0$. Therefore, αs, in the right hand side of the Eq.(7.10) can be replaced by zeros. Then Eq.(7.10) can be written, using Eq.(4.40), as,

$$\left\langle p_{ab}(z,\omega)\right\rangle=e^{-\alpha z}\left\langle p(z,\omega)\right\rangle. \tag{7.11}$$

$$=U(\omega)\cdot H_{24}^{ab}(z,\omega) \tag{7.12}$$

where,

$$H_{24}^{ab}(z,\omega)=H_{nf}(z,\omega)e^{-\alpha z}, \tag{7.13}$$

is the velocity to free field pressure(average) with absorption. Then, using this transfer function, Eq.(7.4) can be modified, to include the absorption, as,

$$V_6^{ab}(z_2,\omega)=\left[\frac{H_{24}(z_2,\rho_2,c_2,\omega)}{H_{24}(z_1,\rho_1,c_1,\omega)}\cdot V_6(z_1,\omega)\right]\cdot e^{-\alpha(z_2-z_1)}. \tag{7.14}$$

In the above equation, $V_6^{ab}(z_2,\omega)$ is the received voltage signal with absorption, the term in the

brackets is the received voltage signal without absorption(see Eq.(7.4)) and the term with exponential is the absorption factor. Then, Eq.(7.14) can be written as,

$$V_6^{ab}(z_2,\omega) = V_6(z_2,\omega)\cdot e^{-\alpha(z_2-z_1)}. \tag{7.15}$$

Inverse Fourier transform of the both sides of the Eq.(7.15) will give the corresponding time signals,

$$v_6^{ab}(t) = v_6(t)\cdot e^{-\alpha(z_2-z_1)}. \tag{7.16}$$

$v_6^{ab}(t)$ in the Eq.(7.16) can be taken as the measured signal. Then, this equation can be used to calculate the absorption between the distance z_1 and z_2, using the calculated and measured signals in Figs.(7.5) and (7.8). The measured signal contains both the diffraction effect and absorption and the simulated signal contains only the diffraction effects.

The absorption coefficient is, then,

$$\frac{20\log\left(\frac{|v_6^{ab}(z_2,t)|}{|v_6(z_2,t)|}\right)}{(z_2-z_1)} dB/m. \tag{7.12}$$

Calculation of absorption of the measurement pair1 needs an additional data processing. The simulated signal has to be corrected for the difference in the input voltage signals shown in Fig.(7.4). Consider the Eqs.(7.1) and (7.2). The frequency spectrum of the input signal, $V_0(\omega)$, in these equations are no longer equal. As the frequencies of the input signals are equal, the spectrums of the input signals in Eqs.(7.1) and (7.2) can be replaced by $A_1V(\omega)$ and $A_2V(\omega)$ respectively, where A_1 and A_2 are the amplitudes of the measured input voltage signals for z = 100.50mm and z = 401.86mm respectively. This will change the Eq.(7.4) by a multiplicative factor A_2/A_1. As this factor is a frequency independant constant, the correct voltage output signal can be found by direct multiplication of the simulated signal by A_2/A_1. In order to prevent any confusion, the simulated signal corrected for amplitude difference is denoted as $v_6^{ab}(t)$ and uncorrected signal is denoted with a prime as $v_6^{'ab}(t)$.

From the Table(7.1), the average absorption coefficient is 9.01dB/m. To be with the same scale as in Ref.(7), deviding the absorption coefficient in dB/m by (8.69*1000) gives α = 0.001mm^{-1}. The value of $k\left(=\frac{2\pi}{\lambda}\right)$ for this pair(Table(7.1)) of measurements is 3.8339mm^{-1}. That is, this measurement pair satisfy the condition, $\alpha \ll k$. For the pair2, from Table(7.2), average absorption coefficient is 9.48dB/m and α is 0.001mm^{-1} and k is 3.9420mm^{-1}. This pair of measurements also satisfy the condition, $\alpha \ll k$. The calculated absorption from the two pairs of measurements are given in Table(7.3).

	Pair1	Pair2
The ampltude of the simulated signal, $v_6^{'ab}(t)$. (vlots).	0.32	0.01091
Amplitude correction factor, A_2/A_1,	7.75/7.50	1
Corrected amplitude, $v_6^{ab}(t) = v_6^{'ab}(t)*A_2/A_1$. (volts)	0.3306	0.01091
The amplitude of the measured signal, $v_6^{ab}(t)$, (volts)	0.237	0.00765
Distance between the receiver locations of the two mesurements (mm)	301.36	301.36
The absorp. coeff, from the measurements, using Eq.(7.12). (dB/m)	9.59	10.23
The average absorp. coeff. from Tables(7.1) & (7.2). (dB/m)	9.01	9.48

Table 7.3 Absorption from the measurements.

7.5 DISCUSSION & CONCLUSION

There are two different measurements of separation of transducers involved in the analysis of each of pair1 and pair2. Both measurements could possibly have error. The separation measurements were made with an internal micrometer. It is very difficult to decide when the tip of the device touches the face of the transducer. Inaddition, the face of the transducers are made of rubber like material which makes it even more difficult. One can easily make a few hundredths of a millimeter error in the measurement of separation. The Figs.(7.10) and (7.11) demonstrate that a few hundredths of a millimeter can easily lead to an error of couple of hundred nano seconds.

The parameters used in the calculations for testing of the programme, DIF2FILD, and the parameters of pair1 are same. Hence, the theoritical phase correction of diffraction of pair1, is 216.6ns.

In the analysis, measurements "X" and "Z" were chosen as the environmental differences between these measurements are very small. But the same kind of analysis has been done for measurements "X" and "Y". That is, using the measurements for the transducer separation, 0.10050m, the voltage signal for the transducer separation, 0.20836m, was predicted. This analysis is not documented because of short of time. Since absorption is not implemented in the simulation, one should expect the simulated signal to be larger than the measured. But to the surprise, the measured signal was larger than the simulated. The reason to this must be the increase in transmitting response of the transmitter. The average temperature for the series of measurements "X" was 20.129°C and for measurements "Y" was 21.194°C. In this temperature variation the transmitting response of the transmitter has increased. Exact measurements are not available to prove this, but the tendency of the behaviour for the frequency, 210kHz, can be seen in Fig.(5.15) in Ref.(15). The use of sensitivity plots in explaining the shape of the received signal was pointed out in the discussion in Chapter 3 in Sec.(3.5).

CHAPTER 8

SUMMERY AND CONCLUSION

The effects of the acoustic part of a transit-time flow meter on pulse forming, at no flow conditions, are studied in this work. The effects of diffraction and of the transducer dynamics on pulse forming are studied individually and as a system. Pulse forming mechanisms in the transducers and of diffraction are studied using the impulse responses and time convolutions. The effects of the total system on the form of the whole pulse are studied using the frequency domain methods; the Fourier methods. An experiment was performed and the results are analysed and discussed.

The active face of a circular transducer, an imaginary circular surface of dimension equal to the transducer placed coaxially in front of it and the medium in between are considered as a linear time invariant filter. The transient response(average pressure), for an impulsive velocity, of this filter is found and compared with the earlier results[23]. Pulse forms for a uniform sinusoidal velocity burst are calculated and presented as a function of S and ka values. The pulse forms are also compared with that of the far-field and near-field point receiver models.

The response of the system, for open circuit conditions, with the model for real transducer, is simulated. The effect of the matching layer on the initial transient, ringing and the signal level is discussed. It is indicated that, with proper models for the transducer, propagation and electronics, the simulations will guide the experimenter to interpret the received signal and hence to make correct measurements.

The pulse form from the experiment, for z(separation of the transducers) = 401.86mm, was predicted theoretically with the propagation model, using the measured pulse form for z = 100.50mm as the input. The predicted pulse form was not in good agreement with the measured one. Possible reasons for this deviation are discussed.

In the analysis of the experimental results, it was assumed that the environmental condition and the input voltage signals of the two measurement situations are identical. But, these assumptions were not fulfilled in the experiment. In experiments, where the requirements are achieved, this method can be used to calculate the diffraction correction. For example, in Pulse Echo Overlap(PEO) method, the echoes compared are measured at exactly the same environmental conditions and have the same input voltage signal. Moreover this method does not need a model for the transducers.

Appendix A-1

Velocity to average pressure impulse response.

Velocity to average pressure transfer function is given by (see Eq.(4.41b),

$$H_{nf}(\omega) = \rho_0 c\left[e^{-j\omega t_z} - \frac{4}{\pi}\int_0^{\infty} e^{-j\omega t(\theta)} \sin^2\theta d\theta \right] \tag{A-1-1}$$

where

$$t_z = z/c, \tag{A-1-2}$$

$$t(\theta) = (z^2+4a^2\cos^2\theta)^{1/2}/c \tag{A-1-3}$$

Velocity to average pressure impulse response is given by the inverse Fourier transform of the velocity to average pressure transfer function. Taking inverse Fourier transform of Eq.(A-1-1),

$$h_{nf}(t) = \frac{1}{2\pi}\int_{-\infty}^{\infty} H_{nf}(\omega) e^{j\omega t} d\omega \tag{A-1-4}$$

$$= \rho_0 c\left[\frac{1}{2\pi}\int_{-\infty}^{\infty} e^{-j\omega t_z} e^{j\omega t} d\omega - \frac{1}{2\pi}\int_{-\infty}^{\infty} \frac{4}{\pi}\int_0^{\pi/2} e^{-j\omega t(\theta)} \sin^2\theta d\theta e^{j\omega t} d\omega \right] \tag{A-1-5}$$

$$= \rho_0 c\left[\frac{1}{2\pi}\int_{-\infty}^{\infty} e^{-j\omega t_z} e^{j\omega t} d\omega - \frac{4}{\pi}\int_0^{\pi/2} \left(\frac{1}{2\pi}\int_{-\infty}^{\infty} e^{-j\omega t(\theta)} e^{j\omega t} d\omega \right) \sin^2\theta d\theta \right] \tag{A-1-6}$$

$$= \rho_0 c\left[\delta(t - t_z) - \frac{4}{\pi}\int_0^{\pi/2} \delta(t - t(\theta)) \sin^2\theta d\theta \right] \tag{A-1-7}$$

From Eq.(A-1-3),

$$t(\theta) = \frac{\sqrt{z^2 + 4a^2\cos^2\theta}}{c} \tag{A-1-8}$$

$$\cos^2\theta = \frac{c^2[t(\theta)]^2 - z^2}{4a^2} \tag{A-1-9}$$

Differentiating Eq.(A-1-8) with respect to θ gives,

$$d\theta = \frac{-c^2 t(\theta)}{4a^2 \sin\theta \cos\theta} d\left[t(\theta)\right] \qquad \text{(A-1-10)}$$

Substituting for $d\theta$ and $\sin^2\theta$ in Eq.(A-1-7) from Eq.(A-1-10) and Eq.(A-1-9) gives,

$$h_{nf}(t) = \rho_0 c\left[\delta(t-t_z) - \frac{1}{\pi a^2}\int_{t_z}^{t_{4az}} \delta(t-t(\theta)) \frac{c^2 t(\theta)\sqrt{4a^2 - c^2\left[t(\theta)\right]^2 + z^2}}{\sqrt{c^2\left[t(\theta)\right]^2 - z^2}} d\left[t(\theta)\right]\right] \qquad \text{(A-1-11)}$$

where

$$t_{4az} = (4a^2+z^2)^{1/2}/c \qquad \text{(A-1-12)}$$

The above integration takes values[8] only when $t = t(\theta)$. Therefore,

$$h_{nf}(t) = \rho_0 c\left[\delta(t-t_z) - \frac{c^2 t}{\pi a^2}\sqrt{\frac{z^2 + 4a^2 - c^2 t^2}{c^2 t^2 - z^2}}\right] \qquad t_z \le t \le t_{4az} \qquad \text{(A-1-13)}$$

or

$$h_{nf}(t) = \rho_0 c\left[\delta(t-t_z) - \frac{c^2 t}{\pi a^2}\sqrt{\frac{t_{4az}^2 - t^2}{t^2 - t_z^2}}\right] \qquad t_z \le t \le t_{4az} \qquad \text{(A-1-14)}$$

Appendix(A-2)

Convolution integral for the near-field finite receiver model.

Consider the convolution integral given Eq.(4.88). The equation is rewritten and renumbered as (A.2.1).

$$p_{nf}(z,t) = h_{nf}(z,t) \otimes u(t) \tag{A.2.1}$$

where

$$h_{nf}(z,t) = h_{1nf}(z,t) + h_{2nf}(z,t) \tag{A.2.2}$$

$$h_{1nf}(z,t) = \rho_0 c\delta(t-t_z), \tag{A.2.3}$$

$$h_{2nf}(z,t) = -\frac{\rho_0 c^3 t}{\pi a^2}\left[\frac{t_{4az}^2 - t^2}{t^2 - t_z^2}\right]^{\frac{1}{2}} \quad t_z < t \le t_{4az}, \tag{A.2.4}$$

and

$$u(t) = U_0\left[\mathbf{U}(t)-\mathbf{U}(t-T')\right]\sin\omega_0 t. \tag{A.2.5}$$

$$p_{nf}(z,t) = \int_{-\infty}^{\infty} u(t-\tau)\left[h_{1nf}(z,\tau) + h_{2nf}(z,\tau)\right]d\tau \tag{A.2.6}$$

$$p_{nf}(z,t) = \int_{-\infty}^{\infty} u(t-\tau)\rho_0 c\delta(\tau - t_z)d\tau + \int_{-\infty}^{\infty} u(t-\tau)h_{2nf}(z,\tau)d\tau. \tag{A.2.7}$$

Using the sifting property of the Direc delta function,

$$p_{nf}(z,t) = \rho_0 c u(t-t_z) + \int_{t_z}^{t} u(t-\tau)h_{2nf}(z,\tau)d\tau. \tag{A.2.8}$$

The second term in the above expression for $p_{nf}(z,t)$ has to be calculated, as pointed out in the beginning of the Sec.(4.3), numerically. The singularity in the function, $h_{2nf}(z,t)$, makes the task little difficult. The following method was used to calculate the integration. (The method to integrate the function at the singularity was suggested by Westrheim. This method is implemented in the programme for calculating the whole convolution integral in Eq.(A-2-1) given in Appendix(B-1). The programme was written by me and tested out with the consultation of Westrheim.)

The second term in the Eq.(A-2-8) is splitted into two parts. With this splitting, Eq.(A-2-8) can be written as,

$$p_{nf}(z,t) = \rho_0 c u(t-t_z) + \int_{t_z}^{t_z+\Delta} u(t-\tau) h_{2nf}(z,\tau) d\tau + \int_{t_z+\Delta}^{t} u(t-\tau) h_{2nf}(z,\tau) d\tau, \quad \text{(A.2.9)}$$

where Δ is a small interval in the neighborhood of t_z. To minimise the writting the following aberiviations are used.

$$I_1 = \rho_0 c\, u(t-t_z), \quad \text{(A.2.9a)}$$

$$I_2 = \int_{t_z}^{t_z+\Delta} u(t-\tau) h_{2nf}(z,\tau) d\tau \quad \text{(A.2.9b)}$$

and

$$I_3 = \int_{t_z+\Delta}^{t} u(t-\tau) h_{2nf}(z,\tau) d\tau . \quad \text{(A.2.9c)}$$

Substituting for $h_{2nf}(z,t)$ in Eq.(A.2.9b) gives,

$$I_2 = \int_{t_z}^{t_z+\Delta} u(t-\tau) \frac{-\rho_0 c^3 \tau}{\pi a^2} \left[\frac{t_{4za}^2 - \tau^2}{\tau^2 - t_z^2} \right]^{\frac{1}{2}} d\tau \quad \text{(A.2.10)}$$

Let,

$$\tau = t_z + \Delta', \quad \text{(A.2.11)}$$

where

$$\Delta' \in [t_z , t_z+\Delta]. \quad \text{(A.2.12)}$$

Then

$$d\tau = d\Delta' \quad \text{(A.2.13)}$$

$$I_2 = \int_0^{\Delta} u(t-t_z-\Delta') \frac{-\rho_0 c^3 (t_z+\Delta')}{\pi a^2} \left[\frac{t_{4az}^2 - (t_z+\Delta')^2}{(t_z+\Delta')^2 - t_z^2} \right]^{\frac{1}{2}} d\Delta' \quad \text{(A.2.14)}$$

Since $\Delta' \ll t_z$, t_{4az}, higher order terms in Δ' can taken to be negligible and the change in the velocity signal is assumed to be very small in the interval Δ, I_2 can be approximated as follows.

$$I_2 \approx u(t-t_z) \frac{-\rho_0 c^3 t_z (t_{4az}^2 - t_z^2)^{\frac{1}{2}}}{\pi a^2} \int_0^{\Delta} \left[\frac{1}{2\Delta'} \right]^{\frac{1}{2}} d\Delta' \quad \text{(A.2.15)}$$

$$= u(t - t_z)\frac{-\rho_0 c^3 t_z \sqrt{2\Delta(t_{4za}^2 - t_z^2)}}{\pi a^2} \qquad \text{(A.2.16)}$$

The integral I_2 is proportional to the square root of the interval, Δ. Therefore, smaller the interval, Δ, higher the accuracy of the integral I_2.

The integration I_3 can be calculated using usual numerical integration methods. The integration takes different limits in different rang of time, t. This is explained shortly.

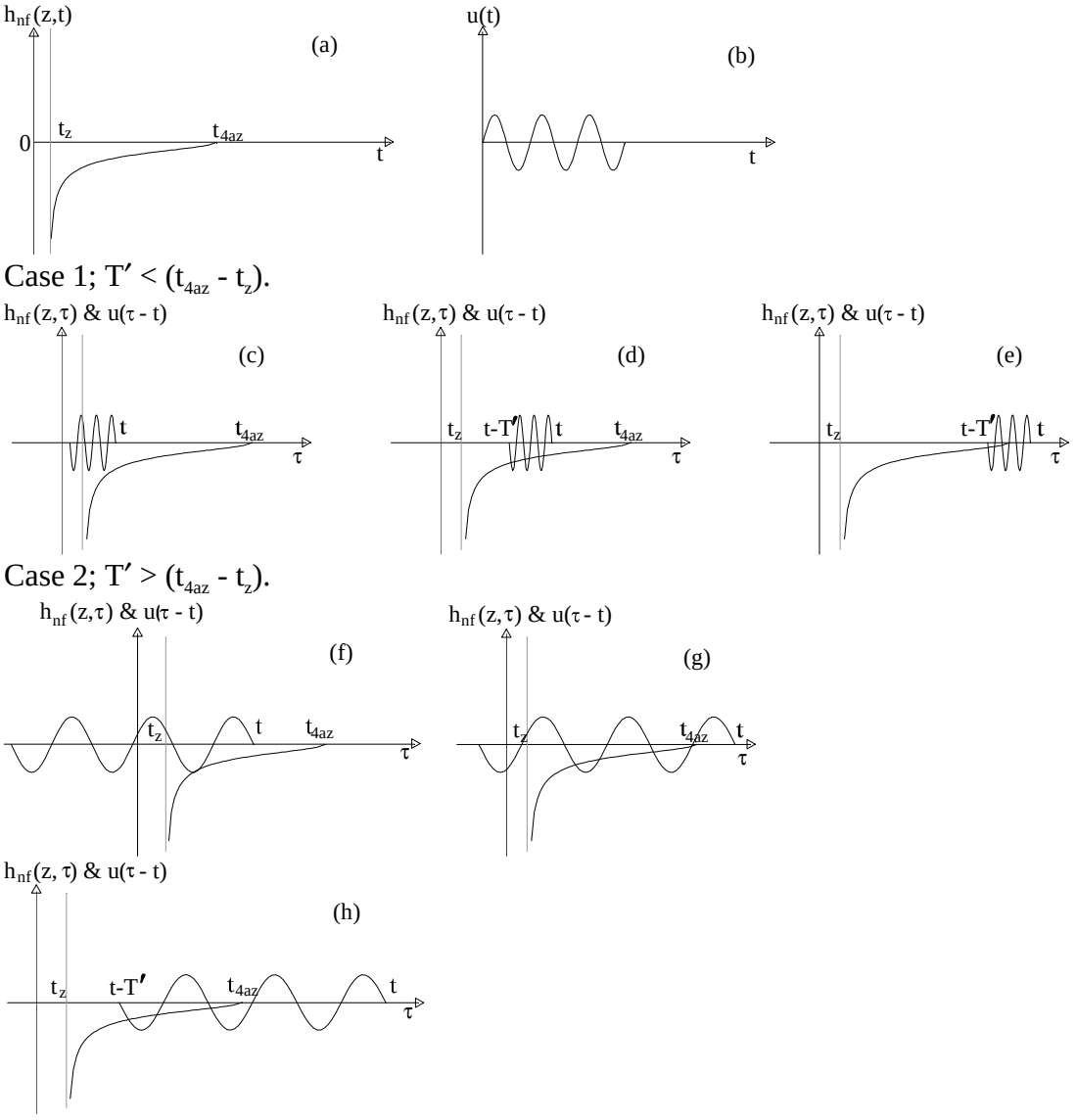

Figure A.2.1 (a) a portion of the impulse response, $h_{2nf}(z,t)$ (b) velocity signal, u(t). (c), (d) and (e) functions in the integrand of I_3 for different ranges of t while $T' < (t_{4az} - t_z)$. (f), (g) and (h) functions in the integrand of I_3 for different ranges of t while $T' > (t_{4az} - t_z)$.

Fig.(A.2.1)(a) and (b) show the impulse response function and the velocity function involved in the integration I_3, given in Eq.(A.2.9c). These figures and the rest are not drawn to scale. Considering the duration of the velocity function, the integration splits into two cases; $T' < (t_{4az} - t_z)$ and $T' > (t_{4az} - t_z)$ where T' is the duration of the velocity function and $(t_{4az} - t_z)$ is the duration of the impulse response.

Fig.(A.2.1)(c) represents the functions in the integrand of the following integral,

$$I_3 = \int_{t_z+\Delta}^{t} u(t-\tau)h_{2nf}(z,\tau)d\tau \qquad t_z \le t \le t_z + T' \qquad \text{(A.2.17)}$$

Similarly the Figs.(A.2.1)(d) and (e) represent the functions in the integrand of the integrals given in Eqs.(A.2.18) and (A.2.19) respectively.

$$I_3 = \int_{t-T'}^{t} u(t-\tau)h_{2nf}(z,\tau)d\tau \qquad t_z + T' \le t \le t_{4az} \qquad \text{(A.2.18)}$$

$$I_3 = \int_{t-T'}^{t_{4az}} u(t-\tau)h_{2nf}(z,\tau)d\tau \qquad t_{4az} \le t \le t_{4az} + T' \qquad \text{(A.2.19)}$$

Since the impulse response is larger than the input signal, there is no steady state in the signal.

The Figs.(A.2.1)(f),(g) and (h) show the functions in the integrand of the integrals given in Eqs.(A.2.20), (A.2.21) and (A.2.22) respectively.

$$I_3 = \int_{t_z+\Delta}^{t} u(t-\tau)h_{2nf}(z,\tau)d\tau \qquad t_z \le t \le t_{4az} \qquad \text{(A.2.20)}$$

$$I_3 = \int_{t_z+\Delta}^{t_{4az}} u(t-\tau)h_{2nf}(z,\tau)d\tau \qquad t_{4az} \le t \le t_z + T' \qquad \text{(A.2.21)}$$

$$I_3 = \int_{t-T'}^{t_{4az}} u(t-\tau)h_{2nf}(z,\tau)d\tau \qquad t_z + T' \le t \le t_{4az} + T' \qquad \text{(A.2.22)}$$

In the range, $(t_z + T') < t$, there is no contribution from the integrals I_1 and I_2 for both cases.

Appendix (A-3)

Diffraction factor for a circular receiver

The Fig(A-3-1) shows plane waves incident on a circular receiver making an angle, θ, with the normal to the face of the receiver. This plane wave can be denoted as $p(t) = P_0\, e^{j(\omega t - kR)}$, where R is the distance between the centre of receiver and the source of the plane wave. The free-field pressure, denoted as P_4 in the text, due this plane wave at the centre of the receiver is $P_0\, e^{-jkR}$. The pressure at the centre of the receiver in the presence of a receiver, assuming the receiver as an infinite plane baffle, is $2P_4$.

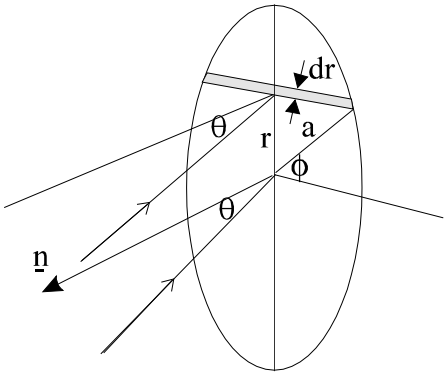

Figure(A-3-1)Plane wave incident on the surface of the receiver.

Consider a small stripe of thickness, dr, on the receiver at a distance, r, from the centre of the receiver. Since the pressure along this stripe is constant, the total pressure on this stripe, dp, is,

$$dp = P_0\, e^{-jk(R + r\sin\theta)}\, 2a\cos\varphi\, dr \qquad \text{(A-3-1)}$$

where a is the radius of the receiver.

The force, F_b(or the open circuit force in the text), on the receiver face, then, is,

$$F_b = \int_{-a}^{a} 2P_0\, e^{-jk(R + r\sin\theta)}\, 2a\cos\varphi\, dr \qquad \text{(A-3-2)}$$

From the figure it can be seen that $r = a\sin\varphi$, then $dr = a\cos\varphi\, d\varphi$. The force, F_b, then will be

$$F_b = 2P_4 \int_{-\frac{\pi}{2}}^{\frac{\pi}{2}} e^{-jkr\sin\theta}\, 2a^2\cos^2\varphi\, d\varphi \qquad \text{(A-3-3)}$$

$$F_b = 2P_4\, 2a^2\, \pi \frac{J_1(ka\sin\theta)}{(ka\sin\theta)} \qquad \text{(A-3-4)}$$

$$F_b = 2 P_4 A \frac{2 J_1(ka \sin\theta)}{(ka \sin\theta)} \quad \text{(A-3-5)}$$

where A is the area of the receiver.

or

$$F_b = DA\ P_4 \quad \text{(A-3-6)}$$

where D is known as the diffraction factor.

For normal incidence the diffraction factor, D, becomes 2.

Appendix (A-4)

Pulse form as a function of S and ka values.

The average pressure $p_{nf}(z,t)$ is given by,

$$p_{nf}(z,t) = \int_{-\infty}^{\infty} h_{nf}(z,\tau)u(t-\tau)d\tau \qquad \text{(A-4-1)}$$

where

$$h_{nf}(z,t) = \rho_0 c\left[\delta(t-t_z) - \frac{c^2 t}{\pi a^2}\sqrt{\frac{t_{4az}^2 - t^2}{t^2 - t_z^2}}\right] t_z < t \le t_{4az} \qquad \text{(A-4-2)}$$

where

$$t_z = \frac{z}{c} \qquad \text{and} \qquad t_{4az} = \frac{\sqrt{4a^2+z^2}}{c}$$

$$u(t) = [U(t) - U(t-NT)]\sin\omega t \qquad \text{(A-4-3)}$$

$$p_{nf}(z,t) = \int_{-\infty}^{\infty} \rho_0 c\left[\delta(\tau - t_z) - \frac{c^2\tau}{\pi a^2}\sqrt{\frac{t_{4az}^2 - \tau^2}{\tau^2 - t_z^2}}\right] \times [U(t-\tau) - U(t-\tau-NT)]\sin\omega(t-\tau)d\tau \qquad \text{(A-4-4)}$$

$$p_{nf}(z,t) = p_{1nf}(z,t) + p_{2nf}(z,t) \qquad \text{(A-4-5)}$$

where

$$p_{1nf}(z,t) = \rho_0 c\int_{-\infty}^{\infty} \delta(\tau - t_z)[U(t-\tau) - U(t-\tau-NT)]\sin\omega(t-\tau)d\tau \qquad \text{(A-4-6)}$$

$$p_{2nf}(z,t) = -\rho_0 c\int_{-\infty}^{\infty} \frac{c^2\tau}{\pi a^2}\sqrt{\frac{t_{4az}^2 - \tau^2}{\tau^2 - t_z^2}}[U(t-\tau) - U(t-\tau-NT)]\sin\omega(t-\tau)d\tau \qquad \text{(A-4-7)}$$

In terms of normalised time the Eqs.(A-4-6) and (A-4-7) can be written as follows. Defining,

$$\hat{t} = \frac{t}{T}, \hat{\tau} = \frac{\tau}{T}, \hat{t}_z = \frac{t_z}{T} \;\&\; \hat{t}_{4az}\,\frac{t_{4az}}{T} \qquad \text{(A-4-8)}$$

$$p_{1nf}(z,\hat{t}) = \rho_0 c \int_{-\infty}^{\infty} \delta(\hat{\tau}T - \hat{t}_z T)\left[U(\hat{t}T - \hat{\tau}T) - U(\hat{t}T - \hat{\tau}T - NT)\right] \times \sin\omega(\hat{t}T - \hat{\tau}T)d(\hat{\tau}T) \tag{A-4-9}$$

$$p_{1nf}(z,\hat{t}) = \rho_0 c \int_{-\infty}^{\infty} \delta(\hat{\tau} - \hat{t}_z)T\left[U(\hat{t} - \hat{\tau})T - U(\hat{t} - \hat{\tau} - N)T\right] \times \sin\omega T(\hat{t} - \hat{\tau})Td\hat{\tau} \tag{A-4-10}$$

Using

$$\delta(at) = \frac{1}{|a|}\delta(t) \tag{A-4-11}$$

$$U(at) = U(t) \tag{A-4-12}$$

$$p_{1nf}(z,\hat{t}) = \rho_0 c \int_{-\infty}^{\infty} \delta(\hat{\tau} - \hat{t}_z)\left[U(\hat{t} - \hat{\tau}) - U(\hat{t} - \hat{\tau} - N)\right]\sin 2\pi(\hat{t} - \hat{\tau})d\hat{\tau} \tag{A-4-13}$$

Using sifting property of the Dirac delta function,

$$p_{1nf}(z,\hat{t}) = \rho_0 c\left[U(\hat{t} - \hat{t}_z) - U(\hat{t} - \hat{t}_z - N)\right]\sin 2\pi(\hat{t} - \hat{t}_z). \tag{A-4-14}$$

$$\hat{t}_z = \frac{z}{\left(a^2/\lambda\right)}\frac{a^2}{\lambda}\frac{1}{cT} = s\frac{a^2}{\lambda^2} = s\frac{(ka)^2}{4\pi^2}. \tag{A-4-15}$$

The above relation proves that $p_{1nf}(z,\hat{t})$ is a function is a function of S and ka only.

Recalling Eq.(A-4-7),

$$p_{2nf}(z,t) = -\rho_0 c \int_{-\infty}^{\infty} \frac{c^2\tau}{\pi a^2}\sqrt{\frac{t_{4az}^2 - \tau^2}{\tau^2 - t_z^2}}\left[U(t-\tau) - U(t-\tau-NT)\right]\sin\omega(t-\tau)d\tau$$

and considering the duration of $h_{nf}(z,t)$, it can be written as,

$$p_{2nf}(z,t) = -\rho_0 c \int_{0}^{t} \frac{c^2\tau}{\pi a^2}\sqrt{\frac{t_{4az}^2 - \tau^2}{\tau^2 - t_z^2}}\left[U(t-\tau) - U(t-\tau-NT)\right]\sin\omega(t-\tau)d\tau. \tag{A-4-16}$$

Substituting for t and τ from (A-4-8), $p_{2nf}(z,t)$ can be written as follows,

$$d\tau = Td\hat{\tau}$$

$$\tau = 0 \rightarrow \hat{\tau} = 0$$

$$\tau = t \rightarrow \hat{\tau} = \hat{t}$$

$$p_{2nf}(z,\hat{t}) = -\rho_0 c\int_0^{\hat{t}} \frac{c^2\hat{\tau}T}{\pi a^2}\sqrt{\frac{\hat{t}_{4az}^2-\hat{\tau}^2T^2}{\hat{\tau}^2T^2-\hat{t}_z^2T^2}}\left[U(\hat{t}T-\hat{\tau}T)-U(\hat{t}T-\hat{\tau}T-NT)\right] \times \sin\omega(\hat{t}T-\hat{\tau}T)d(\hat{\tau}T) \quad \text{(A-4-17)}$$

Using

$$U(at) = U(t)$$

$$p_{2nf}(z,\hat{t}) = -\rho_0 c\int_0^{\hat{t}} \frac{c^2\hat{\tau}T^2}{\pi a^2}\sqrt{\frac{\hat{t}_{4az}^2-\hat{\tau}^2}{\hat{\tau}^2-\hat{t}_z^2}}\left[U(\hat{t}-\hat{\tau})-U(\hat{t}-\hat{\tau}-N)\right] \times \sin 2\pi(\hat{t}-\hat{\tau})d\hat{\tau} \quad \text{(A-4-18)}$$

$$p_{2nf}(z,t) = -\rho_0 c\int_0^{\hat{t}} \frac{\hat{\tau}4\pi}{(ka)^2}\sqrt{\frac{\hat{t}_{4az}^2-\hat{\tau}^2}{\hat{\tau}^2-\hat{t}_z^2}}\left[U(\hat{t}-\hat{\tau})-U(\hat{t}-\hat{\tau}-N)\right] \times \sin 2\pi(\hat{t}-\hat{\tau})d\hat{\tau} \quad \text{(A-4-19)}$$

$$t_{4az}^2 = \frac{4a^2+z^2}{c^2} = \frac{4a^2}{c^2}+\left(\frac{z}{c}\right)^2$$

$$\hat{t}_{4az}^2 = \frac{4a^2f^2}{c^2}+\left(\frac{z}{a^2/\lambda}\right)^2\left(\frac{a^2}{\lambda}\right)^2\frac{1}{c^2T^2}$$

$$\hat{t}_{4az}^2 = \frac{4(ka)^2c^2}{4\pi^2c^2}+\frac{s^2a^4f^4}{c^4}$$

$$\hat{t}_{4az}^2 = \frac{(ka)^2}{\pi^2}+\frac{s^2(ka)^4}{16\pi^4}$$

Since $\hat{t}_z$ and $\hat{t}_{4az}$ are functions of S and ka only, $p_{2nf}(z,t)$ is also a function of S and ka only. Therefore the total function $p_{nf}(z,t)$ is a function of S and ka only.

Appendix(A-5)

Transfer functions of transmitting transducer in Laplace domain

TRANSMITTER

THE MASON MODEL

Voltage to velocity transfer function of the transmitter, in Eq.(5.3f), is,

$$H_{tr1}(\omega) = \frac{\phi}{\left(Z_a + Z_b^* + Z_{r2}\right) + Z_b^* \dfrac{\left(Z_a + Z_{r2}\right)}{\left(Z_a + Z_{r1}\right)}} \tag{A-5-1}$$

where

$$Z_b^* = Z_b - \frac{\phi^2}{j\omega C_0} . \tag{A-5-2}$$

In Laplace domain,

$$Z_a = jZ_0 \tan\left(\frac{k\ell}{2}\right) = Z_0 \left(\frac{e^{\frac{s\tau_0}{2}} - e^{-\frac{s\tau_0}{2}}}{e^{\frac{s\tau_0}{2}} + e^{-\frac{s\tau_0}{2}}} \right), \tag{A-5-3}$$

$$Z_b = \frac{Z_0}{j\sin\left(k\ell\right)} = \frac{2Z_0}{e^{s\tau_0} - e^{-s\tau_0}}, \tag{A-5-4}$$

and

$$Z_b^* = \frac{2Z_0}{e^{s\tau_0} - e^{-s\tau_0}} - \frac{\phi^2}{sc_0} \tag{A-5-5}$$

where, $k = \frac{\omega}{c}$, $\tau_0 = \frac{\ell}{c}$ and s is the Laplace variable.

Denote $s\tau_0$ by x and ϕ^2/sc_0 by k for simplicity.

Take the denominator of Eq.(A-5-1), and substitute for Z_a and Z_b^* give,

$$H_{tr1}(s) = \frac{(Z_0 + Z_{r2} - k)e^{x} + (Z_0 - Z_{r2} + k)e^{-x}}{e^{x} - e^{-x}} + \left(\frac{2Z_0}{e^{x} - e^{-x}} - k\right)\left[\frac{(Z_0 + Z_{r2})e^{\frac{x}{2}} - (Z_0 - Z_{r2})e^{-\frac{x}{2}}}{(Z_0 + Z_{r1})e^{\frac{x}{2}} - (Z_0 - Z_{r1})e^{-\frac{x}{2}}}\right] \quad \text{(A-5-6)}$$

$$= \frac{\left[(Z_0 + Z_{r2} - k)e^{x} + (Z_0 - Z_{r2} + k)e^{-x}\right]\left[(Z_0 + Z_{r1})e^{\frac{x}{2}} - (Z_0 - Z_{r1})e^{-\frac{x}{2}}\right] + \left[2Z_0 + k(e^{x} - e^{-x})\right]\left[(Z_0 + Z_{r2})e^{\frac{x}{2}} - (Z_0 - Z_{r2})e^{-\frac{x}{2}}\right]}{(e^{x} - e^{-x})\left[(Z_0 + Z_{r1})e^{\frac{x}{2}} - (Z_0 - Z_{r1})e^{-\frac{x}{2}}\right]} \quad \text{(A-5-7)}$$

Denote the numerator of the above equation by N_1 and the denominator by N_2. Then,

$$N_1 = \begin{bmatrix} (Z_0 + Z_{r2} - k)(Z_0 + Z_{r1})e^{\frac{3x}{2}} - (Z_0 + Z_{r2} - k)(Z_0 - Z_{r1})e^{\frac{x}{2}} \\ + (Z_0 - Z_{r2} + k)(Z_0 + Z_{r1})e^{-\frac{x}{2}} - (Z_0 - Z_{r2} + k)(Z_0 - Z_{r1})e^{-\frac{3x}{2}} \\ + 2Z_0(Z_0 + Z_{r2})e^{\frac{x}{2}} - 2Z_0(Z_0 - Z_{r2})e^{-\frac{x}{2}} - k(Z_0 + Z_{r2})e^{\frac{3x}{2}} \\ + k(Z_0 - Z_{r2})e^{\frac{x}{2}} + k(Z_0 + Z_{r2})e^{-\frac{x}{2}} - k(Z_0 - Z_{r2})e^{-\frac{3x}{2}} \end{bmatrix} \quad \text{(A-5-8)}$$

$$= e^{\frac{3x}{2}}\begin{bmatrix} (Z_0 + Z_{r2})(Z_0 + Z_{r1}) - k(2Z_0 + Z_{r1} + Z_{r2}) + (Z_0 + Z_{r2})(Z_0 + Z_{r1})e^{-x} \\ + k(2Z_0 - Z_{r1} - Z_{r2})e^{-x} - (Z_0 - Z_{r2})(Z_0 - Z_{r1})e^{-2x} + k(2Z_0 + Z_{r1} + Z_{r2})e^{-2x} \\ - (Z_0 - Z_{r2})(Z_0 - Z_{r1})e^{-3x} - k(2Z_0 - Z_{r1} - Z_{r2})e^{-3x} \end{bmatrix}. \quad \text{(A-5-9)}$$

Adding some dummies,

$$N_1 = e^{\frac{3x}{2}}\begin{bmatrix} (Z_0 + Z_{r1})(Z_0 + Z_{r2})(1 + e^{-x}) - (Z_0 - Z_{r1})(Z_0 - Z_{r2})(1 + e^{-x})e^{-2x} \\ - k(2Z_0 + Z_{r1} + Z_{r2}) - \boldsymbol{k(2Z_0 + Z_{r1} + Z_{r2})e^{-x}} + \boldsymbol{k(2Z_0 + Z_{r1} + Z_{r2})e^{-x}} \\ - \mathbf{k(2Z_0 - Z_{r1} - Z_{r2})e^{-2x}} - k(2Z_0 - Z_{r1} - Z_{r2})e^{-3x} + \mathbf{k(2Z_0 - Z_{r1} - Z_{r2})e^{-2x}} \\ + k(2Z_0 - Z_{r1} - Z_{r2})e^{-x} + k(2Z_0 + Z_{r1} + Z_{r2})e^{-2x} \end{bmatrix} \text{(A-5-10)}$$

$$N_1 = e^{\frac{3x}{2}}\begin{bmatrix} (Z_0 + Z_{r1})(Z_0 + Z_{r2})(1 + e^{-x}) - (Z_0 - Z_{r1})(Z_0 - Z_{r2})(1 + e^{-x})e^{-2x} \\ - k(2Z_0 + Z_{r1} + Z_{r2})(1 + e^{-x}) - k(2Z_0 - Z_{r1} - Z_{r2})(1 + e^{-x})e^{-2x} \\ + 4kZ_0(1 + e^{-x})e^{-x} \end{bmatrix} \quad \text{(A-5-11)}$$

Defining,

$$k_1 = (Z_0 + Z_{r1})(Z_0 + Z_{r2}) - k(2Z_0 + Z_{r1} + Z_{r2}) \quad \text{(A-5-12)}$$

$$k_2 = 4kZ_0 \quad \text{(A-5-13)}$$

$$k_3 = (Z_0\text{-}Z_{r1})(Z_0\text{-}Z_{r2})+k(2Z_0\text{-}Z_{r1}\text{-}Z_{r2}) \tag{A-5-14}$$

$$\underline{\underline{N_1 = e^{\frac{3x}{2}}(1+e^{-x})\left[k_1 + k_2e^{-x} - k_3e^{-2x}\right]}} \tag{A-5-15}$$

$$N_2 = (e^{x} - e^{-x})\left[(Z_0 + Z_{r1})e^{\frac{x}{2}} - (Z_0 - Z_{r1})e^{-\frac{x}{2}}\right] \tag{A-5-16}$$

$$= (Z_0 + Z_{r1})e^{\frac{3x}{2}} - (Z_0 - Z_{r1})e^{\frac{x}{2}} - (Z_0 + Z_{r1})e^{-\frac{x}{2}} + (Z_0 - Z_{r1})e^{-\frac{3x}{2}}, \tag{A-5-17}$$

adding some dummies,

$$= e^{\frac{3x}{2}}\begin{bmatrix} Z_0 + \boldsymbol{Z_0e^{-x}} - \boldsymbol{Z_0e^{-x}} + Z_{r1} + Z_{r1}e^{-x} - Z_0e^{-x} + \mathbf{Z_0e^{-2x}} - \mathbf{Z_0e^{-2x}} \\ - Z_0e^{-2x} - Z_{r1}e^{-2x} + Z_0e^{-3x} - Z_{r1}e^{-3x} \end{bmatrix} \tag{A-5-18}$$

$$\underline{\underline{N_2 = e^{\frac{3x}{2}}(1+e^{-x})\left[(Z_0 + Z_{r1}) - 2Z_0e^{-x} + (Z_0 - Z_{r1})e^{-2x}\right]}}. \tag{A-5-19}$$

Combining these results,

$$\underline{\underline{H_{tr1}(s) = \phi\left[\frac{(Z_0 + Z_{r1}) - 2Z_0e^{-x} + (Z_0 - Z_{r1})e^{-2x}}{k_1 + k_2e^{-x} - k_3e^{-2x}}\right]}} \tag{A-5-20}$$

SIMPLIFIED MODEL

Transfer function of this model is,

$$H_{tr2}(\omega) = \frac{\phi}{(Z_a + Z_b + Z_{r2}) + Z_b\dfrac{(Z_a + Z_{r2})}{(Z_a + Z_{r1})}}. \tag{A-5-21}$$

Consider the denominator of the Eq.(A-5-21). Substituting for Z_a and Z_b from Eqs.(A-5-2) and (A-5-4) gives,

$$\begin{aligned} H_{tr2}(s) = {} & \frac{(Z_0 + Z_{r2})e^{x} + (Z_0 - Z_{r2})e^{-x}}{e^{x} - e^{-x}} \\ & + \left(\frac{2Z_0}{e^{x} - e^{-x}}\right)\left[\frac{(Z_0 + Z_{r2})e^{\frac{x}{2}} - (Z_0 - Z_{r2})e^{-\frac{x}{2}}}{(Z_0 + Z_{r1})e^{\frac{x}{2}} - (Z_0 - Z_{r1})e^{-\frac{x}{2}}}\right] \end{aligned} \tag{A-5-22}$$

This equation is exactly same as Eq.(A-5-6) with k = 0. There fore the simplified form of the Eq.(A-5-22) can be found by putting k = 0 in Eq.(A-5-20). That is,

$$\underline{\underline{H_{tr2}(s) = \phi\frac{(Z_0 + Z_{r1}) - 2Z_0e^{-s\tau_0} + (Z_0 - Z_{r1})e^{-2s\tau_0}}{(Z_0 + Z_{r1})(Z_0 + Z_{r2}) - (Z_0 - Z_{r1})(Z_0 - Z_{r2})e^{-2s\tau_0}}}} \tag{A-5-23}$$

APPENDIX B-1

PROGRAM CONVLSN

This is an iterative program in FORTRAN to calculate I_1, I_2, and I_3 numerically and to find the pressure $p_{nf}(z,t)$. This program uses a sine burst as an input velocity signal to convolve with the impulse response of the radiation coupling filter and finds the output pressure signal from the filter. It is also possible to calculate a portion of the output signal or a single point in the output signal with this program. By increasing the number of points in the decided time interval, one can achive the desired resolution. The program estimates the integration I_2 in the initial interval using the Eq(A-2-16). The initial interval may be decided by the user, a default value is set to 10^{-11}sec. The integration I_3 is calculated using a subroutine, QROMB[11].

The following variables are used in the program.

INPUT SIGNAL PARAMETERS:

AMPL	:	Amplitude of the input sin burst.
WFRQ	:	Frequency of the input signal
PERI	:	Number of periods in the input burst.

RADIATION COUPLING FILTER PARAMETERS:

A	:	Radius of the sound source.
D	:	Distance between the source and the receiver.
C	:	Velocity of sound in the medium.

INTEGRATION VARIABLES:

TS	:	The time at which the signal being calculated (Time Sample).
SS	:	Starting time of the portion of the signal to be calculated(Signal Start).
SE	:	End time of the portion of the signal to be calculated (Signal End).
N	:	Number of points in the portion of the signal to be calculated.
T1	:	Starting time of the impulse response (t_z, used in the text).
T2	:	End time of the impulse response (t_{4za}, used in the text).
ILS	:	Lower limit of the integration (Integration Limit Start).
ILE	:	Upper limit of the integration (Integration Limit End).
TI1	:	Initial interval (Time Interval 1).
TINT	:	Interval between time samples Time INTerval).
SUMM1	:	Estimated integral in the initial interval (I_2, used in the text).
SUMM2	:	Calculated integral in the rest of the interval (I_3, used in the text).
SIG1	:	Result of convolution between the input signal and the delta function in the impulse response.
SIG2	:	Result of convolution between the input signal and the rest of the impulseresponse (SUMM1+SUMM2).
ANS	:	Total result.

```
      SUBROUTINE QROMB(I,A,B,SS)
      DOUBLE PRECISION A,B,SS,DSS,S,H,ER
      PARAMETER(EPS=1.D-5,JMAX=25,JMAXP=JMAX+1,K=5,KM=4)
      DIMENSION S(JMAXP),H(JMAXP)
      H(1)=1.D0
      ER = 1.D-15
      IF (I .EQ. 2) THEN
      SS = 0
      RETURN
      ELSE
      END IF
      DO 11 J=1,JMAX
       CALL TRAPZD(A,B,S(J),J)
       IF (J.GE.K) THEN
        L=J-KM
        CALL POLINT(H(L),S(L),K,0.0D0,SS,DSS)
        IF (ABS(SS-ER).LT.EPS*ABS(ER)) RETURN
        ER = SS
       ENDIF
       S(J+1)=S(J)
       H(J+1)=0.25D0*H(J)
11    CONTINUE
      PAUSE 'Too many steps.'
      END

      SUBROUTINE TRAPZD(A,B,S,N)
      DOUBLE PRECISION A,B,S,FUNC,DEL,SUM,X
      IF (N.EQ.1) THEN
       S=0.5D0*(B-A)*(FUNC(A)+FUNC(B))
       IT=1
      ELSE
       TNM=IT
       DEL=(B-A)/TNM
       X=A+0.5D0*DEL
       SUM=0.D0
       DO 11 J=1,IT
        SUM=SUM+FUNC(X)
        X=X+DEL
11     CONTINUE
       S=0.5D0*(S+(B-A)*SUM/TNM)
       IT=2*IT
      ENDIF
      RETURN
      END

      SUBROUTINE POLINT(XA,YA,N,X,Y,DY)
      DOUBLE PRECISION XA,YA,Y,DY,DIF,DIFT,C,D,HO,HP,W,DEN,X
      PARAMETER (NMAX=10)
      DIMENSION XA(N),YA(N),C(NMAX),D(NMAX)
      NS=1
      DIF=ABS(X-XA(1))
      DO 11 I=1,N
       DIFT=ABS(X-XA(I))
       IF (DIFT.LT.DIF) THEN
        NS=I
        DIF=DIFT
       ENDIF
       C(I)=YA(I)
       D(I)=YA(I)
11    CONTINUE
      Y=YA(NS)
      NS=NS-1
      DO 13 M=1,N-1
       DO 12 I=1,N-M
        HO=XA(I)-X
        HP=XA(I+M)-X
        W=C(I+1)-D(I)
        DEN=HO-HP
        IF(DEN.EQ.0.)PAUSE
        DEN=W/DEN
        D(I)=HP*DEN
        C(I)=HO*DEN
12     CONTINUE
       IF (2*NS.LT.N-M)THEN
        DY=C(NS+1)
       ELSE
        DY=D(NS)
        NS=NS-1
       ENDIF
       Y=Y+DY
13    CONTINUE
      RETURN
      END
```

```
      PROGRAM CONVLSN
      PARAMETER (PI = 3.14159265359D0)
      DOUBLE PRECISION TI1,TS,SUMM1,T1,BT,SS,SH1,C,D,A,
     +ANS,ILS,ILE,T2,TINT,SIG1,SIG2,SUMM2,SE,WFRQ,PERI
      REAL AMPL, RHO
      INTEGER N
      COMMON WFRQ,AMPL,TS,T1,T2,A,C
      CHARACTER*15  FNAME1,SIGN*1

      DO 10 I = 1,20
      WRITE(*,*)
   10 CONTINUE

      WRITE(*,*)'       CONVLSN'
      WRITE(*,*)'       ***********************************************'
      WRITE(*,*)'        This program calculates the output signal
      WRITE(*,*)'        of the  radiation  coupling  filter for a
      WRITE(*,*)'        uniform sinusoidal input signal using convolution.              '
      WRITE(*,*)'
      WRITE(*,*)'        Author : Murugendran Kanagasundram
      WRITE(*,*)'
      WRITE(*,*)'        Date   : 23-03-93
      WRITE(*,*)'       ***********************************************'
      WRITE(*,*)

      WRITE(*,*)'       Further information(Y/Enter)?'
      READ(*,2) SIGN
    2 FORMAT(A1)
      IF (SIGN .EQ. 'Y' .OR. SIGN .EQ. 'y') THEN
      WRITE(*,*)'   This program will prompt the user for datas.      '
      WRITE(*,*)
      WRITE(*,*)'    1. The program uses a rectangular sin burst as  an'
      WRITE(*,*)'       input velocity signal.The user will be prompted'
      WRITE(*,*)'       for the specifications of the signal. This pro-'
      WRITE(*,*)'       gram can be used to calculate the output for an'
      WRITE(*,*)'       arbitary  input  signal  with  some'
      WRITE(*,*)'       changes,but not implemented yet.'
      WRITE(*,*)
      WRITE(*,*)'    2. Since the impulse  response  is infinite at its'
      WRITE(*,*)'       start, the  program  estimates  the convolution'
      WRITE(*,*)'       integral for a small interval(initial interval)'
      WRITE(*,*)'       approximately. This  initial  interval  may  be'
      WRITE(*,*)'       decided by the user.Default value is 10e-11sec.'
      WRITE(*,*)'       For further details, see the documentation.'
      WRITE(*,*)
      WRITE(*,*)'    3. The  program  will  calculate  the  signal  at'
      WRITE(*,*)'       equivally spaced  points in a user defined time'
      WRITE(*,*)'       interval.The number of points will also decided'
      WRITE(*,*)'       by  the  user. By giving  equal  time data and'
      WRITE(*,*)'       number  of  points as 1, one can find the value'
      WRITE(*,*)'       of the signal at one perticular time.'
      WRITE(*,*)
      WRITE(*,*)'       Press enter to continue.'
      READ(*,*)
      ELSE
      END IF

      WRITE(*,*)'Enter freq. in Hz, amplitude in m/s and # of periods of
     +the input signal.'
      READ(*,*) WFRQ, AMPL, PERI
      WRITE(*,*)'Enter velocity of sound in the medium in (m/s) and denc
     +ity of the medium in   Kg/m**3.'
      READ(*,*) C,RHO
      WRITE(*,*)'Enter radious of the source in m.'
      READ(*,*) A
      WRITE(*,*)'Enter the distance between the source and the observati
     +on point in m.'
      READ(*,*) D
      WRITE(*,*)'The initial interval.'
      WRITE(*,*)' (1) Manual (2) Default'
      READ(*,*) J
      IF (J .EQ. 2) THEN
        DTI1 = 1.0D-11
      ELSE
        WRITE(*,*)'Enter the initial interval in sec..'
        READ(*,*) TI1
      END IF
      WRITE(*,*)'Enter time(2) in sec. between which the signal to be ca
     +lculated.'
      READ(*,*) SS,SE
      WRITE(*,*)'Enter # of points that construct the signal.'
      READ(*,*) N
      WRITE(*,*)'Enter a file name.'
      READ(*,1) FNAME1
    1 FORMAT(A15)
      OPEN(10, FILE = FNAME1,STATUS = 'NEW')


      TINT = (SE-SS)/N
      TS = SS
      SH1 = PERI/WFRQ

      DO 20 L = 0,N
       TS = SS + DBLE(L)*TINT
        T1 = D/C
        T2 = SQRT(4*A**2+D**2)/C
        IF (TS .GT. T1 .AND. TS .LT. (T2 + SH1)) THEN
        M = 1
          IF (TS .LT. (T1+TI1))  THEN
            SUMM1 = AMPL*SIN(2.0D0*PI*WFRQ*(TS-T1))*
     +     (-1)*C**2*SQRT(2.0D0*T1*(T2**2 - T1**2)*TS)/(PI*A**2)
            SUMM2 = 0
          ELSE
            SUMM1 = AMPL*SIN(2.0D0*PI*WFRQ*(TS-T1))*
     +     (-1)*C**2*SQRT(2.0D0*T1*(T2**2 - T1**2)*TI1)/(PI*A**2)
            BT = T1+TI1
            IF (TS .LE. T2) THEN
              IF ((TS-SH1) .LE. T1) THEN
                ILS = BT
                ILE = TS
              ELSE
                SUMM1 = 0
                ILS = TS-SH1
                ILE = TS
              END IF
            ELSE
              IF ((TS-SH1) .LE. T1) THEN
                ILS = BT
                ILE = T2
              ELSE
                SUMM1 = 0
                ILS = TS-SH1
                ILE = T2
                IF (L .EQ. N) M = 2
              END IF
            END IF
            CALL QROMB(M,ILS,ILE,SUMM2)
          END IF
          SIG1 = AMPL * SIN(2.0D0*PI*WFRQ*(TS-T1))
          SIG2 = SUMM1 + SUMM2
          IF (TS .GT. T1+SH1) SIG1 = 0
          ANS = (SIG1+SIG2)/AMPL

        ELSE
          ANS = 0.
        END IF
        WRITE(10,*) TS, (TS-T1)*WFRQ, ANS
*Before use the next write statement the initial do loop number should
*be changed to 1.
*       WRITE(*,*) TS*1.0D6,ANS
   20 CONTINUE

      CLOSE(10)

      STOP
      END


      FUNCTION FUNC(TAU)
      DOUBLE PRECISION TAU,FUNC,Y1,Y2,TS,T1,T2,C,A,WFRQ
      REAL AMPL
      PARAMETER (PI = 3.14159265359D0)
      COMMON WFRQ,AMPL,TS,T1,T2,A,C

      Y1  = AMPL * SIN(2.0D0* PI * WFRQ * (TS - TAU))
      IF ((T2**2 - TAU**2) .LE. 0 ) THEN
      Y2 = 0
      ELSE
      Y2 = (-1) * C**2 * TAU * SQRT((T2**2 - TAU**2)/(TAU**2 - T1**2))
     + /(PI * A**2)
      END IF
      FUNC = Y1 * Y2
      RETURN
      STOP
      END
```

APPENDIX B-2

```
      PROGRAM FIELDSIM

*     The program calculates the on-axis sound pressure for a given
*     frequency spectra of an arbitrary volume velocity burst from a
*     piston. The pressure can be calculated according to tree
*     different propagation models, theese are:
*                 (1) planewave model
*                 (2) farfield model
*                 (3) nearfild model, finite receiver
*
*     As an option, the output voltage of the system due to the
*     pressure can be calculated, both in time and frequency domain.
*     The total transfer function of the receiver section is needed.
*
*     The program is mainly written for a combination with responses
*     from FLOSIM, in order to calculate responses due to other
*     propagation models than the farfield model.
*
*     Variables in the main program and the subroutines:
*
*     XW        -             An array as working space
*     TFUNC     -             An array as working space
*     SPEC      -             An array as working space
*     TO        -             A pure time shift (to more efficient use of the array)
*     RAD       -             Radius of the transducer
*     RHO       -             Density of the propagation media
*     C         -             Speed of sound in the propagation media
*     R         -             Axial distance between the transducer faces
*     K         -             Wave number
*     SFRQ      -             Sampling frequency
*     F         -             Frequency variable
*     DF        -             Frequency resolution
*     LIMIT     -             Buffer length
*
*     Written by              : Murugendran Kanagasundram and Steinar Vervik
*     Date                    : 13-11-1993

      INTEGER LIMIT,ULIMIT
      REAL XW,T0,TFUNC
      CHARACTER FILE*25, ANS*1
      PARAMETER (LIMIT=16384, ULIMIT=LIMIT+2)
      DIMENSION XW(ULIMIT),TFUNC(ULIMIT)

      WRITE(*,*)'      ------ FIELDSIM ------'
      WRITE(*,*)
      CALL READFILE(XW)
      CALL INPAR(RAD,RHO,C,R,SFRQ,T0,LIMIT)
    5 WRITE(*,*)'        PROPAGATION MODELS'
      WRITE(*,*)'        ------------------'
      WRITE(*,*)'    (1) plane wave model'
      WRITE(*,*)'    (2) farfield model'
      WRITE(*,*)'    (3) nearfield model, finite receiver'
      WRITE(*,*)
      WRITE(*,*)'    Choose 1, 2 or 3:'
      READ(*,*)MODEL

      IF     (MODEL .EQ. 1) THEN
        CALL PFIELD(TFUNC,RHO,RAD,C,SFRQ,R,T0)
      ELSE IF (MODEL .EQ. 2) THEN
        CALL FFIELD(TFUNC,RAD,RHO,C,SFRQ,R,T0)
      ELSE IF (MODEL .EQ. 3) THEN
        CALL DIFIELD(TFUNC,RHO,RAD,C,SFRQ,R,T0)
      ELSE
        WRITE(*,*)'.....non of the above models chosen!'
        GOTO 5
      END IF

      CALL FRQCONV(XW,TFUNC)

      WRITE(*,*)'Calculate the output voltage (Y/N):'
      READ(*,110)ANS
      IF (ANS .EQ. 'Y' .OR. ANS .EQ. 'y') THEN
        WRITE(*,*)'Enter file containing Hrec'
        CALL READFILE(TFUNC)
        CALL FRQCONV(XW,TFUNC)

        WRITE(*,*)'Calculate the specter of the output voltage (Y/N)?:'
        READ(*,110)ANS

        IF (ANS .EQ. 'Y' .OR. ANS .EQ. 'y') THEN
          WRITE(*,*)'Enter file to store the modified spectra'
          READ(*,100)FILE
          OPEN(10,FILE=FILE,STATUS='NEW')
          DF = SFRQ/(LIMIT-1)
          J=0
          DO 10 I = 1,LIMIT-1,2
c           PHASE = ATAN2(XW(I+1),XW(I))*360/TOPI
c           MAGN  = 20*LOG10(SQRT(XW(I)**2+XW(I+1)**2))
            WRITE(10,*) J*DF, CMPLX(XW(I),-XW(I+1))
            J = J+1
 10       CONTINUE
        ELSE
        END IF
      ELSE
      END IF

      CALL REALFT(XW,LIMIT/2,-1)
      WRITE(*,*)'Enter file to store the time series'
      READ(*,100)FILE
      OPEN(10,FILE=FILE,STATUS='NEW')
      DO 20 I = 1, LIMIT/2
        WRITE(10,*)I,(I-1.)/SFRQ+T0,2*SFRQ*XW(I)/LIMIT
 20   CONTINUE
100   FORMAT(A25)
110   FORMAT(A1)
      CLOSE(10)
      STOP
      END

      SUBROUTINE INPAR(RAD,RHO,C,R,SFRQ,T0,LIMIT)
      WRITE(*,*)'       Input parameters'
      write(*,*)'       ----------------'
      WRITE(*,*)'Enter:'
      WRITE(*,*)'radius of the sendertransducer (m):'
      READ(*,*)RAD
      WRITE(*,*)'the density of the medium (kg/m**3):'
      READ(*,*)RHO
      WRITE(*,*)'the speed of sound in the propagation medium (m/s):'
      READ(*,*)C
      WRITE(*,*)'the axial distance between the transducers (m):'
      READ(*,*)R
      WRITE(*,*)'the sampling frequency (Hz):'
      READ(*,*)SFRQ
      T0 = R/C-0.1*LIMIT/SFRQ
      RETURN
      END

      SUBROUTINE READFILE(XW)
      REAL XW
      INTEGER TLINES,LIMIT,ULIMIT
      COMPLEX C
      CHARACTER TEXT*79, FILE*25
      PARAMETER (LIMIT=16384,ULIMIT=LIMIT+2)
      DIMENSION XW(ULIMIT)

100   FORMAT(A25)
200   FORMAT(A79)

* *   Open file containing the spectra of the input signal * *
      WRITE(*,*)'Open file containing the spectra of the input signal'
      WRITE(*,*)'Enter filename:'
      READ(*,100)FILE
      OPEN(10,FILE=FILE,STATUS='OLD')
      WRITE(*,*)'Enter number of text lines in the header'
      READ(*,*)TLINES
* *   Read header of the file * *
      DO 10 I = 1,TLINES
        READ(10,200)TEXT
 10   CONTINUE
* *   Convert complex data to real
      K=1
      DO 20 J=I+1,I+LIMIT/2
       READ(10,*)N,F,C
       XW(K)   = REAL(C)
       XW(K+1) = -AIMAG(C)
       K=K+2
 20   CONTINUE
      CLOSE(10)
      RETURN
      END

      SUBROUTINE FRQCONV(SPEC,TFUNC)
*     This routine multiplies two frequency spectra

      INTEGER LIMIT,ULIMIT
      PARAMETER (LIMIT=16384,ULIMIT=LIMIT+2)
      DIMENSION SPEC(ULIMIT), TFUNC(ULIMIT)

      SPEC(1) = 0
      DO 10 I = 3,(LIMIT+1),2
        B1 = SPEC(I)
        B2 = SPEC(I+1)
        A4 = TFUNC(I)
        A3 = TFUNC(I+1)
        IF (I .EQ. LIMIT+1) THEN
          B1 = SPEC(2)
```

```
        B2 = 0
        SPEC(2) = (B1*A4 - B2*A3)
      ELSE
        SPEC(I)   = (B1*A4 - B2*A3)
        SPEC(I+1) = (B2*A4 + B1*A3)
      ENDIF
   10 CONTINUE
      RETURN
      END

      SUBROUTINE PFIELD(TFUNC,RHO,RAD,C,SFRQ,R,T0)
*     This routine calculates the transfer function of the
*     planewave model

      INTEGER LIMIT, ULIMIT
      REAL A3,A4,R,RHO,RAD,C,F,K,SFRQ,TFUNC
      PARAMETER (LIMIT=16384,ULIMIT=LIMIT+2,TOPI=6.28318530718)
      DIMENSION TFUNC(ULIMIT)
      COMPLEX P0


      TFUNC(1) = 0
      TFUNC(2) = 0
      J = 1
      DO 10 I = 3,(LIMIT+1),2
        F  = J * SFRQ / (LIMIT-1)
        K  = TOPI * F / C
        P0 = RHO * C * EXP(CMPLX(0.0,(K*R-K*C*T0)))
        A3 = REAL(P0)*2/(TOPI*RAD**2)
        A4 = AIMAG(P0)*2/(TOPI*RAD**2)
        TFUNC(I)   = A3
        TFUNC(I+1) = A4
        J = J + 1
   10 CONTINUE
      RETURN
      END

      SUBROUTINE FFIELD(TFUNC,RAD,RHO,C,SFRQ,R,T0)
*     This routine calculates the transfer function of the
*     farfield model

      INTEGER LIMIT,ULIMIT
      REAL A1,A2,A3,A4,RAD,R,RHO,C,F,K,SFRQ,B
      PARAMETER (LIMIT=16384,ULIMIT=LIMIT+2,TOPI=6.28318530718)
      DIMENSION TFUNC(ULIMIT)
      J = 0
      DO 10 I = 1,(LIMIT+1),2
        F  = J * SFRQ / (LIMIT-1)
        K  = TOPI * F / C
        A1 = COS(K*R-K*C*T0)
        A2 = SIN(K*R-K*C*T0)
        B  = RHO * RAD**2 * TOPI * F / (2 * R)
        A3 = (-1) * A1 * B
        A4 = A2 * B
        TFUNC(I)   = A4*2/(TOPI*RAD**2)
        TFUNC(I+1) = A3*2/(TOPI*RAD**2)
        J = J + 1
   10 CONTINUE
      RETURN
      END

      SUBROUTINE DIFIELD(TFUNC,RHO,RADI,C,SFRQ,RR,T0)
*     This routine calculates the transfer function of the
*     nearfield model, finite receiver

      REAL A,B,A3,A4,RR,RHO,RADI,C,F,K,SFRQ,TFUNC
      DOUBLE PRECISION C1,D1
      INTEGER LIMIT, ULIMIT
      PARAMETER (LIMIT=16384,ULIMIT=LIMIT+2,TOPI=6.28318530718)
      DIMENSION TFUNC(ULIMIT)
      COMPLEX PM, P0, H
      COMMON R,K,RAD

      R = RR
      RAD = RADI

      TFUNC(1) = 0
      TFUNC(2) = 0
      J = 1
      DUMMY = 0
      DO 10 I = 3,(LIMIT+1),2
        IF (I .GT. DUMMY+100) THEN
          WRITE(*,*)I
          DUMMY=I
        END IF
        F  = J * SFRQ / (LIMIT-1)
        K  = TOPI * F / C
        CALL QROMB(1,0.0D0,TOPI/4.0D0,C1)
        CALL QROMB(2,0.0D0,TOPI/4.0D0,D1)
        A  = 1.0-C1*4.0*2.0/TOPI*COS(K*R)-D1*4.0*2.0/TOPI*SIN(K*R)
        B =    D1*4.0*2.0/TOPI*COS(K*R)-C1*4.0*2.0/TOPI*SIN(K*R)
        PM = CMPLX(A,(-1)*B)
        P0 = RHO * C * EXP(CMPLX(0.0,(K*R-K*C*T0)))
        H  = PM * P0
        A3 = REAL(H)*2/(TOPI*RAD**2)
        A4 = AIMAG(H)*2/(TOPI*RAD**2)
        TFUNC(I)   = A3
        TFUNC(I+1) = A4
        J = J + 1
   10 CONTINUE
      RETURN
      END

*     Routines from Numerical Recipes, numerical integration

      SUBROUTINE QROMB(I,A,B,SS)
      DOUBLE PRECISION A,B,SS,DSS,S,H,ER
      PARAMETER(EPS=1.D-4,JMAX=25,JMAXP=JMAX+1,K=5,KM=4)
      DIMENSION S(JMAXP),H(JMAXP)
      H(1)=1.D0
      ER = 1.D-10
      DO 11 J=1,JMAX
        CALL TRAPZD(I,A,B,S(J),J)
        IF (J.GE.K) THEN
          L=J-KM
          CALL POLINT(H(L),S(L),K,0.D0,SS,DSS)
          IF (ABS(SS-ER).LT.EPS*ABS(ER)) RETURN
          ER = SS
        ENDIF
        S(J+1)=S(J)
        H(J+1)=0.25D0*H(J)
   11   CONTINUE
      PAUSE 'Too many steps.'
      END

      SUBROUTINE TRAPZD(I,A,B,S,N)
      DOUBLE PRECISION A,B,S,FUNC,DEL,SUM,X
      IF (N.EQ.1) THEN
        S=0.5D0*(B-A)*(FUNC(I,A)+FUNC(I,B))
        IT=1
      ELSE
        TNM=IT
        DEL=(B-A)/TNM
        X=A+0.5D0*DEL
        SUM=0.D0
        DO 11 J=1,IT
          SUM=SUM+FUNC(I,X)
          X=X+DEL
   11     CONTINUE
        S=0.5D0*(S+(B-A)*SUM/TNM)
        IT=2*IT
      ENDIF
      RETURN
      END

      SUBROUTINE POLINT(XA,YA,N,X,Y,DY)
      DOUBLE PRECISION XA,YA,Y,DY,DIF,DIFT,C,D,HO,HP,W,DEN,X
      PARAMETER (NMAX=10)
      DIMENSION XA(N),YA(N),C(NMAX),D(NMAX)
      NS=1
      DIF=ABS(X-XA(1))
      DO 11 I=1,N
        DIFT=ABS(X-XA(I))
        IF (DIFT.LT.DIF) THEN
          NS=I
          DIF=DIFT
        ENDIF
        C(I)=YA(I)
        D(I)=YA(I)
   11   CONTINUE
      Y=YA(NS)
      NS=NS-1
      DO 13 M=1,N-1
        DO 12 I=1,N-M
          HO=XA(I)-X
          HP=XA(I+M)-X
          W=C(I+1)-D(I)
          DEN=HO-HP
          IF(DEN.EQ.0.)PAUSE
          DEN=W/DEN
          D(I)=HP*DEN
          C(I)=HO*DEN
   12     CONTINUE
        IF (2*NS.LT.N-M)THEN
          DY=C(NS+1)
        ELSE
          DY=D(NS)
          NS=NS-1
        ENDIF
        Y=Y+DY
```

```
 13   CONTINUE
      RETURN
      END

      FUNCTION FUNC(I,A)
*     Calculates the integrand (connected to the nearfield, finite
*     receiver transfer function)

      DOUBLE PRECISION A,FUNC
      REAL R,K,RAD
      INTEGER I
      COMMON R,K,RAD

      IF (I .EQ. 1) THEN
      FUNC=COS(K*SQRT(R**2+4.D0*RAD**2*(COS(A))**2))*(SIN(A))**2
      END IF

      IF (I .EQ. 2) THEN
      FUNC=SIN(K*SQRT(R**2+4.D0*RAD**2*(COS(A))**2))*(SIN(A))**2
      END IF
      RETURN
      END

*     Routines from Numerical Recipes, FFT and IFFT routines

      SUBROUTINE REALFT(DATA,N,ISIGN)
      REAL*8 WR,WI,WPR,WPI,WTEMP,THETA
      DIMENSION DATA(*)
      THETA=6.28318530717959D0/2.0D0/DBLE(N)
      C1=0.5
      IF (ISIGN.EQ.1) THEN
        C2=-0.5
        CALL FOUR1(DATA,N,+1)
      ELSE
        C2=0.5
        THETA=-THETA
      ENDIF
      WPR=-2.0D0*DSIN(0.5D0*THETA)**2
      WPI=DSIN(THETA)
      WR=1.0D0+WPR
      WI=WPI
      N2P3=2*N+3
      DO 11 I=2,N/2+1
        I1=2*I-1
        I2=I1+1
        I3=N2P3-I2
        I4=I3+1
        WRS=SNGL(WR)
        WIS=SNGL(WI)
        H1R=C1*(DATA(I1)+DATA(I3))
        H1I=C1*(DATA(I2)-DATA(I4))
        H2R=-C2*(DATA(I2)+DATA(I4))
        H2I=C2*(DATA(I1)-DATA(I3))
        DATA(I1)=H1R+WRS*H2R-WIS*H2I
        DATA(I2)=H1I+WRS*H2I+WIS*H2R
        DATA(I3)=H1R-WRS*H2R+WIS*H2I
        DATA(I4)=-H1I+WRS*H2I+WIS*H2R
        WTEMP=WR
        WR=WR*WPR-WI*WPI+WR
        WI=WI*WPR+WTEMP*WPI+WI
 11   CONTINUE
      IF (ISIGN.EQ.1) THEN
        H1R=DATA(1)
        DATA(1)=H1R+DATA(2)
        DATA(2)=H1R-DATA(2)
      ELSE
        H1R=DATA(1)
        DATA(1)=C1*(H1R+DATA(2))
        DATA(2)=C1*(H1R-DATA(2))
        CALL FOUR1(DATA,N,-1)
      ENDIF
      RETURN
      END

      SUBROUTINE FOUR1(DATA,NN,ISIGN)
      REAL*8 WR,WI,WPR,WPI,WTEMP,THETA
      DIMENSION DATA(*)
      N=2*NN
      J=1
      DO 11 I=1,N,2
        IF(J.GT.I)THEN
          TEMPR=DATA(J)
          TEMPI=DATA(J+1)
          DATA(J)=DATA(I)
          DATA(J+1)=DATA(I+1)
          DATA(I)=TEMPR
          DATA(I+1)=TEMPI
        ENDIF
        M=N/2
 1      IF ((M.GE.2).AND.(J.GT.M)) THEN
          J=J-M
          M=M/2
        GO TO 1
        ENDIF
        J=J+M
 11   CONTINUE
      MMAX=2
 2    IF (N.GT.MMAX) THEN
        ISTEP=2*MMAX
        THETA=6.28318530717959D0/(ISIGN*MMAX)
        WPR=-2.D0*DSIN(0.5D0*THETA)**2
        WPI=DSIN(THETA)
        WR=1.D0
        WI=0.D0
        DO 13 M=1,MMAX,2
          DO 12 I=M,N,ISTEP
            J=I+MMAX
            TEMPR=SNGL(WR)*DATA(J)-SNGL(WI)*DATA(J+1)
            TEMPI=SNGL(WR)*DATA(J+1)+SNGL(WI)*DATA(J)
            DATA(J)=DATA(I)-TEMPR
            DATA(J+1)=DATA(I+1)-TEMPI
            DATA(I)=DATA(I)+TEMPR
            DATA(I+1)=DATA(I+1)+TEMPI
 12       CONTINUE
          WTEMP=WR
          WR=WR*WPR-WI*WPI+WR
          WI=WI*WPR+WTEMP*WPI+WI
 13     CONTINUE
        MMAX=ISTEP
      GO TO 2
      ENDIF
      RETURN
      END
```

APPENDIX B-3

```
      PROGRAM TRNSRESP

*     This program is calculating some portion, up to nine times
*     the reverbaration time of the transducer, of the transient
*     response of a lossless thickness mode vibrating piezoelectric
*     transduser.
*
*     The particle velocity is calculated for a uniform
*     sinusoidal voltage pulse.

*     Variables in the main program and the subroutines:
*
*               TMP         - An array as working space
*               ANS         - An array as working space
*               TS          - Discrete version of time, t, in the convolution
*                             integral
*               TAU         - Time variable
*               T           - Sample interval
*               ILS         - Integration limit, lower
*               ILE         - Integration limit, upper
*               SUM1        - Convolution without the delta-terms in the impulse
*                 response
*               SUM2        - Convolution with the delta-terms in the impulse
*                 response
*               RT          - Reverberation time of the transducer
*               INT         - RT/N, the interval between the time samples
*               CRS         - Beginning time of a particular term in the impulse
*                             response

*               C0          - Clamped capasitance
*               CP          - Speed of sound in the piezoelectric material
*               Fi          - Electromechanical coupling factor
*               Z0          - Characteristic impedance of the transducer
*               Z1          - Characteristic impedance of the backing media
*               Z2          - Characteristic impedance of the radiation media

*               R0  - Reflection coeff. at x3 = 0
*               RL  - Reflection coeff. at x3 = L
*               T0  - Transmission coeff. at x3 = 0
*               TL  - Transmission coeff. at x3 = L
*               B   - Beta in the text
*               C1  - Constant defined in the text
*               C2  - Constant defined in the text
*               AF  - Ampitude factor
*
*               Written by     : Steinar Vervik and Murugendran Kanagasundram
*               Date           : 24-7-1993

      INTEGER NUNIT, CH, CH1
      REAL INT, ANS(4000)
      CHARACTER*15 INFILE
      COMMON /COMB1/ B,RT,T
      COMMON /COMB2/ R0,RL
      COMMON /COMB3/ T0,TL,C1,C2

  100 FORMAT(25(/))
      WRITE(*,100)
      WRITE(*,*)'- Transient transducer respons -'
      WRITE(*,*)'--------------------------------'
      WRITE(*,*)
      CALL INPAR(R0,RL,T0,TL,C1,C2,B,A,RT,AF)
      WRITE(*,*)'Choose the input.'
      WRITE(*,*)'    1) Dirac delta  2) sin burst'
      READ(*,*) CH
      IF (CH .EQ. 1) THEN
        CALL IMPRES(A,AF,M,N,ANS)
      ELSE
        CALL INSIG(PL,T)
        WRITE(*,*)'Choose transducer model.'
        WRITE(*,*)'  1) Effect of regeneration excluded'
        WRITE(*,*)'  2) Effect of regeneration included'
        READ(*,*) CH1
        CALL CONV(CH1,PL,A,AF,M,N,ANS)
      END IF

      INT = RT/N
      WRITE(*,*)'Enter a file to store total result.'
      READ(*,1) INFILE
    1 FORMAT(A15)
      CALL OPENER(INFILE,NUNIT,'NEW')
      DO 10 J = 1,M*N
        WRITE(NUNIT,*) (J-1)*INT/RT,AF*ANS(J)
   10 CONTINUE

      STOP
      END

      SUBROUTINE INPAR(R0,RL,T0,TL,C1,C2,B,A,RT,AF)

      CALL PIEZO(Z0,FI,C0,A,RT)

      CALL MEDIA(Z1,Z2,A)

      R0 = (Z0-Z1)/(Z0+Z1)
      RL = (Z0-Z2)/(Z0+Z2)
      T0 = 1+R0
      TL = 1+RL
      C1 = FI**2/C0*(T0*TL)/Z0
      C2 = FI**2/(2*C0)*(R0*TL+RL*T0)/Z0
      B  = FI**2/(2*C0)*(T0+TL)/Z0
      AF = FI*TL/(2*Z0)

      RETURN
      END

      SUBROUTINE PIEZO(Z0,FI,C0,A,RT)
      REAL L
      PARAMETER (PI = 3.141592654)

      WRITE(*,*)'Piezoelectric material (default PZT-5A)'
      WRITE(*,*)'---------------------------------------'
      WRITE(*,*)'Enter the thickness of the element (mm):'
      READ(*,*)L
      WRITE(*,*)'Give the radius of the element     (mm):'
      READ(*,*)R
      L = L/1000.0
      R = R/1000.0
      A = PI*R**2

*     Piezoelectric constants    *
      CD    = 14.7E10
      E33   = 15.8
      EPS33 = 830.0*8.85E-12
      RHO   = 7750.0

      CP = SQRT(CD/RHO)
      C0 = A/L*EPS33
      FI = A/L*E33
      Z0 = RHO*CP*A
      RT = L/CP

      RETURN
      END

      SUBROUTINE MEDIA(Z1,Z2,A)

      WRITE(*,*)
      WRITE(*,*)'medium'
      WRITE(*,*)'------'
      WRITE(*,*)'Enter the spesific impedances (rayl):'
      WRITE(*,*)'radiation medium:'
      READ(*,*)Z2
      WRITE(*,*)'backing medium:'
      READ(*,*)Z1
      Z1 = Z1*A
      Z2 = Z2*A

      RETURN
      END

      SUBROUTINE CONV(CH,PL,A,AF,M,N,ANS)
*     This routine calculates the convolution of a given input
*     signal, f(t), with the impulse response of the transducer,
*     h(t).

      REAL ANS(4000),TMP(4000),TS,ILS,ILE,RT,PL,SUM1,SUM2,INT,CRS
      INTEGER M,N,CH
      COMMON /COMB1/ B, RT ,T
      COMMON /COMB4/ TS
      CHARACTER*15 INFILE, SIGN*1

      IF (CH .EQ. 1 .OR. CH .EQ. 2) THEN
        WRITE(*,*)'Enter, # of terms in the impulse response.'
        READ(*,*) M
        WRITE(*,*)'Enter, # of points to be calculated in one revebarat
     +ion period.'
        READ(*,*) N
        WRITE(*,*)'Do you want to save the effect of each term in the i
     +mpulse response?'
        READ(*,2) SIGN
      ELSE
      END IF

      INT   = RT/N

      DO 20 I = 1,M
```

```
      DO 30 J = 1, (I-1)*N
        TMP(J) = 0
30    CONTINUE
      DO 40 K = (I-1)*N+1, M*N
        TS = INT*(K-1)
        ILE = TS
        CRS = ((I-1)*N)*INT
        IF (CH .EQ. 2) THEN
          IF ((TS - PL) .LE. CRS) THEN
            ILS = CRS
          ELSE
            ILS = TS-PL
          END IF
          IF (K .EQ. ((I-1)*N+1)) THEN
            SUM1 = 0
          ELSE
            CALL QROMB(ILS,ILE,SUM1,I)
          END IF
        ELSE
          SUM1 = 0
        END IF
        IF ((CRS+PL) .GT. TS) THEN
          SUM2 = FUNCIN(TS,CRS,I)
        ELSE
          SUM2 = 0
        END IF
        TMP(K) = SUM1+SUM2
40    CONTINUE
 2    FORMAT(A1)
      IF (SIGN .EQ. 'Y' .OR. SIGN .EQ. 'y') THEN
        WRITE(*,*)'Enter a file to store response due to term #',I
        READ(*,1) INFILE
 1      FORMAT(A15)
        CALL OPENER(INFILE,NUNIT,'NEW')
        DO 50 J = 1, M*N
          WRITE(NUNIT,*) (J-1)*INT/T,AF*TMP(J)
50      CONTINUE
      ELSE
      END IF
      DO 60 J = 1, M*N
        ANS(J) = ANS(J) + TMP(J)
60    CONTINUE
20 CONTINUE

   RETURN
   END

   SUBROUTINE INSIG(PL,T)
*    This routine gives the input voltage pulse

   REAL WFRQ, AMPL, PL, OMG
   PARAMETER (PI = 3.141592654)
   COMMON /COMB5/ OMG, AMPL

   WRITE(*,*)'Enter, amplitude, freq., and # of periods of the input
  +signal.'
   READ(*,*) AMPL, WFRQ, PERI

   PL = PERI/WFRQ
   OMG = 2 * PI * WFRQ
   T = 1/WFRQ

   RETURN
   END

   FUNCTION FUNCIN(TS,T0,L)
*    The function gives the correct weight for the delta
*    terms in the impulse response

   REAL TS, T0, Y, OMG, A0
   INTEGER L, C1, C2, K1, K2
   COMMON /COMB2/ R0, RL
   COMMON /COMB5/ OMG, AMPL
   SAVE C1, C2, K1, K2
   DATA C1 /1/, C2 /1/, K1/2/, K2/3/
   IF (L .LT. 2) THEN
     A0 =1.
   ELSE
     IF (L-AINT(L/2)*2 .EQ. 0) THEN
       IF (L .GT. K1) C1 = C1 + 1
       A0 = (-1)*(R0*RL)**(C1-1)*(1+R0)
       K1 = L
     ELSE
       IF (L .GT. K2) C2 = C2 + 1
       A0 = R0*(R0*RL)**(C2-1)*(1+RL)
       K2 = L
     END IF
   END IF

   Y = A0 * AMPL * SIN(OMG*(TS-T0))
   FUNCIN = Y

   RETURN
   END

   FUNCTION FUNC(TAU,L,X)
   REAL RT, Y1, Y3
   DOUBLE PRECISION FUNC, Y2, K11, K21, K22, K31, K32,
  + K33, K41, K42, K43, K44, K51, K52, K53, K54, K55, K61, K62, K63,
  + K64, K65, K66, K71, K72, K73, K74, K75, K76, K77, K81, K82, K83,
  + K84, K85, K86, K87, K88
   INTEGER L, X
   COMMON /COMB1/ B, RT ,T
   COMMON /COMB4/ TS
   IF (L .EQ. 1) THEN
     CALL K1(K11)
     Y2=K11*EXP(B*TAU)
   ELSE IF (L .EQ. 2) THEN
     CALL K2(K21,K22)
     Y1=(TAU-RT)
     Y2=(-1)*(K21+K22*Y1)*EXP(B*Y1)
   ELSE IF (L .EQ. 3) THEN
     CALL K3(K31,K32,K33)
     Y1=(TAU-2*RT)
     Y2=(K31+K32*Y1+K33*Y1**2/2)*EXP(B*Y1)
   ELSE IF (L .EQ. 4) THEN
     CALL K4(K41,K42,K43,K44)
     Y1=(TAU-3*RT)
     Y2=(-1)*(K41+K42*Y1+K43*Y1**2/2+K44*Y1**3/6)*EXP(B*Y1)
   ELSE IF (L .EQ. 5) THEN
     CALL K5(K51,K52,K53,K54,K55)
     Y1=(TAU-4*RT)
     Y2=(K51+K52*Y1+K53*Y1**2/2+K54*Y1**3/6+K55*Y1**4/24)*
  +     EXP(B*Y1)
   ELSE IF (L .EQ. 6) THEN
     CALL K6(K61,K62,K63,K64,K65,K66)
     Y1=(TAU-5*RT)
     Y2=(-1)*(K61+K62*Y1+K63*Y1**2/2+K64*Y1**3/6+K65*Y1**4/24+
  +     K66*Y1**5/120)*EXP(B*Y1)
   ELSE IF (L .EQ. 7) THEN
     CALL K7(K71,K72,K73,K74,K75,K76,K77)
     Y1=(TAU-6*RT)

 Y2=(K71+K72*Y1+K73*Y1**2/2+K74*Y1**3/6+K75*Y1**4/24+K76*Y1**5/
  +     120+K77*Y1**6/720)*EXP(B*Y1)
   ELSE
     CALL K8(K81,K82,K83,K84,K85,K86,K87,K88)
     Y1=(TAU-7*RT)
     Y2=(-1)*(K81+K82*Y1+K83*Y1**2/2+K84*Y1**3/6+K85*Y1**4/24+
  +     K86*Y1**5/120+K87*Y1**6/720+K88*Y1**7/5040)*EXP(B*Y1)
   END IF

   IF (X .EQ. 1) THEN
     Y3 = 1
   ELSE
     Y3 = FUNCIN(TS,TAU,1)
   END IF
   FUNC = Y2*Y3
   RETURN
   END

*    Calculations of the regeneration coefficients in the
*    impulse responses

   SUBROUTINE K1(K11)
   DOUBLE PRECISION K11
   COMMON /COMB1/ B, RT, T
   COMMON /COMB2/ R0, RL
   COMMON /COMB3/ T0, TL, C1, C2

   K11 = B

   RETURN
   END

   SUBROUTINE K2(K21,K22)
   DOUBLE PRECISION K21, K22
   COMMON /COMB1/ B,RT,T
   COMMON /COMB2/ R0, RL
   COMMON /COMB3/ T0,TL,C1,C2

   K21 = T0*B + C1

   K22 = C1*B

   RETURN
   END

   SUBROUTINE K3(K31,K32,K33)
   DOUBLE PRECISION K31, K32, K33
   COMMON /COMB1/ B,RT,T
   COMMON /COMB2/ R0, RL
   COMMON /COMB3/ T0,TL,C1,C2

   K31 = R0*B + T0*C1 + C2 + 2*R0*RL*B

   K32 = T0*C1*B + C2*B + R0*RL*B**2 + C1**2

   K33 = C1**2*B

   RETURN
   END
```

```
      SUBROUTINE K4(K41,K42,K43,K44)
      DOUBLE PRECISION K41,K42,K43,K44
      COMMON /COMB1/ B,RT,T
      COMMON /COMB2/ R0, RL
      COMMON /COMB3/ T0,TL,C1,C2

      K41 = R0*C1 + T0*C2 + 2*T0*R0*RL*B + 2*R0*RL*C1

      K42 = R0*C1*B + T0*C2*B + T0*R0*RL*B**2 + T0*C1**2 + 2*C1*C2 +
     +     4*R0*RL*C1*B

      K43 = T0*C1**2*B + 2*C1*C2*B + 2*R0*RL*C1*B**2 + C1**3

      K44 = C1**3*B

      RETURN
      END

      SUBROUTINE K5(K51,K52,K53,K54,K55)
      DOUBLE PRECISION K51,K52,K53,K54,K55
      COMMON /COMB1/ B,RT,T
      COMMON /COMB2/ R0, RL
      COMMON /COMB3/ T0,TL,C1,C2

      K51 = R0*C2 + 2*R0**2*RL*B + 2*T0*R0*RL*C1 + 2*R0*RL*C2 +
     +     3*(R0*RL)**2*B

      K52 = R0*C2*B + R0**2*RL*B**2 + R0*C1**2 + 2*T0*C1*C2 + C2**2 +
     +     4*T0*R0*RL*C1*B + 4*R0*RL*C2*B + 3*(R0*RL)**2*B**2 +
     +     3*R0*RL*C1**2

      K53 = R0*C1**2*B + 2*T0*C1*C2*B + C2**2*B + 2*T0*R0*RL*C1*B**2 +
     +     2*R0*RL*C2*B**2 + (R0*RL)**2*B**3 + T0*C1**3 + 3*C1**2*C2 +
     +     6*C1**2*R0*RL*B

      K54 = T0*C1**3*B + 3*C1**2*C2*B + 3*C1**2*R0*RL*B**2 + C1**4

      K55 = C1**4*B

      RETURN
      END

      SUBROUTINE K6(K61,K62,K63,K64,K65,K66)
      DOUBLE PRECISION K61,K62,K63,K64,K65,K66
      COMMON /COMB1/ B,RT,T
      COMMON /COMB2/ R0, RL
      COMMON /COMB3/ T0,TL,C1,C2

      K61 = 2*R0**2*RL*C1 + 2*T0*R0*RL*C2 + 3*T0*(R0*RL)**2*B +
     +     3*C1*(R0*RL)**2

      K62 = 2*R0*C1*C2 + T0*C2**2 + 4*R0**2*RL*C1*B + 4*T0*R0*RL*C2*B
     +
     +     3*T0*(R0*RL)**2*B**2 + 3*T0*C1**2*R0*RL + 6*R0*RL*C1*C2  +
     +     9*C1*(R0*RL)**2*B

      K63 = 2*R0*C1*C2*B + T0*C2**2*B + 2*R0**2*RL*C1*B**2 +
     +     2*T0*R0*RL*C2*B**2 + T0*(R0*RL)**2*B**3 + R0*C1**3 +
     +     3*T0*C1**2*C2 + 3*C1*C2**2 + 6*T0*C1**2*R0*RL*B +
     +     12*R0*RL*C1*C2*B + 9*C1*(R0*RL)**2*B**2 + 4*C1**3*R0*RL

      K64 = R0*C1**3*B + 3*T0*C1**2*C2*B + 3*C1*C2**2*B +
     +     3*T0*C1**2*R0*RL*B**2 + 6*R0*RL*C1*C2*B**2 +
     +     3*C1*(R0*RL)**2*B**3 + T0*C1**4 + 4*C1**3*C2 +
     +     8*C1**3*R0*RL*B

      K65 = T0*C1**4*B + 4*C1**3*C2*B + 4*C1**3*R0*RL*B**2 + C1**5

      K66 = C1**5*B

      RETURN
      END

      SUBROUTINE K7(K71,K72,K73,K74,K75,K76,K77)
      DOUBLE PRECISION K71,K72,K73,K74,K75,K76,K77
      COMMON /COMB1/ B,RT,T
      COMMON /COMB2/ R0, RL
      COMMON /COMB3/ T0,TL,C1,C2

      K71 = 2*R0**2*RL*C2 + 3*R0*(R0*RL)**2*B + 3*(R0*RL)**2*C2 +
     +     3*T0*(R0*RL)**2*C1 + 4*(R0*RL)**3*B

      K72 = R0*C2**2 + 4*R0**2*RL*C2*B + 3*R0*(R0*RL)**2*B**2 +
     +     3*R0**2*RL*C1**2 + 6*T0*R0*RL*C1*C2 + 3*R0*RL*C2**2 +
     +     9*(R0*RL)**2*C2*B + 9*T0*(R0*RL)**2*C1*B +
     +     6*(R0*RL)**3*B**2 + 6*(R0*RL)**2*C1**2

      K73 = R0*C2**2*B + 2*R0**2*RL*C2*B**2 + R0*(R0*RL)**2*B**3 +
     +     3*R0*C1**2*C2 + 3*T0*C1*C2**2 + C2**3 + 6*R0**2*RL*C1**2*B +
     +     12*T0*R0*RL*C1*C2*B + 6*R0*RL*C2**2*B + 4*(R0*RL)**3*B**3 +
     +     4*R0*RL*T0*C1**3 + 12*R0*RL*C1**2*C2 +
     +     18*(R0*RL)**2*C1**2*B + 9*T0*(R0*RL)**2*C1*B**2 +
     +     9*(R0*RL)**2*C2*B**2

      K74 = 3*R0*C1**2*C2*B + 3*T0*C1*C2**2*B + C2**3*B +
     +     3*R0**2*RL*C1**2*B**2 + 6*T0*R0*RL*C1*C2*B**2 +
     +     3*R0*RL*C2**2*B**2 + 3*(R0*RL)**2*C2*B**3 +
     +     3*T0*(R0*RL)**2*C1*B**3 + (R0*RL)**3*B**4 + R0*C1**4 +
     +     4*T0*C1**3*C2 + 6*(C1*C2)**2 + 8*R0*RL*T0*C1**3*B +
     +     24*R0*RL*C1**2*C2*B + 18*(R0*RL)**2*C1**2*B**2 +
     +     5*R0*RL*C1**4

      K75 = R0*C1**4*B + 4*T0*C1**3*C2*B + 6*(C1*C2)**2*B +
     +     4*R0*RL*T0*C1**3*B**2 + 12*R0*RL*C1**2*C2*B**2 +
     +     6*(R0*RL)**2*C1**2*B**3 + T0*C1**5 + 5*C1**4*C2 +
     +     10*R0*RL*C1**4*B

      K76 = T0*C1**5*B + 5*C1**4*C2*B + 5*R0*RL*C1**4*B**2 + C1**6

      K77 = C1**6*B

      RETURN
      END

      SUBROUTINE K8(K81,K82,K83,K84,K85,K86,K87,K88)
      DOUBLE PRECISION K81,K82,K83,K84,K85,K86,K87,K88
      COMMON /COMB1/ B,RT,T
      COMMON /COMB2/ R0, RL
      COMMON /COMB3/ T0,TL,C1,C2

      K81 = 3*R0*(R0*RL)**2*C1 + 4*(R0*RL)**3*C1 + 4*T0*(R0*RL)**3*B +
     +     3*T0*(R0*RL)**2*C2

      K82 = 9*R0*(R0*RL)**2*C1*B + 6*R0**2*RL*C1*C2 +
     +     6*T0*(R0*RL)**2*C1**2 + 6*T0*(R0*RL)**3*B**2 +
     +     9*T0*(R0*RL)**2*C2*B + 3*T0*R0*RL*C2**2 +
     +     16*(R0*RL)**3*C1*B + 12*(R0*RL)**2*C1*C2

      K83 = 4*R0**2*RL*C1**3 + 9*R0*(R0*RL)**2*C1*B**2 +
     +     12*R0**2*RL*C1*C2*B + 3*R0*C1*C2**2 +
     +     18*T0*(R0*RL)**2*C1**2*B + 12*T0*R0*RL*C1**2*C2 +
     +     4*T0*(R0*RL)**3*B**3 + 9*T0*(R0*RL)**2*C2*B**2 +
     +     6*T0*R0*RL*C2**2*B + T0*C2**3 + 10*(R0*RL)**2*C1**3 +
     +     24*(R0*RL)**3*C1*B**2 + 36*(R0*RL)**2*C1*C2*B +
     +     12*R0*RL*C1*C2**2

      K84 = 8*R0**2*RL*C1**3*B + 4*R0*C1**3*C2 +
     +     3*R0*(R0*RL)**2*C1*B**3 + 6*R0**2*RL*C1*C2*B**2 +
     +     3*R0*C1*C2**2*B + 5*T0*R0*RL*C1**4 +
     +     18*T0*(R0*RL)**2*C1**2*B**2 + 24*T0*R0*RL*C1**2*C2*B +
     +     6*T0*(C1*C2)**2 + T0*(R0*RL)**3*B**4 +
     +     3*T0*(R0*RL)**2*C2*B**3 + 3*T0*R0*RL*C2**2*B**2 +
     +     T0*C2**3*B + 30*(R0*RL)**2*C1**3*B + 20*R0*RL*C1**3*C2 +
     +     16*(R0*RL)**3*C1*B**3 + 36*(R0*RL)**2*C1*C2*B**2 +
     +     24*R0*RL*C1*C2**2*B + 4*C1*C2**3

      K85 = R0*C1**5 + 4*R0**2*RL*C1**3*B**2 + 4*R0*C1**3*C2*B +
     +     10*T0*R0*RL*C1**4*B + 5*T0*C1**4*C2 +
     +     6*T0*(R0*RL)**2*C1**2*B**3 + 12*T0*R0*RL*C1**2*C2*B**2 +
     +     6*T0*(C1*C2)**2*B + 6*R0*RL*C1**5 +
     +     30*(R0*RL)**2*C1**3*B**2 + 40*R0*RL*C1**3*C2*B +
     +     10*C1**3*C2**2 + 4*(R0*RL)**3*C1*B**4 +
     +     12*(R0*RL)**2*C1*C2*B**3 + 12*R0*RL*C1*C2**2*B**2 +
     +     4*C1*C2**3*B

      K86 = R0*C1**5*B + T0*C1**6 + 5*T0*R0*RL*C1**4*B**2 +
     +     5*T0*C1**4*C2*B + 12*R0*RL*C1**5*B + 6*C1**5*C2 +
     +     10*(R0*RL)**2*C1**3*B**3 + 20*R0*RL*C1**3*C2*B**2 +
     +     10*C1**3*C2**2*B

      K87 = T0*C1**6*B + C1**7 + 6*R0*RL*C1**5*B**2 + 6*C1**5*C2*B

      K88 = C1**7*B

      RETURN
      END

*     End coeff. calculations  *

      SUBROUTINE OPENER(FNAME,NUNIT,STAT)

      INTEGER N, NUNIT
      CHARACTER FNAME*15, STAT*3
      SAVE N
      DATA N/10/

      OPEN(N,FILE = FNAME,STATUS = STAT)
      NUNIT = N
      N = N + 1
      RETURN
      END

      SUBROUTINE IMPRES(A,AF,M,N,ANS)
*     This subroutine calculates the regenerative part of the impulse
*     response

      REAL ANS(4000), TMP(4000), TS, RT, INT, PL, OMG, AMPL
      DOUBLE PRECISION FUNC
      INTEGER M,N
      PARAMETER (PI = 3.141592654)
      COMMON /COMB1/ B, RT ,T
      COMMON /COMB4/ TS
      COMMON /COMB5/ OMG, AMPL
```

```
      WRITE(*,*)'Calculates the regenerative part of the impulse'
      WRITE(*,*)'response'

      M = 8
      WRITE(*,*)'Enter, #  of points to be calculated in one revebara
     +tion period.'
      READ(*,*) N

      INT = RT/N

      DO 20 I = 1,M
      WRITE(*,*) I
        DO 30 J = 1, (I-1)*N
          TMP(J) = 0
   30   CONTINUE
        DO 40 K = (I-1)*N+1, M*N
          TS = INT*(K-1)
          TMP(K) = FUNC(TS,I,1)
   40   CONTINUE
    2   FORMAT(A1)
        DO 60 J = 1, M*N
          ANS(J) = TMP(J)
   60   CONTINUE
   20 CONTINUE

      RETURN
      END

*     Rutines from Numerical Recipes, numerical integration

      SUBROUTINE QROMB(A,B,SS,W)
      INTEGER W
      PARAMETER(EPS=1.E-6,JMAX=25,JMAXP=JMAX+1,K=5,KM=4)
      DIMENSION S(JMAXP),H(JMAXP)
      H(1)=1.
      DO 11 J=1,JMAX
        CALL TRAPZD(A,B,S(J),J,W)
        IF (J.GE.K) THEN
          L=J-KM
          CALL POLINT(H(L),S(L),K,0.,SS,DSS)
          IF (ABS(DSS).LT.EPS*ABS(SS)) RETURN
        ENDIF
        S(J+1)=S(J)
        H(J+1)=0.25*H(J)
   11   CONTINUE
      PAUSE 'Too many steps.'
      END

      SUBROUTINE TRAPZD(A,B,S,N,W)
      DOUBLE PRECISION FUNC
      INTEGER W
      IF (N.EQ.1) THEN
        S=0.5*(B-A)*(FUNC(A,W,2)+FUNC(B,W,2))
        IT=1
      ELSE
        TNM=IT
        DEL=(B-A)/TNM
        X=A+0.5*DEL
        SUM=0.
        DO 11 J=1,IT
          SUM=SUM+FUNC(X,W,2)
          X=X+DEL
   11     CONTINUE
        S=0.5*(S+(B-A)*SUM/TNM)
        IT=2*IT
      ENDIF
      RETURN
      END

      SUBROUTINE POLINT(XA,YA,N,X,Y,DY)
      PARAMETER (NMAX=10)
      DIMENSION XA(N),YA(N),C(NMAX),D(NMAX)
      NS=1
      DIF=ABS(X-XA(1))
      DO 11 I=1,N
        DIFT=ABS(X-XA(I))
        IF (DIFT.LT.DIF) THEN
          NS=I
          DIF=DIFT
        ENDIF
        C(I)=YA(I)
        D(I)=YA(I)
   11   CONTINUE
      Y=YA(NS)
      NS=NS-1
      DO 13 M=1,N-1
        DO 12 I=1,N-M
          HO=XA(I)-X
          HP=XA(I+M)-X
          W=C(I+1)-D(I)
          DEN=HO-HP
          IF(DEN.EQ.0.)PAUSE
          DEN=W/DEN
          D(I)=HP*DEN
          C(I)=HO*DEN
   12     CONTINUE
        IF (2*NS.LT.N-M)THEN
          DY=C(NS+1)
        ELSE
          DY=D(NS)
          NS=NS-1
        ENDIF
        Y=Y+DY
   13   CONTINUE
      RETURN
      END
```

APPENDIX B-4

```
      PROGRAM DIF2FIELD
*********************************************************************
This programme calculates the output voltage signal for a given separation of the
transmitter and receiver, using the simulated or measured voltage output signal for a
different transmitter-receiver separation


      Author:     Murugendran Kanagasundram
      Date  :     1-12 94.
*********************************************************************



      REAL  SFRQ, RAD, R, K, K1, R1, S, CA1, CA2, RHO1, RHO2, AF,T01
      DOUBLE PRECISION C1,D1,C2,D2
      INTEGER  LIMIT, P, STIM, ETIM, T
      COMMON R, K, K1, RAD, R1
      PARAMETER  (LIMIT = 16384, TOPI = 6.28318530718)
      DIMENSION  PSAM(LIMIT)
      CHARACTER*15 FNAME2, FNAME4
      COMPLEX PM1, PM2, H, P0

      WRITE(*,*)'GIVE THE SAMPLING FREQ..'
      READ(*,*) SFRQ

    2 FORMAT(A1)
    1 FORMAT(A15)

      WRITE(*,*)'ENTER THE FILE WITH THE DATA.'
      READ(*,1) FNAME2
      OPEN(20, FILE = FNAME2, STATUS = 'OLD',
     +   ACCESS = 'SEQUENTIAL')

      WRITE(*,*) 'ENTER THE STARTING AND ENDING SAMPLE # OF THE PULSE.'
      READ(*,*) STIM, ETIM


      PSAM(1) = 0
      I = 2
      READ(20,*) T,S
    3 IF (T .GE. STIM .AND. T .LE. ETIM) THEN
        PSAM(I) = S
        I = I + 1
        READ(20,*) T,S
        GO TO 3
      ELSE IF (T .LT. STIM) THEN
        READ(20,*) T,S
        GO TO 3
      ELSE
      END IF

      DO 40 J = I,LIMIT
        PSAM(J) = 0
   40 CONTINUE

      P = LIMIT / 2
      CALL REALFT(PSAM,P,1)

      WRITE(*,*)'ENTER THE RADIOUS OF THE SOURCE IN (m).'
      READ(*,*) RAD
      WRITE(*,*)'ENTER DISTANCE BETWEEN SOURCE AND OBSERVATION POINTS'
      WRITE(*,*)'1 AND 2 IN (m).'
      READ(*,*) R, R1
      WRITE(*,*)'ENTER THE VELOCITY OF SOUND DURING THE MEASUREMENTS A'
      WRITE(*,*)'T OBSERVATION POINTS 1 AND 2 IN (m/s).'
      READ(*,*) CA1,CA2
      WRITE(*,*)'Enter the density of the medium during the measurement'
      WRITE(*,*)'s at observation points 1 and 2 in (kg/m**3).'
      READ(*,*)RHO1, RHO2
      AF = (RHO2*CA2)/(RHO1*CA1)
      T01= R1/CA2-0.1*LIMIT/SFRQ


      WRITE(*,*)'Choose the model: (1)Plane wave (2)Near-field'
      READ(*,*)K

      IF (K .EQ. 1) THEN
        PSAM(1) = 0.
        J = 1
        DO 70 I = 3,(2*P+1), 2
          F   = J * SFRQ /(2 * P)
          K   = TOPI * F / CA1
          K1  = TOPI * F / CA2
          P0  = AF*EXP(CMPLX(0.0,(K1*R1-K*R-K1*CA2*T01)))
          H   = P0
          A3  = REAL(H)
          A4  = AIMAG(H)
          B11 = PSAM(I)
          B22 = PSAM(I+1)
          IF (I .EQ. (2*P+1)) THEN
            B11 = PSAM(2)
            B22 = 0
            PSAM(2) = (B11*A3 - B22*A4)
          ELSE
            PSAM(I)   = (B11*A3 - B22*A4)
            PSAM(I+1) = (B22*A3 + B11*A4)
          END IF
          J = J + 1
   70   CONTINUE
      ELSE
        PSAM(1) = 0.
        J = 1
        DUMMY = 0
        DO 80 I = 3,(2*P+1), 2
          IF (I .GT. DUMMY+100) THEN
            WRITE(*,*)I
            DUMMY = I
          ENDIF
          F   = J * SFRQ /(2 * P)
          K   = TOPI * F / CA1
          K1  = TOPI * F / CA2
          CALL QROMB(1,1,0.0D0,TOPI/4.0D0,C1)
          CALL QROMB(2,1,0.0D0,TOPI/4.0D0,D1)
          CALL QROMB(1,2,0.0D0,TOPI/4.0D0,C2)
          CALL QROMB(2,2,0.0D0,TOPI/4.0D0,D2)
          A1 =1.0-C1*4.0*2.0/TOPI*COS(K*R)  -D1*4.0*2.0/TOPI*SIN(K*R)
          B1 =    D1*4.0*2.0/TOPI*COS(K*R)  -C1*4.0*2.0/TOPI*SIN(K*R)
          A2 =1.0-C2*4.0*2.0/TOPI*COS(K1*R1)-D2*4.0*2.0/TOPI*SIN(K1*R1)
          B2 =    D2*4.0*2.0/TOPI*COS(K1*R1)-C2*4.0*2.0/TOPI*SIN(K1*R1)
          PM1=CMPLX(A1,(-1)*B1)
          PM2=CMPLX(A2,(-1)*B2)
          P0 =AF*EXP(CMPLX(0.0,(K1*R1-K*R-K1*CA2*T01)))
          H  =P0*PM2/PM1
          A3 =REAL(H)
          A4 =AIMAG(H)
          B11= PSAM(I)
          B22= PSAM(I+1)
          IF (I .EQ. (2*P+1)) THEN
            B11 = PSAM(2)
            B22 = 0
            PSAM(2) = (B11*A3 - B22*A4)
          ELSE
            PSAM(I)   = (B11*A3 - B22*A4)
            PSAM(I+1) = (B22*A3 + B11*A4)
          END IF
          J = J + 1
   80   CONTINUE
      END IF

      WRITE(*,*)'ENTER A FILE TO STORE DATA.'
      READ(*,1) FNAME4
      OPEN(40, FILE = FNAME4, STATUS = 'NEW',
     +ACCESS = 'SEQUENTIAL')

      CALL REALFT(PSAM,P,-1)

      WRITE(*,*)'Writing to file.'
      DO 100 I = 1,LIMIT
        WRITE(40,*)(I-1)+(STIM-1)+T01*SFRQ,PSAM(I)/P
*       WRITE(40,*)I,PSAM(I)/P
  100 CONTINUE


      CLOSE(20)
      CLOSE(40)
      STOP
      END

      SUBROUTINE QROMB(I,M,A,B,SS)
      DOUBLE PRECISION A,B,SS,DSS,S,H,ER
      PARAMETER(EPS=1.0D-5,JMAX=30,JMAXP=JMAX+1,K=5,KM=4)
      DIMENSION S(JMAXP),H(JMAXP)
      H(1)=1.0D0
      ER = 1.0D-10
      DO 11 J=1,JMAX
        CALL TRAPZD(I,M,A,B,S(J),J)
        IF (J.GE.K) THEN
          L=J-KM
          CALL POLINT(H(L),S(L),K,0.0D0,SS,DSS)
          IF (ABS(SS-ER).LT.EPS*ABS(ER)) RETURN
          ER = SS
        ENDIF
        S(J+1)=S(J)
        H(J+1)=0.25D0*H(J)
```

```
11    CONTINUE
      PAUSE 'Too many steps.'
      END

      SUBROUTINE TRAPZD(I,M,A,B,S,N)
      DOUBLE PRECISION A,B,S,FUNC,DEL,SUM,X
      IF (N.EQ.1) THEN
       S=0.5D0*(B-A)*(FUNC(I,M,A)+FUNC(I,M,B))
       IT=1
      ELSE
       TNM=IT
       DEL=(B-A)/TNM
       X=A+0.5D0*DEL
       SUM=0.0D0
       DO 11 J=1,IT
        SUM=SUM+FUNC(I,M,X)
        X=X+DEL
11     CONTINUE
       S=0.5D0*(S+(B-A)*SUM/TNM)
       IT=2*IT
      ENDIF
      RETURN
      END

      SUBROUTINE POLINT(XA,YA,N,X,Y,DY)
      DOUBLE PRECISION XA,YA,Y,DY,DIF,DIFT,C,D,HO,HP,W,DEN,X
      PARAMETER (NMAX=10)
      DIMENSION XA(N),YA(N),C(NMAX),D(NMAX)
      NS=1
      DIF=ABS(X-XA(1))
      DO 11 I=1,N
       DIFT=ABS(X-XA(I))
       IF (DIFT.LT.DIF) THEN
        NS=I
        DIF=DIFT
       ENDIF
       C(I)=YA(I)
       D(I)=YA(I)
11    CONTINUE
      Y=YA(NS)
      NS=NS-1
      DO 13 M=1,N-1
       DO 12 I=1,N-M
        HO=XA(I)-X
        HP=XA(I+M)-X
        W=C(I+1)-D(I)
        DEN=HO-HP
        IF(DEN.EQ.0.)PAUSE 'ERROR'
        DEN=W/DEN
        D(I)=HP*DEN
        C(I)=HO*DEN
12     CONTINUE
       IF (2*NS.LT.N-M)THEN
        DY=C(NS+1)
       ELSE
        DY=D(NS)
        NS=NS-1
       ENDIF
       Y=Y+DY
13    CONTINUE
      RETURN
      END

      FUNCTION FUNC(I,M,A)
      DOUBLE PRECISION A,FUNC
      REAL RAD,K,K1,R,R1
      INTEGER I,M
      COMMON R,K,K1,RAD,R1

      IF (M .EQ. 1) THEN
       IF (I .EQ. 1) THEN
       FUNC=COS(K*SQRT(R**2+4.*RAD**2*(COS(A))**2))*(SIN(A))**2
       END IF

       IF (I .EQ. 2) THEN
       FUNC=SIN(K*SQRT(R**2+4.*RAD**2*(COS(A))**2))*(SIN(A))**2
       END IF
      ELSE
       IF (I .EQ. 1) THEN
       FUNC=COS(K1*SQRT(R1**2+4.*RAD**2*(COS(A))**2))*(SIN(A))**2
       END IF

       IF (I .EQ. 2) THEN
       FUNC=SIN(K1*SQRT(R1**2+4.*RAD**2*(COS(A))**2))*(SIN(A))**2
       END IF
      END IF
      RETURN
      END
```

APPENDIX C-1

Transducer parameter (PZT-5A)

Density(ρ_0)	7750kg/m^3
Velocity of sound(c)	4355.2m/s
stiffness constant(c_{33}^D)	$1.47*10^{11}$ N/m^2
Piezo electric stress coefficient(e_{33})	15.8C/m^2
Dielectric constant(ε_{33})	$830*8.85*10^{-12}$

REFERENCES

1. **Lawrence E. Kinsler, Austin R. Frey, Alan B. Coppens** and **James V. Sanders**, *Fundmentals of Acoustics* Third Editions, page 178, John Wiley & sons, 1982

2. **A. Lygre, M. Vestrheim, P. Lunde** and **V. Berge**, *Numerical simulations of ultrasonic flowmeters*, Ultrasonics International 87 Conf. Proc..

3. **Per Lunde** and **Magne Vestrheim,** *Piezoelectric transducer modelling, thickness mode vibration***,** page 49, Report, Ref. No. CMI-91-A10003.

4. **Murugendran Kanagasundram** and **Magne Vestrheim**, *Pulse forming effects in ultrasound transit-time flowmeters, no flow conditions*, 15th Scandinavian Cooperation Meeting in Acoustics/Hydrodynamics,Ustaoset Høyfjellshotel 2-5 Feb. 1992.

5. **B.Rayleigh,** *The Theory of Sound, Volume II*, page 107, Dover publications,1945.

6. **A.O.Williams, Jr.**, *The Piston Source at High Frequncies*, J. Acoust. Soc. Am. 23(1), Jan. 1951.

7. **A.S.Khimunin,** *Numerical Calculation of the Diffraction Corrections for the Precise Measurement of Ultrasound Absorption*, page 178, Acustica, Vol.27, Heft 4, 1972.

8. **M.Braun,** *Differential equations and their applycations (Third Edition) short version*, page 196, A Springer-Verlag publication.

9. **A.Papoulis,** *The Fourier integral and its applications*, page 135, McGraw-Hill Book Company, Inc. 1962.

10. **E.Skudrzyk,** *The foundations of Acoustics, Basic Mathamatics and Basic Acoustics* page 505, Springer-Verlag, Wien New York,1971.

11. **William H. Press**, **Brain P. Flannery**, **Saul A. Teukolsky** and **William T. Vetterling**, *Numerical Recipes The Art of Scientific Computing (FORTRAN Version)*, Cambridge University Press, 1989.

12.

13. **W.D.Munk,** *Ultrasonic flowmeter — a new approach to gas measurement*, PIPE LINE INDUSTRY, April 1983.

14. **Richard E. Challis** and **John A. Harrison,** *Rapid solutions to the transient response of piezoelectric elements by z-transform techniques*, J. Acoust. Soc. Am. **74**(6), December 1983.

15. **Steinar Vervik**, *Transitt-tidsbestemmelse for Ultralyd Strømningsmetre. Nullstrømningsforhold*, Dissertation for the Cand. Scient. degree, in Norwegian, Dept. of Physics, University of Bergen, Norway, Jan. 1995.

16. **K.Beissner**, *Free-field Reciprocity Calibration in the Transition Range between near Field and far Field*, page 164, ACUSTICA, Vol 46, 1980.

17. *Precision method for free-field calibration of one-inch standerd condenser microphones by the reciprocity technique*, page 9, International Electrotechnical Commission, Publication 486,1974.

18. *Characteristics and calibration of hydrophones for opration in the frequency rang 0.5 MHz to 15 MHz*, page 11, International Electrotechnical Commission, Publication 866, 1987.

19. Reference 17, page 9.

20. **Asle Lygre, Trond Folkestad, Reidar Sakariassen** and **Dag Aldal,** *A new multi-path ultrasonic flow meter for gas*, 10th North Sea Flow Measurement Workshop, NEL, Glasgow, 27-29 Oct.1992, Ref.nr.: CMR-92-A10005.

21 Reference 1, page 177.

22 **Louis V. King**, *On The Acoustic Radiation Field of The Piezo-Electric Oscillator and The Effect of Viscosity on Transmission*, Canad. J. Res., 11(2), page 135-155, 1934.

23 **Theodore L. Rhyne**, *Radiation coupling of a disk to a plane and back or a disk to a disk: An exact solution*, J. Acoust. Soc. Am., 61(2), Feb. 1977

24 **Peter R. Stepanishen**, *Transient Radiation from Pistons in an Infinite Planar Baffle*, J. Acoust. Soc. Am., 49(5) part 2, 1971.

25 **Philip M. Morse** and **K. Uno Ingard**, *Theoritical Acoustics*, page 377,Princeton University press, Princeton, New Jersey.

26 **William L. Beaver**, *Sonic nearfields of pulsed piston radiator*, J. Acoust. Soc. Am., 56(4), Oct. 1974.

27 **Magne Vestrheim,** *Akustiske Transdusere*, lecture notes for the course in acoustic transducers(Norwegian), course No. F272, Dept. of Physics, University of Bergen, May 1990.

28 **Warren P. Mason**, *Physical Acoustics Principles and Methods*, Vol. 1- part A, Academic Press, New York and London, 1964.

29 Reference 28, page 237.

30 **M. Redwood**, *Transient Performance of a Piezoelectric Transducer*, J. Acoust. Soc. Am, 33(4), Apr. 1961.

31 Reference 9, Appendix I.

32 **James W. Nilsson**, *Electric Circuits Second Edition*, page 126, World Student Series Edition, Addison-Wesley Puplishing Company.

33 **Erling A. Hammer**, *Ultrasonics in the oil and gas industry*, Lecture at Cranfield institute of technology, Fluid engineering and instrumentation, Short course, Ultrasonics sensors and systems, March 26-29, 1990.

34 **Nils Sponheim**, *Transient Ultrasonc Fields of Efficient Broadband Piezoelectric Transducers*, Dissertation for the degree of Dr. ing., Institutt for fysikalsk elektronikk, University of Trondheim, Norway, Aug. 1985.

35 **Kan Cao**, *Kalibreringsmetoder for Høyfrekvens Ultralyd Transdusere for Gass*, Hovedfagsoppgave(Dissertation for the Cand. Scient degree, in Norwegian), Dept. of Physics, University of Bergen, Norway, July 1992.

36 **A.S.Khimunin**, *Numerical Calculation of the Diffraction Corrections for the Precise Measurement of Ultrasound Phase Velocity*, Acustica, Vol. 32, 1975.

37 **J.L.Leander**, *Effects of Viscosity and Chemical Relaxation on Acoustic Pulse Propagation in Seawater*, Ultrasonics, Vol 27, Nov. 1989.

38 **Gerald R. Harris**, *Review of Transient Field Theory for a Baffled Planer Piston*, J. Acoust. Soc. Am. 70(1), July 1981.

39 **M. E. Nolan** and **J. G. O'Hair**, *An Ultrasonic Flowmeter for the Accurate Measurement of High Pressure Gas Flows*, Flow Metering and Proving Techniques..., The Inst. of Meas. & Contr., London 1983.

40 **Franklin F. Kuo**, *Network Analysis and Synthesis*, 2nd Edition, page 40, Wiley International Edition, 1966, John Wiley & Sons, New York.

41 **Henry Stark, Franz B. Tuteur** and **John B. Anderson**, *Modern Electrical Communications analog, digital, and optical systems*, Second Edition, page 60, Printice Hall International, 1988.

42 **Didier Cassereau, Daniel Guyomar** and **Mathias Fink,** *Time Deconvolution of Diffraction Effects - Application to Calibration and Prediction of Transducer Waveforms*, page 1076, J. Acoust. Soc. Am. 84(3), Sep. 1988.

43 *Measurement of Fluid Flow in Closed Conduits-Methods Using Transit Time Ultrasonic Flowmeters*, 8th Working Draft, ISO/TC 30/WG 20 N 88 E, 1994.

44 **K. J. Zanker** and **W. R. Freund Jr.**, *Developments of Multipath Transit Time Ultrasonic Gas Flow Meters*, The north sea flow measurement workshop, 24th-27th Oct. 1994.

45 **Peter R. Stepanishen** and **George Fisher**, *Experimental verification of the impulse response method to evaluate transient acoustic fields*, page1610-1617, J. Acoust. Soc. Am. 69(6), June 1981.

46 **Jonathan A. Harrison**, **Geoffrey N. Cook-Martin**, and **Richard E. Challis**, *Radiation coupling between two coaxial disks of different diameter: An exact solution and detailed experimental verification*, page 1009-1022, J. Acoust. Soc. Am. 76(4), Oct. 1984.

47 **Lawrence E. Kinsler** and **Austin R. frey**, *Fundamentals of acoustics*, second edition, John Wiley & Sons, Inc., 1962.